T CENTER FOR NEUTRON RESEARCH

1999 PROGRAMS

AND

ACCOMPLISHMENTS

MATERIALS

SCIENCE AND

ENGINEERING

LABORATORY

NISTIR 6437

UNITED STATES
DEPARTMENT OF
COMMERCE

TECHNOLOGY
ADMINISTRATION

NATIONAL
INSTITUTE OF
STANDARDS AND
TECHNOLOGY

From Research to the "Real World"

NCNR research provides information key to applications
in automotive spring design, computer hard drive reading
heads, and materials thermally stabilizing gratings in
fiber optics communications. Over 1600 researchers
from the U.S. and around the world were drawn to
NCNR's unique facility in 1999.

NIST CENTER FOR NEUTRON RESEARCH

1999 PROGRAMS AND ACCOMPLISHMENTS

J. Michael Rowe, Director

Ronald L. Cappelletti, Editor
Linda K. Clutter, Assistant Editor

January 2000

U.S. DEPARTMENT OF COMMERCE
William M. Daley, Secretary

Technology Administration
Dr. Cheryl L. Shavers, Under Secretary of Commerce for Technology

National Institute of Standards and Technology
Raymond G. Kammer, Director

CONTENTS

Once again, it is a pleasure to be able to reflect on the accomplishments of the NIST Center for Neutron Research over the past year. In the reactor operations area, 1999 was another outstanding year. In spite of an unsheduled maintenance shutdown, the reactor operated 250 days, with a reliability factor of better than 90%. The cold source availability for the period was 98%; i.e. the cold source held the reactor from operation 4 days during the year. The remaining spent fuel in the storage pool was shipped, providing space for at least five years operation. Also, an order has been placed for a new cooling tower which will not only provide needed capability for the next 25 years, but will also reduce the plume visible during cold weather. Last, steady progress has been made in preparing for a license renewal application to the Nuclear Regulatory Commission, in order to extend the period of operation beyond 2004.

We have also made great progress in instrumentation, with the back scattering spectrometer operational; with the spin echo spectrometer now being used for real measurements; and with the disk chopper spectrometer being commissioned. All three of these instruments will be available to "friendly" users in the next proposal cycle. Other work is also advancing well–the perfect crystal small angle scattering spectrometer (part of the NSF/NIST CHRNS) is being installed at the reactor; the first phase of the high intensity filter analyzer spectrometer is ready to begin installation; and the design and manufacture of new thermal neutron spectrometers is underway. This simultaneous development program has put severe strains on our resources, but we can now look forward to many years of benefit from the results.

Finally, as always, the results are seen in the output of the researchers who use the facility. As was done last year, we are presenting highlights of this work in the following chapters of this report. I think that all can agree that the results truly speak for themselves.

Mike Rowe

Modern technological society is dependent upon increasingly sophisticated use of materials, many of whose attributes are dictated by their sub-microscopic structural and dynamical properties. Our knowledge of these properties is provided by a wide range of scientific techniques of which the many types of scattering (for example, X-rays, light, electrons, neutrons) are arguably the most important. Of these probes, neutrons are perhaps least familiar, but they provide important advantages for many types of measurements.

Neutrons, as prepared for use at modern sources, are moving at speeds comparable to those of atoms moving at room temperature, thus providing the ability to probe dynamical behavior. At the same time, neutrons are well matched to measurements at length scales ranging from the distances between atoms to the size of biological or polymer macromolecules. Neutrons are sensitive to the magnetic properties of atoms and molecules, allowing study of the underlying magnetic properties of materials. They also scatter quite differently from normal hydrogen atoms than they do from heavy hydrogen (deuterium), allowing selective study of individual regions of molecular systems. Finally, neutrons interact only weakly with materials, providing the opportunity to study samples in different environments more easily (at high pressures, in shear, in reaction vessels, etc.), and making them a non-destructive probe. These favorable properties are offset by the relative weakness of the best neutron sources compared to X-ray or electron sources, and by the relatively large facilities required to produce neutrons. As a result, major neutron sources are operated as national user facilities to which researchers come from all over the U.S. (and abroad) to perform small scale science using the special measurement capabilities provided.

In addition to scattering measurements, neutrons can be used to probe the atomic composition of materials by means of capture and resultant radioactive decay. The characteristics of the decay act as "fingerprints" for particular atomic nuclei, allowing studies of environmental samples for pollutants (e.g. heavy metals), characterization of Standard Reference Materials, and many other essential measurements. While the scattering and capture users of neutrons are little concerned with understanding the inherent properties of the neutron, there are important areas in physics that can be explored by carefully measuring fundamental neutron behavior. Examples include the lifetime of the free neutron, an important quantity in the theory of astrophysics; the beta decay process of the neutron, the

details of which are stringent tests of nuclear theory; and the effects of various external influences such as gravity or magnetic fields on neutrons.

The NCNR utilizes neutrons produced by the 20 MW NIST Research Reactor to provide facilities, including the nation's only internationally competitive cold neutron facility, for all of the above types of measurements to a national user community. There are approximately 35 stations in the reactor and its associated beams that can provide neutrons for experiments. At the present time 26 of these are in active use, of which 6 provide high neutron flux positions in the reactor for irradiation, and 20 are beam facilities. A schematic layout of the beam facilities and brief descriptions of available instrumentation are given below. More complete descriptions can be found at http://www.ncnr.nist.gov.

These facilities are operated both to serve NIST mission needs and as a national facility, with many different modes of access. Some instrumentation was built years ago, and is not suited to general user access; however, time is available for collaborative research. NIST has recently built new instrumentation, and reserves 1/3 of available time for mission needs with the balance available to general users. In other cases, instrumentation was built and is operated by Participating Research Teams (PRT). PRT members have access to 75% of available time, with the balance available to general users. In a special case, NIST and the National Science Foundation established the Center for High Resolution Neutron Scattering at the NCNR, with a 30-m Small Angle Scattering (SANS) instrument, a cold neutron triple axis spectrometer, and a perfect crystal SANS under construction. For these facilities, most time is available for general users. While most access is for research, whose results are freely available to the general public, proprietary research can be performed under full cost recovery. Each year, approximately 1600 researchers (persons who participated in experiments at the facility, but did not necessarily come here) from all areas of the country, from industry, academe, and government use the facility for measurements not otherwise possible. The research covers a broad spectrum of disciplines, including chemistry, physics, biology, materials science, and engineering.
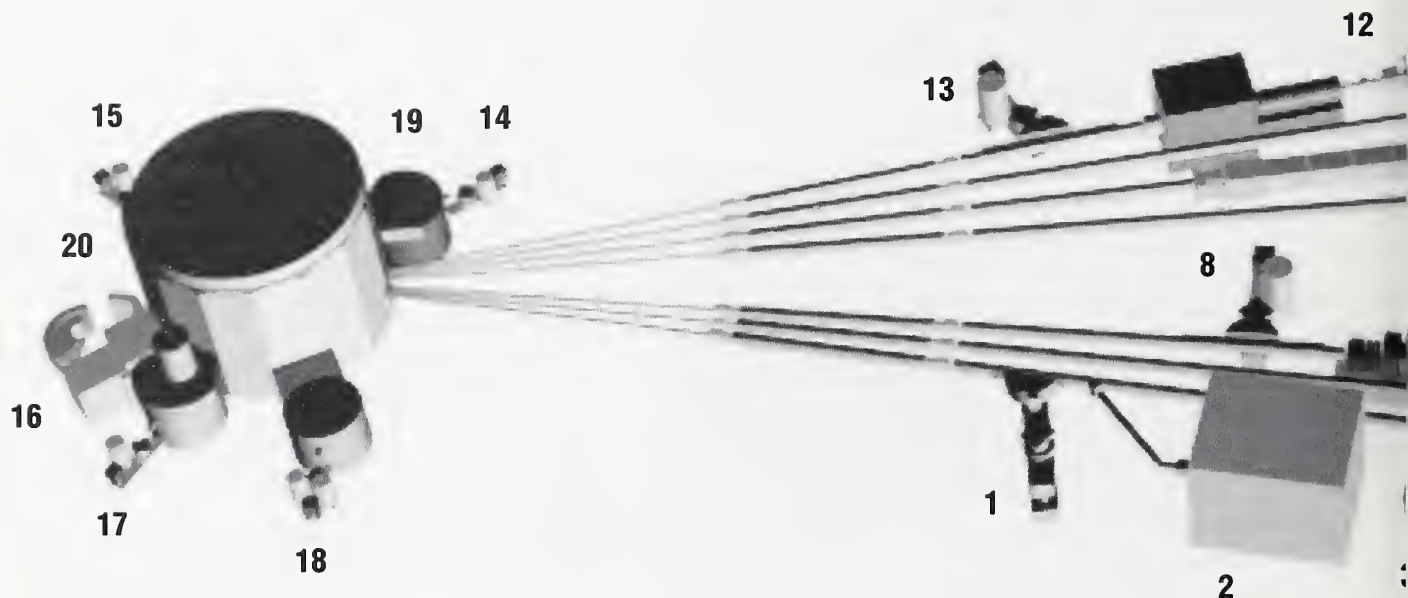
1 Horizontal Sample Reflectometer

Horizontal surface of sample allows reflectivity measurements of free surfaces, liquid vapor interfaces, as well as polymer coatings.

2 Neutron Interferometry and Optics Station

Includes perfect silicon interferometer; vibration isolation system provides exceptional phase stability and fringe visibility.

3 Prompt Gamma Activation Analysis

Cold neutron fluxes allow detection limit for H of 1 to 10 micrograms. Focused beams available for profiling.

4 NG-7 30m SANS

Small Angle Neutron Scattering instrument for microstructure measurement sponsored by NIST, the Exxon-Mobil Research and Engineering Co., the University of Minnesota, and Texaco R&D.

5 Neutron Physics Station

A cold neutron beam 150 x 60 mm^2, available for fundamental neutron physics experiments.

6 Fermi Chopper TOF Spectrometer

A hybrid time-of-flight spectrometer for inelastic scattering, with wavelengths between 0.23 and 0.61 nm. The wavelength is chosen by focusing pyrolytic graphite crystal, while the beam is pulsed by a simple Fermi chopper.

7 Spin Echo Spectrometer

A neutron spin echo spectrometer offering neV energy resolution, based upon Julich design, sponsored by NIST, Julich and Exxon-Mobil.

8 SPINS Spectrometer

Spin Polarized Inelastic Scattering, a cold neutron triple axis spectrometer with spin polarization capabilities for high resolution studies, and position sensitive detector capability, sponsored by the National Science Foundation and NIST; part of Center for High Resolution Neutron Scattering (CHRNS).

9 Disk Chopper TOF Spectrometer

Versatile time-of-flight spectrometer, with beam pulsing and monochromatization effected by 7 disk choppers. Used for studies of dynamics in condensed matter, including macromolecular systems.

11 10 9 7 6 5 4
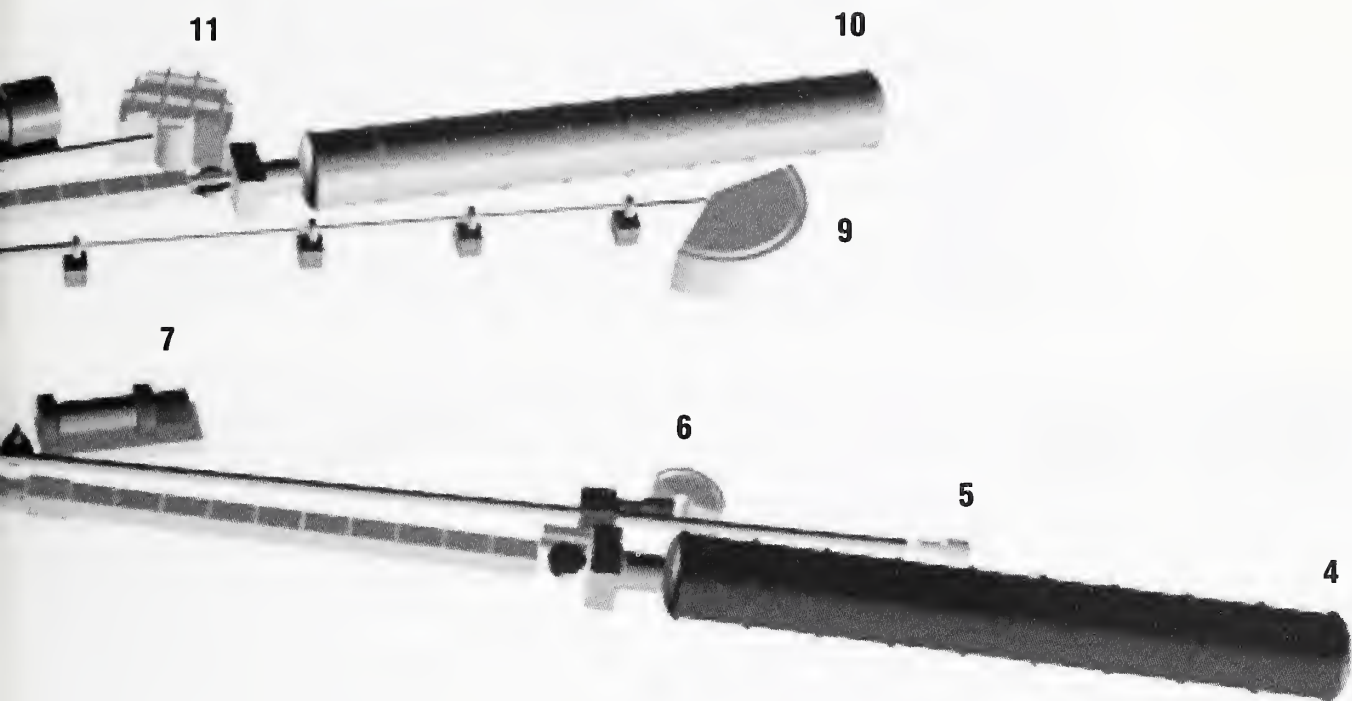
10 NG-3 30m SANS

Instrument for microstructure measurement sponsored by the National Science Foundation and NIST; part of CHRNS.

11 Back Scattering Spectrometer

High intensity, very high resolution back scattering spectrometer, with many innovative features, and energy resolution of approximately 1 μeV.

12 8M SANS

Instrument for polymer characterization, sponsored by Polymers Division.

13 Vertical Sample Reflectometer

Instrument for measuring subsurface structure with polarization analysis capability. Reflectivities down to 10^{-8} can be measured.

14 BT-8 Residual Stress Diffractometer

Diffractometer optimized for depth profiling of residual stress in large components.

15 BT-9 Triple Axis Spectrometer

Triple axis crystal spectrometer for measurements of excitations and structure.

16 BT-1 Powder Diffractometer

Powder diffractometer with 32 detectors; incident wavelengths of 0.208, 0.154, and 0.159 nm, with highest resolution of $\delta d/d = 8 \times 10^{-4}$.

17 BT-2 Triple Axis Spectrometer

Triple axis crystal spectrometer with polarized beam capability for measurement of magnetic dynamics and structure.

18 BT-4 Filter Spectrometer

A triple axis crystal spectrometer with a Be or Be/Graphite filter analyzer option for chemical spectroscopy.

19 Cold Neutron Depth Profiling

A station for quantitative profiling of subsurface impurities and coatings, based on neutron capture and emission of a charged particle.

20 Thermal Column

A very well-thermalized beam of neutrons used for radiography, tomography, dosimetry, and other experiments.

Photograph by L. A. Shuman

1. An incoming SANS image excites the interest of Martin Vigild (center) as Frank Bates (standing), Newell Washburn (right) and Ken Hanley, all of the University of Minnesota, look on.

2. NCNR's Peter Gehring describes the analyzer of the spin polarized triple axis spectrometer (SPINS) to NCNR Summer School participants.

1

2
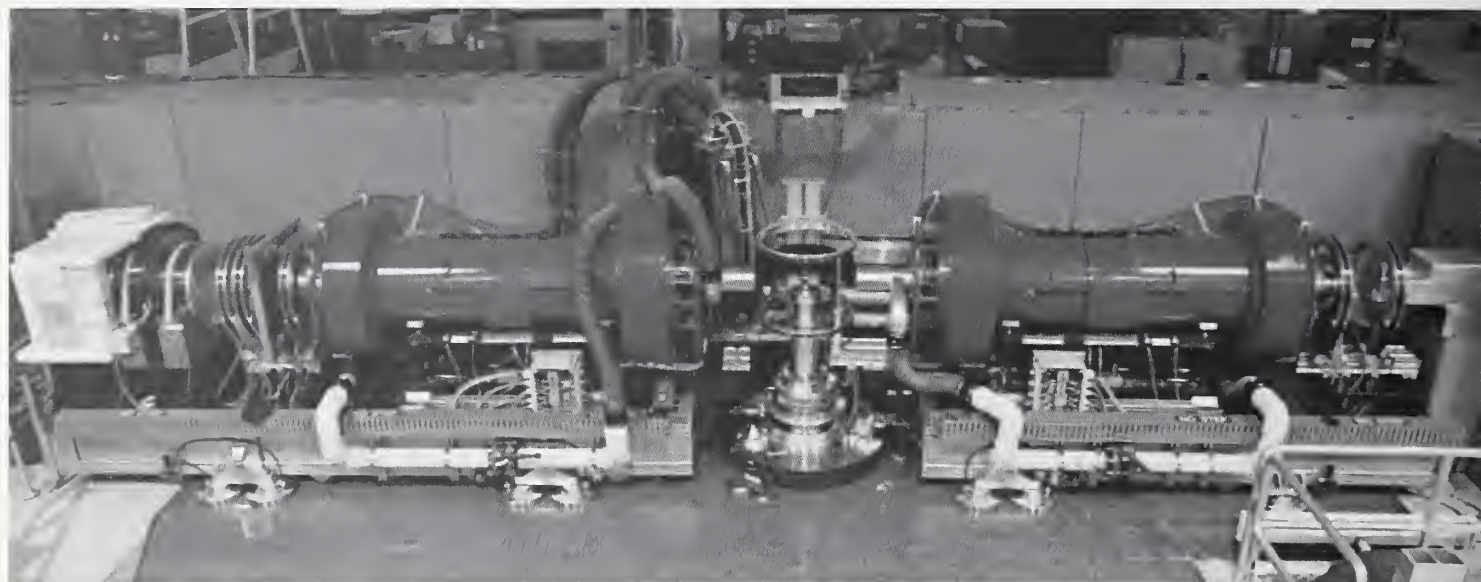
3

3. The Spin Echo Spectrometer (NSE) at NCNR, commissioned this year, is described in a Research Highlight in this issue.

4. Stephen FitzGerald (Oberlin College) loads a sample at the HFBS.

5. Gudrun Schmidt (NIST, Polymers Division) awaits the display of an updated SANS image.

4

5
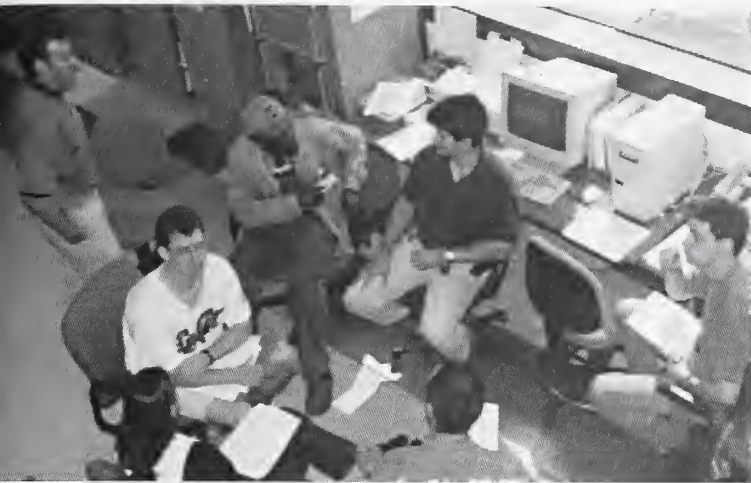
6. NCNR Summer School participants interacting at the recently commissioned high-flux back-scattering spectrometer (HFBS).

7. Silke Rathgeber and So Hyun Park (both at NCNR), ready to load a sample at the NSE.

8. The science/engineering/technical team which built and put the HFBS into operation.

6
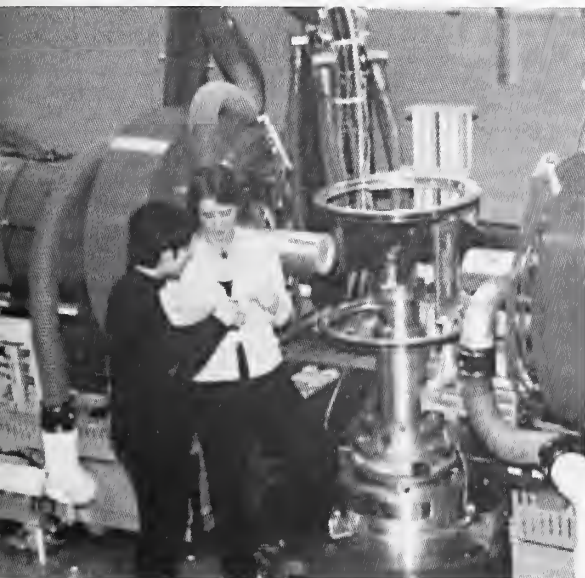
Photograph by L. A. Shuman

7   8

9. John Copley (NCNR) in front of the soon-to-be commissioned disk chopper time-of-flight spectrometer (DCS).

10. Dave Clem and Mike Rinehart (both of NCNR) installing biological shielding at the DCS.
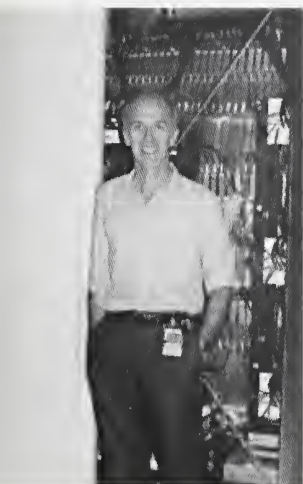
9   10

SUPERLATTICE MAGNONS

A powerful technique for optimizing material properties is to deposit alternating layers of different materials to form a thin film superlattice. In particular, magnetic and non-magnetic materials grown as a superlattice exhibit a variety of tunable couplings between the magnetic layers. Control of these couplings by varying the layer materials and thicknesses has lead to dramatic increases in performance in certain device applications. A prime example is the recent use of layered magneto-resistive films in high-performance magnetic recording heads and sensors. The inter-layer magnetic coupling can survive across as many as 30 non-magnetic atomic planes due to its one-dimensional nature, but the coupling strength is always much weaker than bulk material magnetic interactions.

The behavior of the magnetic fluctuations (magnons) in these weakly coupled layer systems is of interest because it provides a direct measure of the magnetic interactions responsible for the magnetic structure, and leads to a better understanding of the unique layer to layer couplings. Until now, the only measurements that have probed these fluctuations have used Brillouin light scattering [1], or ferromagnetic-resonance techniques [2], both of which measure only the longest wavelength dynamics. These measurements have found interesting resonances associated with the superlattice structure.

It is important to directly measure the magnons at shorter wavelengths in order to determine the dispersion, which directly relates to the magnetic interactions, both within and between layers, and whether or not the magnetic fluctuation waves propagate between layers. Only inelastic magnetic scattering techniques can provide this information, but with current neutron scattering sources the intensities from such measurements can be prohibitively low, because the amount of magnetic material in the films is so small.

In order to overcome this difficulty we have made neutron inelastic scattering measurements on a very large superlattice of alternating layers of dysprosium and yttrium. Dysprosium is the magnetic constituent, and it has the strongest neutron magnetic-scattering of all the elements. In order to maximize the amount of Dy, 350 bilayers composed of 43 Å of Dy and 28 Å of Y (designated $[Dy_{43}/Y_{28}]_{350}$) were grown by MBE techniques on a 2.5 cm X 1.3 cm substrate resulting in 3 mg of Dy in the sample.
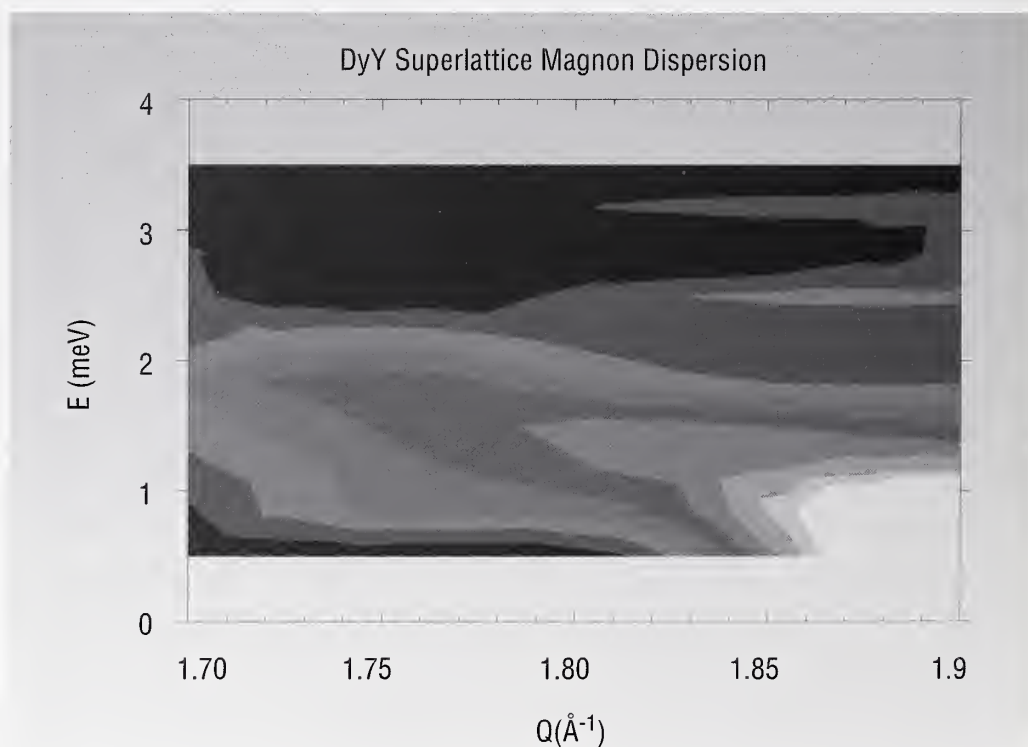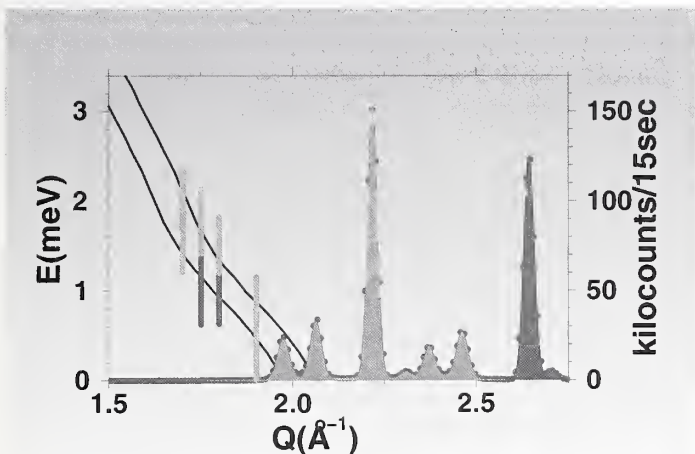

FIGURE 1. Inelastic magnetic scattering from a $[Dy_{43}/Y_{28}]_{350}$ superlattice, obtained by subtracting 10K data from 75K data, shown as an intensity map in Q-energy space. The highest intensity is 300 counts/ 30 minutes and decreases by 30 counts for each level. A magnetic Bragg peak is just off the graph at Q = 1.97 Å⁻¹.

A. Schreyer
Institut für Experimentalphysik
Festkörperphysik
Ruhr-Universität Bochum
D-44780 Bochum, Germany

R. W. Erwin and C. F. Majkrzak
NIST Center for Neutron Research
National Institute of Standards and Technology
Gaithersburg, MD 20899-8562

J. Kwo
Lucent Technologies
Bell Laboratories
Murray Hill, NJ 07974

The magnetic structure of this superlattice has previously been determined to be the basal-plane helical structure of bulk Dy with a coherence length greater than 4 bilayers. The helix progresses remarkably undisturbed through the conduction electrons of the non-magnetic yttrium, but with a turn-angle that is different than in the dysprosium. The coupling strength across the yttrium has been measured by applying a uniform external magnetic field. The coupling breaks down when the external field provides 0.2 meV per Dy atom in the basal-plane, while the equivalent zone-boundary magnetic fluctuation in bulk Dy is greater than 5 meV per Dy atom.

The inelastic neutron scattering measurements were performed at the NIST Center for Neutron Research on the cold-neutron spectrometer SPINS. A multi-component crystal was used to analyze the energy of the scattered neutrons in order to enhance the measured intensity while sacrificing wave-vector (Q) resolution. Measurements were performed at 75 K as a compromise between the size of the ordered magnetic moment and the thermal population of magnons. The magnons of interest are those propagating along the superlattice growth direction or the c-axis of the hcp rare-earth structure. Lower magnon energies produce higher thermal populations, but become contaminated with elastic background scattering,

so it is necessary to subtract scans taken at low temperatures where the magnons have become depopulated in order to remove this background. The resulting magnetic signal is shown in Figure 1 as a color-coded intensity map in Q-energy space. There is a clear ridge of intensity which moves to higher energies as Q moves away from the magnetic Bragg peak at 1.97 Å^{-1}. We have concentrated on the magnon branches that extend towards smaller Q since they move away from the intense magnetic and nuclear Bragg peaks that produce a large elastic background. This measured dispersion is compared with bulk Dy in Figure 2, which also shows the diffraction pattern along the growth direction (c-axis) of the superlattice. The bulk Dy dispersion is shown as lines originating from the magnetic Bragg peaks at Q = 1.97 Å^{-1} and Q = 2.06 Å^{-1}. The measured magnons are shown as bars centered on the measured peak positions and with lengths representing the full-width-at-half-maximum-intensity. The agreement with the bulk dispersion is quite good. There is no evidence in these data of the influence of the yttrium layers other than possibly the splitting of the dispersion into two branches because of the superlattice structure as shown by separate bars at both Q = 1.8 Å^{-1} and at Q = 1.75 Å^{-1}. The observed modes are not over-damped, but we cannot measure the damping under the current experimental conditions. Also, these data would have to be extended to smaller Q, in order to approach the interface thickness. We are currently designing additional focusing configurations so that the instrumental resolution will be better optimized for measurements of this dispersion surface.

REFERENCES

[1] B. Hillebrands and G. Güntherodt in *Ultrathin Magnetic Structures I + II*, edited by B. Heinrich and J. A. C. Bland (Springer Verlag, 1994).

[2] C. F. Majkrzak et al., Adv. in Phys. **40**, 99 (1991).

FIGURE 2. The dispersion along the growth direction (c-axis) measured for the [Dy$_{48}$Y$_{23}$]$_{350}$ superlattice is plotted against the energy scale on the left side. It is compared to the measured dispersion in bulk dysprosium (solid lines) expected to originate from each of the superlattice magnetic Bragg peaks. (Only the negative Q branches from the two low Q Bragg peaks are shown). On the right side the diffraction scan for this sample showing the superlattice peaks is displayed. This film is so large that the sample diffraction peaks are as strong as the substrate peak shown in blue on the right.

ANTIFERROMAGNETIC SPIN REORIENTATION IN EXCHANGE-BIASED Fe$_3$O$_4$/NiO SUPERLATTICES

The magnetic hysteresis loop of a ferromagnetic material can be displaced along the field axis as a result of magnetic exchange coupling to an antiferromagnet. This "exchange-biasing" phenomenon was discovered over 40 years ago in oxidized Co particles [1] and has been observed in a variety of thin films and multilayers. Artificial spin-valve structures with exchange-biased layers show great promise for applications as magnetoresistive sensors in read heads. Recent theories [2-4] make specific predictions about the origin of exchange biasing and the response of the antiferromagnetic layer.

High-angle neutron diffraction is an ideal probe as the antiferromagnet gives rise to distinct reflections of magnetic origin. We have performed neutron diffraction studies of exchange-biased [001] Fe$_3$O$_4$/NiO superlattices on the SPINS and BT-9 triple-axis spectrometers. These measurements confirm that the NiO layers retain their bulk antiferromagnetic structure in which ferromagnetic {111} planes alternate direction along each <111> axis. Our data show that exchange biasing is associated with domain walls that form and "freeze" within the antiferromagnetic NiO layer. Upon field cooling into the exchange-biased state, magnetic domains lock within the NiO layers and do not change with subsequent application of magnetic fields. In contrast, the antiferromagnetic domain sizes in unbiased samples prepared by cooling in zero field depend sensitively on the strength of the applied field.
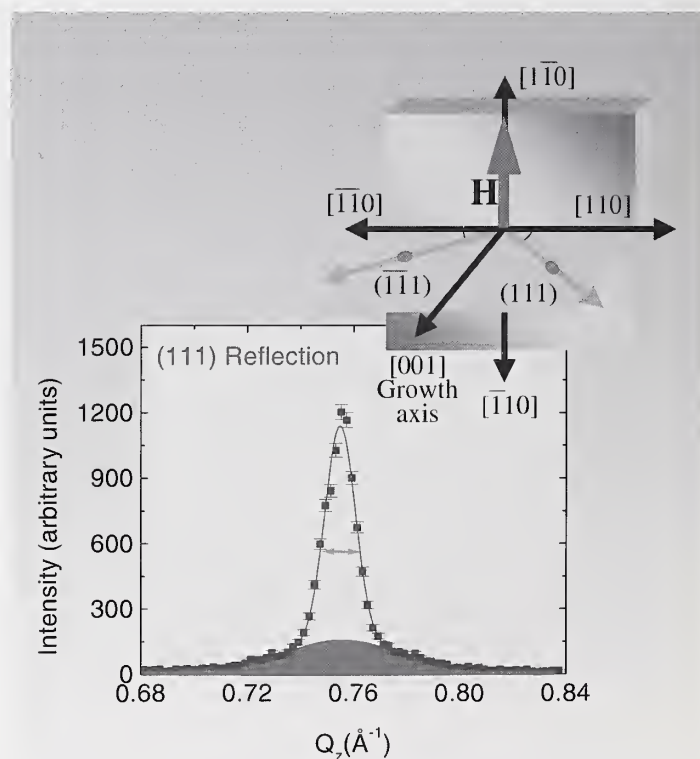
We focus here on a Fe$_3$O$_4$(10 nm)/NiO(20 nm) superlattice deposited using oxygen plasma-assisted molecular beam epitaxy. Measurements of the magnetic hysteresis loop show little evidence of exchange biasing after cooling in zero field. Strong exchange biasing is induced upon field cooling the superlattices from high temperatures. For our superlattice, the biasing field at 30 K is 0.043 T after field cooling from 550 K.

For the diffraction experiments the sample was oriented as shown in the inset of Figure 1. Vertical magnetic fields, H, were applied in the sample plane. In this configuration, the (1 1 1) and ($\bar{1}$ $\bar{1}$ 1) NiO antiferromagnetic reflections lie in the scattering plane. Using a horizontal-field magnet, the (1 $\bar{1}$ 1) and ($\bar{1}$ 1 1) reflections could be accessed by rotating the sample 90° about the growth

axis. Figure 1 shows a typical growth-axis (00l) scan through the (111) reflection for the superlattice. Structural stacking faults [5] at the NiO/Fe$_3$O$_4$ interfaces limit the coherence of the Fe$_3$O$_4$ structural and magnetic order to a single Fe$_3$O$_4$ layer. As a result, we can easily separate the broad Fe$_3$O$_4$ and narrow NiO contributions to the reflection and track the latter as a function of field.

The neutron scattering data reveal that the magnetic domain sizes in the antiferromagnetic NiO depend on the presence or absence of exchange biasing. Figure 2 shows the full-width-at-half-maximum (FWHM) for the (111) NiO peak scanned along the (00l) and (ll0) directions after cooling in a 6 T field (i.e., exchange-biased state) and cooling in zero field (i.e., unbiased state). After field cooling, the FWHM of the NiO reflection scanned along the (00l) growth direction shows no dependence on field.

The antiferromagnetic domain size along the growth direction, determined from the inverse of the FWHM, remains constant

FIGURE 1. Growth-axis (00l) scan through the (111) reflection for the Fe$_3$O$_4$(10 nm)/NiO(20 nm) superlattice after cooling to 78 K in a 6 T field parallel to [$\bar{1}$10]. The broad Fe$_3$O$_4$ peak is shown in red, and the remaining scattering is from the NiO. The green arrow marks the FWHM of the NiO peak. The inset shows the scattering diagram.

J. A. Borchers and R. W. Erwin
NIST Center for Neutron Research
National Institute of Standards and Technology
Gaithersburg, MD 20899-8562

Y. Ijiri
Department of Physics, Oberlin College
Oberlin, OH 44074

S.-H. Lee
NIST Center for Neutron Research
National Institute of Standards and Technology
Gaithersburg, MD 20899-8562
and
University of Maryland
College Park, MD 20742

D. M. Lind and P. G. Ivanov
Department of Physics, Florida State University
Tallahassee, FL 32306

Aron Qasba
Department of Physics
Massachusetts Institute of Technology
Cambridge, MA 02139

near 750 Å after field cooling. This contrasts with the pronounced field-dependence of the FWHM observed after cooling in zero field (Figure 2). In this state, the FWHM is smallest near zero field, but approaches the constant field-cooled value when the magnitude of the field is greater than 2 T. The corresponding domain size varies from approximately 1200 Å in zero field to 800 Å in high fields. Growth-plane (ll0) scans through the NiO reflection show a similar difference between the field dependence of the FWHM after cooling in zero field and cooling in a 6 T field (Figure 2).

Upon field cooling, domain walls both parallel and perpendicular to the growth direction lock into the antiferromagnetic layer, presumably due to the exchange coupling between the NiO antiferromagnetic moments and the Fe_3O_4 moments that are aligned parallel to the cooling field. After cooling in zero field, the domains are larger, but reversibly decrease in size in high fields (Figure 2) as the magnetic frustration increases. Consistent with several theoretical predictions [2,3] we believe that exchange biasing may originate from magnetic frustration that leads to "frozen" domain walls in the field-cooled state.

We also observe that the magnitude of the ordered NiO moments in all four of the {111} domains in the Fe_3O_4/NiO super-lattices depends upon applied field. After cooling in a large vertical field, the intensity of the antiferromagnetic (111) NiO reflection reversibly decreases as the field is increased. (The behavior is qualitatively similar after cooling in zero field.) Analogous field-cooled measurements of the ($1\bar{1}1$) NiO peak were performed in a horizontal field and surprisingly show a comparable intensity decrease. Some of the NiO moments thus seem to disappear out of all four {111} domains. We speculate that these NiO spins may become disordered as a result of the high internal fields. Simultaneously, some of the NiO moments reorient perpendicular to the Fe_3O_4 magnetization direction in high fields [6]. While this "spin-flop" response is favored by some theoretical models [4], it does not appear to be directly responsible for the exchange biasing for these samples.

Future studies will focus on the characteristics and origin of the "spin-flop" response of the NiO spin structure to large magnetic fields. In addition, we will further explore the differences between the antiferromagnetic domains for the exchange-biased and unbiased conditions.

REFERENCES:

[1] W. H. Meiklejohn and C. P. Bean, Phys. Rev. **102**, 1413 (1956); **105**, 904 (1957).

[2] A. P. Malozemoff, J. Appl. Phys. **63**, 3874 (1988).

[3] T. C. Schulthess and W. H. Butler, Phys. Rev. Lett. **81**, 4516 (1998).

[4] N. C. Koon, Phys. Rev. Lett. **78**, 4865 (1997).

[5] J. A. Borchers, R. W. Erwin, S. D. Berry, D. M. Lind, J. F. Ankner, E. Lochner, K. A. Shaw and D. Hilton, Phys. Rev. **B 51**, 8276 (1995).

[6] J. A. Borchers, Y. Ijiri, D. M. Lind, P. G. Ivanov, R. W. Erwin, S.-H. Lee and C. F. Majkrzak, J. Appl. Phys. **85**, 5883 (1999).
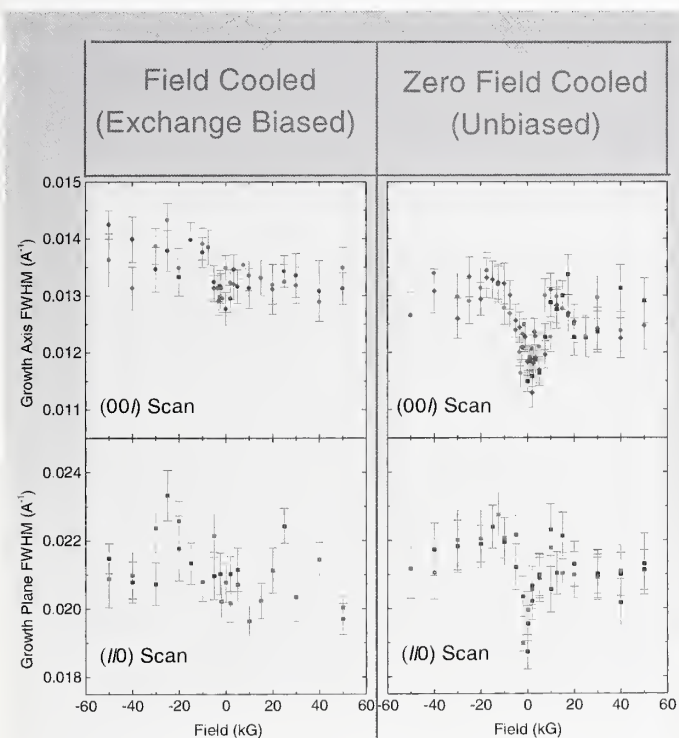
FIGURE 2. Full-width-at-half-maximum (FWHM) of the (111) NiO reflection as a function of field at 78 K after cooling in a 6 T field and after cooling in zero field. The top plots show the FWHM of the peak along the (00l) direction. The bottom plots show the FWHM from (ll0) scans. The black, blue and red data are from each field cycle.

# SPIN DENSITY WAVE ORDER IN THE SUPERCONDUCTING STATE OF La$_2$CuO$_{4+y}$

In the high temperature (high-T$_c$) superconductors, the multiple roles played by the electrons continue to defy theoretical understanding. It appears that all high-T$_c$ superconductors are based on structures with CuO$_2$ planes, in which the electrons on neighboring copper ions are strongly coupled magnetically. In systems based on La$_2$CuO$_4$, antiferromagnetism is a dominant feature of the phase diagram at low doping levels, and conventional itinerant-electron behavior dominates in the high doping regime. Intermediate doping levels are described by neither, but this is where the superconducting properties are optimal. In our experiments, we focus on the evolution of magnetic properties from the insulating antiferromagnet to the superconductor.

It is becoming increasingly apparent that incommensurate spin structures are universal to the high-T$_c$ superconductors. Especially noteworthy is the observation of static incommensurate magnetic ordering coexisting with superconductivity in La$_{1.6-x}$Nd$_{0.4}$Sr$_x$CuO$_4$ and recently in La$_{2-x}$Sr$_x$CuO$_4$ [1, 2]. Further experiments are needed to understand the coexistence of the incommensurate spin density waves (SDW) and superconductivity, the details of the spin structure, and the influence of pinning potentials.

A crystal of La$_2$CuO$_{4+y}$ with a superconducting transition at ~ 42K was produced by doping pure La$_2$CuO$_4$ electrochemically with a large quantity of excess oxygen (y $\approx$ 0.12). The superconducting shielding signal measured after cooling in zero field is shown in Figure 1A. The transition is very sharp with an onset T$_c$ ~ 42 K. Our initial characterization suggests that the crystal is a bulk superconductor with a hole concentration similar in density and homogeneity to that of La$_{2-x}$Sr$_x$CuO$_4$ crystals with x $\approx$ 0.15.

At temperatures below the superconducting T$_c$, we observe elastic magnetic scattering at a quartet of incommensurate positions centered around (100), which is the Bragg position for the antiferromagnetism in the undoped insulator. Surprisingly, we find that the incommensurate wavevectors are not precisely along the Cu-O-Cu bond direction, but are rotated by about 3°.

In Figure 2A we show elastic scans along the in-plane H direction through an incommensurate position for various temperatures using 5 meV neutrons. Below 42 K, the observed peaks are extremely sharp and are resolution-limited, while above 42 K
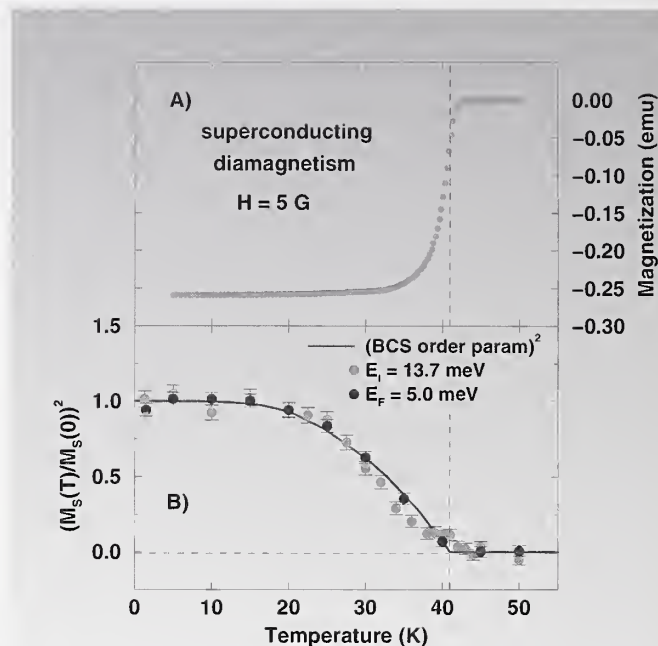
FIGURE 1. A) Magnetic susceptibility measured after cooling in zero field. B) Peak intensity of the incommensurate elastic scattering as a function of temperature. The measurement was performed with two different neutron energies of 13.7 meV and 5 meV. The solid line denotes the BCS superconducting order parameter squared, with a T$_c$ of ~ 41K.

the peaks disappear. The solid lines in the figure are Gaussians convolved with the instrumental resolution which indicate that the in-plane static magnetic order is correlated over distances larger than 400 Å. From this, we conclude that static long-range magnetic order exists in the superconducting state of La$_2$CuO$_{4+y}$. Also, the SDW order is not specific to a tetragonal crystal structure as previously believed since this crystal is orthorhombic; it is a more general phenomenon.

We then investigated how the static spin arrangement is correlated between CuO$_2$ planes. The L-dependence of the incommensurate scattering is shown in Figure 2B. The intensity modulation of both the (10L)- and (01L)-centered scattering is reminiscent of the spin structure of the undoped parent compound La$_2$CuO$_4$. The solid lines in both panels represent fits to Gaussian lineshapes convolved with the instrumental resolution, assuming a model for the stacking arrangement and spin direction identical to that of

Y. S. Lee, R. J. Birgeneau, and M. A. Kastner
Department of Physics
Massachusetts Institute of Technology
Cambridge, MA 02139

Y. Endoh, S. Wakimoto, and K. Yamada
Department of Physics
Tohoku University
Aramaki Aoba
Sendai 980-77, Japan

R. W. Erwin and S.-H. Lee
NIST Center for Neutron Research
National Institute of Standards and Technology
Gaithersburg, MD 20899-8562

G. Shirane
Department of Physics
Brookhaven National Laboratory
Upton, NY 11973

pure La_2CuO_4. Here, the only free parameters are the width and a single overall intensity scale factor. The agreement is clearly satisfactory, with the fit indicating that the spins are correlated across ~3 CuO_2 planes. We conclude that the stacking arrangement of the magnetically ordered planes in our La_2CuO_{4+y} sample follows that of undoped insulating La_2CuO_4, even though the magnetic order in the CuO_2 planes is incommensurate. This is the first direct evidence that the magnetism of the doped superconductor mimics the magnetism in the undoped insulator in such a specific way.

We show in Figure 1B the peak intensity of the elastic signal as a function of temperature measured using both 13.7 meV and 5 meV neutrons. The fact that one obtains identical results for the temperature dependences of the intensities with these two different neutron energies and, concomitantly, energy resolutions indicates that the scattering is truly elastic. The intensity of the elastic scattering turns on at approximately the same transition temperature as superconductivity. Noting that the intensity of the magnetic scattering is proportional to the square of the magnetic order parameter, we plot the square of the BCS order parameter curve over the data using a T_c of ~41K. The agreement indicates that the magnetism exhibits mean field behavior just like conventional superconductivity. This is very surprising given the two dimensionality of the ordered magnetism. The size of the ordered moment is 0.15 μ_B, which is 25% of the ordered moment in pure La_2CuO_4. Our results argue against an itinerant electron description of the incommensurate magnetism since it is difficult to see how a delocalized model can support interplanar spin correlations and choose the same preferred spin direction as in insulating La_2CuO_4. It appears that the spins are localized and ordered in this high temperature superconductor.

REFERENCES

[1] J. M. Tranquada et al., Phys. Rev. Lett. **78**, 338 (1997).
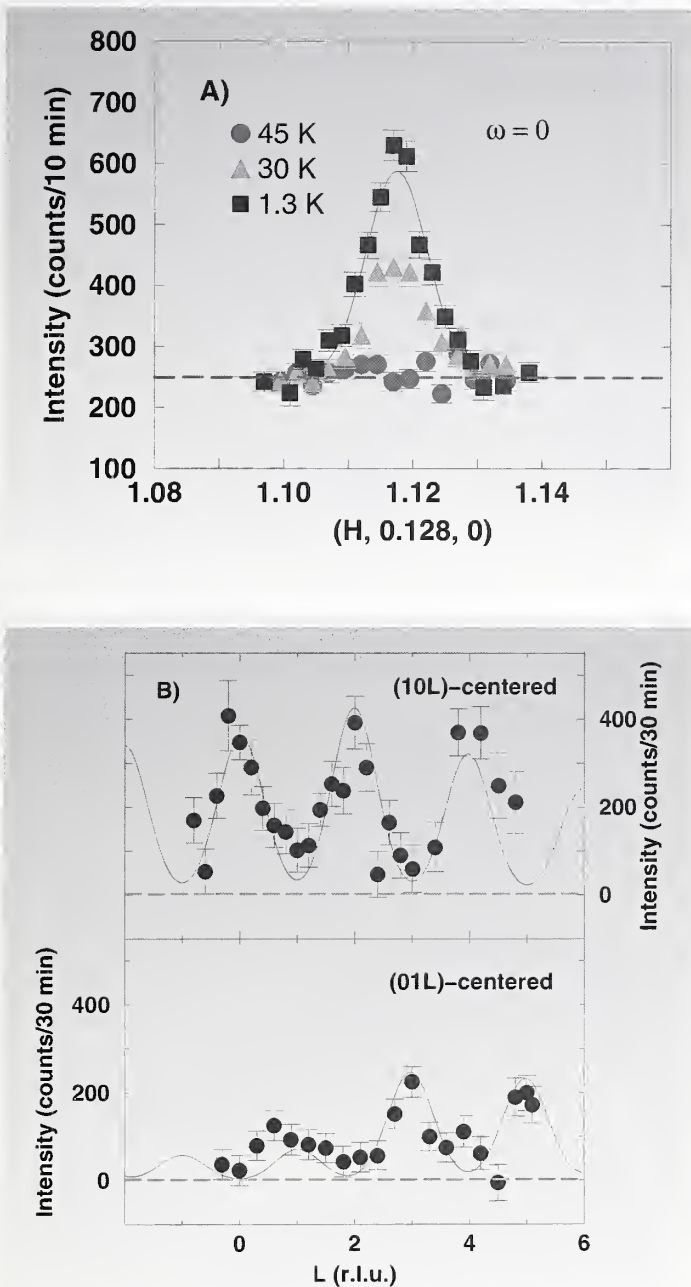[2] H. Kimura et al., Phys. Rev. **B59**, 6517 (1999).

FIGURE 2 A) Scans along the in-plane H direction over one of the incommensurate SDW peaks for various temperatures. B) The top panel shows the L-dependence of the SDW scattering centered about the (10L) position. The bottom panel shows scattering centered about the (01L) position.

LOCAL SPIN RESONANCE AND SPIN-PEIERLS-LIKE PHASE TRANSITION IN ZnCr₂O₄

Most magnets order when the thermal energy drops below a microscopic energy scale for magnetic interactions. The topology of certain lattices can, however, reduce the energy gain associated with long range ordering thus favoring more entropic phases. Figure 1 shows one such lattice, the tetravalent site in the pyrochlore structure that forms a network of corner-sharing tetrahedra. As shown in the figure, antiferromagnetically (AFM) interacting spins on the lattice cannot satisfy all their exchange interactions simultaneously. This phenomenon, called geometrical frustration, can lead to macroscopic classical ground state degeneracy and offers the possibility of qualitatively new states of matter. Theoretical studies have in fact shown that spins with nearest neighbor antiferromagnetic Heisenberg interactions on the pyrochlore lattice do not have a long range ordered phase at all.

Pyrochlore magnets studied experimentally so far exhibit a continuous phase transition at a finite temperature, T_f, into a glassy phase with static short range correlations [1]. Spinel antiferromagnets, AB_2O_4, in which the octahedral B site forms the same magnetic lattice as in the pyrochlore structure, however behave quite differently. For instance, $ZnCr_2O_4$ exhibits a first order phase transition to a long- range ordered Néel phase at $T_c = 12.5$ K, much less than the Curie-Weiss temperature $|\theta_{CW}| = 393$K. We have explored this ordered phase and the corresponding phase transition through inelastic neutron scattering [2].

Figure 2 provides an overview of our neutron scattering results as a color image of $\tilde{I}(Q, \omega)$ at three temperatures. For $T > T_c$, Figures 2 (a) and (b) show a constant-Q ridge centered at $Q \sim 1.5$ Å^{-1} and extending beyond 10 meV. The ridge indicates quantum critical fluctuations of small AFM clusters, most likely antiferromagnetically correlated tetrahedra, and closely resembles those obtained in similar experiments on other frustrated AFM. For $T < T_c$, however, the low energy spectral weight concentrates into a sharp constant-energy mode centered at $\hbar\omega = 4.5$ meV $\approx |J|$ $\gg k_B T_c$. The wave vector dependence of this resonance intensity reveals that it is an excitation among antiferromagnetically correlated nearest neighbor spins. Though they can not be seen in Figure 2(c), there are in fact magnetic Bragg peaks in the elastic scattering channel (see Figure 3(b)), which provide evidence for long-range order for $T < T_c$. It is unusual that excitations of such localized character exist in a long-range ordered phase. The reso-
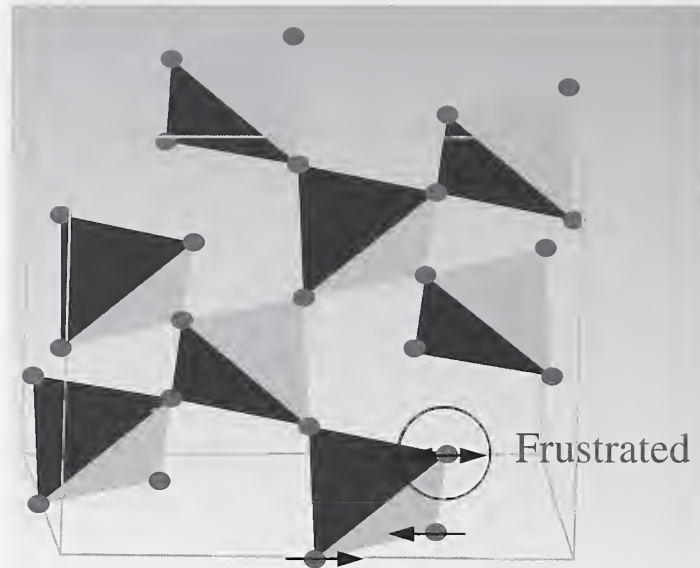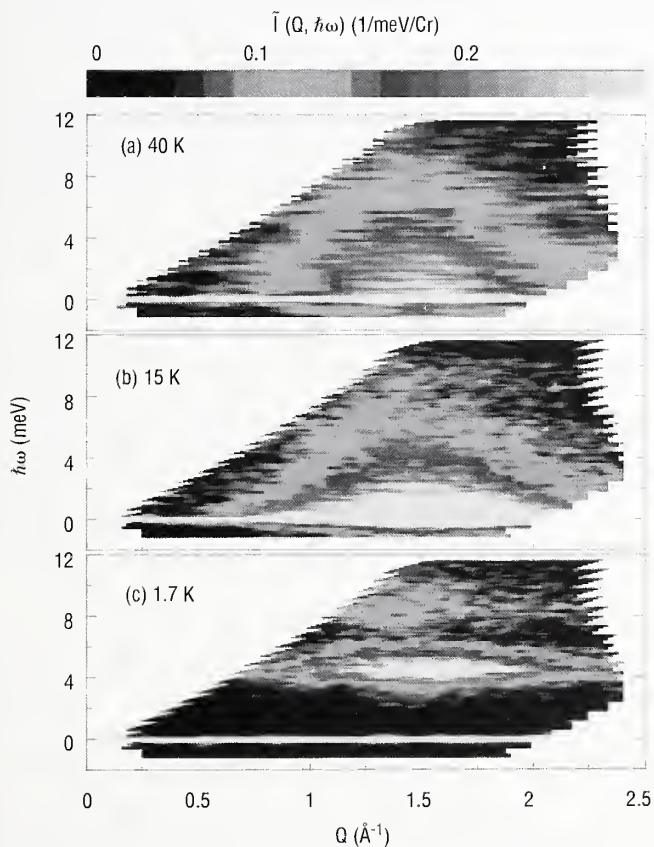

FIGURE 1: A network of corner-sharing tetrahedra. When two spins in a tetrahedron are aligned antiparallel to each other then the third spin can not satisfy its antiferromagnetic interaction with the other two spins simultaneously.

nance indicates the presence of weakly interacting spin clusters within the ordered phase, which is a key feature of geometrically frustrated magnets.
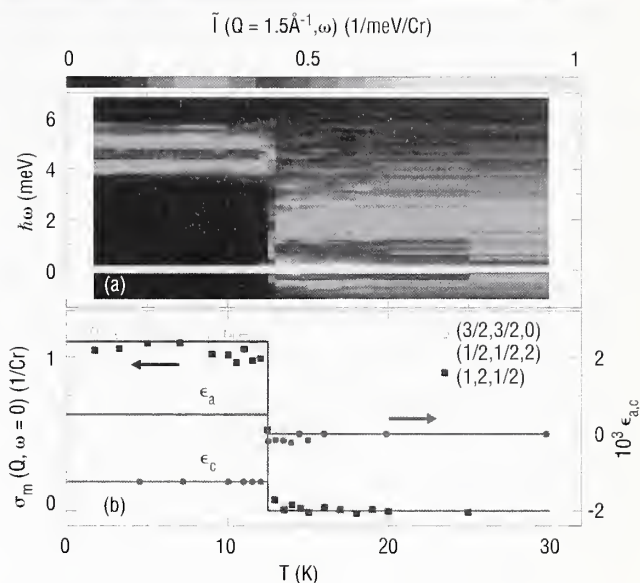
Theoretical work indicates that magnetic order cannot develop in an isotropic spin system with nearest neighbor antiferromagnetic Heisenberg interactions on the pyrochlore lattice. It is natural to ask what deviation from this model causes order to develop in $ZnCr_2O_4$? To answer the question we probed the temperature dependence of static and dynamic features of this system in the vicinity of the phase transition. Figure 3 shows that long range antiferromagnetic order (blue squares in frame (b)) and the local spin resonance (frame (a)) appear simultaneously in a spectacular first order transition. It also shows that magnetic ordering is accompanied by a cubic to tetragonal lattice distortion (red circles in frame (b)). The lattice distortion plays a crucial role in relieving frustration and allowing long-range order to develop. It is well known that exchange interaction between Cr^{3+} ions whose oxygen coordination octahedra share an edge are strongly dependent on the oxygen bond angles and hence the metal ion spacing. As a consequence the tetragonal strain $\epsilon_a > 0$ and $\epsilon_c < 0$ yields weaker AFM interactions between spins occupying the same basal plane and stronger AFM interactions between all other spin pairs. This reduces

S.-H. Lee
NIST Center for Neutron Research
National Institute of Standards and Technology
Gaithersburg, MD 20899-8562
and
University of Maryland
College Park, MD 20742

C. Broholm, NCNR and
Department of Physics and Astronomy
The Johns Hopkins University
Baltimore, MD 21218

T.H. Kim
Francis Bitter Magnet Laboratory
Massachusetts Institute of Technology
Cambridge, MA 02139

S. W. Cheong
Department of Physics and Astronomy
Rutgers University
Piscataway, NJ 08854
and
Bell Laboratories, Lucent Technologies
Murray Hill, NJ 07974

W. Ratcliff II
Department of Physics and Astronomy
Rutgers University
Piscataway, NJ 08854

the energy of a particular long range ordered spin configuration with respect to the low energy degenerate manifold thus allowing the system to achieve long range order. The overall picture that emerges is that of two distinct phases in competition: a cubic cooperative paramagnet and a tetragonal long-range ordered antiferromagnet. Though the spin Hamiltonian has a lower expectation value in the latter phase, the lattice energy is greater and the entropy is lower in the tetragonal phase. The phase transition occurs when the free energy of the tetragonal low entropy phase drops below that of the disordered cubic paramagnet.

There are strong analogies between the phase transition in $ZnCr_2O_4$ and the spin-Peierls (SP) transition. In both cases the high T phase is nearly quantum critical and can lower its energy through a lattice distortion. In both cases the transition occurs from

FIGURE 3: (a) Image of inelastic neutron scattering for Q = 1.5 Å⁻¹. (b) T-dependence of magnetic Bragg scattering from a powder, σ_m (blue squares), and of lattice strains measured n a single crystal (red circles).

a strongly correlated paramagnet: $T_c \ll \theta_{CW}$, and in both cases low energy spectral weight is moved into a finite energy peak.

There are also important differences between the two transitions. The low T phases are qualitatively different, the transition in $ZnCr_2O_4$ is a first order one, while the SP transition is second order, and the change in entropy at T_c plays an important role in $ZnCr_2O_4$, but not in a SP transition. The central idea that finite lattice rigidity can preclude a spin liquid at T=0 however does carry over and should be relevant for any frustrated magnet when other symmetry breaking interactions are sufficiently weak.

REFERENCES

[1] J. S. Gardner, B. Gaulin, S.-H. Lee, C. Broholm, N. P. Raju, J. E. Greedan, Phys. Rev. Lett. **83**, 211 (1999).

[2] S.-H. Lee, C. Broholm, T. H. Kim, W. Ratcliff II and S. W. Cheong, Phys. Rev. Lett., in press.

FIGURE 2: Contour maps of the magnetic neutron scattering intensity at temperatures spanning the phase transition at T_c = 12.5(5) K. The data were taken by utilizing a flat analyzer and two-dimensional position-sensitive detector at the SPINS spectrometer.
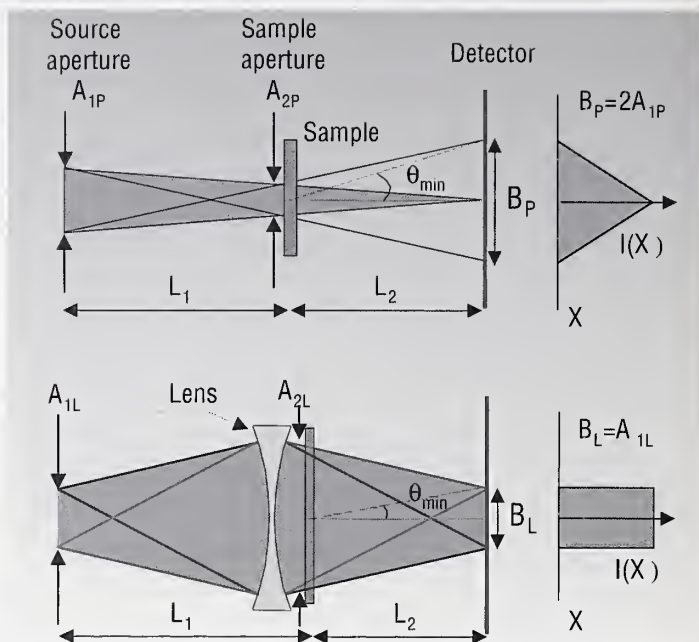
COMPOUND REFRACTIVE OPTICS IMPROVE RESOLUTION OF 30-METER SANS INSTRUMENT

In the most favorable cases, cold neutrons can be deflected through an angle of a degree or two by grazing incidence reflection, but by only an arc second or two by refraction. Hence grazing incidence reflection optics has long been considered the most promising means for focusing neutrons for applications such as small-angle neutron scattering (SANS). Numerous attempts over more than 30 years to produce highly reflective surfaces for neutrons have been vitiated, however, by SANS from the mirror surfaces themselves, which blurs the focus. The best mirrors produced thus far are only marginally better for SANS than pinhole collimation, i.e., circular apertures separated by long distances.

Scientists at Bell Laboratories recently took a fresh look at this problem and proposed that multiple refraction from relatively high index, low absorbing material could be superior to reflection optics or conventional pinhole collimation for SANS. Initial measurements [1] at Risø National Laboratory, Denmark, demonstrated the proposed focusing effect, but did not make quantitative comparisons with reflection optics or pinhole collimation for application in SANS instruments. Measurements made recently at the NCNR in collaboration with the Bell Labs scientists [2] have addressed these issues and have demonstrated and quantified the significant
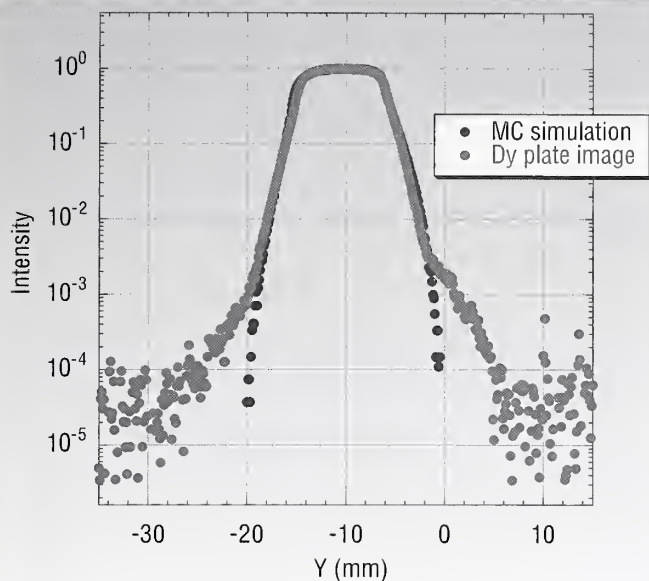

FIGURE 2 Upper panel, conventional SANS pinhole collimation. The source and sample apertures, A_{1p} and A_{2p}, respectively, determine the shape and extent of the beam profile, I(x), at the detector plane. Lower panel, focusing lens geometry. Ideally, the source aperture, A_{1L}, alone determines the beam profile.

improvement in resolution that can be achieved with compound refractive optics.

Our tests were made with the same set of cylindrical biconcave MgF_2 (magnesium fluoride) lenses used in the Risø study. Up to 30 lenses were placed end-to-end near the sample position of the 30-m SANS instrument to focus neutrons, emanating from a circular source aperture 15 m upstream, onto the plane of instrument's two-dimensional detector. Figure 1 shows an array of 28 lenses for focusing 8.44 Å neutrons at a distance of 15 m from the sample, next to a set of 6 lenses for focusing 18 Å neutrons at the same distance.

For this geometry, as depicted in Figure 2, the lenses ideally produce a 1:1 image of the source aperture at the detector independent of the size of the sample. Since the scattering signal is proportional to sample size, the lens system can, in principle, be used to improve resolution more efficiently, by reducing the size of the source aperture, than is possible with pinhole collimation where both the source aperture and sample size must be reduced proportionally to improve angular resolution. Aberrations and small-angle scattering by the lenses could, however, blur the image to

FIGURE 1. Now installed in the pre-sample flight path of the NG-7 30-meter SANS instrument are two sets of MgF_2 biconcave lenses that can be inserted into the beam under computer control. The 28-lens array in the foreground focuses 8.44 Å neutrons at a distance of 15 m from the lenses, and the 6-lens set focuses 18 Å neutrons at the same distance. Each lens is 25 mm in diameter, has a radius of curvature of 25 mm, and is 1mm thick in the center.

S.-M. Choi, J. G. Barker and C. J. Glinka
NIST Center for Neutron Research
National Institute of Standards and Technology
Gaithersburg, MD 20899-8562

Y. T. Cheng
NeuTek
Darnestown, MD 20878

P. L. Gammel
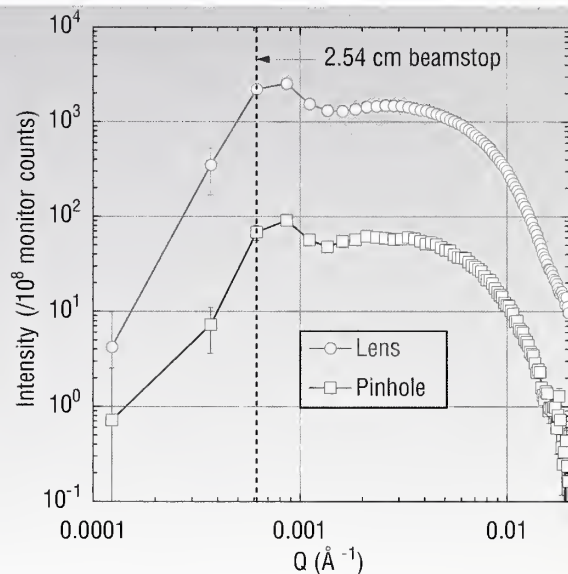Bell Laboratories, Lucent Technologies
Murray Hill, NJ 07974

FIGURE 3. Red dots are measured points along the vertical profile of the image formed by the 28 lens array shown in Fig. 1 of a 9.5 mm diameter source of neutrons 15 m upstream from the lenses. The blue dots are a Monte Carlo calculation of the profile that includes the effects of spherical and chromatic aberrations as well as the broadening caused by gravity. The shoulder in the measured profile at Y = 0 is due to a residual fast neutron component in the beam.

FIGURE 4. Small-angle scattering from voids in a single crystal (2.5 cm in diameter and 1 cm thick) of fast-neutron-irradiated aluminum. The measurements were made under equivalent resolution conditions (i.e. nearly identical beam spot size at the detector) using both simple pinhole collimation and the 28 biconcave lens array shown in Figure 1. The integrated gain in intensity due to the lenses is approximately 26.

such a degree that any advantage over pinhole collimation, which does produce a sharply defined beam spot at the detector, would be lost.

To accurately measure the intensity profile produced by the lenses, a dysprosium foil was positioned at the focal plane and exposed to the focused beam for approximately two hours. The activated foil was then placed in contact with a high resolution image plate which stored the image produced by the emitted gamma rays with a spatial resolution of better than 0.1 mm. A typical profile obtained from reading out the image plate is shown in Figure 3. Also plotted in the figure is a Monte Carlo calculation of the profile that includes the effects of spherical and chromatic aberrations as well as the broadening caused by gravity. The measured profile agrees with the simulation down to intensity levels of 10^{-3} of the peak intensity and has an overall signal-to-background ratio in the wings approaching 10^5, which is highly satisfactory for most SANS measurements.

The practical benefit provided by the lenses is demonstrated by the SANS data from voids in a single crystal (2.5 cm in diameter

and 1 cm thick) of fast-neutron-irradiated aluminum shown in Figure 4. The measurements were made under equivalent resolution conditions (i.e. nearly identical beam spot size at the detector) using both simple pinhole collimation and the 28 biconcave lens array shown in Figure 1. The first data point unaffected by the beam stop in both data sets occurs at $Q \approx 0.001 \, \text{Å}^{-1}$, but the scattered intensity per unit area is more than 10 times higher by using the lenses to illuminate a much larger area of the sample.

The focusing lenses shown in Figure 1 are now installed for routine use in the NCNR's 30-meter SANS instrument on guide NG-7. Further testing is planned to understand, and hopefully eliminate, the sources of parasitic scattering that contribute to the tails of the beam profile seen in Figure 3, prior to installing a lens system in the NIST/NSF 30-meter SANS instrument on guide NG-3.

REFERENCES

[1] M. R. Eskildsen, P. L. Gammel, E. D. Isaacs, C. Detlefs, K. Mortensen, D. J. Bishop, Nature **391**, 563-566 (1998).

POLYMER BRUSH
RESPONSE TO SOLVENT FLOW

The presence of polymer chains grafted or adsorbed onto a surface can dramatically alter the forces that affect interactions between surfaces. The equilibrium properties of such polymer brush systems have been studied for the past two decades, yielding general agreement between theory and experiment. Conversely, the non-equilibrium properties of polymer brushes are still under intense theoretical and experimental investigation. Of particular interest is the response of a brush to the frictional forces imposed by solvent flow. The behavior of polymer brushes subjected to flow has important technological implications for the rheology of colloidal dispersions stabilized by polymer layers, for the lubrication properties of polymer coated interfaces, for biocompatibility of medical implant devices, and for permeation flow through polymer-containing porous media [1].

The height of a polymer brush is determined by the equilibrium conformation of the tethered chains, which depends on both the grafting density and quality of solvent. The basic physics governing the static behavior of a polymer brush result from a competition between two opposing tendencies: 1) elastic contraction, as the chains attempts to maximize their entropy by adopting random walk configurations, and 2) monomer-monomer interactions, such as polymer-polymer repulsions, and polymer-solvent wetting [2, 3].

Polymer chain stretching in densely grafted brushes has been studied by many different techniques including surface forces apparatus [4], neutron reflectivity [5], and small angle neutron scattering (SANS) [6]. In general, there is good agreement with results from experiment, simulations and analytical calculations [3].

Oscillatory shear measurements performed with a surface forces apparatus suggest that the normal forces between a pair of brush surfaces are altered when sheared. However, these measurements do not give the actual brush profile either with or without shear. Effective hydrodynamic thickness measurements of polymer brushes under shear indicate a thickening of the brush; whereas neutron reflectivity experiments on adsorbed PS-PEO block copolymer brushes on a silica surface show no effect of shear on the brush density profile in good solvent, and a slight increase in poor solvent. These earlier reflectivity measurements were limited to shear rates of ~ 10,000 s^{-1} [7] since the adsorbed PS-PEO block copolymer

FIGURE 1. Schematic illustrating the effect of shear on grafted brushes predicted by Miao *et al.* [8] Such an effect would be consistent with the present data.
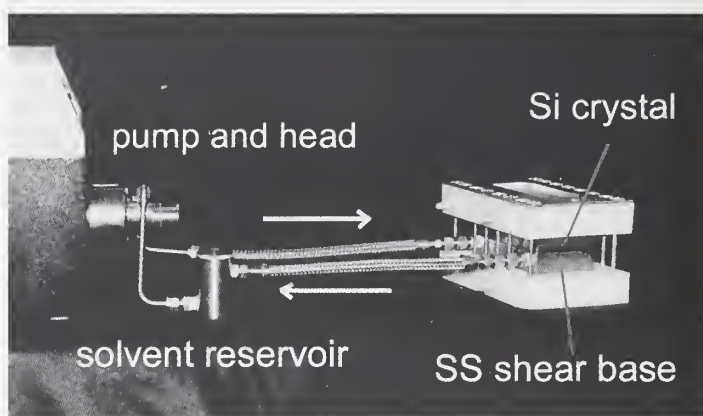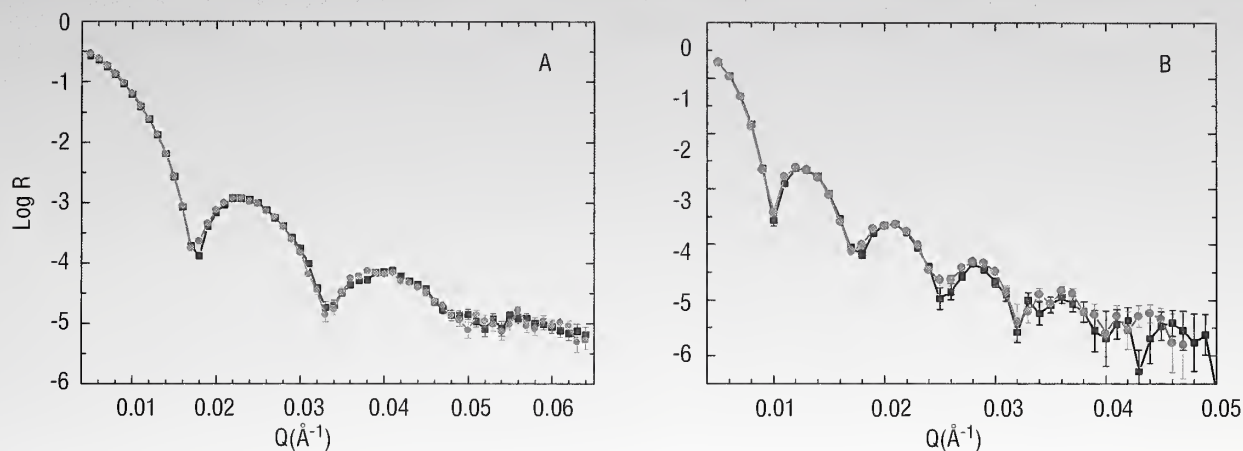

FIGURE 2: Shear cell. Arrows denote solvent flow direction. The polystyrene brush is grafted onto the Si crystal.

brushes have a tendency to come off the surface at higher shear rates.

Predictions from theoretical calculations of brush profiles under shear span the gamut of possibilities, ranging from brush thickening to brush compression, including no effect of shear flow on the density profile [3]. Miao *et al* [8]. predict that the response of a brush to the solvent shear flow is displayed as chain tilting toward and chain stretching along the direction of flow. However, the overall conformational properties such as brush thickness remain essentially unaffected (Figure 1).

We have performed neutron reflectivity measurements on a chemically grafted polymer in both good and poor solvents at shear rates over an order of magnitude greater than previously reported. Our neutron reflectivity experiments measure the segment density profile of the polymer brushes under shear in an experimental cell similar to the one used by Baker *et al*. [9], (Figure 2). We use deuterated polystyrene (d-PS), 83 kg/mol, with a trichloro-silane end group to bind the d-PS brush chemically onto a single crystal Si surface [5]. We used a good solvent, toluene, and a poor

Robert Ivkov, Paul Butler, and Sushil K. Satija
NIST Center for Neutron Research
National Institute of Standards and Technology
Gaithersburg, MD 20899-8562

L.J. Fetters
Exxon
Annandale, NJ 08801

FIGURE 3: Representative shear data for deuterated polystyrene brush under shear in cyclohexane (A), and toluene (B). In both cases, black circles represent shear of 0 s⁻¹, whereas red squares represent data taken at 30,000 s⁻¹.

solvent, cyclohexane, as the solvent media. The dry brush height was measured by x-ray reflectivity to be 17.5 nm. Without shear the brush extends to 31 nm in cyclohexane and 75 nm in toluene. We measured the brush profile at several shear rates, up to 130,000 s^{-1}, yet we see no effect of shear on the brush density profiles in either solvent (Figure 3). No desorption of the polymer brush was ever observed. In fact, the neutron reflectivity profiles at 0 s^{-1} and 130,000 s^{-1} look identical, indicating less than a 2-3% change in the brush density profile.

We have also been able to establish that the slight shear induced swelling reported by Baker *et al.* [7] for a poor solvent (cyclohexane), was probably due to frictional heating of the solvent. In high shear fields, heat generated from friction between the solvent and interior surfaces of the apparatus does not readily dissipate, causing a ∼ 2-3 °C rise in the temperature of the shear cell. We were able to demonstrate that the brush height in cyclohexane is unaffected by shear when the cell temperature is carefully controlled. An elevated cyclohexane temperature swells the brush as the solvent quality improves. Naturally, these effects were not observed in toluene.

Thus, our neutron reflectivity data represent the first comprehensive measurements of shear effects on the density profile of a grafted polymer brush into regimes that are predicted by some to

display an effect. We cannot, at this time determine if the brush responds as predicted by Miao *et al.* [8], or if there is insufficient solvent penetration into the brush to exert enough force on the chains to induce conformational changes. Future measurements will distinguish between these cases.

REFERENCES

[1] J. L. Harden and M. E. Cates, J. Phys. II France **5**, 1093 (1995).

[2] P.-G. de Gennes, Macromolecules **13**, 1069 (1980).

[3] S. Grest, Adv. Polym. Sci., in press.

[4] G. Hadziannou, S. Patel, S. Granick, and M. Tirrell, J. Am. Chem. Soc. **108**, 2869 (1986).

[5] A. Karim, S. K. Satija, J. F. Douglas, J. F. Ankner, and L. J. Fetters, Phys. Rev. Lett. **73**, 3407 (1994).

[6] P. Auroy, Y. Mir, and L. Auvray, Phys. Rev. Lett. **69**, 93 (1992).

[7] S. M. Baker, A. Callahan, G. Smith, C. Toprakcioglu, and A. Vradis, Physica B **241-243**, 1041 (1997).

[8] M. L. Miao, H. Guo, M. J. Zuckermann, Macromolecules **29**, 2289 (1996).

[9] S. M. Baker, G. S. Smith, R. Pynn, P. Butler, J. Hayter, W. Hamilton, and L. Magid, Rev. Sci. Instrum. **65**, 412 (1994).

MACROMOLECULAR CONFORMATION IN ULTRATHIN POLYMER FILMS

Since thin polymeric films are ubiquitous in technological applications such as paints, lubricants, and adhesives, a critical characterization of their thermophysical properties is essential. A central premise in the development of theories for predicting the properties of polymer melts in confined geometries is that chains maintain their unperturbed Gaussian conformation, which they adopt in the bulk, in the direction parallel to the surfaces under all conditions [1,2]. These assumptions, which form the foundations of the important field of polymer thin films, have been questioned on the basis of indirect experimental findings [3,4]. We have utilized the power of small angle neutron scattering, especially the high neutron flux at NCNR, to unequivocally characterize the chain structure and conformation in ultrathin polymer films, and thus have resolved this important fundamental question.

The experimental measurements of chain conformations and system thermodynamics in thin films have remained elusive due to the small amounts of sample material involved. To illustrate this point, a thin film of 10 nm incurs a decrease in signal by $\approx 1 \times 10^4$ from a typical bulk polymer sample. In this case, the noise is comparable to the signal, complicating the experiments. Prior to upgrades of the cold neutron source at the NCNR, data collection times were prohibitive. Improvements in sample preparation, which are discussed in detail elsewhere [5,6], have allowed us to measure molecular size and conformation of an isotopically labeled blend of polystyrene (25 wt% d-PS/75 wt% h-PS) in films as thin as 12 nm. Two blends of nominally matched molecular weight, Mn, of 270,000 and 650,000, respectively, were utilized. These were labeled 270k and 650k, respectively. Solutions of the blends were spin cast on silicon substrates (Semiconductor Processing) and annealed at 120°C ($T_g \approx 105°C$).

The scattered intensity for a 15 nm thick film of the 270k blend is compared to an analogous bulk sample in Figure 1. It is clear from the figure that, on a unit volume basis, the thin film scattering is higher than that of the bulk. We postulated that this difference is attributable to the scattering from the imperfections at both the air and the substrate interfaces, which is driven by the relatively high neutron contrast at these boundaries. To evaluate this component, films of pure d-PS were spin cast under identical conditions and their scattering measured.

The pure d-PS film data were fit with a simple Debye-Bueche form factor to obtain parameters for a roughness term. The blend film data were then fit by scaling this roughness term and adding a component obtained from the Random Phase Approximation (RPA) model. In the fitting, two RPA model parameters were also varied: the blend chain radius of gyration (R_g) and the Flory interaction parameter. The combined model is illustrated as the solid line in Figure 1 along with the roughness term (long dashed line) and RPA term (short dashed line). The fact that the RPA term is very close to the data for the bulk blend illustrates that the film and bulk
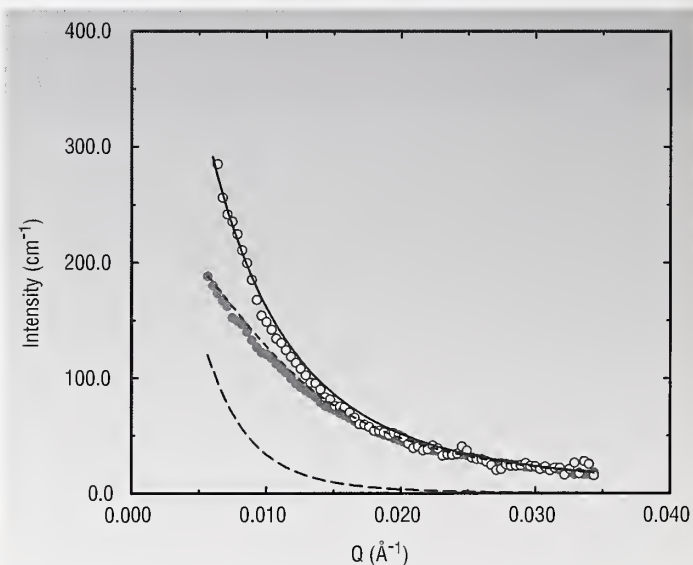
FIGURE 1. Plots of I(Q) as a function of Q for dPS/hPS blends of Mn = 270k. Filled symbols, bulk sample; open symbols, data for a film of thickness D = 18 nm. The fit to these data (solid line) was obtained by utilizing both a roughness term (long dashed line) as well as the standard RPA form (short dashed line).

R.L.Jones, S.K.Kumar
Department of Materials Science and Engineering
Pennsylvania State University
University Park, PA., 16802

D.L.Ho, R.M. Briber
Department of Materials and Nuclear Engineering
University of Maryland
College Park, MD., 20742

T.P. Russell
Polymer Science Department
University of Massachusetts
Amherst, MA., 01003

samples have nearly the same R_g. Using this combined model, R_g was determined for films ranging in thickness over two decades ($0.5 R_g < D < 50 R_g$). The molecular size was found to be independent of film thickness (Figure 2). Since the scattering vector is primarily in the surface plane, this conclusion is consistent with theoretical assumptions and suggests that chain conformation in the direction parallel to the surfaces are unaffected by confinement.

Our results clearly show that, in the thinnest films, the volume pervaded by a coil is decreased as compared to the bulk. This is because the R_g in the direction parallel to the surfaces is unaffected, while the corresponding quantity in the third direction is strongly reduced. In conjunction with other studies, which indicate a thickness-independent density in ultrathin polymer films, these conclusions indicate decreased intermolecular entanglement in thin polymer films. Since entanglement density directly affects the dynamic properties of polymeric systems, we contend that unusual thin film properties, such as the anomalous thickness dependence of diffusion coefficients and glass transition temperatures, are caused by this reduced entanglement density near a surface.

With thin films as a model system, and continuing increases in cold neutron flux, SANS at the NCNR is now an appropriate tool to study a host of problems involving interfacial structure, finite size phase behavior, and nano-patterning in systems as far ranging as engineering thermoplastics to biological systems. These, and related problems, are the focus of investigation in our research groups.

REFERENCES
[1] D. N. Theodorou, Macromolecules **21**, 1400 (1988).
[2] S. K. Kumar, M. Vacatello, D. Y. Yoon, J. Chem. Phys. **89**, 5206 (1988).
[3] P. M. Calvert, Nature **384**, 311(1996).
[4] C. W. Frank et al., Science **273**, 912 (1996).
[5] D. L. Ho et al., Macromolecules **31**, 9247 (1998).
[6] R. L. Jones et al., Nature **400**, 146 (1999).

FIGURE 2. Plots of ratios of R_g and I(0), derived from the RPA component (short dashed line in Figure 1) of the fits to the blend thin film data, to their corresponding bulk values. The ratios are plotted versus the ratio of the film thickness to the bulk R_g. Data are displayed for blends with Mn = 270k (filled circles) and Mn = 650k (open circles).

PROBING THE LOCATION OF THE TERMINAL GROUPS OF A DENDRIMER

Dendrimers represent a new class of macromolecules developed in recent years. Typically, a dendrimer structure has a tri- or tetrafunctional core, which is surrounded by several 'generations' of stepwise added trifunctional monomers, leaving the last generation with a large number of terminal units as shown in Figure 1. The molecular weight doubles with each generation, leading to high molecular weights, and causing the dendrimer to become very compact and crowded.

Many of the potential technological applications of dendrimers depend on their segment density distribution. Previous scattering studies have shown that dendrimers have uniform interiors and are quite spherelike in their shape [1]. The location of the terminal groups is also of importance, since they are usually different chemically from the rest of the dendrimer. This invites a number of applications such as the support of catalysts or drugs or their use as hyperfunctional crosslink sites. The accessibility of these terminal groups depends on their location compared to the other dendrimer units.

The location of the terminal units can be measured by labeling the last generation of the dendrimer with deuterium and using contrast matching techniques to determine their location. Figure 1 shows the labeled groups in red and the rest of the dendrimer in blue. By choosing the proper mix of h- and d- solvents, the interior of the dendrimer will be matched, making only the labeled end groups visible in small angle neutron scattering (SANS).

A sixth generation polyamidoamine (PAMAM) dendrimer was reacted with acrylonitrile (vinyl-d3) to give the deuterium labeling for the SANS. Ethylene diamine was reacted with the dendrimer to give a labeled seventh generation dendrimer. A similar reaction was used to make a seventh and eighth generation dendrimer without labeling. Solutions of unlabeled eighth generation dendrimer were made in mixtures of CH_3OH and CD_3OH for determination of the match point. Three samples were analyzed, an unlabeled dendrimer in CD_3OH (high contrast), an unlabeled dendrimer in the match mixture (dendrimer matched), and the labeled dendrimer in the match mixture (interior matched).

FIGURE 1. Dendrimer structure with labeled terminal units.
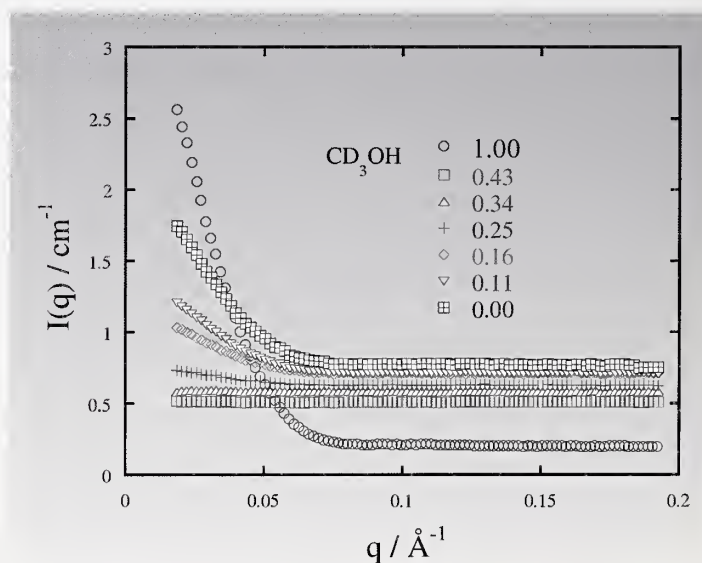
FIGURE 2. SANS from G8 dendrimer in CD_3OH/CH_3OH mixtures.

Andreas Topp, Barry J. Bauer, and
Eric. J. Amis
Polymers Division
National Institute of Standards and Technology
Gaithersburg, MD 20899-8542

June W. Klimash, Ralph Spindler, and
Donald A. Tomalia
Michigan Molecular Institute
1910 West Saint Andrews Road
Midland, MI 48640

SANS was performed at the 30 m facilities at NIST. The spectrometers were operated at a wavelength of $\lambda = 6$ Å, and a wavelength spread of $\Delta\lambda/\lambda = 0.15$.

Figure 2 is a plot of SANS of dendrimer solutions with different CD_3OH contents. The intensity is the strongest in pure CD_3OH, weakens as CH_3OH is added and increases again when pure CH_3OH is used. The coherent scattering intensity varies as $I \sim (b_S - b_D)^2$ where b_D is the contrast of the dendrimer and b_S is the average contrast of the solvent mixture.

Figure 3 is a plot of the square root of the scattered intensity versus solvent composition with the values to the right made negative so that a straight line can be put through all of the data points. The zero intersection is at a mass fraction of 60.5 CH_3OH which was the composition used in the matching experiments.

Figure 4 is a plot of the SANS of the three G7 samples. The circles give the scattering from the high contrast sample, showing strong scattering typical of large spherical dendrimers. The diamonds show the SANS of the same dendrimer, but under match conditions. This sample has no measurable coherent scattering sig-nal, demonstrating that the match conditions have been achieved. The labeled dendrimer SANS is given by the squares. The scattering is weak because only the labeled terminal groups scatter.

A Guinier analysis of the scattering of the high contrast sample gives the radius of gyration (R_g) of the whole dendrimer, and the labeled - contrast match sample gives the R_g of only the terminal groups. The R_g of the whole dendrimer is (34.2 ± 0.2) Å, while the R_g of the terminal groups is (39.3 ± 1.0) Å.

The terminal groups of a seventh generation PAMAM dendrimer are 15% larger than the average of all of the units. Therefore, the terminal units of a dendrimer are concentrated in the outer shell of a dendrimer.

REFERENCES

[1] T. J. Prosa, B. J. Bauer, E. J. Amis, D. A. Tomalia, R. Scherrenberg, J. Polym. Sci.:Polym. Phys. **35**, 2213, (1997).
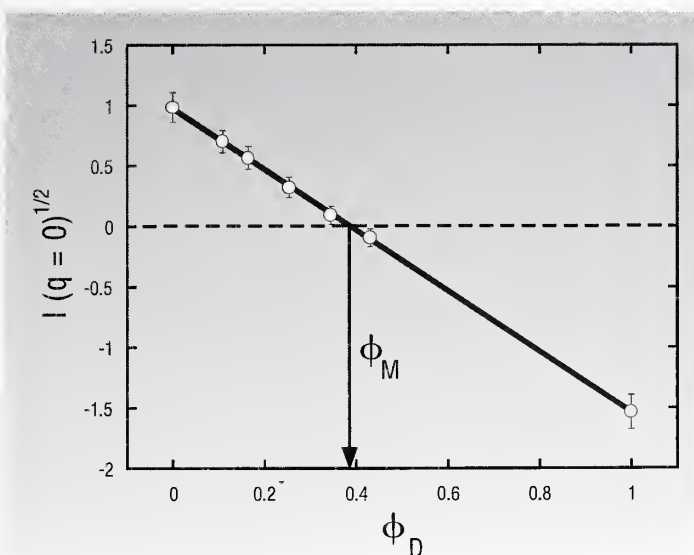
FIGURE 3. Location of the match point.
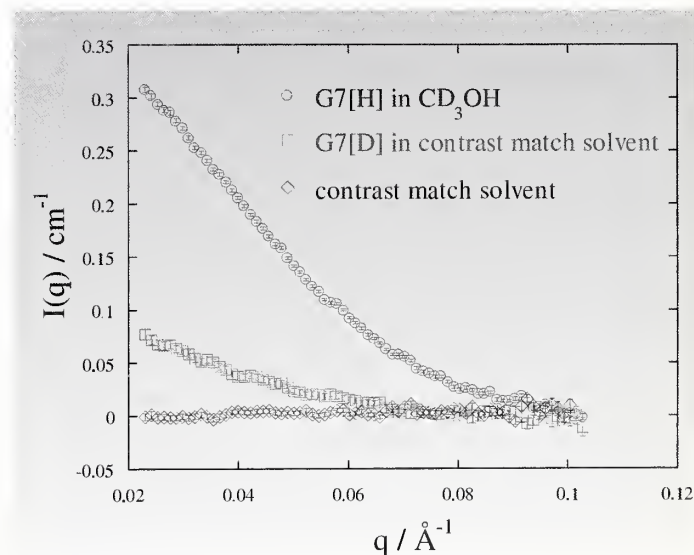
FIGURE 4. SANS of labeled and unlabeled G7 dendrimer in match and high contrast solvents.

SELF-ASSEMBLIES OF MEMBRANE ACTIVE PEPTIDES

In recent years we have made progress by neutron diffraction in a major structural challenge, namely in detecting and analyzing the structures of peptide assemblies in fluid membranes [1,2]. These experiments were performed with membranes in the form of oriented multilayers. Originally the samples were investigated in full hydration so that the physical properties of the lipid bilayers were close to those at physiological conditions. However, it was soon realized that new phenomena involving peptide-lipid interactions occur when the sample hydration is varied. In general, in full hydration, the peptide organization in each membrane is uncorrelated to the neighboring membranes. As the hydration level decreases, the peptides become correlated between bilayers, even though the membranes are still fluid. In many cases, further dehydration strengthens the correlation such that the peptide organization in the multilayers crystallizes [2]. The crystallization provides the possibility for high-resolution diffractional studies. Investigations along this line might also lead to useful information for crystallization of membrane proteins.

Antimicrobial peptides are inducible innate host defense molecules found in all multicellular organisms, including humans and plants. These peptides have a folded size comparable to the membrane thickness. All evidence indicates that antimicrobial peptides act by permeabilizing the cell membranes of microorganisms. But the molecular mechanisms of their actions are still not clear. We have found that all peptides, when they are bound to lipid bilayers, exhibit two distinct oriented circular dichroism spectra, one at low peptide-to-lipid ratios (P/L) and another at high P/L. This indicates that each peptide has two different physical states of binding to a membrane.

The transition from the low to the high P/L spectrum occurs over a narrow range of P/L as if there is a threshold concentration, called P/L*. At concentrations below P/L*, the peptides are embedded in the headgroup region, as suggested by the peptide orientation and the membrane thinning effect. At concentrations above P/L*, neutron in-plane scattering showed that the peptides form pores in the membranes, while no pores were detected below P/L*. The detection was achieved by exploiting the sensitivity of neutrons to
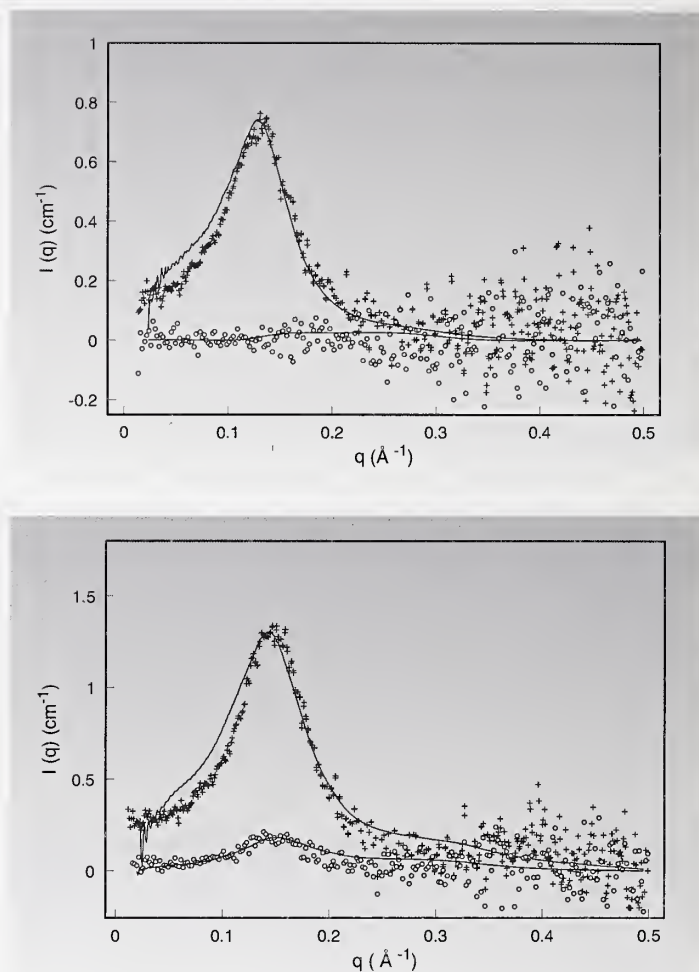
FIGURE 1. In-plane SANS from alamethicin in DLPC lipid bilayers at a high peptide-to-lipid ratio where the peptides self-assemble to form channels through the lipid bilayer as depicted in Figure 2. In the upper panel, the channels were filled with either D_2O (+), giving strong scattering contrast, or H_2O (o). In the lower panel the lipid was deuterated, providing stronger scattering contrast with H_2O in the channels (+) compared with D_2O (o). These data were taken at ANL.

D_2O, which had replaced the water in the membrane pores. As an example, Figure 1A and B show neutron in-plane scattering taken at Argonne National Laboratory (ANL) of alamethicin in protonated lipid bilayers (1A) and in deuterated lipid bilayers (1B), with D_2O or H_2O filling the pore channels. The peak in these data is due to the fairly regular pore spacing and is most pronounced when

Huey W. Huang
Rice University
Department of Physics
Houston, TX 77005-1892
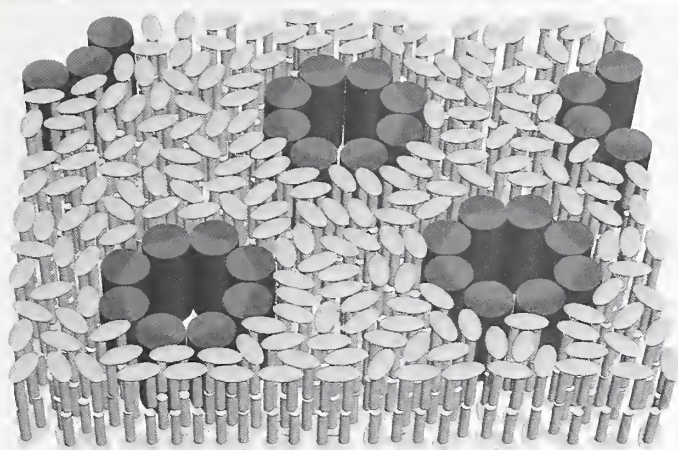
FIGURE 2. Model for the channels formed by octamers of alamethicin in DLPC bilayers that is consistent with the in-plane SANS data shown in Figure 1.
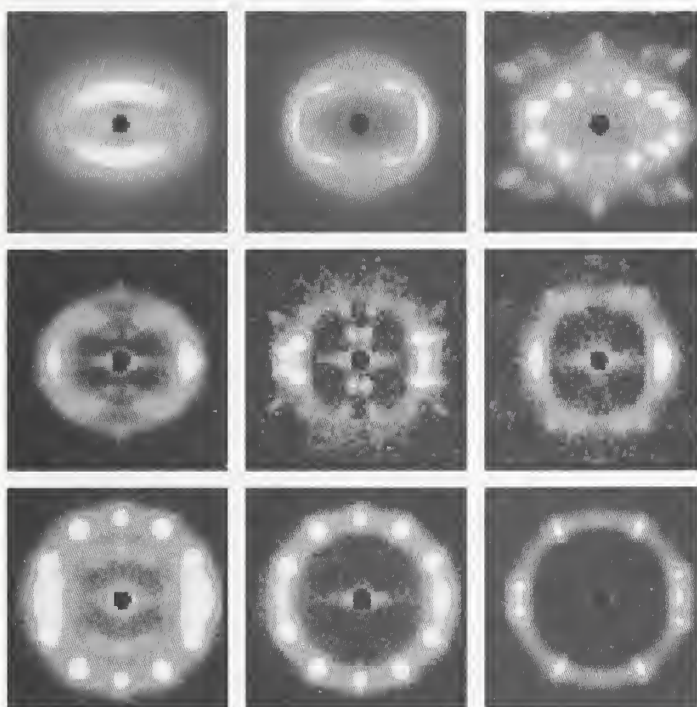
FIGURE 3. Examples of SANS patterns from channel-forming peptides in lipid bilayers at various temperatures and stages of dehydration. The upper left panel is for magainin pores in fully hydrated fluid bilayers. As this and other peptide/lipid systems studied are dehydrated, the pores in adjacent bilayers become correlated and eventually crystallize.

there is a strong contrast, either between D_2O and protonated lipid, or between H_2O and deuterated lipid. All four sets of data are consistent with the model shown in Figure 2 once the differences in contrast are taken into account (solid curves). Thus we concluded that alamethicin in DLPC bilayers forms octameric pores in the barrel-stave fashion.

Interestingly, the barrel-stave model is not the only possible pore formation. We have detected another type, called toroidal pores, in which the lipid monolayer bends continuously from one leaflet to another like the inside of a torus [1]. However, while the evidence for the pores is clear by the detection of the water (D_2O) channels through the lipid bilayers, the evidence for the pore structures is indirect. Thus the discovery of the crystalline phases is an important new development for the field of antimicrobial peptides.

We developed a method of off-plane scattering [2] to record the diffraction pattern on a SANS instrument that includes both the in-plane and out-of-plane momentum components. Figure 3 exhibits some typical diffraction patterns as recorded on the NG-3 30-meter SANS instrument's detector by this method. The top left panel shows the diffraction pattern of magainin pores in fully hydrated fluid bilayers. When the sample was slightly dehydrated, the pattern changed to the top middle panel. Our analysis [2] showed that the positions of the magainin pores in each bilayer become correlated with the pores in adjacent bilayers, even though the bilayers are still in the fluid phase. The cause of this correlation was hypothesized to be due to the hydration force. Upon further dehydration or cooling, the pore arrangement crystallized into a lattice (the left panel of the middle row) having ABCABC stacking of hexagonally ordered planes.

REFERENCES

[1] K. He, S. J. Ludtke, D. L. Worcester, and H. W. Huang. Biochemistry **34**, 16764 (1995); Biophys. J. **70**, 2659 (1996); S. J. Ludtke, K. He, W. T. Heller, T. A. Harroun, L. Yang, and H. W. Huang. Biochemistry **35**, 13723 (1996)

[2] L. Yang, T. M. Weiss, T. A. Harroun, W. T. Heller, and H. W. Huang. Biophys. J. **75**, 641 (1998); **77**, 2648 (1999)

# SHEAR ORIENTATION OF VISCOELASTIC POLYMER-CLAY SOLUTIONS

Shear-induced structural changes in complex fluids of anisotropic species are a very general phenomenon, occurring in polymer solutions, liquid crystalline materials and block copolymer melts. The purpose of our work is to investigate the influence of shear on the structure of a highly viscoelastic, aqueous clay-polymer solution. Many structural models have been proposed for such solutions [1-3], but little is definitively known about mesoscopic properties or shear behavior. This information is important in the production of nanocomposite materials [4].

In our work, we use small-angle neutron scattering (SANS) to study a solution of the synthetic hectorite type clay, Laponite LRD (Laporte Industries Ltd.), and poly(ethylene-oxide) (PEO) ($M_w = 10^6$ g/mol). The results reported here are for a highly viscoelastic solution containing a mass fraction of 3 % LRD and 2% PEO at room temperature. The clay particles produce transparent dispersions of disk shaped particles ca. 300 Å in diameter and ca. 10 Å thick [5,6]. The pH and ionic strength of the solutions were controlled by the addition of NaOH and NaCl, respectively.

Figure 1 shows the shear rate dependence of the birefringence of the clay-polymer solution. A distinct minimum in the birefringence is observed at a critical shear rate of approximately 40 s^{-1}. The source of the shear dependence of the birefringence is due to the alignment of the clay particles and the PEO. Previous work demonstrated that the sign of the birefringence of the clay particles oriented along a flow field is negative, therefore at low shear rates, the orientation of the clay dominates the birefringence. Above the critical shear rate, the birefringence due to the orientation of the polymer chains dominates.

A double logarithmic plot of viscosity, η, versus shear rate shows that the solution is shear-thinning over the entire range according to a power law with exponent m = -0.65. No signature of the critical shear rate is observed in the viscosity behavior.

The SANS shear cell utilized has been described previously [2]. The instrument was configured in both "radial" (incident beam parallel to the shear gradient along the cylinder diameter) and "tangential" (incident beam passing between the cylinders, parallel to the flow direction) geometries. Using 9 Å wavelength neutrons gives a Q range between 0.0027 Å^{-1} and 0.0199 Å^{-1}. The primary contrast in the SANS experiment used to detect the orientation of
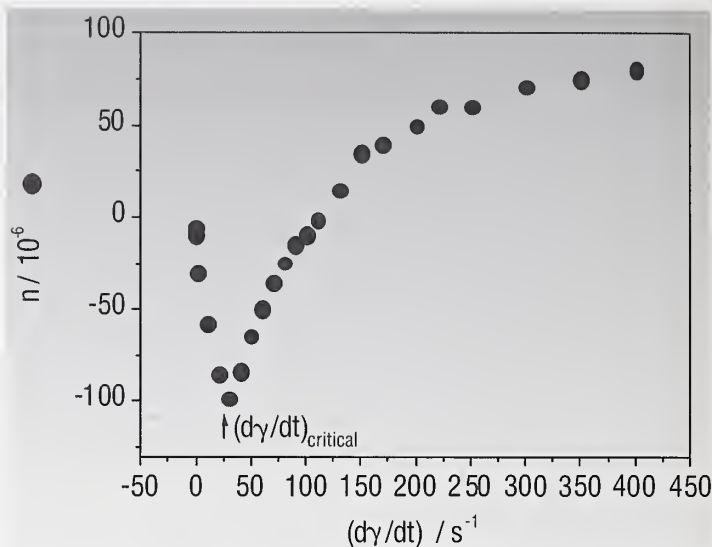
FIGURE 1. Optical birefringence as a function of shear rate. The arrow indicates $(d\gamma/dt)_{critical}$, the shear rate where the minimum in the birefringence occurs.

the clay platelets and polymer chains under shear is between D$_2$O and the other solution components.

The results obtained from the polymer-clay solutions in the "radial" and "tangential" beam configurations are summarized in Figure 2. At low shear rates, a diffuse isotropic ring of SANS intensity is observed (Figure 2a). The diffuse ring corresponds to an average spacing between platelets of 800-1100 Å. With increasing shear rate, the ring becomes more diffuse (Figure 2b) and an anisotropic streak develops parallel to the vorticity axis of the flow field (the cylinder axis). If we neglect the main reflected beam which appears as a background streak in the gradient direction for tangential beam measurements (Figure 2d), the anisotropic streak becomes the dominant feature in both scattering geometries with increasing shear rate. After cessation of shear, the streaks relaxed to an isotropic state in less than 2 minutes.
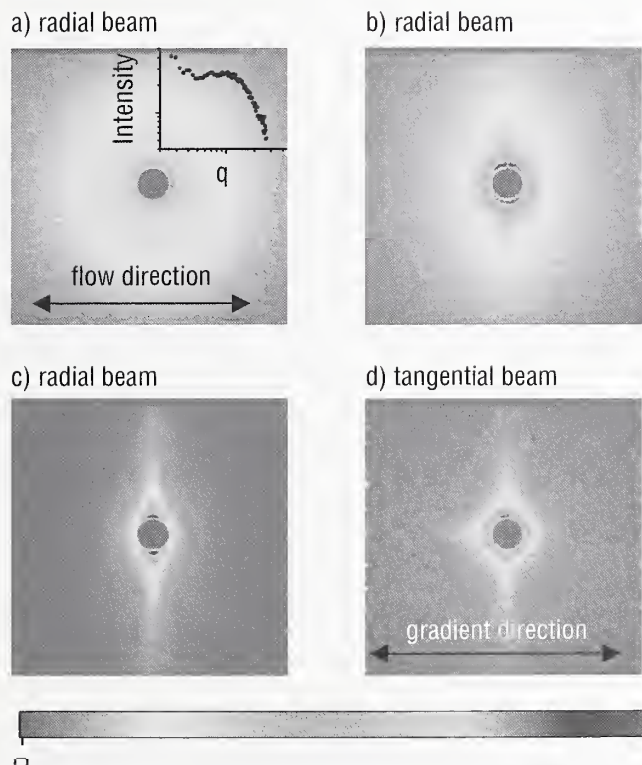
To account for the SANS and birefringence results, our current understanding is that the polymer chains are in a dynamic adsorption/desorption equilibrium with the clay particles to form a network. The peak position in the quiescent scattering pattern in Figure 2a is an indication of the mesh size of this network (~ 1000 Å). A 2% solution of only PEO, at the same pH, polymer and salt concentration showed no anisotropic SANS scattering at shear rates up to 100 s^{-1}. Similarly a 3% aqueous clay solution

Gudrun Schmidt, Alan I. Nakatani, Alamgir Karim, and Charles C. Han
Polymers Division
National Institute of Standards and Technology
Gaithersburg, MD 20899-8544

Paul D. Butler
NIST Center for Neutron Research
National Institute of Standards and Technology
Gaithersburg, MD 20899-8562

shows no evidence of an anisotropic SANS pattern. Therefore, we can conclude that the anisotropic SANS pattern observed in the clay-polymer solutions is due to this coupling between clay platelets and polymer, allowing a higher orientation than either single component in solution can produce. From the birefringence data, the clay particles orient at low shear rates, while strong orientation of the PEO does not occur until the critical shear rate is exceeded. Since the clay platelets and the PEO chains are of comparable size (both about 300 Å), the lack of internal flexibility of the rigid clay particles makes them much easier to align than the flexible polymer chains.

According to SANS patterns from both beam configurations (Figure 2) the shear flow results in an alignment of clay platelets orienting with their surface normals in the vorticity direction. One would expect the surface normals to orient along the gradient direction of the flow field, however, the type of orientation observed

in these clay-polymer solutions is also observed in some liquid crystalline lamellar phases, block copolymer solutions, and melts. The critical shear rate is the shear rate at which the rate of chain desorption is slower than the terminal relaxation time of the chain, hence chain extension is observed in the birefringence.

On cessation of shear, the stress on the network decays almost immediately, and the recovery of the isotropic structure is controlled by the relaxation of the stretched chains. As the chains retract, the coupling of the chains to the clay allows the platelets to randomize in orientation in the local viscous environment. The recovery from anisotropy is much faster than expected from simple Brownian motion of only the clay particles in a medium of the same viscosity as the clay-polymer solution exhibited macroscopically, and is indicative of the dynamic coupling of the polymer chains to the clay. Future work will compare the relative rates of the relaxation in the PEO and clay with the cooperative adsorption/desorption kinetics which occur during deformation.

REFERENCES

[1] A. Mourchild, A. Delville, J. Lambard, E. Lecolier, P. Levitz, Langmuir **11**, 1942 (1995)

[2] H. J. M. Hanley, G. C. Straty, Langmuir **10**, 3362 (1994).

[3] F. Pignon, A. Magnin, J. M. Piau, J. Rheol. **42**, 1349 (1998).

[4] S. Rossi, P. F. Luckham, S. Zhu, Rev. I Fr. Petrol **52**, 199 (1997).

[5] J. D. F. Ramsay, S. W. Swanton, J. Bunce, J. Soc. Faraday Trans. **86**, 3919 (1990).

[6] F. Pignon, A. Magnin, J. M. Piau, B. Cabane, P. Lindner, O. Diat, Phys. Rev. E **56**, 3281 (1997).

FIGURE 2. SANS patterns of the clay-polymer solutions as a function of shear rate in the radial geometry (a-c) and tangential geometry (d) at shear rates of a) 0.5 s⁻¹, b) 20 s⁻¹, c) 90 s⁻¹, d) 90 s⁻¹.

New biomimetic membrane materials, of fundamental importance in understanding such key biological processes as molecular recognition, conformational changes, and molecular self-assembly, can be characterized using neutron reflectometry. In particular, scattering length density (SLD) depth profiles along the normal to the surface of a model biological bilayer, which mimics the structure and function of a genuine cell membrane, can be deduced from specular neutron reflectivity data collected as a function of wavevector transfer Q. Specifically, this depth profile can be obtained by numerically fitting a computed to a measured reflectivity. The profile generating the best fitting reflectivity curve can then be compared to cross-sectional slices of the film's chemical composition predicted, for example, by molecular dynamics simulations [1]. However, the uniqueness of a profile obtained by conventional analysis of the film's reflectivity alone cannot be established definitively without additional information. In practice, significantly different SLD profiles have been shown to yield calculated reflectivity curves with essentially equivalent goodness-of-fit to measured data [2], as illustrated in Figure 1.

The existence of multiple solutions, only one of which can be physical, is especially problematic in cases where a key additional piece of structural or compositional information is lacking as can happen in the investigation of these biological membrane systems.

Why this inherent uncertainty? The neutron specular reflection amplitude for a model SLD can be computed exactly from first principles; the square of its modulus gives the measurable reflectivity. It is firmly established, however, that the complex amplitude is necessary and sufficient for a unique solution of the inverse problem, that of recovering the SLD from reflection measurements. Unambiguous inversion requires both the magnitude and phase of reflection. Once these are known, practical methods [3] exist for extracting the desired SLD.

In fact, considerable efforts were made about a quarter century ago to solve the analogous "phase problem" in X-ray crystallography using known constraints on the scattering electron density [4] and by the technique of isomorphic substitution [5]. Variations of the latter approach have been applied to reflectivity, using a known reference layer in a composite film in place of atomic substitutions. These solution methods, however, were tied to the Born approximation,

FIGURE 1. Family of scattering length density profiles obtained by model-independent fitting of the reflectivity data in the inset. The profile represented by the blue dashed line is unphysical for this Ti/TiO film system yet generates a reflectivity curve that fits the data with essentially equivalent goodness-of-fit (all the reflectivity curves corresponding to the SLD's shown are plotted in the inset but are practically indistinguishable from one another).

FIGURE 2. Reflectivity curves for the thin film system depicted schematically in the inset, one for a Si fronting (red triangles), the other for Al_2O_3 (black circles). The curve in the lower part of the Figure (blue squares) is the real part of the complex reflection amplitude for the films obtained from the reflectivity curves by the method described in the text.

C. F. Majkrzak, N. F. Berk, S. Krueger
NIST Center for Neutron Research
National Institute of Standards and Technology
Gaithersburg, MD 20899-8562

C. W. Meuse, V. Silin, J. Woodward, A. L. Plant
NIST Biological Division
National Institute of Standards and Technology
Gaithersburg, MD 20899-8311

M. Tarek
Department of Chemistry
University of Pennsylvania
Philadelphia, PA 19103

which generally is valid in crystal structure determination but which fails catastrophically at low Q (low glancing angles) in reflection from slab-shaped samples such as thin films. Exact inversion requires accurate knowledge of the reflection amplitude over the entire Q-range, especially at low Q.

In this decade the reflection phase problem has been exactly solved using a protocol of three reflectivity measurements on composite films consisting of the film of interest in intimate contact with each of three known reference layers [6, 7]. Subsequently, variations using only two measurements have been shown to partially solve the phase problem, an additional procedure being required to choose between two solution branches, only one of which is physical [8, 9]. In the past year [10], an exact solution has been found for a two measurement strategy in which the film surround, either the fronting (incident) or backing (transmitting) medium, is varied. This new approach is simpler to apply than reference layer methods and is adaptable to many experiments. Surround variation neutron reflectometry has been successfully applied to the challenging type of biological membrane depth profiling described earlier.

In Figure 2 are plotted a pair of neutron reflectivity curves measured for the layered film structure schematically depicted in the upper right inset, one with Si and the other with Al_2O_3 as the fronting medium. The lower part of Figure 2 shows the real part of the complex reflection amplitude for the multilayer as extracted from the reflectivity data, according to the method described above, and which was subsequently used to perform the inversion to obtain the SLD shown in Figure 3. For comparison, the SLD predicted by a molecular dynamics simulation is also shown in Figure 3, along with a slightly distorted version, corresponding to a truncated reflectivity data set, which indicates the spatial resolution of an SLD obtainable in practice. This latter SLD was obtained by inversion of the reflection amplitude computed for the exact model SLD, but using values only up to the same maximum Q value ($0.3 Å^{-1}$) over which the actual reflectivity data sets were collected. Overall, agreement between the experimentally determined profile and the theoretical prediction is remarkable, essentially limited only by the Q-range of the measurement. Surround variation neutron reflectivity thus makes it possible to measure complicated thin film structures without the ambiguity associated with curve fitting. The veridical SLD profile is obtained directly by a first principles inversion.

REFERENCES:

[1] M. Tarek, K. Tu, M.L. Klein, and D. J. Tobias, Biophys. J. **77**, 964 (1999).

[2] N. F. Berk and C. F. Majkrzak, Phys. Rev. B **51**, 11296 (1995).

[3] P. E. Sacks, Wave Motion **18**, 21 (1993).

[4] H. A. Hauptman, Science **233**, 178 (1986).

[5] J. M. Cowley, *Diffraction Physics*, 2nd Ed., (North Holland, Amsterdam, 1990) p .131.

[6] C. F. Majkrzak and N. F. Berk, Phys. Rev. B **52**, 10825 (1995).

[7] V.O. deHaan, A. A. van Well, S. Adenwalla, and G..P. Felcher, Phys. Rev. B **52**, 10830 (1995).

[8] T. Aktosun and P. E. Sacks, Inverse Problems **14**, 211 (1998).

[9] C. F. Majkrzak and N. F. Berk, Physica B **267-268**, 168 (1999).

[10] C. F. Majkrzak and N. F. Berk, Phys. Rev. B **58**, 15416 (1998).

FIGURE 3. SLD profile (red line) resulting from a direct inversion of the Re r of Figure 2 compared with that predicted by a molecular dynamics simulation (white line) as discussed in the text. The headgroup for the Self-Assembled-Monolayer (SAM) at the Au surface in the actual experiment was ethylene oxide and was not included in the simulation but, rather, modelled separately as part of the Au. Also, the Cr-Au layer used in the model happened to be 20 Å thicker than that actually measured in the experiment.

MULTI-TECHNIQUE STUDIES OF ULTRATHIN SiO$_2$ FILMS

Current gate dielectrics in silicon based devices are only a few nm thick. Optical techniques such as ellipsometry are used to monitor film thicknesses and optical properties in production. However, for the current integrated circuit (IC) generation the accuracy of ellipsometry degrades because parameters such as thickness and index of refraction (which reflects the composition) become strongly correlated. Thus, it is difficult to unambiguously determine these parameters simultaneously, and the accuracy of ellipsometry would benefit from an independent calibration. In reflectometry techniques, on the other hand, these parameters are nearly decoupled. The thickness of a layer is approximately inversely proportional to the oscillation period of the reflected intensity, whereas the differences in scattering length density SLD (also an indicator of composition) between the layers is related to the amplitude of the oscillations. Neutron reflectometry (NR) is better suited than X-ray reflectometry (XR) for the study of the SiO$_2$/Si system because there is a relatively large contrast (or difference in SLD) between the scattering length densities of the two materials: 65%, vs. 7.6% for X-rays.

Consider as an example a sample with a nominally 10 nm thick thermal oxide film on silicon. This moderate thickness was chosen to increase our confidence in the results of the various characterization methods, while remaining thin enough that the results are relevant to film of technological interest. Figure 1 shows spectroscopic ellipsometry (SE) data and corresponding best fits for the sample with surface contamination and after an organic cleansing. Nominally, the only change is a decrease in the thickness of the contamination layer [1].

In XR data (Figure 2) two oscillation periods are observed for the contaminated sample. The high frequency oscillation corresponds to the SiO$_2$ film, whereas the low frequency modulation is due to the thinner contamination layer (which is not present after cleaning, indicating removal of the contamination.)

The NR measurements (Figure 3) were done in a vacuum to reduce the air scattering background. This allowed us to achieve a very large range in reflectivity, over 10^8, which is among the best examples in NR measurements to date. A slightly thinner contamination layer in NR is consistent with the fact that the XR was done in air, during which the contamination was growing. This was confirmed by changes in XR scans immediately following those in Figure 2. The average of the 5 measurements of the SiO$_2$ film thickness was 10.27 ± 0.13 nm The excellent agreement among the results for the three different techniques increases our confidence in the parameters extracted via these models. Thus the XR and
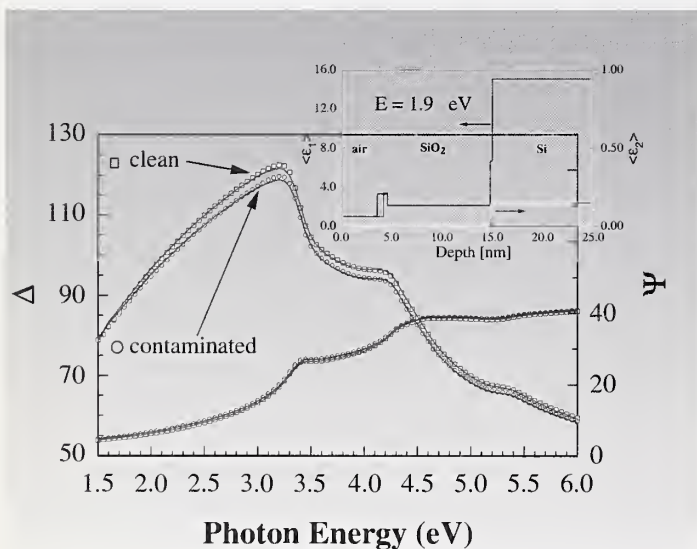
FIGURE 1. Comparison of spectroscopic ellipsometry experimental data, Ψ and Δ, to the fits (solid line) for the clean and surface contaminated sample. The inset shows $<\varepsilon 1>$ and $<\varepsilon 2>$ as a function of depth determined by the fit.
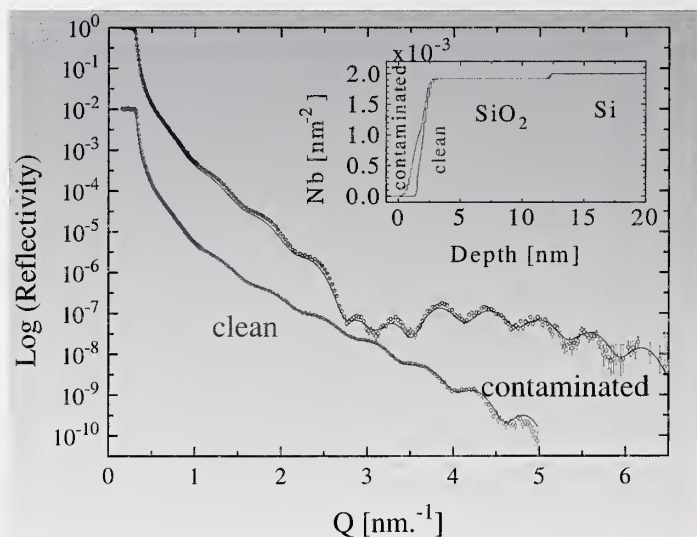
FIGURE 2. X-ray reflectivity and best fits for the clean and surface contaminated sample. The inset shows the scattering length density profile determined by the fits.

J. A. Dura and C. F. Majkrzak
NIST Center for Neutron Research
National Institute of Standards and Technology
Gaithersburg, MD, 20899-8562

C. A. Richter, N. V. Nguyen and J. R. Ehrstein
Semiconductor Electronics Division
National Institute of Standards and Technology
Gaithersburg, MD, 20899-8122
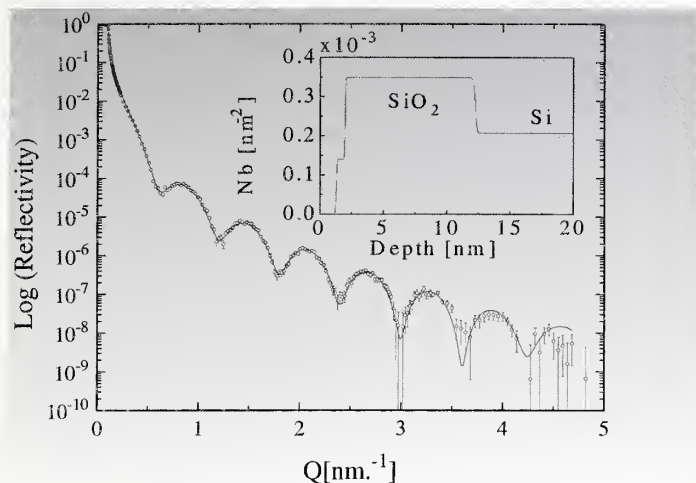
FIGURE 3. Neutron Reflectivity data and best fit for a sample with surface contamination. The inset is the scattering length density profile determined by the fit.

particularly the NR corroborate the correct analysis required in SE (which is the technique most practical in monitoring production).

To further investigate the applicability of these techniques to thinner SiO_2 layers, we simulated the SE and the XR and NR curves for 6 nm, 4 nm, and 2 nm thick layers of SiO_2. For a realistic and consistent set of roughness parameters in the models, we used the average values obtained from the actual measurements previously discussed. The SE simulation, Figure 4a, shows distinct differences in both the magnitude and shape of D among the three thicknesses shown. In models of XR, shown in Figure 4b, only very weak oscillations are seen for even the thickest of the SiO_2 layers because of the low contrast between SiO_2 and Si. However, in NR, strong oscillations are clearly seen above the 10^{-8} lower limit, demonstrated in Figure 3, for SiO_2 layers as thin as 2 nm. Therefore both NR and SE are well suited for the study of SiO_2 films as thin as 2 nm. Encouraged by these models, we obtained NR data for a thinner, 2.4 nm, sample. While these data are not yet fit to a model curve, we note that both the reflected intensities and oscillation amplitude are similar to those of the 2.0 nm model, indicating similar interface widths.

We have shown that three different techniques can offer complimentary information on the structure of thin SiO_2 films on Si. All offer a significant degree of sub-monolayer thickness sensitivity, although in NR there is a much higher contrast between SiO_2 and Si than in XR.
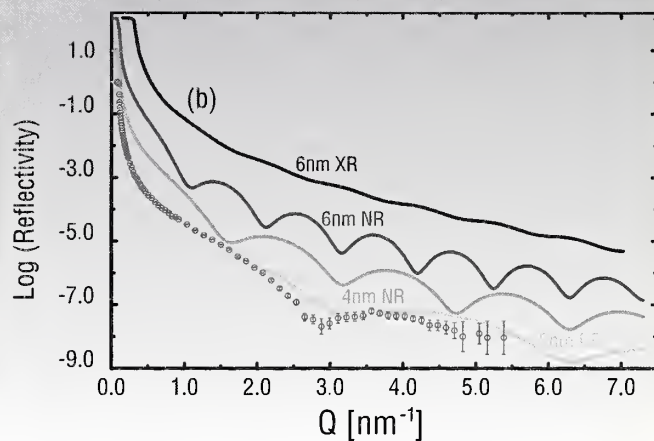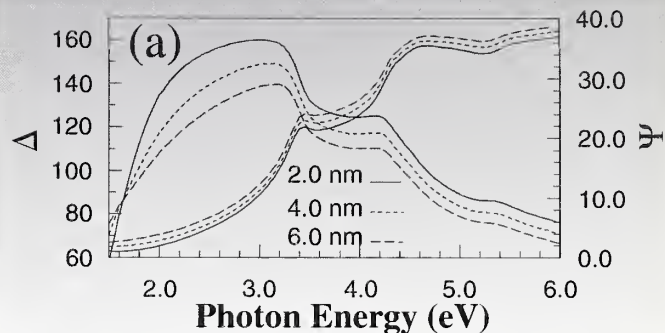
FIGURE 4. Model calculations for thin SiO_2 films of thickness indicated in the figure, on Si. a) Spectroscopic ellipsometry, and b) unless otherwise noted solid lines are neutron reflectometry models. For clarity the 6 nm (4 nm) films are shifted up by 2(1) orders of magnitude. The data points are for a ~ 2.4 nm film.

REFERENCES

[1] For details see: "Neutron Reflectivity, X-ray Reflectivity, and Spectroscopic Ellipsometry Characterization of Thin SiO_2 on Si," J. A. Dura, C. A. Richter, C. F. Majkrzak, and N. V. Nguyen, Appl. Phys. Lett. **73**, 2131 (1998).

CERTIFICATION OF AN ION-IMPLANTED ARSENIC IN SILICON STANDARD REFERENCE MATERIAL

The secondary-ion mass spectrometry (SIMS) community in the United States recently undertook a round-robin study to calibrate the implanted dose of arsenic in silicon by consensus. Variations in dose determination among laboratories were as high as 30%, reflecting primarily the errors of the respective in-house standards. By contrast, in an international round-robin exercise sponsored by the International Standards Organization (ISO), the United States laboratories achieved a relative standard deviation of 4% for nine independent determinations of the boron content in an unknown boron-doped silicon sample. This level of agreement was only possible because all the laboratories used SRM 2137 Boron Implant in Silicon as a common reference material. These results demonstrate the need for a common arsenic reference material to improve inter-laboratory reproducibility. Furthermore, SEMATECH (a consortium of semiconductor manufacturers) recently listed SRM implants of phosphorus and arsenic in silicon as high priority industrial needs. Consequently, a Standard Reference Material (SRM 2134 Ion-Implanted Arsenic in Silicon) was produced at NIST, using a wafer from the SIMS intercomparison. The material for this SRM was provided by a major ion implanter manufacturer who supplied three 200 mm diameter wafers that had been implanted with arsenic at an energy of 100 keV (in the same batch). One of the wafers was diced and distributed to 12 participating laboratories for the arsenic round-robin study described above. Each of the remaining wafers could provide 221 SRM units, enough for an estimated 10 year supply. One of the remaining wafers was therefore diced into 1 cm x 1 cm pieces with a wafer saw for use as SRM 2134. Because of the specificity and matrix independence of instrumental neutron activation analysis (INAA), this technique was chosen as the primary method for certification of the arsenic implanted dose.

NIST currently certifies elemental concentrations in SRMs using one of three modes: (1) a primary method at NIST with confirmation by other method(s), (2) two independent critically-evaluated methods at NIST, and (3) one method at NIST and different methods by outside collaborating laboratories.

Certification using a primary method is only possible when all potentially significant sources of uncertainty have been evaluated explicitly for the application of the method and the matrix under investigation. In addition, confirmation of measurements by a primary NIST method is accomplished by one or more of the following: determination of certified constituents in

Table 1. Individual Uncertainty Components for Determination of Arsenic in SRM 2134

Source of Uncertainty	Individual Uncert. (1s)%
Basis Measure - Sample Area / Micrometer Accuracy	0.012
Basis Measure - Sample Area / Precision (n = 26)[1]	0.0089
Concentrations of Comparators (Standards)	0.106
Mass Determination - Comparators	0.041
Isotopic Variability	0
Blank and Blank Correction (n = 10^2)[1]	0.013
Irradiation Geometry Differences	0.039
Neutron Self - Shielding/Scattering Differences	0.024
Timing	0
Irradiation Interferences	Negligible
Measurement Replication (n = 9)[1]	0.081
Counting Statistics - Standards (n = 10^5)[1]	0.073
Counting Geometry Differences	0.009
Pulse-Pileup	0.066
Dead-Time Effects (inadequacy of LT extension)	Negligible
Decay Timing Effects (Half life related)	0.053
Gamma-Ray Self Shielding	0.004
Gamma-Ray Interferences	0.00004
Peak Integration Method	0.033
Overall	0.189

[1] "n" indicates degrees of freedom which are listed for Type A sources of uncertainty

Robert R. Greenberg, Richard M. Lindstrom, and David S. Simons
Analytical Chemistry Division
National Institute of Standards and Technology
Gaithersburg, MD 20899-8395

other Standard Reference Materials (SRMs) or Certified Reference Materials (CRMs) of similar matrix and constituent concentration range; a second NIST technique with appropriate controls; or results of measurements from selected outside collaborating laboratories with appropriate experience.

In order to certify the arsenic concentration in SRM 2134 using INAA as a primary method it is therefore necessary to evaluate all significant sources of uncertainty explicitly. For this set of measurements, we considered sources of uncertainty greater than 0.01% relative to be significant. The results of a complete evaluation of all sources of uncertainty are listed in Table 1. This evaluation yielded an expanded relative uncertainty of 0.38% (as defined by ISO and NIST) and gives an approximate level of confidence of 95%. The arsenic concentration observed was 91.20 ng/cm^2 ± 0.35 ng/cm^2. No evidence indicating significant heterogeneity among samples could be seen when the observed sample-to-sample precision was compared to what was expected from counting statistics combined with other sources of analytical variability.

In conclusion, we have successfully applied INAA as a primary method for the certification of this new SRM. The observed relative expanded uncertainty of 0.38% is considerably smaller than the 1% value desired by the semiconductor industry. This new SRM should greatly enhance the U. S. semiconductor industry's ability to achieve accurate and reproducible analytical results for this key dopant in silicon.

THE ROTATIONAL DYNAMICS OF H₂ IN POROUS VYCOR GLASS

Porous materials play an increasingly important role in the exploration of fundamental scientific issues related to diverse technological applications including adhesion, lubrication, tribology and the engineering of materials. Surface interactions and finite size effects both play a key role in the qualitative modification of the properties of the materials contained within the porous host. Due to its light mass and weak electronic interactions, molecular hydrogen is an ideal system to probe the effects of surface interactions. H_2 is well described as a quantum rigid rotor with discrete energy levels labeled by the rotational quantum number, J, and energies given by $E_J = BJ(J+1)$ where B is the rotational constant which is equal to 7.35 meV for H_2. These energy levels can be studied by using neutrons to stimulate the J = 1 to J = 0 transition of the H_2 molecule, a process that is normally doubly forbidden due to the quantum statistics obeyed by H_2. When neutron stimulated conversion occurs, the neutron gains an amount of energy equal to the rotational energy of the molecule. This results in an extremely clean signal since all other processes are frozen out at the low temperatures of these measurements.

Studies of the rotational levels of H_2 adsorbed in Vycor, a commercially available porous glass, were carried out for pore fillings ranging from 0.10 (corresponding to less than a single monolayer on the pore surface) to 0.92 (corresponding to nearly full pores). As can be seen in Figure 1, at low filling fractions only a single broad peak at 10 meV is present which can be attributed to the scattering from an adsorbed layer of H_2 strongly bound to the pore surface. The appearance of scattering at 14 meV, corresponding to the free molecule transition, for fillings above 0.45 is associated with the appearance of "bulk"-like material in the pore center. The clear separation of the scattering from molecules adsorbed on the walls and in the pore center suggests that these are quite distinct states which we refer to as the bound and bulk-like states, respectively.

The shift in the energy of the rotational transition at low fillings can be directly related to the interaction of the molecules with the surface [2]. Figure 2 shows the shift of the J = 1 to J = 0 transition as a function of the rotational energy barrier for the molecule. From Figure 2 one finds that the observed rotational energy of 10 meV corresponds to an orientational potential with a barrier height of $V_B/B_H = 2.7$ ($V_B = 19.8$ meV). The magnitude
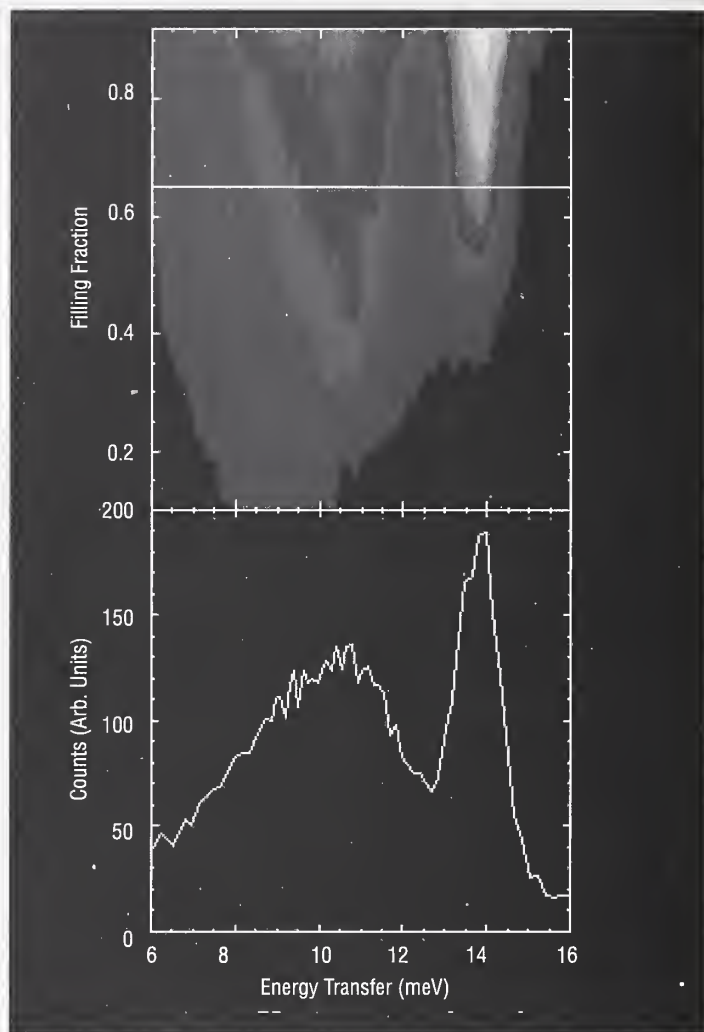
FIGURE 1. The top panel shows a contour plot of the inelastic scattering from H_2 in Vycor at various pore fillings at 6 K. The bottom panel is a cut through the contour plot at f = 0.65 (indicated by the line).

of this potential is quite large, comparable to that seen in alpha alumina, a catalyst used for ortho-H_2 enrichment [3], and on leached glass [4].

Careful inspection of the data reveals that the peak due to the bound state actually shifts from 9.1 meV to 10.1 meV between filling fractions, f, of 0.20 and 0.27. Thus for f between 0.27 and 0.45, the bound state may be separated into a layer in direct contact with the pore wall and a layer that feels a weaker orientational potential. The scattering from these two layers can be separately determined assuming the intensity from the first layer varies linearly with filling.

D. W. Brown
Manual Lujan Jr. Neutron Scattering Center
Los Alamos National Laboratory
Los Alamos, NM 87545

P. E. Sokol
Department of Physics
The Pennsylvania State University
University Park, PA 16802

S. A. FitzGerald
Department of Physics
Oberlin College
Oberlin, OH 44074
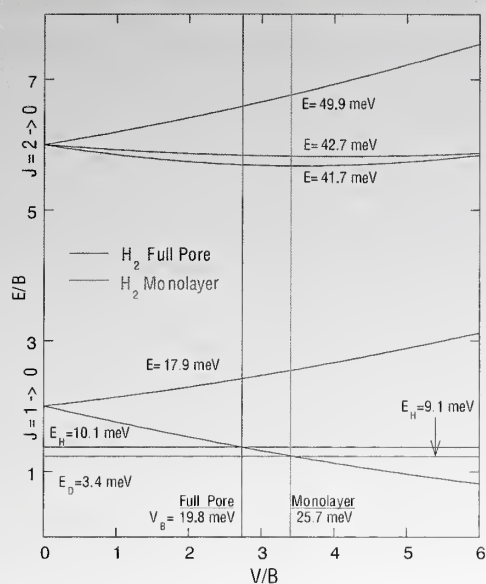
FIGURE 2. Shift of the rotational energy levels of H_2 as a function of barrier height.

FIGURE 3. Distribution of potential barriers felt by the molecules in the first (red) and second (blue) layers.

The scattering from the second surface layer can be obtained from the difference of the monolayer and bilayer spectra. The scattering from the second layer is centered at $E = 11.3$ meV, compared to the first layer which is centered at 9.1 meV, indicating that the second layer interacts less strongly with the wall.

The width of the peak we associate with the bulk-like molecules is due entirely to instrumental resolution. This is consistent with the view of these molecules as being free rotors with a single well defined value for B. On the other hand, the width of the peak which we attribute to the bound layer is much broader than the instrumental resolution. A single well defined orientational potential would yield a shift in the peak location, as observed, but no additional broadening, since the energy levels would still be well defined. Thus, we attribute this additional width to a distribution of orientational potentials which can also be directly extracted using the model of White and Lassettre [2] (Figure 2). After correcting for instrumental effects, the strength of the scattering at a given energy is directly proportional to the number of molecules which feel the corresponding orientational potential. Thus, plotting the scattering as a function of V/B_H, directly yields the distribution of orientational potentials shown in Figure 3. As can be seen, the orientational potential for the first layer is broad, asymmetric, and centered at

$V_B = 3.5B_H$, whereas the potential of the second layer is relatively narrow and centered at $V_B = 2.0B_H$, indicating a weaker interaction with the surface.

The data allow us to draw the following picture of the adsorption of molecular hydrogen on a porous glass surface. The first monolayer is bound tightly to the rough pore surface. The rough surface prevents free rotation of the molecule, altering the rotational energy states. The second layer perceives the surface roughness smoothed by the presence of the first layer, and accordingly, the rotational transitions are affected to a lesser degree. Subsequent to the completion of the second monolayer, the H_2 molecules sense no significant orientational interaction from the glass surface. This is in agreement with the picture presented by Katsaros et al [5], in which surface roughness is created by dangling bonds on the pore surface.

REFERENCES

[1] J. Dekinder, A. Bouwen and D. Schoemaker, Phys Rev B **52**, 15872 (1995)

[2] D. White and E. N. Lassettre, J. of Chem. Phys. **32**, 72 (1960)

[3] I. F. Silvera, Rev. of Modern. Phys. **52**, 393 (1980).

[4] M. Mohnke and W. Saffert, *Gas Chromatography*, edited by M. Swaay (Butterworths, London, 1962), p. 216.

[5] F. Katsaros, et al., Physica B **234**, 402 (1997).

FIRST-PRINCIPLES COMPUTATIONAL AND NEUTRON SCATTERING STUDY OF PROTONIC CONDUCTORS

Fuel cells, which produce electricity via hydrogen oxidation to water, have emerged in the last decade as one of the key technologies for meeting the world's energy needs well into the 21st century. Solid-oxide fuel cells (SOFCs) are the most promising among the many different types of fuel cells being developed. However, the required high operating temperature of an SOFC places stringent requirements on its component materials. Potential candidates to replace the oxygen-conducting electrolyte used in current SOFCs include the perovskite-based high-temperature protonic conductors (HTPCs), since switching from anionic to protonic conduction can lower the practical operating temperature from 1300 K to around 1000 K.

We undertook neutron vibrational spectroscopy (NVS) measurements of various HTPCs (namely, $SrCeO_3$ and $SrZrO_3$ aliovalently doped with different rare earth cations) in order to probe the bonding potentials experienced by the residual protons incorporated as OH^- species via steaming. At high temperatures, these protons migrate from site to site, giving rise to protonic conduction. The NVS measurements revealed the existence of dopant-related perturbations to the bending-mode energies of OH^- in $SrCe_{0.95}M_{0.05}H_xO_{3-\delta}$ (M = Sc, Ho, and Nd), confirming the trapping effects of the

dopants. The bending-mode energy could be correlated with the size of the dopant cation, generally increasing for smaller cations. NVS measurements of $SrZr_{0.95}M_{0.05}H_xO_{3-\delta}$ (M = Sc, Y, and Nd) indicated differences in the OH^- bending-mode energies between the cerates and zirconates. These differences reflect changes in the lattice potential experienced by the protons, which ultimately effects the proton jump rates and therefore the performance of these materials for use in fuel cells.

An understanding of the dynamics of the undoped perovskites is the first step towards a comprehensive picture of the protonated doped materials. To explore this in more detail, we performed *ab initio* total-energy calculations using the CAmbridge Serial Total Energy Package (CASTEP). We calculated the Q = 0 phonons in the primitive unit cell (i.e., $Zr_4Sr_4O_{12}$) of undoped strontium zirconate and compared with the experimental density of states (DOS) at room temperature, as shown in Figure 1. While at low energies, the calculated modes are almost at the same energies as observed modes, at high energies, we overestimate the energies of the modes by about 10%. However there is still a one-to-one correspondence between the main experimental and calculated spectral
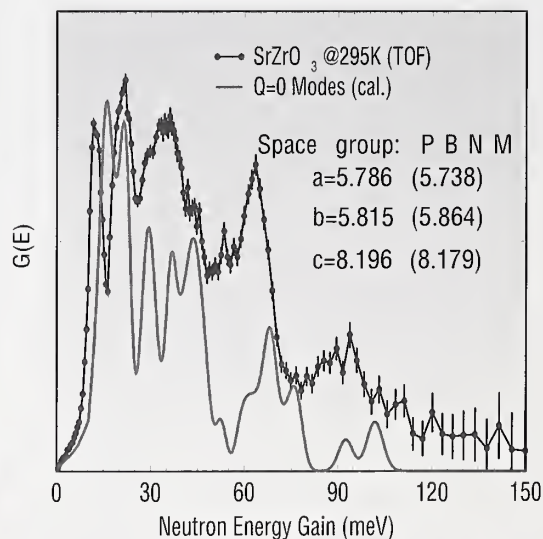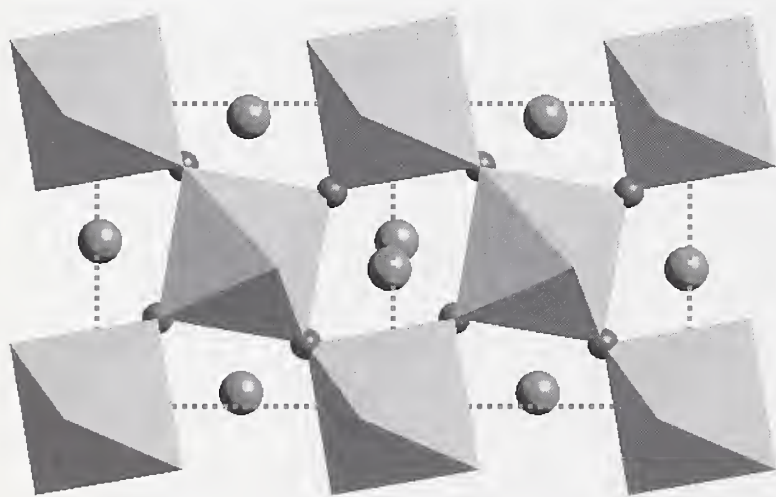
FIGURE 1. LEFT: A view of the structure of undoped $SrZrO_3$ in the [001] direction. RIGHT: Vibrational spectra for $SrZrO_3$ measured by neutron time-of-flight spectroscopy. The space group and the lattice parameters are also shown. Numbers in parentheses are the theoretical values. The lower solid line is the DOS of the Q = 0 phonons calculated from first principles.

**T. Yildirim, T. J. Udovic, C. Karmonik, and
D. A. Neumann**
NIST Center for Neutron Research
National Institute of Standards and Technology
Gaithersburg, MD 20899

features, allowing us to identify the modes observed by our NVS measurements.

In order to model the dynamics of protons trapped in Sc-doped $SrZrO_3$, we replaced one of the Zr atoms in the $\sqrt{2} \times \sqrt{2} \times 1$ supercell by (Sc + H), which yields a cell formula $Sr_8Zr_7ScHO_{24}$ (See Figure 2). We performed calculations for protons at either the "undoped" (U) or "doped" (D) sites. Even though the MO_6 octahedra are quite rigid, the distortions due to the presence of the proton at these sites are quite large.

These distortions are also reflected by the vibrational spectrum of the proton. The two tangential OH- bending modes depend strongly on the proton siting. At the Sc site, the lowest tangential mode is found at 122.9 meV. However at the Zr site, the mode is much softer at 88.5 meV. Interestingly, we observe new features in our NVS spectra at these energies upon proton addition. To further investigate this effect, we performed "embedded cluster" calculations in which the vibrational spectrum of the $H-MO_6$ cluster is calculated while all other atoms are kept at their equilibrium positions. The similarity between experiment and the calculated spectrum from $H-ZrO_6$ + $H-ScO_6$ clusters suggests that the mode observed near 120 meV is due to protons trapped at the Sc sites

while some portion of the peak near 80 meV is due to protons at the undoped sites. Thus NVS can be used to determine the hydrogen occupancy of the various sites.

For a better understanding of the protonic conduction in these materials, we calculated the total energy of the system as the proton migrates from Zr to Sc sites. We found that the doped site has a much lower energy (-1.13 eV) than the undoped site. The two sites are separated by an energy barrier of 1.5 eV. Hence, we expect that most of the protons are trapped at the dopant site. This is primarily because the proton prefers to be closer to the Sc cation, which has a charge of +3 compared to +4 for Zr. Yet, one also has to consider steric effects; i.e., if the dopant cation has a larger radius, then the proton may prefer to occupy the Zr site, despite the larger Coulomb interaction. Thus these calculations indicate that the protonic transport is sensitive to the competition between short-range repulsive and Coulomb interactions, and suggest that the use of a large dopant cation is one important step in developing a HTPC with increased protonic conductivity. We are currently testing the usefulness of the calculated proton potentials for predicting the protonic diffusional motions observed experimentally via quasielastic scattering measurements.
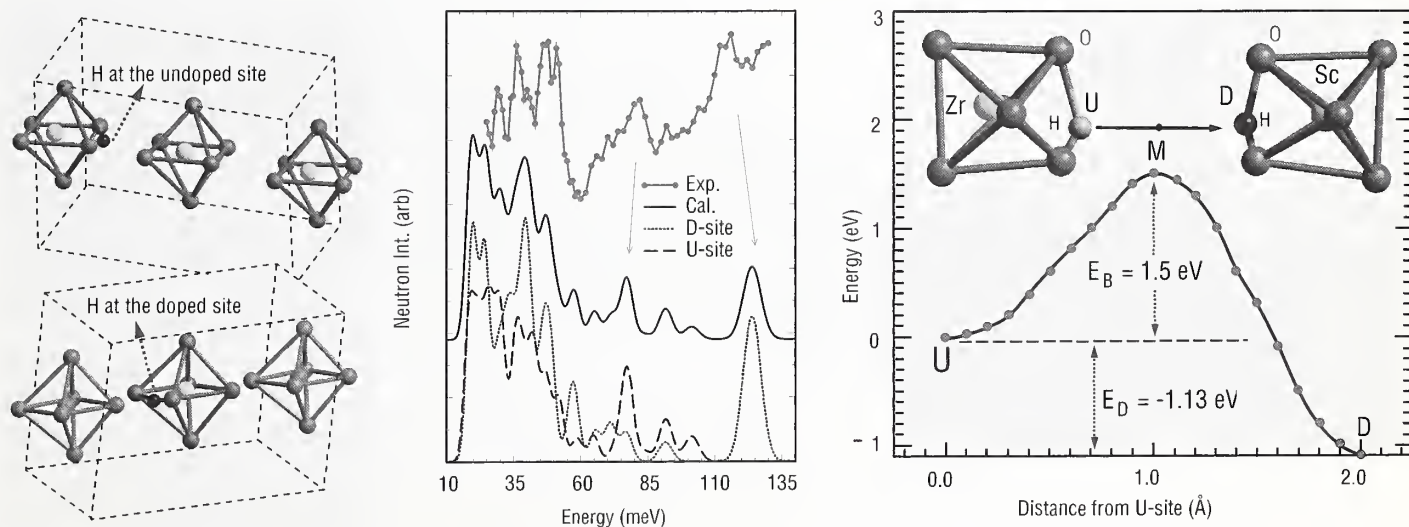
FIGURE 2. LEFT: Optimized structures when the proton is trapped at the undoped site (top) and at the doped site (bottom). **MIDDLE:** Comparison of the neutron vibrational spectrum of $SrCe_{1-x}Sc_xH_yO_3$ (top) and $SrZr_{1-x}Sc_xH_yO_3$ (calculated). Dashed and dotted lines shown at the bottom are the contributions from the $H-MO_6$ clusters, where M = Zr (undoped site) and Sc (doped site), respectively. **RIGHT:** Potential energy of the crystal as the proton migrates from the undoped site (U) to the doped site (D).

MAGNETIC TRAPPING OF ULTRACOLD NEUTRONS

The first successful demonstration of magnetic trapping of neutrons was performed this past year at NIST [1]. The techniques developed should lead to improved precision in the measurement of the neutron beta-decay lifetime, thereby expanding our knowledge of the weak nuclear force and our understanding of the creation of matter during the Big Bang.

Magnetic traps are formed by creating a magnetic field minimum in free space. The confining potential depth is determined by the magnetic moment of the neutron and the difference between the magnitude of the field at the edge of the trap and at the minimum. A neutron in a low-field-seeking state (one with its magnetic moment anti-aligned with the local magnetic field vector) feels a force pushing it towards the trap minimum and will remain confined within the trapping region.

In order to load a neutron into a static conservative trap, its energy must be lowered while it is in the potential well. We rely on a loading technique that employs the "superthermal process" [2]. Superfluid helium fills the trapping region and serves as a neutron scattering medium. A neutron with kinetic energy near 11 K (where the free neutron and Landau-Feynman dispersion curves cross) that passes through the helium can lose nearly all of its energy in a single scattering event. Neutrons that scatter to energies less than the trap depth (1 mK) and in the appropriate spin state are trapped. Neutrons in this energy range are called ultracold neutrons (UCN).

Isotopically pure superfluid helium is contained in a tube located inside the superconducting magnet and centered axially within its trapping field (see Figure 1). The superconducting magnet, trapping region, and other key parts of the apparatus reside within a cryogenic dewar. The incident neutron beam is collimated, passes through the trapping region, and is absorbed by the beam stop. As the beam traverses the trapping region, about 1% of the neutrons scatter in the helium. Some of these neutrons are trapped and the remainder are absorbed by shielding materials that surround the helium. Low-field-seeking UCN are trapped and remain in the trapping region until they decay.
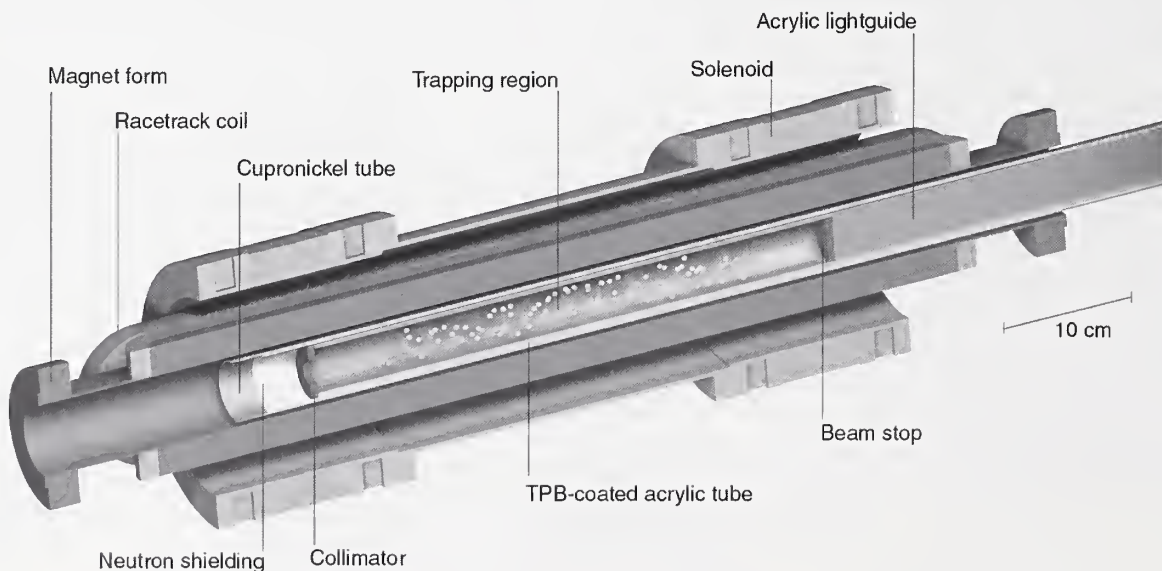
FIGURE 1. Half section view of the neutron trapping apparatus. A beam of cold neutrons enters from the left, is collimated, passes through the trapping region and is absorbed at the rear. Scattered neutrons (yellow) in the low-field-seeking spin state and with energy below the trap depth are magnetically confined. Electrons from neutron beta-decay create EUV scintillations in the superfluid helium which are wavelength shifted to the visible and transported to the photomultiplier (to the right).

P. R. Huffman, M. S. Dewey and F. E. Wietfeldt
Ionizing Radiation Division
National Institute of Standards and Technology
Gaithersburg, MD 20899-8461

**C. R. Brome, J. S. Butterworth, S. N. Dzhosyuk,
C. E. H. Mattoni, D. N. McKinsey and J. M. Doyle**
Department of Physics, Harvard University
Cambridge, MA 02138

R. Golub and K. Habicht
Hahn-Meitner-Institut
Berlin, Germany

K. J. Coakley
Statistical Engineering Division
National Institute of Standards and Technology
Boulder, CO 80303

G. L. Greene and S. K. Lamoreaux
Los Alamos Neutron Science Center
Los Alamos National Laboratory
Los Alamos, NM 87545

The trapped neutrons are detected when they decay. When a trapped neutron decays (into an electron, proton and anti-neutrino), the resulting high-energy electron travels through the helium leaving a trail of ionized helium atoms. These ions quickly combine with neutral helium atoms to form metastable diatomic molecules. Most of these molecules decay within 10 ns, emitting a pulse of light in the extreme ultraviolet (EUV), $\lambda \sim 70-90$ nm. This pulse of scintillation light is the signal of a neutron decaying in the trap.

In an experimental run, the cold neutron beam is allowed to pass through the trapping region, after which the beam is blocked and pulses of light are counted. A background signal, with both constant and time-varying components obscures the trapped neutron signal. These backgrounds are subtracted by collecting data where the magnetic field is on during the initial loading phase, so that

UCN are confined by the trap and subtracting data where the magnetic field is off initially, so that no neutrons are trapped. Equal numbers of each data set were taken, pooled and subtracted to give the background subtracted data.

Two sets of background subtracted data were collected: set I with a trap depth of 0.76 mK (Figure 2a) and set II with a lower trap depth of 0.50 mK (Figure 2b) due to problems with the magnet. For each set, the pooled background subtracted data are modeled to extract the amplitude and lifetime of the decaying neutron signal. The best fit values for the initial counting rates combined with the measured detection efficiency gives $N_I = 560 \pm 160$ and $N_{II} = 240 \pm 65$. Calculations using the known beam flux, trap geometry and the theory of the superthermal process predict $N_I = 480 \pm 100$ and $N_{II} = 255 \pm 50$, in good agreement with the measured values. The best fit value for the trap lifetime, $\tau = 750^{+330}_{-200}$ s is consistent with the presently accepted value of the neutron beta-decay lifetime of 886.7 ± 1.9 s [3].

To verify that our signal is in fact due to trapped neutrons, we doped the isotopically pure ^{4}He with ^{3}He at a concentration of 2×10^{-7} ^{3}He/^{4}He. This amount of ^{3}He absorbs the trapped neutrons in less than 1 s without affecting anything else in the experiment (less than 1% of the cold neutron beam is absorbed by ^{3}He). The data (Figure 2d) is modeled with the lifetime fixed at $\equiv 750$ s, yielding $N_{3He} = 53 \pm 63$, consistent with zero. This confirms that our signal is due to trapped neutrons.

Magnetic trapping of neutrons is a new technique that should allow a higher precision measurement of the neutron lifetime, and offers the prospect of precision much greater than the current limit of one part in 10^3. In order to realize the potential of this technique, we are in the process of improving our apparatus in many ways, including increasing the size and depth of the trap. We expect to make a competitive neutron lifetime measurement in the near future.

FIGURE 2. Counting rate as a function of time after the neutron beam is turned off (pooled background subtracted data). (a) Trapping data set I, $N_I = 560 \pm 160$, (b) Trapping data set II, $N_{II} = 240 \pm 65$, (c) Combined trapping signal, $\tau = 750^{+330}_{-200}$ s, (d) Combined ^{3}He data, $N_{3He} = 53 \pm 63$.

REFERENCES:

[1] P. R. Huffman et al. (Submitted to Nature).

[2] R. Golub, D. Richardson, and S. K. Lamoreaux *Ultra-Cold Neutrons* (Adam Hilger, Bristol, UK 1991).

[3] Particle Data Group, "Review of Particle Physics," Eur. Phys. J. C **3**, 1 (1998).

CHARGE DISPROPORTIONATION AND MAGNETIC ORDERING IN CaFeO$_3$

Transition metal oxides adopting the perovskite crystal structure (or one of its relatives) have occupied a place in the scientific limelight for nearly fifty years now. Beginning with the discovery of ferroelectricity in BaTiO$_3$, following World War II, the dielectric properties of perovskites have been extensively studied over this entire period. Today perovskite dielectrics, due to their widespread usage in telecommunication, are still extensively studied. The discovery of superconductivity first in doped BaBiO$_3$, and later in the cuprates, such as YBa$_2$Cu$_3$O$_{7-X}$, triggered an unprecedented avalanche of scientific activity in the late 1980's and early 1990's. More recently, phenomena such a collosal magnetoresitance, (CMR), charge, orbital and spin ordering, and phase separation in the manganate perovskites, (Ln$_{1-x}$A$_x$)MnO$_3$ (Ln = lanthanide ion, A = alkaline earth ion) have captured the imagination of the condensed matter scientific community.

Ultimately the electronic and magnetic properties of a material depend upon the behavior of the outermost or valence electrons. In a first row transition metal oxide the valence electrons are shared, though not equally, between the 3d orbitals of the transition metal ion and the 2p orbitals of oxygen. In compounds with the perovskite structure the oxygen atoms are arranged in an octahedral geometry about the transitional metal ion, each oxygen is then shared by two transition metal ions to form a three dimensional network of corner sharing MO$_6$ octahedra. The octahedral coordination removes the energetic degeneracy of the 3d orbitals, forming the familiar triply degenerate t$_{2g}$ and doubly degenerate e$_g$ set of orbitals. The e$_g$ orbitals point directly at the oxygen ligands to form a strongly antibonding σ* bond. In contrast, the t$_{2g}$ orbitals have a smaller overlap with the oxygen 2p orbitals, which leads to a weakly antibonding π* band. If this covalent bonding interaction between the transition metal and oxygen is weak, the valence electrons are localized and a magnetic insulator is typically observed. If we increase the strength of the interaction sufficiently, either by increasing the electronegativity of the transition metal ion or the spatial overlap of the metal 3d and oxygen 2p orbitals, partial delocalization of the valence electrons can occur. Frequently, this leads to metallic conductivity. In a number of transition metal oxides the metal-oxygen interaction strength is such that delocalized

FIGURE 1. The low temperature structure of CaFeO$_3$. The green spheres depict the calcium ions. The other shaded objects represent iron centered octahedra, where an oxygen atom can be found at each vertex and an iron atom at the center of each octahedron. The purple and blue objects represent Fe^{3+} centered and Fe^{5+} centered octahedra respectively.

electrons and metallic conductivity are seen at higher temperatures but give way to a magnetically ordered, insulating ground state upon cooling.

LaMnO$_3$, SrFeO$_3$ and CaFeO$_3$ are isoelectronic, they each have an electronic configuration of t$_{2g}$^{3}e$_g$^{1}. According to the Jahn-Teller theorem, the presence of a single localized electron in the doubly degenerate e$_g$ set of orbitals is not a stable situation. LaMnO$_3$ responds to this instability by undergoing a cooperative Jahn-Teller distortion of the MnO$_6$ octahedra, producing two long and four short Mn-O bonds, Thereby, removing the degeneracy of the e$_g$ orbitals. SrFeO$_3$ takes a different approach, by delocalizing its e$_g$ electrons to form a σ* band. The contrasting behavior of these two materials can be understood in terms of the strength of the metal-oxygen

Patrick M. Woodward
Department of Chemistry
Ohio State University
Columbus, OH 43210

David E. Cox and Evagalia Moshopoulou
Department of Physics
Brookhaven National Laboratory
Upton, NY 11973

Arthur W. Sleight
Department of Chemistry
Oregon State University
Corvallis, OR 97331-4003

interaction. Contrasting $LaMnO_3$ to $SrFeO_3$, the oxidation state of the transition metal increases from +3 to +4, which leads to an increase in the metal-oxygen interaction strength, increasing the width of the σ^* band and stabilizing a metallic ground state. Since they both contain Fe^{4+}, one might expect that $CaFeO_3$ and $SrFeO_3$ would behave very much alike. However, Ca^{2+} is smaller than Sr^{2+}, which causes a tilting of the FeO_6 octahedra to satisfy the valence requirements of calcium. This seemingly subtle distortion has several important consequences. The Fe-O-Fe bond is distorted away from the linear geometry observed in $SrFeO_3$ (the Fe-O-Fe angle is 158° in $CaFeO_3$). This reduces the spatial overlap of the Fe e_g and O 2p orbitals and the width of the σ^* band, decreases. The reduction in bandwidth triggers an electron localization that occurs just below room temperature (290 K). Once electron localization occurs, a cooperative Jahn-Teller distortion to the $LaMnO_3$ crystal structure is expected.

However, $CaFeO_3$ refuses to conform with expectations. Instead $CaFeO_3$ undergoes a charge disproportionation (CD), $2Fe^{4+}$ $(t_{2g}^3 e_g^1) \rightarrow Fe^{3+} (t_{2g}^3 e_g^2) + Fe^{5+} (t_{2g}^3 e_g^0)$. Evidence for a CD in $CaFeO_3$ was first proposed over 20 years ago, based on Mössbauer studies [1]. However, crystallographic confirmation of this rare phenomenon has proven elusive. Through the combined use of synchrotron x-ray (X7a-NSLS) and neutron powder diffraction (BT-1 at NCNR), we have elucidated the crystal structure of $CaFeO_3$ in its CD state for the first time. The resulting structure (Figure 1) clearly shows the presence of two chemically and crystallographically distinct Fe sites. The average Fe-O bond length about the "Fe^{5+}" site is 1.872(6) Å, while the same distance about the "Fe^{3+}" site is 1.974(6) Å. The ordered arrangement of Fe^{3+}/Fe^{5+} is such that each Fe^{3+} is surrounded by six Fe^{5+} ions, and vice versa (NaCl or G-type ordering), optimizing the Coulomb stabilization of the CD state. Alternately, the CD process can be viewed as the condensation of a breathing phonon mode.

In addition to electronic properties, there has long been both technological and fundamental scientific interest in the magnetic properties and interactions in perovskites containing transition metal ions. Goodenough's study of the various antiferromagnetic structures observed in the $(La_{1-x}Ca_x)MnO_3$ system was vital in the development of the Goodenough-Kanamori rules of superexchange [2]. These rules correctly predict an A-type antiferromagnetic structure for $LaMnO_3$. Using the same rules, we would expect $CaFeO_3$ to have a simple ferromagnetic ground state. Perhaps not surprisingly, our investigation showed that again $CaFeO_3$ defies expectations. Low temperature neutron powder diffraction data reveals instead an incommensurate antiferromagnetic ground state ($T_N \approx 120$ K). Analysis of the data shows the magnetic structure to be either a screw spiral or a sinusoidal amplitude-modulated structure. In either case, it would appear that a long range AFM interaction (probably between next-neighbors) is present in addition to the nearest neighbor FM superexchange interaction.

REFERENCES

[1] M. Takano, N. Nakanishi, Y. Takeda, S. Naka and T. Takada, Mater. Res. Bull. **12**, 923 (1977).

[2] J. B. Goodenough, *Magnetism and the Chemical Bond*, Interscience, New York (1963).

BOND VALENCE ANALYSIS OF RUTHENATES

Bond valence analysis allows us to evaluate, for any compound whose bonding scheme is known or assumed, the bond distances that the atoms would form in an ideal structure in which all atomic valences are exactly balanced. In a significant number of cases this information is sufficient to make accurate predictions about the real crystal structure of the compound.

The bond valence method is based on two concepts that can be stated in the following way.

(i) A bond valence $v_{ij} = v_{ji}$ is assigned to a bond between atoms i and j, of valences $V(i)$ and $V(j)$, so that

$$\sum_{1}^{n(i)} {}_j v_{ij} = V(i) \quad \text{and} \quad \sum_{1}^{n(j)} {}_i v_{ji} = V(j) \qquad (1)$$

where $n(i)$ and $n(j)$ are the number of atoms in the coordination spheres of i and j, respectively. This principle of local valence balance is a generalization of Pauling's principle of local charge balance in ionic crystals, and is known as the *valence sum rule* [1].

(ii) The sum of the bond valences around any loop in the structure, taken with alternating signs, is equal to zero

$$\sum_{loop} v_{ij} = 0 \qquad (2)$$

Equation (2) expresses the mathematical conditions that result in the most regular distribution of the valences among the bonds in a structure and is known as the equal valence rule [1]. The system of equations (1) and (2) allows us to evaluate the valences of all the individual bonds if we know how the atoms are bonded together in a structure [2]. The description of atomic bonding in terms of bond valences is useful because the length d_{ij} of a bond between atoms i and j is a function only of the bond valence n_{ij}. The relationship between these two quantities is expressed by the empirical formula

$$d_{ij} = R_{ij} - 0.37 \ln v_{ij} \qquad (3)$$

where the bond valence parameter R_{ij} depends on the nature and the oxidation states of atoms i and j forming the bond, and expresses the length of a bond of unit valence. Values of R_{ij} can be evaluated from the bond distances of known structures and are tabulated for most chemical species [3,4]. By means of equations (1-3) we may evaluate the expected bond lengths for any known atomic configura-
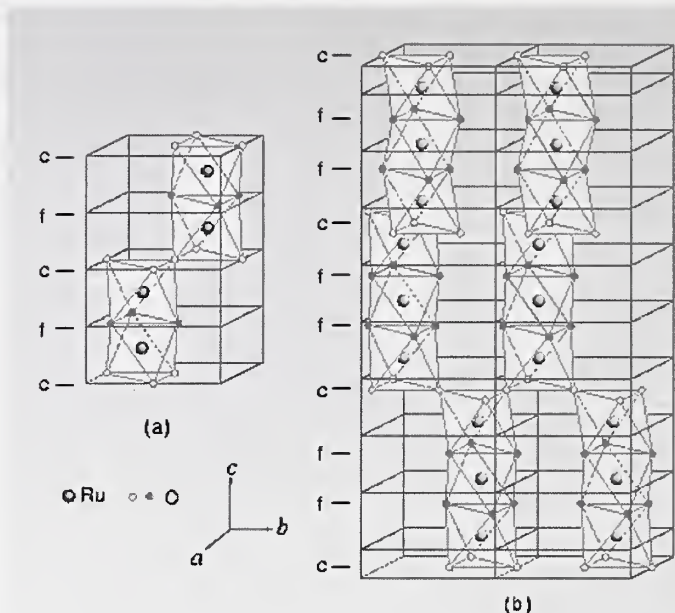
FIGURE 1. Schematic representation of (a) the 4-layer structure of $TRuO_3$ (T = 0.875 Ba + 0.125 Sr); and (b) the 9-layer structure of $BaRuO_3$. For clarity only the Ru and O atoms are shown in the figure. The symbols c and f indicate the layers on which the RuO_6 octahedra share corners and faces, respectively.

tion. These distances satisfy exactly the valence requirements of the atoms and, in general, differ significantly from those determined experimentally. The discrepancies are in some cases due to the electronic behavior of particular cations, which may cause distortions not accounted for by the bond valence model (for example, lone pair distortions around cations such as Bi^{3+} and Pb^{2+}, or Jahn-Teller distortions around Mn^{3+} and Cu^{2+}). In the majority of cases, however, the bond lengths calculated with equations (1-3) are incommensurate under the constraints imposed by the crystal geometry, and have to be stretched or compressed in order to fit them into a particular configuration. Since these changes introduce strains into the structure, the process of adapting the theoretical model to the requirements of a space group symmetry must be carried out in such a way that the violations of the bond valence sum rule and of the equal valence rule are kept as small as possible. We have recently applied the concepts discussed above to the determination of the crystal structures of $TRuO_3$ (T = 0.875Ba + 0.125Sr) [5] and $BaRuO_3$ [6], using initially only the information obtained from the indexing of the neutron diffraction patterns of these materials (i.e. crystal system symmetry and lattice parameters), and ignoring any

A. Santoro
NIST Center for Neutron Research
National Institute of Standards and Technology
Gaithersburg, MD 20899-8562

I. Natali Sora
INFM and Department of Physics and Chemistry
University of Brescia
25123 Brescia, Italy

Q. Huang
Department of Physics
University of Maryland
College Park, MD 20742

other structural details obtained in the experimental work. Since T^{2+} and Ba^{2+} have ionic radii similar to that of O^{2-}, we may expect that the structures of $TRuO_3$ and $BaRuO_3$ are built with some sphere packing mechanism. This assumption is corroborated by the fact that in both cases the a-parameter calculated from the average r of the ionic radii of A and O (A = T, Ba) for the composition AO_3 is in good agreement with the experimental values, and by the fact that the ionic radius of Ru^{4+} is quite close to the radius of the octahedral void formed by the close packing of oxygen anions. The periodicity n of the stacking sequences of the AO_3 layers in the vertical direction of the c-axis, evaluated with the formula $n = c/(2r\sqrt{2/3})$, shows that $TRuO_3$ and $BaRuO_3$ have 4- and 9-layer structures, respectively, in which the RuO_6 octahedra are related to one another as indicated in Figures 1a and 1b.

In order to fit this configuration, the theoretical bond lengths calculated with equations (1-3) have to be changed, and in particular the A-O bonds have to be compressed, on the average, and the

Ru-O bonds have to be stretched. This process of relaxation of the initial model is carried out by modifying the structural parameters obtained from sphere packing geometry in such way that the violations of equations (1) and (2) are contained within reasonable bounds [7]. The results of the bond valence analysis of $BaRuO_3$ are reported in Table 1, where they are compared with the corresponding values determined experimentally. Similar results, reported in reference [5], were obtained for $TRuO_3$. The agreement between the observed and calculated structures is quite good for both compounds, and the differences between bond distances are well within 0.02Å. This result proves that, at least in favorable cases, the bond valence method may yield an accurate model of the structure without requiring more information than that needed to index a powder pattern. More importantly, however, it shows that the need to satisfy the valence requirements of the atoms with an acceptably regular distribution of the bond valences, is the driving force in determining the magnitude and the direction of the atomic shifts allowed by the symmetry, and that, as a consequence, non-bonded metal-metal and oxygen–oxygen interactions do not play an important role in the way in which the structures of these ruthenates are built. In particular, the shifts that pull together the oxygen atoms forming the shared faces of the RuO_6 octahedra (thus providing a shielding effect to Ru-Ru interactions) are specifically designed to improve the local valence balance of the Ru and O atoms involved in the Ru-O bonds. Application of the method to structural types other than perovskites is now under consideration.

Models of the Structure of BaRuO$_3$ (R$\bar{3}$m).

	1	2	3	4
Lattice parameters (Å) and atomic positions				
a	5.754	5.754	5.747(1)	0.007
c	21.142	21.626	21.602(1)	0.024
x	1/6	0.1769	0.1769(1)	0.0000
z_1	1/9	0.1087	0.1082(1)	0.0005
z_2	2/9	0.2185	0.2175(1)	0.0010
z_3	7/18	0.3844	0.3829(1)	0.0015
Bond distances (Å)				
Ba(1)-O(1)	2.877	2.877	2.8733(1)	0.004
-O(2)	2.877	2.938	2.926(2)	0.012
Ba(2)-O(1)	2.877	2.988	3.002(2)	-0.014
-O(2)	2.877	2.882	2.880(2)	0.002
-O(2')	2.877	2.957	2.945(3)	0.012
Ru(1)-O(1)	2.034	2.001	2.005(2)	-0.004
Ru(2)-O(1)	2.034	1.995	1.974(1)	0.021
-O(2)	2.034	1.995	2.007(2)	-0.012

Note. 1, commensurate structure derived from sphere packing geometry; 2, model obtained with the relaxation process discussed in the text; 3, experimental results; 4, difference between calculated and observed values. The theoretical bond distances calculated with equations (1-3) are: T-O = 2.932Å, Ba-O = 2.948Å and Ru-O = 1.984Å.

REFERENCES

[1] D. Brown, Acta Cryst. **B48**, 553 (1992).

[2] M. O'Keeffe, Structure and Bonding **71**, 161 (1989).

[3] D. Altermalt and I. D. Brown, Acta Cryst. **B41**, 240 (1985); I. D. Brown and D. Altermalt, Acta Cryst. **B41**, 244 (1985).

[4] N. E. Breese and M. O'Keeffe, Acta Cryst. **B47**, 192 (1991).

[5] A. Santoro, I. Natali Sora and Q. Huang, J. Solid State Chem. **143**, 69 (1999).

[6] A. Santoro, I. Natali Sora and Q. Huang, (in preparation)

[7] I. D. Brown, Z. Kristall. **199**, 255 (1992).

RESIDUAL STRESSES IN COLD-COILED HELICAL AUTOMOMOTIVE SPRINGS

Most front-wheel-drive automotive suspension systems use helical springs. The process chosen to produce these is, like any other engineering dilemma, determined by quality, performance, price, environmental issues, etc. Ford Motor Company has developed a potentially cost saving cold-coiling process in which less time is spent treating spring metal at elevated temperatures. The pronounced residual stress pattern within the as-cold-coiled spring is undesirable for its unpredictable effect on fatigue and corrosion behavior, and Ford evaluates these stresses by X-ray measurements of the surface stress field along with modeling of the internal stresses. The success of these at-home procedures requires an independent verification of the actual residual stress field over the cross-section of the original wire stock. The only available well-established method for this is neutron diffraction, and that is where NCNR expertise comes into play.

Generally, there are two ways to coil a spring: hot coiling and cold-coiling. Hot coiling implies that the spring is wound from stock at or above the recrystallization temperature. The strength and fatigue resistance are controlled afterwards by an appropriate heat treatment. Cold-coiling means that the helical winding takes place at a low temperature after the spring has been hardened and tempered. Cold-coiling allows the high temperature heat treatments to take place on the bar stock, which is easier to handle then the coiled end-product. The resulting residual stresses can be essentially eliminated by a relatively low temperature tempering treatment following the cold coiling.

The idea is to measure the residual stress field in a number of specimens that represent various stages of the production process. Using neutron diffraction one can determine the effect of the prior processing on the residual stress state of that particular stage in the process. Of equal importance, these measurements can serve to verify well established elasto-plastic models that are being used to predict the formation of residual stress. Finally one can look for a way to correlate the residual stress at the surface to the stress field as a whole.

We have looked at three cold-coiled springs. The first spring is an as-cold coiled spring. The second one is cold-coiled followed by a relatively low temper. The third one is identical to the second one, but in addition to being tempered the spring has been compressed to the point where the length of the spring is equal to the
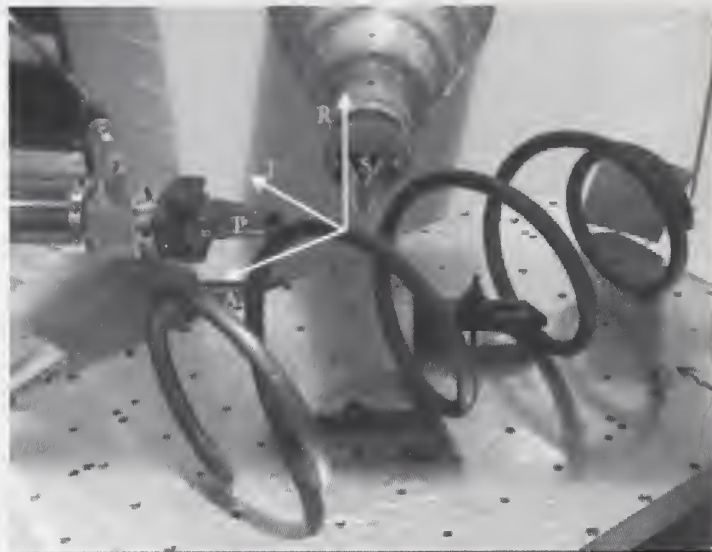
FIGURE 1. Experimental setup. The three arrows indicate three directions of measured lattice spacing with respect to the specimen: A = axial, R = radial, T = tangential. In the current configuration, the spacing of planes whose normal is parallel to T is being measured. The sampling volume is defined by the primary aperture P and secondary aperture S, respectively.

number of windings times the wire thickness. After this the spring was allowed to relax. A small part of this torsion strain is in the plastic region, so this spring is slightly shorter than all the others. In the automotive industry this process is know as "bulldozing".

The measurements were carried out on the Double Axis system for Residual stress, Texture and Single crystal analysis (DARTS) at beam tube 8 (BT-8) in the NIST Center for Neutron Research. This instrument is specifically designed for residual stress measurements, and to that effect is equipped with very accurately positioned apertures as is shown in Figure 1.

For these experiments the apertures were chosen to allow a sampling volume of $2 \times 2 \times 2$ mm^3. The residual stress in the three springs across the cross-section of the originally 14 mm thick wire stock was determined by detecting the diffracted monochromatic neutron intensity with a position sensitive detector. The neutron wavelength was chosen such that the [211] Fe planes would scatter diffracted intensity over approximately 90°. The specimen was rotated and translated in this geometry, such that the sampling volume was scanned across this cross-section allowing the elastic (residual) strain to be determined from the small shifts in scattering angle. This was done in three mutually perpendicular directions.

Jiri Matejicek and Paul C. Brand
NIST Center for Neutron Research
National Institute of Standards and Technology
Gaithersburg, MD 20899-8562

A. R. Drews
Ford Research Laboratory
Dearborn MI 48121
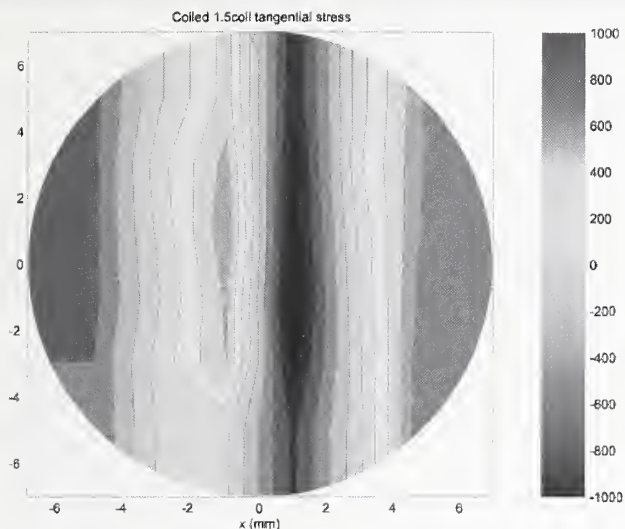
FIGURE 2. Contour map of the residual stress in the direction of the length of the coiled bar stock, plotted on the bar stock cross-section. With reference to Figure 1, this is the tangential direction. This map represents the as-cold-coiled spring. The left and right side of the map represent the convex and concave sides respectively.

FIGURE 3. Same as Figure 2, these data representing the as-tempered spring. The data for the as-bulldozed spring, though not given here, look essentially the same.

These strain measurements allowed us to calculate the residual stress in three perpendicular directions from the equations published by Allen *et al.* [1] in each of the three specimens. For every specimen, the stress free lattice parameter was determined on the basis that the net force on the cross-section under investigation had to be zero.

From these experiments a set of interesting observations can be made. First is the notion that the residual stress pattern across the wire stock in the as-coiled spring is very pronounced and exactly matches what one would expect when a cylindrical bar is plastically bent into a hoop, a process much resembling helical coiling. With reference to Figure 2 we note essentially uniaxial residual stress in the length direction of the original wire stock. Through the diameter of the stock, the stress goes from highly compressive at the convex side to highly tensile at the concave side. On its way through the cross-section the stress level changes sign three times, while the maximum compressive and tensile stresses are −600 MPa and +800 MPa respectively. For the tempered and bulldozed specimens the pattern is roughly the same, albeit at a much reduced level. The stress range being from −170 to +160 MPa as depicted in Figure 3.

The uncertainties in these stress levels are around ±30 MPa. This means that the bulldozing process does not introduce addition residual stresses, a fact that can be well understood considering that the plastic deformation under pure torsion is essentially uniform and thus cannot contribute to the residual stress state.

These results will allow Ford to correlate their model predictions and X-ray residual stress measurements to the complete residual stress field. This constitutes a powerful tool in optimizing the parameters of the spring manufacturing process.

REFERENCES:

[1] A. J. Allen, M. T. Hutchings, C. G. Windsor, and C. Andreani: "Neutron Diffraction Methods for the Study of Residual Stress Fields" Advances in Physics, **34**, 445-473 (1985).

THE NCNR NEUTRON
SPIN ECHO SPECTROMETER

The first experiments have been performed on the NCNR's Neutron Spin Echo (NSE) Spectrometer, which is the only spectrometer of its kind in the United States. This cold neutron spectrometer allows studies of dynamic processes in macromolecular systems that are relevant to, among others, polymer [1] and biomedical [2] sciences. It covers a time-scale of 0.01–100 ns and a length-scale of 2–200 Å with the equivalent of extremely high energy resolution and moderate Q-resolution. Unlike the other high-resolution inelastic instruments at the NCNR which measure in the energy domain, the NSE spectrometer measures, in the time domain, the real part of the intermediate scattering function, I(Q,t). This is done by using the neutron's spin precession in a magnetic field as a clock to determine the energy transfer in the scattering process.

The NSE spectrometer, developed in partnership with Exxon Research and Engineering and the Forschungszentrum Jülich in Germany [3], is located at the end position of the NG-5 guide. The guide is tapered horizontally and then deviated so that the spectrometer is out of the direct line of sight of the reactor core, thereby reducing the background and the radiation load on the sample region [4]. The taper is followed by a Neutron Velocity Selector (NVS), which transmits a $\Delta\lambda/\lambda = 10\%$ FWHM band of neutrons to the spectrometer. The last element of the guide is a transmission polarizer [5], which produces a polarized beam of neutrons with spin anti-parallel to the beam direction for wavelengths greater than 5 Å. The neutrons precess, from the first $\pi/2$-flipper (1) to the sample, through a phase angle that is determined by the time that the neutron spends in the solenoidal magnetic field (4) and the field integral along the neutron path. Near the sample, a π-flipper (2) rotates the spin by 180° around the vertical axis. If the solenoid on the second arm of the spectrometer provides the same field integral for the scattered neutron and if the scattering is elastic, the neutron will precess through the same phase angle as along the first arm and will end up with the original spin orientation at the final $\pi/2$ flipper (3). This $\pi/2$-flipper rotates the spin back into the horizontal plane. If the neutron is scattered quasielastically, it will precess a slightly different number of times in the second arm of the spectrometer and end up at the second $\pi/2$-flipper rotated by some angle that is proportional to the wavelength shift. The analyzer (7) projects the component of the neutron spin that is parallel to the field direction onto the detector.

Figure 2 shows the detector count rate as a function of current in the phase coil (5), which changes the field integral on one arm of the spectrometer. The field integrals for the first and second arms of the spectrometer are equal at the echo point where the amplitude is at a maximum, since for an elastic scatterer the neutrons all arrive at the analyzer in phase. As the phase current is changed, the neutron spins rotate away from the polarization axis of the analyzer (7) and the count rate is changed. The period of this oscillation is proportional to the mean wavelength. The envelope of the
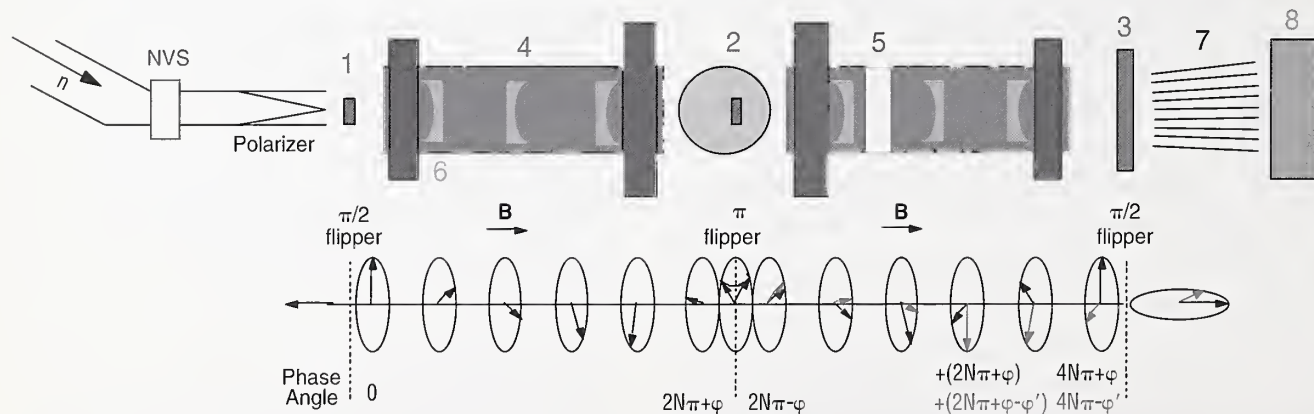
FIGURE 1: (Top) Schematic plan view of the NSE spectrometer. The numbers refer to spectrometer elements as described in the text. (Bottom) Changes of neutron spin orientation passing through the spectrometer elements for elastically (black) and inelastically (blue) scattered neutrons.

Nicholas Rosov
NIST Center for Neutron Research
National Institute of Standards and Technology
Gaithersburg, MD 20899-8562

Silke Rathgeber
NIST Center for Neutron Research
National Institute of Standards and Technology
Gaithersburg, MD 20899-8562
and
University of Maryland
College Park, MD 20742

Michael Monkenbusch
Institut für Festkörperforschung
Forschungzentrum Jülich GmbH
52425 Jülich
Germany

FIGURE 2: Phase scan of an echo for an elastic scatterer (Grafoil). A is the amplitude at the echo point; N_{ON} and N_{OFF} are counting rates with the π-flipper on and off, respectively, and the $\pi/2$ flippers off.
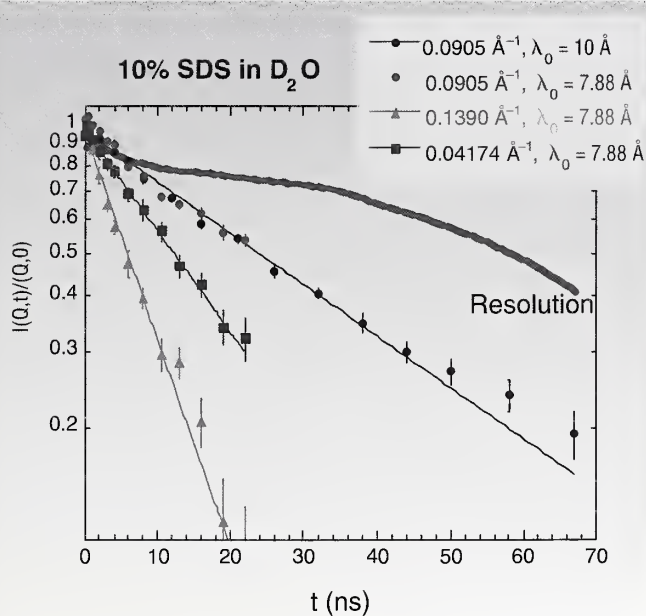
FIGURE 3: Normalized and resolution-corrected measurements of the intermediate scattering function at the indicated Q-values for 10% SDS in D_2O at room temperature. The resolution curve is a normalized measurement of an elastic scatterer (Grafoil) at 10 Å.

oscillations gives the wavelength distribution. The amplitude A is proportional to I(Q,t), which can be normalized by measuring the difference in intensity with the π-flipper on and off, $N_{ON}-N_{OFF}$. For the normalizing measurement, which is proportional to I(Q,t=0), the $\pi/2$-flippers are off since there is no precession of the neutrons in this configuration. Instrumental resolution effects are removed by dividing the normalized sample signal by the normalized values from an elastic scatterer.

We have also verified the operation of the correction elements (6) which allow non-axial and divergent neutrons to satisfy the echo condition. These are essential for operation at high fields. The value of the resolution amplitude at 25 ns in Figure 3 would be at least a factor of ten smaller without the contribution of the correction elements.

As an example of the science that is available through NSE, we have reproduced the measurements of Hayter and Penfold [6] on a micellar solution of 10% sodium dodecylsulfate (SDS) in D_2O. Figure 3 shows the normalized intermediate scattering function versus time at several Q values at, well below, and well above the interaction peak in the structure factor. The effective diffusion constant $D_{eff}(Q)$, obtained from I(Q,t) ; exp(-$D_{eff}(Q)Q^2$t), varies inversely with the structure factor, reaching a minimum at the structure factor peak, an effect analogous to DeGennes narrowing. As a result, in a dilute solution of interacting micelles, one may unambiguously separate the structure factor from the form factor, which may not be done with only a SANS measurement.

REFERENCES

[1] B. Ewen and D. Richter, Adv. Polym. Sci. **134**, 1 (1997)

[2] M-C. Bellissent-Funel et al, JACS **120**, 7347 (1998)

[3] M. Monkenbusch, R. Schäztler, and D. Richter. Nucl. Instr. Meth. Phys. Res. A **399**, 301–323 (1997).

[4] J. R. D. Copley, J. Neutron Res. **2**, 95 (1994).

[5] T. Krist, C. Lartigue, and F. Mezei, Physica B **180-181**, 1005 (1992).

[6] J. B. Hayter and J. Penfold. J. Chem. Soc. Faraday Trans. I **77**, 1851-1863 (1981).

SERVING THE SCIENTIFIC AND TECHNOLOGICAL COMMUNITIES

Providing neutron beam methods to the US research community is a central purpose of the NCNR. Intense neutron sources are scarce, as are the advanced instruments needed to fully exploit them. Expert scientists will always recognize opportunities to perform research with the most powerful tools available, so that the existence of the NCNR as the nation's premier reactor-based neutron facility stimulates considerable demand from the community. However, in order to foster the best possible science, many of our procedures and activities are designed to encourage researchers to learn more about our capabilities, and eventually to obtain instrument time through proposals and collaborations. The first instruments became operational in the NCNR guide hall in 1991, and a formal proposal system was started to accommodate users from universities, industry and government laboratories. Since then, the quantity and the diversity of research carried out at the NCNR has grown steadily, and the number of research participants (Figure 1) is now several times larger than it was just a few years ago.
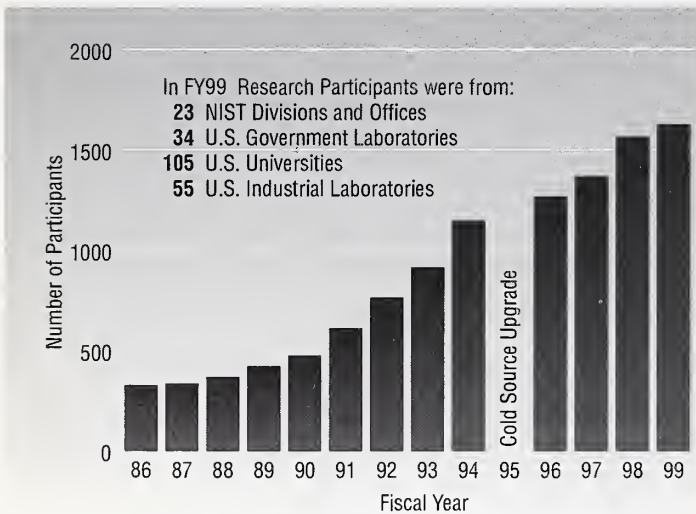
FIGURE 1. Research participants at the NCNR.

THE USER PROGRAM

NIST has always relied on advice from accomplished scientists to assist in formulating policy. The Program Advisory Committee (PAC) is the body primarily responsible for proposal review and recommending user policies for the NCNR, working closely with the Center's Director and staff. Its current membership includes Sanat Kumar (Penn State University, chair), Robert M. Briber (University of Maryland), Michael K. Crawford (DuPont), Dieter K. Schneider (Brookhaven National Laboratory), Thomas P. Russell (University of Massachusetts), Sunil K. Sinha (Argonne National Laboratory), Emile A. Schweikert (Texas A&M University), Laurence Passell (Brookhaven National Laboratory), and Gabrielle G. Long (NIST).

At their meeting in May 1999, the PAC made several recommendations for improving the current system. They felt that program proposals for longer-term projects had not had their intended effect of reducing the burden for external reviewers, and should be discontinued for the time being. Noting a potential for large increases in instrument time for biology-related proposals in the next few years, the addition of another PAC member with expertise in that area was recommended. The PAC discussed the results of a recent independent survey of user satisfaction, coordinated by Anne Mayes of MIT. Ideas for obtaining more feedback from users were also considered. Incidentally, Professor Mayes, the head of the NCNR User's Group, recently won the American Physical Society's Dillon Medal, partly for work carried out using NCNR instruments.

Most of the PAC meeting was devoted to proposal review. With the help of several written reviews for each proposal from selected experts, the PAC considered 151 proposals requesting 1138 instrument-days, and allocated 514 instrument-days to 95 proposals for SANS, reflectometry, SPINS, and time-of-flight instruments. The PAC usually meets twice a year, but because of a planned shutdown for cold source and reactor upgrades, only one meeting was held in 1999.
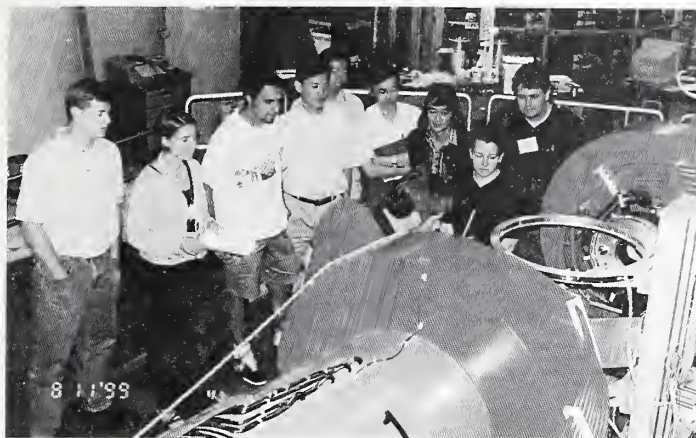
FIGURE 2: Nick Rosov explains the operation of the Neutron Spin Echo Spectrometer to summer school participants.

SUMMER SCHOOL ON METHODS AND APPLICATIONS OF NEUTRON SPECTROSCOPY

Each summer for the past five years, the NCNR has held a one-week school to introduce researchers to the methods of neutron scattering. Organized by senior staff members John Copley and Peter Gehring, the 1999 summer school was devoted to spectroscopy with neutrons, with an emphasis on the opportunities afforded by new instruments in the guide hall. Most of the 32 participants, chosen from almost 60 who applied, were graduate students and post-doctoral fellows. The curriculum consisted of lectures by NCNR staff and experts from other institutions, tours of the facility, and four three-hour, hands-on, sessions at instruments in the guide hall. Informal discussions among students and the resident staff were also an important part of the school's activities.

Beginning with lectures on the fundamental concepts of nuclear and magnetic scattering, the agenda turned to talks on applications of neutron spectroscopy to a wide range of research topics. Subsequent presentations covered the reactor and cold source, specific scattering techniques, computer modeling and ab initio calculations, and the operating principles of various spectrometers used in the experimental sessions. In the latter, students and staff used time-of-flight, backscattering, triple-axis, and neutron spin-echo spectrometers to measure, respectively, quasielastic scattering from water, rotational tunneling in solid methyl iodide, magnetic excitations in a geometrically frustrated antiferromagnet, and

coherent scattering from the time domain in a system of spherical micelles. (The last example is illustrated in the article on the Neutron Spin Echo Spectrometer.) The lecture materials will be placed on the NCNR website, in order to reach as wide an audience as possible.

THE CENTER FOR HIGH-RESOLUTION NEUTRON SCATTERING (CHRNS)

Supported by the National Science Foundation (NSF), CHRNS is a very important component of the user program. It operates a suite of three instruments, including a 30-m SANS machine, the SPINS triple-axis spectrometer, and a double-crystal, high-resolution SANS. The last of these is under construction. Approximately 40% of the instrument time allocated by the PAC goes to experiments carried out on CHRNS instruments. The NSF is currently reviewing the CHRNS renewal proposal, which requests support for upgrading existing instruments and including an improved 9-m SANS instrument within CHRNS. Approval would mean an increase of more than 50% in CHRNS' capacity to serve users.

COLLABORATIONS

Direct collaborations on specific experiments remain a common way for users to pursue their ideas using NCNR facilities, accounting for approximately 60% of the number of instrument-days. The thermal-neutron triple-axis spectrometers are mainly scheduled in this way. Most of the time reserved for NIST on these and all other NCNR instruments is also devoted to experiments that are collaborations with non-NIST users.

Another mode of access to the NCNR is through Participating Research Teams (PRTs). In this case, groups of researchers from various institutions join forces to build and operate an instrument. Typically, 50 to 75% of the time on the instrument is then reserved for the PRT, and the remaining time is allocated to general user proposals. For example, a PRT involving Exxon-Mobil, the University of Minnesota, Texaco R&D and NIST cooperates on the NG-7 30-m SANS instrument. Similar arrangements involving other PRTs apply to the horizontal-sample reflectometer, the high-resolution powder diffractometer, and the neutron spin-echo spectrometer.

INDEPENDENT PROGRAMS

There are a number of programs of long standing located at the NCNR which involve other parts of NIST, universities, industrial laboratories, or other government agencies.

The **Polymers Division** of the Materials Science and Engineering Laboratory has two major program elements at the NCNR. In the first, the purpose is to help the U.S. microelectronics industry in addressing their most pressing materials measurement and standards issues. In today's ICs and packages, the feature size on a chip is ever shrinking, approaching 250 nm, while the size of a polymer molecule is typically 5-10 nm. As feature size shrinks, the structure and properties of interfaces play an increasingly important role in controlling the properties of the polymer layers used in interconnects and packages. NIST scientists use both neutron reflectivity and other neutron scattering methods to characterize polymer/metal interfaces with regard to local chain mobility, moisture absorption, glass transition temperature and crystalline structure. In the second program element, the objective is to understand underlying principles of phase behavior and phase separation kinetics of polymer blends, both in the bulk and on surfaces, in order to help control morphology and structure during processing. SANS and reflectivity measurements in equilibrium, in transient conditions, and under external fields, provide essential information for general understanding as well as for specific application of polymer blend/alloy systems. Customers include material producers and users, ranging from chemical, rubber, tire, and automotive companies, to small molding and compounding companies. The focus of research on polymeric materials includes commodity, engineering and specialty plastic resins, elastomers, coatings, adhesives, films, foams, and fibers.

The **Exxon-Mobil Research and Engineering Company** is a member of the Participating Research Team (PRT) that operates, maintains, and conducts research at the NG-7 30m SANS instrument and the recently commissioned NG-5 Neutron Spin Echo Spectrometer. The mission is to use those instruments, as well as other neutron scattering techniques, in activities that complement research at Exxon-Mobil's main laboratories as well as at its affiliates' laboratories around the world. The aim of these activities is to deepen understanding of the nature of Exxon-Mobil's products and processes, so as to improve customer service and to improve the return on shareholders' investment. Accordingly, and taking full advantage of the unique properties of neutrons, most of the experiments use SANS or other neutron techniques to study the structure and dynamics of hydrocarbon materials, especially in the fields of polymers, complex fluids, and petroleum mixtures. Exxon-Mobil regards its participation in the NCNR and collaborations with NIST and other PRT members not only as an excellent investment for the company, but also as a good way to contribute to the scientific health of the nation.

The **Nuclear Methods Group** (Analytical Chemistry Division, Chemical Science and Technology Laboratory) has as its principal goals the development and application of nuclear analytical techniques for the determination of elemental compositions with greater accuracy, higher sensitivity and better selectivity. A high level of competence has been developed in both instrumental and radiochemical neutron activation analysis (INAA and RNAA). In addition, the group has pioneered the use of cold neutron beams as analytical probes with both prompt gamma activation analysis (PGAA) and neutron depth profiling (NDP). PGAA measures the total amount of a particular analyte present throughout a sample by the analysis of the prompt gamma-rays emitted during neutron capture. NDP, on the other hand, determines concentrations of several important elements (isotopes) as a function of depth within the first few micrometers of a surface by energy analysis of the prompt charged-particles emitted during neutron bombardment. These techniques (INAA, RNAA, PGAA, and NDP) provide a powerful combination of complementary tools to address a wide variety of analytical problems of great importance in science and technology, and are used to help certify a large number of NIST Standard Reference Materials. During the past several years, a large

part of the Group's efforts has been directed towards the exploitation of the analytical applications of the guided cold-neutron beams available at the NIST Center for Neutron Research. The Group's involvement has been to design and construct state-of-the-art cold neutron instruments for both PGAA and NDP and provide facilities and measurements for outside users, while retaining and utilizing our existing expertise in INAA and RNAA.

The **Center for Food Safety and Applied Nutrition** of the U. S. Food and Drug Administration (FDA) directs and maintains a neutron activation analysis (RNAA) facility at the NCNR. This facility provides agency-wide analytical support for special investigations and applications research, complementing other analytical techniques used at FDA with instrumental (INAA), neutron-capture prompt-gamma (PGAA), and Radiochemical Neutron Activation Analysis (RNAA) procedures, radioisotope X-ray fluorescence spectrometry (RXRFS), and low-level gamma-ray detection. This combination of analytical techniques enables diverse multi-element and radiological information to be obtained for foods and related materials. The RNAA facility supports agency quality assurance programs by developing in-house reference materials, by characterizing food-related reference materials with NIST and other agencies, and by verifying analyses for FDA's Total Diet Study Program annually. Other studies include the development of RXRFS methods for screening foodware for the presence of Pb, Cd and other potentially toxic elements, use of INAA to investigate bromate residues in bread products, and use of PGAA to investigate boron nutrition and its relation to bone strength. The FDA's RNAA laboratory personnel frequently provide intra-agency technical assistance, the most recent example being participation in the production of the document "Accidental Radioactive Contamination of Human Food and Animal Feeds: Recommendations for State and Local Agencies" by the Center for Devices and Radiological Health.

The **Neutron Interactions and Dosimetry Group** (Physics Laboratory) provides measurement services, standards, and fundamental research in support of NIST's mission as it relates to neutron technology and neutron physics. The national and industrial interests served include scientific instrument calibration, electric power production, radiation protection, defense nuclear energy systems, radiation therapy, neutron radiography, and magnetic resonance imaging. The Group's activities may be represented as three major activities. The first is <u>Fundamental Neutron Physics</u> - including operation of a neutron interferometry and optics facility, development of neutron spin filters based on laser polarization of ^{3}He, measurement of the beta decay lifetime of the neutron, and investigations of other coupling constants and symmetries of the weak interaction. This project involves a large number of collaborators from universities and national laboratories. The second is <u>Standard Neutron Fields and Applications</u> - utilizing both thermal and fast neutron fields for materials dosimetry in nuclear reactor applications and for personnel dosimetry in radiation protection. These neutron fields include thermal neutron beams, "white" and monochromatic cold neutron beams, a thermal-neutron-induced ^{235}U fission neutron field, and ^{252}Cf fission neutron fields, both moderated and unmoderated. The third is <u>Neutron Cross Section Standards</u> - including experimental advancement of the accuracy of neutron cross section standards, as well as evaluation, compilation and dissemination of these standards.

Several universities have also established long term programs at the NCNR. The **University of Maryland** is heavily involved in the use of the NCNR, and maintains several researchers at the facility. **Johns Hopkins University** participates in research programs in solid state physics and in instrument development at the NCNR. The **University of Pennsylvania** is working to help develop biological applications of neutron scattering. It is also participating in the construction of a new filter analyzer neutron spectrometer, along with the **University of California at Santa Barbara**, DuPont, Hughes, and Allied Signal. The **University of Minnesota** participates in two PRTs, the NG-7 30-m SANS and the NG-7 reflectometer. The **University of Massachusetts** also participates in the latter PRT.

The reactor operated for 250 full power (20 MW) days during the past year, or 68% of real time. This meets our goal, and was achieved in spite of a shutdown for maintenance early in the fiscal year. The reactor operated with better than 90% predictability–i.e. days operated on the day originally scheduled. This is substantially better operation than is specified in national goal of 85% reliability for user facilities. Just after the end of the fiscal year, another fuel shipment was made, thus clearing additional space in the spent fuel storage pool. This completes our current round of scheduled spent fuel shipments. There is now ample storage space for at least 5 years of continuous 20 MW operation.

As part of preparing for another 20 years of operation past 2004, we have been assessing the present cooling tower. During the past year, a contract for construction of a hybrid wet/dry tower was signed. This new tower will not only meet our cooling needs; it will also reduce the visible plume given off by the tower during the winter months, a substantial additional benefit. The new tower will be erected adjacent to the current one, and will not require an outage until the switch is made. This outage will be scheduled when the new tower is fully ready for use, so as to minimize down time. Extensive planning for the piping changes that will be needed is now underway. It is expected that the new second-generation cold source will be installed at the same time, so as to maximize operating time.

During the coming year, we will take advantage of the normal Christmas shutdown to replace the shim control arms. This operation is required every 4 - 5 years, since the cadmium in the control arms is burned up in service. By utilizing the time period of the holiday shutdown, the entire operation will be done with only 3 weeks of additional shutdown time. Since this period will also be used for required training and requalification of operations personnel, there will be little lost operating time compared to our best possible schedule.

A major highlight of the year was the annual conference of the National Organization of Test, Research and Training Reactors (TRTR) held at NIST, chaired and organized by the group. By all accounts, it was highly successful with the largest number of participants ever. Many distinguished speakers addressed the conference including the Chairman of the Nuclear Regulatory Commission and the Undersecretary of Energy. Also, TRTR became the first professional organization to honor NIST on its forthcoming centennial.

Finally, preparations for a license renewal application are proceeding as planned. We are fortunate to have attracted Dr. Seymour H. (Sy) Weiss to our staff, as Deputy to NCNR Director. He will be leading the relicensing effort and associated reactor upgrades for the coming years, and has already started several tasks related to this effort.

IMPROVEMENTS TO THE PERFORMANCE OF HFBS

The recent commissioning of the high flux backscattering spectrometer (HFBS) has opened up opportunities to a variety of users from around the country to study the dynamics of condensed matter systems with time scales on the order of nanoseconds (10^{-9}) and length scales up to 10 Å. A careful design which incorporates state-of-the-art neutron optics has resulted in a flux on sample as high as that of any other backscattering spectrometer in the world with comparable energy resolution. The first call for proposals for the HFBS was made in FY 1999 and the response was outstanding. Several successful user experiments have already been performed (see Figure 1) with more scheduled in the near future. Although the initial performance of the instrument was impressive, improvements continue to be made.

One of the recent changes to the instrument has been a modification to the data acquisition system. Initially the data were binned to the velocity of the reciprocating silicon monochromator. However the method in which the velocity was determined overemphasized local details of the monochromator motion which were not observed

in the neutron data. A detailed analysis of the performance of the monochromator system indicated that the quality of the data could be improved making a rather simple change in the way that data is collected and stored, namely by binning data versus time during a period of the Doppler monochromator motion. The data are later re-binned to velocity using the average monochromator motion profile. This straightforward change to the way that the data is collected has improved the quality of the data, suppressing the spurious effects observed in the velocity-binning mode.

Improvements have also been made to the Doppler monochromator system which have improved its reliability and performance. One of the problems encountered is associated with the fact that the monochromator is being driven to higher energy transfers than any other Doppler monochromator system in the world. The monochromator, which is vibrated over a distance of 9 cm at high frequencies, can experience accelerations in excess of 100 g's. Prolonged vibration of the monochromator resulted in the silicon wafers coming off of the monochromator surface. Recent changes in the gluing method have dramatically increased the lifetime of the silicon wafers on the monochromator.

Efforts to optimize shielding in various parts of the instrument have resulted in improvements in the signal to noise ratio in the detectors. During normal operation the instrument vessel (which is made up of the sample, analyzer crystals, and the detectors) is evacuated in order to reduce the background due to air scattering. Additional shielding has been installed on the detector assembly and on parts of the analyzer system in the vessel. Improvements have also been made to the shielding on the phase space transform chopper to handle the highly divergent beam from the converging neutron guide. This has resulted in a substantial increase of the signal to noise ratio to almost 600 to 1.

FIGURE 1. Measurement of quasi-elastic scattering from monolayer coverage of alkanes on grafoil performed on the HFBS by H. Taub, D. Fuhrmann, L. Criswell, and K. Herwig. The low temperature data (blue) is resolution limited with a full-width at half maximum of 0.96 µeV. The higher temperature data (red) clearly displays broadening indicative of the diffusive motion of the alkanes.

THE DISK CHOPPER SPECTROMETER

The Disk Chopper Spectrometer (DCS) is an extremely versatile time-of-flight instrument, designed to achieve a broad range of energy resolution full widths, from 12 µeV to 1 meV, by changing chopper speed, wavelength, and/or beam width. Once commissioned, the DCS will be in high demand for experiments on a variety of systems such as proteins, molecular crystals, disordered materials and metal-hydrogen systems. The instrument is to be
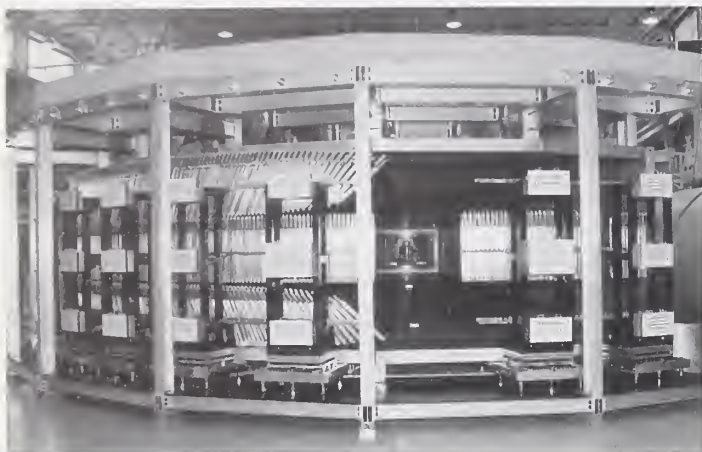
FIGURE 2. Photograph of the DCS detector bank and flight chamber.

included, on a limited basis, in the first Call for Proposals in FY2000.

Over the past twelve months the DCS has seen major progress in a number of important areas. The sample chamber and flight chamber were equipped with beam-handling components, and the insides of both chambers were lined with cadmium. Flow tests were performed in order to complete the design of the gas handling system for the sample and flight chambers; the system had been fabricated and had largely been assembled by the end of the fiscal year. An overhead platform, to be used for sample environment preparation and installation into the sample chamber, has also been designed.

Problems with some of the amplifiers for the DCS detectors prompted us to send the complete inventory to the manufacturer for mutually agreed modifications. On their return discriminator thresholds were individually set, and the full complement of 913 detectors and amplifiers was installed on the detector racks, which were then installed and aligned at the spectrometer. The detectors and voltage distribution assemblies were cabled and fully tested prior to installation of the outer shields. Much work was devoted to troubleshooting and greatly improving the reliability and performance of the VME data acquisition electronics, and to the development of data acquisition software.

PERFECT CRYSTAL SANS DIFFRACTOMETER

A perfect crystal diffractometer (PCD) used for very high resolution small angle neutron scattering (SANS) is being developed jointly by the NCNR and NSF as part of the CHRNS facility. The higher resolution obtained by using perfect silicon crystals increases the maximum size of features that can be measured from 0.1 μm obtained using the current NCNR's two 30 m, pinhole geometry SANS instruments, to 10 μm with the new instrument. The monochromator and analyzer use triple reflections before and after the sample using large channel-cut silicon crystals suppress the "wings" of the beam profile in order to improve the signal-to-noise to values comparable to that obtained from the pinhole instruments. The PCD will cover a Q-range from 0.0004 nm^{-1} to 0.1 nm^{-1} with an expected beam current of 50,000 s^{-1}.

Located on the BT-5 beam tube in the Confinement Building, the layout of the instrument is shown in Figure 3. A vertically and horizontally focusing graphite premonochromator provides a directs the neutron beam away from the main reactor beam towards the perfect crystal monochromator. The monochromator reflects a highly collimated beam to the sample. After the sample, a high precision rotation stage rotates the analyzer crystal to scan the small angle scattering obtained from the sample, which is then collected by the detector. The shields supporting the premonochromator are set on kinematic mounts for accurate repositioning. The monochromator and analyzer are isolated from room vibrations using a heavy pneumatic vibration isolation table.
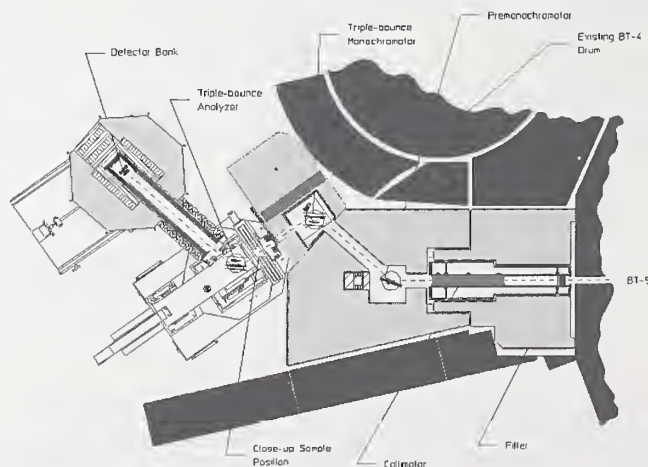
FIGURE 3. Schematic layout of the BT-5 Perfect Crystal Diffractometer.

INSTRUMENTATION DEVELOPMENTS

In 1999, all detailed design work was finished and all purchased parts received. The beam shutter and premonochromator shielding has been installed. Major components yet to be installed are the detector housing, sample position table, and the small monochromator shield. Preliminary characterization measurements leading to instrument commissioning are planned for early 2000.

THE FILTER ANALYZER NEUTRON SPECTROMETER

The new Filter Analyzer Neutron Spectrometer (FANS) is designed to give US researchers access to unprecedented sensitivity for measuring the vibrational spectra of a wide variety of materials. This spectrometer, which will replace the current BT4 instrument, uses cryogenically cooled polycrystals as low energy band-pass filters for neutrons scattered from the sample. A dramatic gain in signal over the existing filter analyzer is achieved primarily through a large increase in the solid angle covered by the secondary spectrometer. The FANS instrument is being developed in two phases. Phase I includes the first of two new filter assemblies and Phase II includes the second filter analyzer and a new monochromator and monochromator drum system.

During the past year, the detailed design of the first filter wedge was completed, the vacuum chamber which encloses the Be and graphite filters was delivered, and the Be and graphite filter wedges were assembled (see Figure 4). Recent tests demonstrated that these filters can be cooled to cryogenic temperatures which is necessary to maximize the performance of the instrument. Furthermore all of the parts for the undercarriage for Phase I have been received, assembled, and operated successfully under load. Most of the shielding and data acquisition system have also been received. Major assembly and installation of Phase I will begin early in 2000.

DEVELOPMENT OF AN ACTIVE DOUBLE FOCUSSING MONOCHROMATOR SYSTEM

The use of vertical or horizontal focussing monochromators to increase the intensity of selected neutrons incident on the sample is well known and widespread. Less common are systems combining these features. Often the machinery employed to do this is cumbersome and results in extraneous material in the beam, increasing the background from unwanted neutrons. For horizontal focussing it is desirable to have maximum flexibility by adjusting many

FIGURE 4. The FANS filter assembly. The first Be filter is in the foreground with the PG filter second and the final Be filter in the background just before the detector bank. A radial collimator is visible in the middle of the assembly.
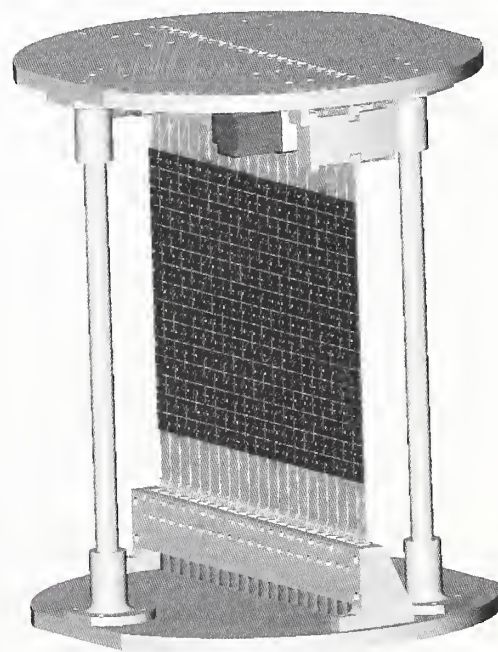
FIGURE 5. A drawing of the active double focussing monochromator system.

monochromator elements while keeping the corresponding mechanical components away from the beam area. By contrast, vertical focussing can be confined to the problem of adjusting only one parameter, the radius of curvature of the array, and admits a correspondingly simpler mechanical solution.

We are currently developing a system that combines completely flexible horizontal focussing with vertical focussing that is achieved by buckling the entire system of separately controllable vertical crystal arrays. Cylindrical curvature is to be accomplished by compressing the system of specially shaped strips upon which the individual monochromating crystals are mounted. This design eliminates extraneous material in the beam, which should result in greatly reduced background.

AN ADVANCED LIQUID HYDROGEN COLD SOURCE

The NIST liquid hydrogen cold source has completed over four years of service. It was installed with three goals: at least double the cold neutron intensity with respect to its predecessor (D_2O ice); operate simply and reliably; and pose no safety threat to the reactor or personnel. It has successfully met or exceeded all these goals. The cold neutron flux increased by a factor of 4 to 6, for wavelengths in the range of 0.2 to 2 nm. The availability of the source has been nearly 99% of the time that the reactor was available (the reactor is shutdown if the source is inoperable). And there have been no hydrogen leaks, nor have any of the insulating vacuums or helium containments been compromised.

Even as Unit 1 was being installed in 1995, however, improvements in the MCNP model (used for Monte Carlo simulations) of the NIST reactor were pointing toward a new, but more complicated cryostat assembly, with a possible additional gain of a factor of two. Better coupling between the reactor fuel and the cold source can be achieved by expanding the cooling jacket into the volume now occupied by the insulating vacuum, so that it partially surrounds the moderator vessel. In this way, the D_2O coolant also serves as an extension of the reactor reflector. Additional changes in the new source are based on our operating experience with the existing LH_2 source and extensive MCNP calculations. Unit 2 will be an ellipsoidal annulus rather than spherical, it will have an evacuated inner vessel, rather than vapor-filled, and the LH_2 layer will

FIGURE 6. NCNR Mechanical Engineering Technician, Scott Slifer, welds the aluminum moderator vessel for the advanced hydrogen cold source.

be up to 30 mm thick, rather than 20 mm, without increasing the LH_2 volume.

The advanced liquid hydrogen cold source is currently being fabricated and will be installed in the NIST reactor next year. Enhanced mechanical design and manufacturing tools are exploited in the fabrication of the advanced source. Components of the hydrogen, insulating vacuum, helium containment, and D_2O vessels are cut from solid blocks of Al 6061 on a computer-controlled, high-speed mill at the NIST Instrumentation shop, and are then welded and thoroughly tested by NCNR staff (see Figure 6). It is expected that the flux of cold neutrons will increase by a factor of 1.8.

IMPROVEMENTS TO NCNR SAMPLE ENVIRONMENT EQUIPMENT

The sample environment equipment has seen a number of changes in FY1999 at the NCNR. One of the most visible accomplishments has been the development of informative webpages that detail sample environment resources, specifications, and even the current operating condition and location for specific devices. This information is easily accessible through the NCNR homepage (http://www.ncnr.nist.gov), allowing guest researchers to plan their experiments and design appropriate sample holders.

Commissioning has begun on a new high magnetic field/ low temperature superconducting magnet system which is financed through a joint collaboration of Johns Hopkins University, NCNR, NEC Research Institute, Princeton, the University of Maryland, and a National Science Foundation IMR grant. The 0.022 Kelvin dilution refrigerator of this new system has already been tested and used on triple axis spectrometers. A 7 Tesla magnet has been temporarily outfitted in the system at this time, with replacement by a much stronger superconducting magnet of 10-12 Tesla in the coming months. The magnet is capable of operating with either a homogeneous magnetic field at the sample position or with a field gradient, a great aid for polarized neutron beam experiments.

This system is top loading, which provides an important capability for experiments requiring multiple sample changes or for quick changeover between consecutive experiments.

From new capabilities to improved sample preparation and screening, the sample environment resources have been significantly expanded during the past year. Listed in Table 1 are further acquisitions, notable modifications, and improvements that combine to offer the researcher more control over the sample conditions. Figure 7 displays a typical cryorefrigerator sample environment. More details are available at the web site mentioned above.

Table 1.

Helium flow cryostat	1.5 – 300 K, dedicated to backscattering spectrometer
Helium flow cryostat	1.5 – 300 K, dedicated to disk chopper time-of-flight spectrometer
Helium flow cryostat	1.5 – 300 K
Pumped helium-3 cryostat insert	0.30 – 300 K, for use with 7 T vertical field magnet
Closed-cycle helium refrigerator	7 – 320 K
Closed-cycle helium refrigerator	10 – 320 K, modified for backscattering spectrometer
Poiseuille flow shear cell	shear rate up to 130,000 s^{-1} near surface
Light scattering particle sizer	2-100 nm diameter
Rheometer	1.7×10^{-3} to 2.7×10^{8} Pascal-seconds, -60 to 600° C, for in-situ measurement during SANS experiments
Lyophilizer	freeze dryer for sample preparation
Kare Fisher titrator	quantitative analysis of water in a sample
Freezer	-20° C, for longer term storage of biological samples
Superconducting magnet power supply	0 - 120 Amps, bi-directional
Dual channel lock-in amplifier	1 mHz – 102 kHz frequency range
Four temperature controllers	programmable, remote operation
Dual channel lock-in amplifier	0 - 120 Amps, bi-directional
Four temperature controllers	programmable, remote operation
Single-crystal windowed tail	for SANS low-temperature electromagnet experiments
Sensitive equipment transport carts	custom-designed to protect valuable equipment

NCNR Sample Environment Geometry Cryorefrigerators
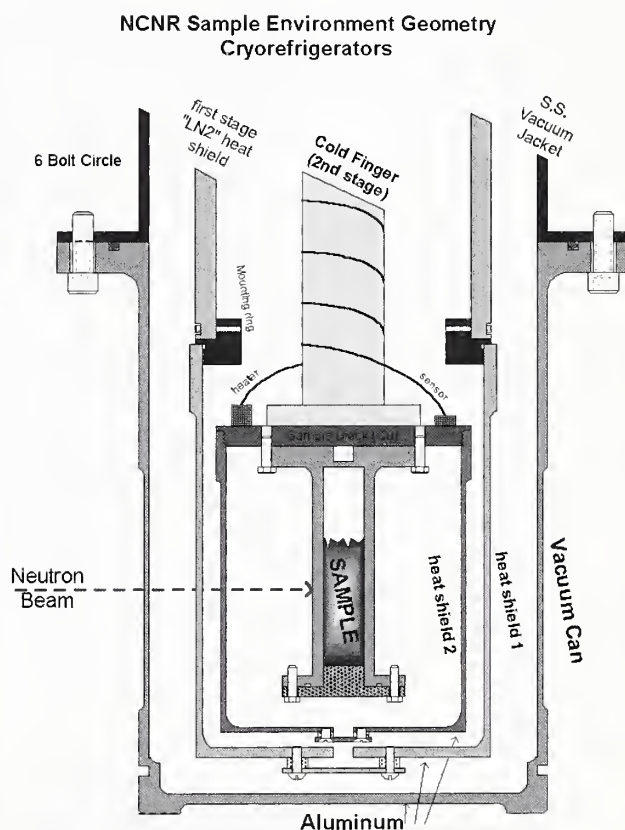
FIGURE 7 Schematic diagram of the sample environment in a cryorefrigerator in the neutron beam.

MATERIALS SCIENCE/ CRYSTALLOGRAPHY

Acid Sites in Zeolite ZSM-5
A. Peters[42], R.-H. Hu[248], S. Purnell[248], B. H. Toby[114], R. Senesi[168], D. A. Neumann[114] and D. H. Olson[231]

Aerogels Investigated by SANS with Contrast Masking Solutions
C. Merzbacher[111], M. Anderson[111] V. Cepak[111] and J. G. Barker[114]

Amorphous Content Determination Methodology
J. K. Stalick[114], R. Senesi[168] and B. H. Toby[114]

Cation Location in Ion Exchanged (Li,Na) Chabazite
L. J. Smith[204] and A. K. Cheetham[204]

Characterization of Ag and Mixed Li/Ag Faujasite Zeolites using Neutron Diffraction
N. Hutson[222], R. Yang[222], B. A. Reisner[114] and B. H. Toby[114]

Characterization of Microcracking in Iron Titanate by SANS
A. J. Allen[118] and E. Fuller[118]

Chemical Ordering in Ni-Mn-Ga Heusler Alloys
R. Overholser[220], M. Wuttig[220] and D. A. Neumann[114]

Comparison of Residual Stress Measurement Techniques
T. Gnäupel-Herold[220], P. C. Brand[114], H. J. Prask[114], S. Spooner[136], B. Pardue[172], D. Nelson[167] and S. Foss[81]

Complex Oxide Structures
A. Sleight[141], I. Radosavljevic[141] and T. Amos[141]

'CONV' and 'STRESS': New Codes for Data Reduction in Neutron Diffraction Residual Stress Measurements
P. C. Brand[114] and T. Gnäupel-Herold[220]

CPD Round Robin on Quantitative Phase Analysis
J. K. Stalick[114]

Crystal Chemistry of Protonic Centers in Zeolites
D. H. Olson[231] and B. H. Toby[114]

Crystal Structure of $Ba_4CaCu_2O_6(CO_3)$
Q. Z. Huang[114, 220] and F. Izumi[106]

Crystal Structure of Dehydrated LaD-LSX
D. H. Olson[231], B. A. Reisner[114] and B. H. Toby[114]

Crystal Structure of Ferroelectric Tetragonal Tungsten Bronze Lead Barium Niobate
Q. Z. Huang[114, 220] and R. Guo[146]

The Crystal Structure of $Pb_5Bi_{18}P_4O_{42}$
H. Steinfink[180] and S. Giraud[180]

Crystal Structure of $Sr_2Nb_2O_7$
Q. Z. Huang[114, 220], T. Vanderah[116] and I. Levin[118]

Defect Structure of $(Cu,Zn)InSe_2$
B. A. Reisner[114], M. Knox[198], A. Stacy[198] and G. Ron[198]

Effect of Annealing on ZrO_2 Phase Composition
J. K. Stalick[114] and J. Ilavsky[40]

Fast Ion Conductors
J. K. Stalick[114], B. Wuensch[94] and E. Ku[94]

Field and Temperature Dependent Neutron Scattering Study of Mn_{12} Magnetic Molecules
T. Yildirim[114] and S.-H. Lee[114, 220]

Grazing Incidence SANS from Plasma Sprayed Coatings
A. J. Allen[118] and H. Boukari[118]

Hydrogen Location in Graphite Nano-Fibers
S. F. Trevino[114, 12] and P. Anderson[131]

Internally Oxidized Palladium Alloys: Particle Size Determination by SANS
J. G. Barker[114]

Investigation of Slow Motion Dynamics in Selective Adsorption
H. Taub[224], D. Fuhrmann[224], L. Criswell[224], K. Herwig[8] and R. M. Dimeo[114]

Intermetallic Compounds of the A_3B_4 Structure
J. K. Stalick[114] and R. Waterstrat[114]

Investigation of the Zr_9Pt_{11} Structure Type
J. K. Stalick[114] and R. Waterstrat[114]

In Situ Neutron Reflectivity Measurements of Deuterium Absorption in Pd Films
B. Heuser[216], A. Munter[216], N. Barber[216], J. A. Dura[114] and C. F. Majkrzak[114]

Kinetics of Gellation of Silica under Shear
C. D. Muzny[129], J. M. Hanley[129] and G. C. Straty[129]

Low Energy Excitations in Deuterated Polystyrene
R. M. Dimeo[114] and J. F. Douglas[124]

Low Temperature Structure of Methyl Halide Films on MgO
J. Larese[23], M. Sprung[23] and A. Freitag[23]

Magnetic Cluster Sizes in Thin Film Magnetic Recording Disks
M. Toney[63], S.-M. Choi[114] and C. J. Glinka[114]

Microstructure Evolution of Fly Ash Blended Cements
A. J. Allen[118] and R. A. Livingston[51]

Modelling of Texture-Strain Relationships Using Neutron Diffraction Data
H. Sitepu[168, 114], J. K. Stalick[114] and H. J. Prask[114]

Morphological and Kinetic Study of Early Calcium-Silicate-Hydrate Gel Development During the Hydration of Cement and Tricalcium Silicate
H. M. Jennings[131], J. J. Thomas[131] and A. J. Allen[118]

MSANS Study of Effects of Feedstock Preparation on the Microstructure of Plasma-Sprayed Ceramic Coatings
A. J. Allen[118], H. Boukari[118] and A. Kulkarni[168]

Negative Thermal Expansion in $AOPO_4$ (A = Ta,Nb) Compounds
A. W. Sleight[141] and T. Amos[141]

Neutron Diffraction of Heusler Alloys
V. G. Harris[111] and Q. Z. Huang[114, 220]

Neutron Diffraction of Single-Wall Carbon Nanotubes
P. Papanek[114], J. E. Fischer[223, 231], Z. Benes[231], D. Colbert[153] and M. Heben[153]

Neutron Diffraction Study of Hydronium Ions in Zeolite (Nd,D)-X
D. H. Olson[231] and B. H. Toby[114]

Neutron Scattering and the Low Energy Excitations in Polycarbonate Copolymers:
C. Soles[124], R. M. Dimeo[114], J. Liu[222], A. Yee[222] and A. Sokolov[114]

A New Phase of Silver Fluoride? No It's $Ag_{10}C_2$!
R. L. Harlow[45]

Order-Disorder in CoFe/Carbon Composites
J. H. Scott[128], M. E. McHenry[27], Z. Turgut[27] and M. Storch[27]

Phase Analysis of Sintered Yttria-Stabilized Zirconia
J. K. Stalick[114] and A. Slifka[121]

Phase Composition Analysis of Plasma-Sprayed Partially Stabilized Zirconia Coatings by Neutron Powder Diffraction Data
H. Sitepu[168, 114] H. J. Prask[114], J. K. Stalick[114], R. Goswani[168] and S. Sampath[168]

Polymerized Fullerenes
S. F. Trevino[114, 12], N. Beck-Tan[12] and L. Balogh[100]

Radiation-Induced Microstructure in Reactor Pressure Vessel Steels
G. R. Odette[204], B. Wirth[204] and D. Klingensmith[204]

Residual Stresses in Powder Metallurgy Test Specimens
T. Gnäupel-Herold[220], H. J. Prask[114], M.-J. Yang[146] and R. German[146]

Residual Stresses in Ti Rib Implants for Children
T. Gnäupel-Herold[220], H. J. Prask[114] and R. Roberts[5]

Residual Stress Measurements on Railroad Rails
T. Gnäupel-Herold[220], P. C. Brand[114], J. Gordon[187], J. Magiera[39], J. Orkisz[39] and H. J. Prask[114]

Rotational Excitations of Methane Confined to Porous Glass
B. Asmussen[86], R. M. Dimeo[114] and D. A. Neumann[114]

SANS and SAXS Determination of the Dispersion in Organic Solvents of Organically Modified Clays for Polymer/Clay Nanocomposites
D. Ho[220], R. M. Briber[220] and C. J. Glinka[114]

SANS Characterization of Hydrides in Uranium
S. Spooner[136], G. Ludtka[136] and J. G. Barker[114]

SANS Investigation of Hydrogen Trapping at Lattice Defects in Palladium
B. Heuser[215] and J. S. King[222]

SANS Study of Fire Retardant Polymer-Clay Nanocomposites
J. M. Hanley[129], C. D. Muzny[129] and J. Gilman[136]

SANS Study of Oil Bearing Sedimentary Rocks
A. Radlinski[14] and G. D. Wignall[136]

Site Distributions in the Structure of $Ba_2Sn_2ZnGa_{10-x}Cr_xO_{22}$ (x = 3 and 4)

Q. Z. Huang[114, 220] and R. Cava[150]

Single-Crystal Elastic Constants from Measurements on Polycrystals

T. Gnäupel-Herold[220], H. J. Prask[114] and P. C. Brand[114]

SiO_2 Ultra Thin Films Round Robin

J. A. Dura[114], C. F. Majkrzak[114] and J. Ehrstein[125]

Size Distribution and Volume Fraction of Copper-Rich Precipitates in Model Reactor Pressure Vessel Steels

D. Balzar[122] and C. J. Glinka[114]

Solute Effects on Membrane Thickness in DOPG and DOPC

J. Pencer[215] and R. Hallett[215]

Structural Ordering in Erbium Doped Bi_2O_3

B. A. Reisner[114], E. Wachsman[210], T. J. Udovic[114] and D. A. Neumann[114]

Structural Studies of Fullerene Superconductors

K. Prassides[236] and D. A. Neumann[114]

Structural Study of $Sr_4Nb_2O_9$ Compound

I. Levin[118], J. Chan[118] and T. Vanderah[118]

Structural Distortions in the $NaSr_3MO_6$ (M = Ru,Rh) Family

B. A. Reisner[114], A. Prieto[198] and A. Stacy[198]

Structural Distortions in Titanites

B. A. Reisner[114] and D. Xirouchakis[103]

Structural Distortions in Zeolite RHO

B. A. Reisner[114]

Structural Studies of Germanium Zeolites

J. B. Parise[168], G. M. Johnson[168] and A. Tripathi[168] and S. Park[168]

Structural Studies of High Silica Zeolite RHO

J. B. Parise[168], A. Tripathi[168] and Y.-J. Lee[168]

Structural Studies of Iodine-Loaded ZSM-5

D. H. Olson[231]

Structural Studies of $Sr_{2\cdots}Rh_{1-x}Ru_xO_4$ Layered Perovskites

P. Woodward[23], B. Kennedy[237] and T. Vogt[23]

Structural Studies of Strontium Niobium Oxides

W. Wong-Ng[118], W. Greenwood[220] and B. H. Toby[114]

A Structural Study of the Ruddlesden-Popper Calcium Manganate $Ca_4Mn_3O_{10}$

M. Greenblatt[159] and I. Fawcett[159]

Structure of Barium Titanate Thin Films on Silicon

C. Bouldin[118], B. Revel[118] and J. A. Borchers[114]

Structure, Cation Ordering and Magnetism in Manganate Spinels

M. Green[156] and D. A. Neumann[114]

Structure of $Ca_2Ta_{2-x}Nb_xO_7$ (x = 0.05 and 0.1)

Q. Z. Huang[114, 220] and R. Roth[114]

Structure Determination of Ca_2RhD_5 by Powder Neutron Diffraction

R. Moyer[185] and B. H. Toby[114]

Structure Determination of Framework Materials with the RHO Topology

B. A. Reisner[114]

Structure Determination of $La_{0.78}Sr_{0.22}RuO_3$

Q. Z. Huang[114, 220], I. Natali Sora[194], A. Santoro[114] and F. T. Vanderah[118]

Structure Determination of Sr_2IrD_5 by Powder Neutron Diffraction

R. Moyer[185] and B. H. Toby[114]

Structure Refinement of a Ferromagnetic Vanadium(III) Sulfate

D. Grohol[94], D. Nocera[94], B. H. Toby[114] and Q. Z. Huang[114, 220]

Structure of Ca_2AlNbO_6 and $CaTiO_3$ Compounds

I. Levin[118], J. Chan[118] and T. Vanderah[118]

Structure of the Layered Cobalt Oxychlorides $Sr_3Co_2O_5Cl_2$ and Sr_2CoO_3Cl

Q. Z. Huang[114, 220], N. McGlothlin[150], D. Ho[150] and R. J. Cava[150]

The Structure of a Lithium Substituted Aluminosilicate RHO

B. A. Reisner[114] and J. B. Parise[168]

Structure and Oxygen Disorder in $Sr_{1.9}Nd_{1.1}Cu_2O_x$

Q. Z. Huang[114, 220] and W. Wong-Ng[118]

Structure of Porous Silica Thin Films

W. Wu[124] and D. Pochan[124]

Structure of 75.25:24.75 CaO-Nb_2O_5

J. Chan[118], I. Levin[118], R. Roth[118], T. Vanderah[118] and B. A. Reisner[114]

Structure Refinements of Alumo- and Gallo-Germanates Using Neutron Scattering Techniques

S. Park[168], J. B. Parise[168] and B. H. Toby[114]

Structure of $Sr_{1.875}Dy_{1.125}Cu_2O_x$

Q. Z. Huang[114, 220] and W. Wong-Ng[118]

Study of Hydronium Ions In Zeolites

D. H. Olson[231] and B. H. Toby[114]

Temperature Dependence in the Structure of Yttrium Tungstate

A. Sleight[141], P. Forster[141] and A. Yokochi[141]

Temperature-Dependent Structure Determination of Ca_2IrD_5 by Powder Neutron Diffraction

R. Moyer[185] and B. H. Toby[114]

Thermal Expansion of II-VI Semiconductors

R. Reeber[130, 13] and K. Wang[130]

Thermal Expansion of Alpha SiC from 15 to 298K

R. Reeber[130, 13], K. Wang[130] and B. H. Toby[114]

Thermal Expanion of HgSe

R. Reeber[130, 13] and K. Wang[130]

X-Ray Reflectometry Analysis of Alkanethiol Deposited on AuO

K. T. Forstner[114], J. A. Dura[114], C. F. Majkrzak[114], J. Woodward[116] and A. L. Plant[116]

Zeolite SRM Characterization

B. H. Toby[114] and R. Senesi[168]

Zirconium Tungstate Studies

A. W. Sleight[141] and N. Duan[141]

POLYMERS

Behavior of Polymer Chains in Porous Media

M. Nieh[146], S. Kumar[146] and R. M. Briber[220]

Chain Conformation in Deformed Elastomers

D. Peiffer[50], M. Rabeony[50] and M. Lin[50]

Chain Conformation in Self-Assembled, Layer-by-Layer Polyelectrolyte Thin Films

M.-P. Nieh[146], S. Kumar[146] and R. M. Briber[220]

Characterization of Dye Distribution in Polymer Thin Films

C. White[124], E. Lin[124] and W. L. Wu[124]

Conformation of Chains in Strained Polymer Networks

C. Cohen[38] and R. M. Briber[220]

Conformation of Polymer Chains Confined in Controlled Pore Glass

R. M. Briber[220], D. Ho[215] and I. Teraoka[148]

Conformation of Random Copolymers in Solution

M. Y. Lin[50] and D. Peiffer[50]

Critical Neutron Reflection Tests of Polymer Interdiffusion Dynamics

R. P. Wool[209], K. A. Welp[209] and W. Dozier[209]

Demixing Kinetics of Polyolefin Blends

N. Balsara[148], H. Wang[148] and B. Hammouda[114]

Dynamics of Polymer Interdiffusion

S. K. Satija[114]

Effects of Polymer Additives on the Formation of Hydrate Crystals

J. M. Hutter[50], H. King[50] and M. Lin[50]

Effects of Pressure on the Lower Critical Ordering Temperature of Diblock Copolymers

A.-V. Ruzette[94] and A. M. Mayes[94]

Effects of Shear on the Phase Behavior of Polyolefin Blends

N. Balsara[148] and A. Lefebvre[148]

Effects of Substrate Interactions on the Ordering of Block Copolymer Films

E. Huang[221], J. DeRouchey[221] and T. P. Russell[221]

Effects of Supercritical CO_2 on the Phase Behavior of Block Copolymer Melts

J. Watkins[221], M. Pollard[221], G. Brown[221], S. Kumar[146] and T. P. Russell[221]

Effects of Surfactants on the Conformation of Grafted Polymer Brushes

T. Cosgrove[196], J. Hone[196] and R. Wesley[196]

Electric Field-Induced Orientation of Diblock Copolymers in Thin Films
J. DeRouchey[221] and T. P. Russell[221]

Glass-Transition Effects on Microphase Separation in PS/PVME Polymer Blends
S. Kumar[146], R. Jones[146], S. Kanath[146], R. M. Briber[220] and L. Ho[215]

Inelastic Neutron Scattering from Filled Elastomers
A. I. Nakatani[124], R. Ivkov[114], P. Papanek[114, 231], H. Yang[163] and M. Gerspacher[163]

In-Plane Structure of PSAN/dPMMA Blends in Thin Films
M.-P. Nieh[146], S. Kumar[146], R. Jones[146] and R. M. Briber[220]

Interdiffusion of Crosslinked Polymer Films
U. Perez-Salas[220], R. M. Birber[220], M. Rafailovich[168], J. Sokolov[168] and N. F. Berk[114]

Interfacial Scattering from Phase-Separated Polymer Blends
H. Jinnai[89], M. Hayashi[89] and C. C. Han[124]

Investigation of the Concentration Profile between Crosslinked Thin Films
R. M. Briber[220], U. A. Perez-Salas[220], M. Rafailovich[168] and J. Sokolov[168]

Kinetics of Shear Alignment of Block Copolymer Blends
R. Krishnamoorti[215], S. Rai[215] and B. Hammouda[114]

Marginal Solvent Scaling of Polystyrene in Naphthalene
J. G. Barker[114]

Membrane Mediated Polymer Interdiffusion
H. Gruell[124], A. Esker[124] and C. C. Han[124].

Microstructure and Properties of Hyperbranched Polymers
N. Wagner[209] and Y. Kim[46]

Morphology of Self-Assembled Aggregates of Amphiphilic Peptides with Applications in Bioengineering
T. Gore[223], H. Bianco[223], Y. Dori[223] and M. Tirrell[223]

Morphology of Single Graft Block Copolymers
S. F. Trevino[114, 12], N. Beck-Tan[12] S. Guido[221] and C. Lee[221]

Neutron Reflectivity from the Monolayers of SAN Random Copolymers
E. Kim[60], H. Kim[88], K. Char[162] and S. H. Lee[162]

Neutron Reflectivity Study of the Phase Separation in dPB/PI Blends Using a Unique Back Transformation Technique
A. Schreyer[114], C. F. Majkrzak[114], N. Berk[114], H. Gruell[124] and C. C. Han[124]

Neutron Studies of Polymer Dynamics in Intercalated Polymer-Clay Nanocomposites
R. Ivkov[124], P. M.Gehring[114], N. Maliszewskyj[114], P. Papanek[114, 231] and R. Krishnamoorti[215]

Nucleation and Growth in Binary Polymer Mixtures Initiated by Pressure Jumps
N. Balsara[148], A Lefebvre[148], H. Lee[148] and B. Hammouda[114]

Phase Behavior of Multi-Component Polymer Systems in Compressible Solvents
J. Watkins[221], G. Brown[221], V. RamachandraRao[221], B. Vogt[221] and T. P. Russell[221]

Phase Behavior of Polystyrene/Polybutadiene Blends with Added Random Copolymer Studied Via Small Angle Neutron Scattering
D. Waldow[144] and R. M. Briber[220]

Phase Separation in Polymer Thin Films
H. Gruell[124], C. C. Han[124] and S. Kumar[146]

Phase Separation in Polyolefin Blends
M. Modi[215] and R. Krishnamoorti[215]

Polyethylene/Polymethylene Blends: Wetting and Phase Transitions
Y. Akpalu[124] and A. Karim[124]
Polymer Brushes Under Shear
R. Ivkov[114], P. D. Butler[114] and S. K. Satija[114]

Polymer Chain Conformation in Thin Films: Deviations from Bulk Behavior in dPS/PS Films
S. Kumar[146], R. Jones[146], R. M. Briber[220], L. Ho[215] and T. P. Russell[221]

Polymer Interdiffusion Near the Polymer/Solid Interface
E. K. Lin[124], D. J. Pochan[124], W. Wu[124], S. K. Satija[114] and R. Kolb[50]

Polymer Liquid-Crystal Ordering at an Interface
G. Lynn[238], E. Lin[124], W. L. Wu[124] and M. Dadmun[238]

Polymer Materials for Medical Implants
A. Bellare[59], A. Gomoll[59] and R. Myers[59]

Polymer Supercritical Fluid Solutions
M. McHugh[82], T. diNoia[82], J. van Zanten[82], C. Kirby[82], T. Kermis[82] and S. Conroy[82]

Polyolefin Polymer Blend Tie Chain Structures
D. Lohse[50], M. Rabeony[50] and R. Garner[50]

Pressure Dependence of the Order-Disorder Transition in Diblock Copolymers
M. Pollard[221] and T. P. Russell[221]

Pressure Effects on Crystallization and Phase Behavior of Binary Polyolefin Blends
R. Krishnamoorti[215], M. Modi[215] and B. Hammouda[114]

Pressure Induced Phase Transitions in Multicomponent Polymer Systems
N. Balsara[148] and A. Lefebvre[148]

SANS from Dendrimer-Hydrophobe Complexes
G. Nisato[124] and E. Amis[124]

SANS Investigations of a New Class of Nylon-6 Polymers
M. Kreitschmann[70] and S. Rathgeber[220]

SANS Study of Phase Separation in Model Polymer Networks
B. Viers[208]

SANS Study of the Thermodynamics of Blends of Star and Linear Polymers
M. D. Foster[196], T. Zook[196] and C. Greenberg[196]

Self-Assembly of Polyethylene-Propylene-Ethylene Triblock Copolymers in Selective Solvents
L. Fetters[50], D. Richter[70], M. Monkenbush[70] and W. Leube[70]

Shear-Induced Order-Disorder Transition in Diblock Copolymer Solutions
C.-I. Huang[223], T. Lodge[223] and C. C. Han[124]

Shear Induced Polymer Desorption
E. Lin[124], R. Kolb[124] and W. L. Wu[124]

Shear-Induced Polymer Melt Desorption from an Attractive Solid Surface
E. K. Lin[124], D. J. Pochan[124], W. Wu[124], S. K. Satija[114] and R. Kolb[50]

Solvent Vapor Induced Swelling of a Polymer Brush
S. K. Satija[114], R. Ivkov[114], P. D. Gallagher[114] and J. A. Dura[114]

Solution Structure of Arborescent Graft Polymers
R. M. Briber[220], S.-W. Choi[114, 220], S.-M. Choi[114], M. Gauthier[249] and B. J. Bauer[124]

Spinodal Decomposition in PS/PI Blends
H. Jinnai[89], M. Hayashi[89] and C. C. Han[124]

Strain-Induced Interfacial Fracture Between Epoxy and Silicon Oxide
M. Kent[85] and W. F. McNamara[85]

Strained Polymer Networks
N. Gilra[38], C. Cohen[38], R. M. Briber[220] and T. Panagiotopolis[220]

Structure and Characterization of Ultrathin Polymer Films
R. L. Jones[146], S. Kumar[146], L.-T. Ho[220] and R. M. Briber[220]

Structure of Filled Elastomer Thin Films
Y. Zuang[168], B. Tan[168], M. Rafailovich[168], J. Sokolov[168] and M. Lin[50, 114]

Structure of Fluorosilicone Networks
F. Horkay[55] and E. Geissler[213]

Structure of Nafion in Various Solvents
S. F. Trevino[114, 12], S. Young[12] and N. Beck-Tan[12]

Surface Segregation in Binary Blends of Topologically Distinct Polymers
M. D. Foster[196], C. C. Greenberg[196] and D. M. Teale[196]

Static Characterization of Star-Like Dendrimers
S. Rathgeber[220] A. Gast[167] and J. Hedrick

Structure and Aggregation Kinetics of Asphaltenes
T. Mason[50] and M. Lin[50]

Structure of Adsorbed Polyelectrolyte Multilayer Thin Films
C. Barrett[94] and A. M. Mayes[94]

Structure and Morphology of Semicrystalline Polymer Thin Films
D. J. Pochan[124], E. K. Lin[124], W. L. Wu[124], S. K. Satija[114], C. F. Majkrzak[114] and R. Kolb[50]

Structure of Polystyrene/Polyisoprene Diblock Copolymer Micelles in Decane
J. Pople[167], J. Hur[167], A. Lee[167], A. Gast[167] and K. Barnes[124]

Temperature Induced Contrast Variation Method in Semicrystalline Polymers
J. Barnes[124], A.Nakatani[124], K. Barnes[124], B. Hammouda[114] and R. Kolb[50]

Thermal Expansion and Glass Transition Behavior of Polymer Films: Effect of the Free Surface and Confinement between Non-Interacting Surfaces
D. J. Pochan[124], E. K. Lin[124], W. Wu[124], S. K. Satija[114] and S. Z. D. Cheng[196]

Thermal Expansion and Glass Transition of Thin Polymer Films Sandwiched Between Polymer Layers
D. J. Pochan[124], E. K. Lin[124] and W. L. Wu[124]

Two-Stage Spinodal Decomposition in a Rubber Blend
M. Hayashi[89] and C. C. Han[124]

COMPLEX FLUIDS

Compatibility of Oil Mixtures at High Temperatures
H. Aldrich[50] and M. Y. Lin[50]

Effect of Shear Combined with a Proximate Surface on Surfactant Sponge Phases and the Sponge to Lamellar Transition
W. A. Hamilton[136], P. D. Butler[114], G. Warr[237] and L. Porcar[136]

Effects of Shear on Phase Boundaries of Bicontinuous Microemulsions
S.-M. Choi[114, 220] and S.-H. Chen[94]

Electrostatic and Counterion-Specific Effects on Micelle Morphology Probed with SANS
L. J. Magid[238], P. D. Butler[114] and Z. Han[124]

Field Driven Phase Transitions in Monolayers and Bilayers of Amphiphiles at Electrode Surfaces
J. Lipkowski[214], J. Majewski[91] and G. Smith[91]

Flow-Induced Microstructural Transitions in Polyampholyte-Polymer Colloid Mixtures
N. Wagner[209], K. A. Vaynberg[209] and R. Sharma[209]

High Pressure Study of Hydrophobic Interactions
M. Lesemann[82], C. Kirby[82], M. Paulaitis[82] and J. VanZanten[82]

Kinetics of Poiseuille Flow-Induced Structures in Solutions of Threadlike Micelles
W. A. Hamilton[135], P. D. Butler[114], Z. Han[179] and L. J. Magid[238]

Kinetics of Polymerization of Rod-Like Micelles
S. R. Kline[114]

Micellar Fluids Near a Solid Interface
C. Sommer[49], W. A. Hamilton[136] and L. J. Magid[238]

Microemulsion Structure at an Interface
G. Warr[237], J. Schulz[237], P. D. Butler[114] and W. A. Hamilton[136]

Microstructure of Alkylpolyglucoside Micelles and Microemulsions
L. D. Ryan[209], D. Ianspetro[209], C. McKelvey[209], J. Silas[209] and E. W. Kaler[209]

Microstructure and Properties of Hyperbranched Polymers
N. Wagner[209], B. Tande[209] and Y. Kim[209]

Microstructure of Shear Thickening and Shear Thinning Suspensions
N. Wagner[209], B. Moranzano[209], B. Schubert[209], B. Tunde[209], P. Middhu[209], A. Vaynberg[209] and R. Butera[47]

Mixed Cationic/Anionic Vesicle Formation Kinetics Using Time-Resolved SANS
P. Huibers[94], L. Shen[94] and I. Goldmints[94]

Octane Wetting of an Air/Water Interface
S. Satija[114] and R. Ivkov[114]

Ordered Structures of Pluronic Micelles in Formamide Solutions
P. Alexandridis[168], L. Yang[168], S. Ahn[168] and Y. Lin[168]

Percolation Transition in L-64 Triblock Copolymer Micelles
S.-M. Choi[114, 220] and S.-H. Chen[94]

Polymeric Surfactants on Modified Surfaces
A. Rennie[21], A. Jackson[143] and R. Thomas[143]

Poiseuille-Flow-Induced Changes in the Structure of Surfactant Micelles
L. Walker[27], B. Poore[27], M. Truong[27], Y. Christanti[27] and B. Hammouda[114]

Pressure-Induced Swelling of Polymer Micelles in Supercritical Fluids
M. McHugh[82], T. diNoia[82], J. van Zanten[82], C. Kirby[82], T. Kermis[82] and S. Conroy[82]

Prewetting at a Hydrophobic Surface in Phenol/Water Mixtures
A. Rennie[21], Z. X. Li[143] and R. Thomas[143]

SANS Characterization of Wax Modifiers for Diesel Fuel
L. Fetters[50], D. Richter[70] and W. Leube[70]

SANS Determination of the Persistence Length in Rod-Like Micelles
L. J. Magid[238] and P. D. Butler[114]

SANS Determination of the Structure of Vitrified Microemulsions
G. Warr[236], P. R. Harrowell[237], A. Widmer-Cooper[237] and P. D. Butler[114]

SANS from Nanodroplet Aerosols
B. Wyslouzil[255], C. Heath[255], K Streletzky[255], G. Wilemski[225] and R. Strey[69]

SANS Investigation of Stimuli Responsive Hybrid Linear-Dendrimer Copolymers in Various Solvents
M. Diallo[25], B. J. Bauer[124] and B. Hammouda[114]

SANS Measurements of Liposome Size Distributions
S. F. Trevino[114, 12], F. Lebeda[252] and G. R. Matyas[11]

SANS Study of Colloidal Interactions of Proteins
O. Velev[209], P. Hinderliter[209], J. Silas[209] and E. W. Kaler[209]

SANS Study of the Factors Affecting the Crystallization of Wax in Fractionated Petroleum
J. Hsu[179] and E. Sheu[179]

SANS Study of Interfacial Curvature in Microemulsions
S.-H. Chen[94] and S.-M. Choi[94]

SANS Study of Organic-Template-Driven Synthesis of Transition Metal Mesoporous Oxides
S. Elder[136] and P. D. Butler[114]

Search for Micelle Formation in Caustic Solutions Used in Bauxite Processing
J. Watson[15], J. M. Hanley[129] and M. Lin[50]

Shear-Induced Structure in Rodlike Micelles
P. D. Butler[114] and C. Sommer[49]

Structural Evolution During Synthesis of SBA-15 and MCF-type Mesoporous Silica
P. Schmidt-Winkel[204], G. D. Stucky[204], S. R. Kline[114] and C. J. Glinka[114]

Structure and Aggregation Behavior of Aqueous Solutions of Fulvic Acid
M. Diallo[61] and C. J. Glinka[114]

Structure and Aggregation of Soot in Flowing Motor Oil
M. Y. Lin[50] and M. Francisco[50]

Structure of Dendritic Diblock Copolymer Langmuir Films
P. Hammond[94] and J. Iyer[94]

Structure of Oil in Water Microemulsions Stabilized by Triblock Copolymer Amphiphiles
J. Lettow[94], A. Zarur[94] and J. Ying[94]

Structure of Ni(OH)$_2$ Sheared Dispersions of Colloidal Hard Plates
A. Rennie[26] and A. Brown[26]

Solvent Effects on the Size and Shape of Dendrimers
S. F. Trevino[114, 12] and N. Beck-Tan[114, 12]

Temperature and Concentrnation Dependence of Polymer(PEO)-Surfactant (SDS) Complexes in Aqueous Solutions
K. Chari[48] and M. Lin[50]

Time-Resolved SANS Study of Microemulsion Polymerization
C. Co[209] and E. W. Kaler[209]

CONDENSED MATTER PHYSICS/MAGNETISM

Antiferromagnetic Ordering of La$_{0.33}$Ca$_{0.67}$MnO$_3$ Thin Films
Y. Ijiri[137], J. A. Borchers[114], J. W. Lynn[114], R. W. Erwin[114], M. Rajeswari[220], M. C. Robson[220], R. Ramesh[220] and V. Venkatesan[220]

Antiferromagnetic Structure Determination: Exchange-Based MnPd-Based Thin Films
J. A. Borchers[114], R. F. Farrow[63], M. Toney[63]

A Bond-Valence Analysis of the Structure of YBa$_2$Fe$_3$O$_8$
I. Natali-Sora[194] and A. Santoro[114]

Characterization of the Antiferromagnetic Order in Exchange-Biased Ni$_{80}$Fe$_{20}$/CoO Bilayers
N. Gokemeijer[80], C. L. Chien[80], Y. Ijiri[137], J. A. Borchers[114] and R. W. Erwin[114]

Characterization of Thin SiO$_2$ on Si by Spectroscopic Ellipsometry, Neutron Reflectivity and X-ray Reflectivity
J. A. Dura[114], C. A. Richter[70], N. V. Nguyen[23] and C. F. Majkrzak[114]

Charge, Orbital Magnetic Ordering and Two-Phase Coexistence in La$_{1/2}$Ca$_{1/2}$MnO$_3$
Q. Z. Huang[114, 220], J. W. Lynn[114], V. Smolyaninova[220], K. Ghosh[220] and R. L. Greene[220], D. C. Dender[114], R. W. Erwin[114] and A. Santoro[114]

Crystal and Magnetic Structure of ZnCr$_{1.4}$Ga$_{0.6}$O$_4$
S.-H. Lee[114, 220], W. Retcliff[159], T. H. Kim[159] and S. Cheong[159]

Crystal and Magnetic Structures in Co$_{2.25}$Ru$_{0.75}$O$_4$ and Co$_{2.25}$Sn$_{0.25}$Ru$_{0.50}$O$_4$
Q. Z. Huang[114, 220], J. W. Lynn[114], R. W. Erwin[114], M. Crawford[45], R. L. Harlow[45] and E. M. McCarron[45]

Crystal and Magnetic Structures of FeOCl
W.-H. Li[104], S. Y. Wu[104], C. G. Wu[104] and J. W. Lynn[114]

Crystal and Magnetic Structures of La$_3$RuO$_7$ and La$_7$Ru$_8$O$_{26}$
Q. Z. Huang[114, 220], R. Cava[150], R. W. Erwin[114] and J. W. Lynn[114]

Crystal and Magnetic Structures of La$_5$R$_2$O$_{12}$
Q. Z. Huang[114, 220], R. Cava[150], R. W. Erwin[114] and J. W. Lynn[114]

Crystal and Magnetic Structures of Sr$_4$Fe$_2$CO$_9$
Q. Z. Huang[114, 220], R. Cava[150], R. W. Erwin[114] and J. W. Lynn[114]

Crystal and Magnetic Structures of TbBaCo$_2$O$_6$
Q. Z. Huang[114, 220], I. Troyanchuk[18] and J. W. Lynn[114]

Crystal Structure and Magnetic Ordering in CoMoO$_3$
Q. Z. Huang[114, 220], J. W. Lynn[114], R. W. Erwin[114] and M. Crawford[45]

Crystal Structure and Magnetic Ordering in Co$_{2.25}$(Sn$_{0.25}$)Ru$_{0.75}$O$_4$
Q. Z. Huang[114, 220] and M. Crawford[45]

Neutron Diffraction Measurements of Nanostructured, Non-Equilibrium Spinel Ferrites
V. G. Harris[111]

Neutron Reflectivity Studies of Fe_3O_4/NiO Exchange-Biased Bilayers
D. M. Lind[52], J. A. Dura[114] and C. F. Majrkzak[114]

Neutron Scattering Study of the Nuclear and Magnetic Structure of RD_3
T. J. Udovic[114], Q. Z. Huang[114, 220], J. W. Lynn[114], R. W. Erwin[114] and J. J. Rush[114]

Neutron Studies of New Incommensurate Magnetic Correlation's Near the Lower Critical Concentration for Stripe Order in $La_{1.6-x}Nd_{0.4}Sr_xCuO_4$
J. M. Tranquada[23], N. Ichikawa[240], P. M. Gehring[114] and S.-H. Lee[114, 220]

Oxygen Isotope Effect on the Spin and Lattice Dynamics of $La_{5/8}Ca_{3/8}MnO_3$
C. P. Adams[114, 220], J. W. Lynn[114], V. Smolyaninova[23], G. M. Zhao[220], R. L. Greene[220] and S.-W. Cheong[93,159]

Polarized Neutron Diffraction Studies of Magnetic Ordering in Exchange-Biased Fe_3O_4/CoO Superlattices
Y. Ijiri[137], J. A. Borchers[114], R. W. Erwin[114], S.-H. Lee[114, 220], C. F. Majrkzak[114], P. J. van der Zaag[147] and R. M. Wolf[147]

Polarized Neutron Reflectrometry Measurements of CoPt Thin Films
M. Toney[63], A. Schreyer[114], J. A. Borchers[114], C. F. Majrkzak[114]

Polarized-Neutron Scattering Measurements of the Oxygen Moment in (La,Sr)MnO₃
P. M. Gehring[114], G. Shirane[23] and H. Hirota[182]

Polarized Neutron Studies of Magnetic Interfacial Roughness in EuTe/PbTe Superlattices
H. Kepa[141, 114], T. Giebultowicz[141], G. Bauer[141], C. F. Majrkzak[114]

Pressure Dependence of the Nuclear and Magnetic Structures in $La_{0.67}Ca_{0.33}MnO_3$
Q. Z. Huang[114, 220], J. W. Lynn[114], A. Santoro[114], S. F. Trevino[114,12]

Pr Magnetic Order and Spin Dynamics in the Cuprates
J. W. Lynn[114], N. Rosov[114], S. N. Barilo[18], L. Kurnevitch[18] and A. Zhokhov[158]

Q-Dependence of the Spin Flip Scattering from Exchange Coupling across $Fe-FeF_2$ Interfaces Measured with Spin Polarized Neutron Diffraction with Polarization Analysis
M. Fitzsimmons[92] and I. Schuller[202]

Reflectivity Measurements on Spin Valve Structures
D. Sarkisov[232] and M. Dabaghian[232]

Refinement of the Ordered Moment in the Quasi-1D Antiferromegnet $CsNiCl_3$
I. Zaliznyak[82, 114] and C. Broholm[82, 114]

Single-Ion Anisotropy and Crystal Field Effects in R_2CuO_4 (R = Nd, Sm, Pr, …)
T. Yildirim[114], R. Sachidanandam[178], A. Aharony[178] and A. B. Harris[231]

Site Distributions and Magnetic Structures in $Al_{0.5}Fe_{0.5-x}Mn_x$, x = 0.05, 0.1, 0.15
V. Harris[111], D. J. Faremi[111], K. B. Hathaway[111], Q. Z. Huang[114, 220], A. Mohan[225] and G. J. Long[225]

Sites Distribution and Magnetic Structure in $La_2(Co_{1-x}Fe_x)_{16}Ti$. X = 0,0.2,0.4
J. K. Liang[68], Q. Z. Huang[114, 220] and A. Santoro[114]

Small-Angle Magnetic Scattering from Nanocrystalline Cobalt
J. Weismüller[193], R. D. Shull[118], R. McMichael[118], U. Erb[151] and J. G. Barker[114]

Spin Chain Direction in Copper Pyrazine Nitrate
M. Stone[82], D. H. Reich[82] and C. Broholm[82, 114]

Spin Dynamics of the Mn Ions in $La_{1-x}Ba_xMnO_3$ and $Pr_{1-x}Ba_xMnO_3$
J. W. Lynn[114], L. Vasiliu-Doloc[132], K. Ghosh[220], R. L. Greene[220] and S. Barilo[18]

Spin Dynamics in $LaTiO_3$
B. Keirner[95,150], A. Ivanov[76], J. W. Lynn[114], Y. Taguchi[240] and Y. Tokura[240]

Spin Dynamics in Single Crystal $La_{.7}Ca_{.3}MnO_3$
C. P. Adams[114, 220], J. W. Lynn[114] and Y. M. Mukovskii[102]

Spin Dynamics of Strongly Doped $La_{1-x}Sr_xMnO_3$
L. Vasiliu-Doloc[132], J. W. Lynn[114], Y. M. Mukovskii[102], A. A. Arsenov[102] and D. A. Shulyatev[102]

Spin Freezing in a Geometrically Frustrated Antiferromagnet, $Y_2Mo_2O_7$
J. Gardner[98], B. Gaulin[98], C. Broholm[82, 114] and S.-H. Lee[114, 220]

Spin-Flop Tendencies in Exchange-Biased Co/CoO Thin Films
J. A. Borchers[114], Y. Ijiri[114], S.-H. Lee[114, 220], C. F. Majrkzak[114], G. Felcher[8], R. Kodama[111], K. Takano[202] and A. E. Berkowitz[202]

Static and Dynamic Properties of Spin and Charge Ordering in $La_{2-x}Sr_xNiO_4$
S.-H. Lee[114, 220], S.-W. Cheong[93] and G. Aeppli[112]

Strain-Induced Changes to the NiO Spin Structure in NiO Thin Films
T. Regan[167], R. White[167] and J. Stohr[63]

Structural Change and Magnetic Ordering in Bilayered $La_{2-2x}Sr_{1+2x}Mn_2O_7$
W.-H. Li[104], S. Y. Wu[104], H. D. Yang[108] and J. W. Lynn[114]

Structural and Magnetic Ordering in DyD_{3-x}
T. J. Udovic[114], Q. Z. Huang[114, 220], J. W. Lynn[114] and R. W. Erwin[114]

Structural and Magnetic Ordering in ErD_{3-x}
T. J. Udovic[114], Q. Z. Huang[114, 220], J. W. Lynn[114] and R. W. Erwin[114]

Structural Phase Transition and Magnetic Order in Heavy Fermion Compounds Ce_3M with M = Al, In and Sn
W.-H. Li[104], K. C. Lee[104] and Y. Y. Chen[93]

Structure and Magnetic Order in $Ba_3MRu_2O_9$, M = Cu, Fe, Co, Ni, In
J. T. Rijssenbeek[146], Q. Z. Huang[114, 220], R. W. Erwin[114] and R. J. Cava[150]

Structure and Magnetic Order in $Sr_3CaRu_2O_9$
Q. Z. Huang[114, 220] and R. J. Cava[150]

Structure and Magnetic Order in $Sr_2Y_{0.8}Ca_{0.2}Co_2O_6$
Q. Z. Huang[114, 220], J. W. Lynn[114], R. W. Erwin[114] and R. J. Cava[150]

Structure and Magnetic Properties in the $Sr_{1-x}(La_{0.5}Na_{0.5})_xRuO_3$ Solid Solution
Q. Z. Huang[114, 220] and R. J. Cava[150]

Structure of $YCo_{0.5}Mn_{0.5}O_{3-x}$, $Tb_{0.5}Ba_{0.5}CoO_x$ and $Nd_{0.5}Ba_{0.5}CoO_x$
Q. Z. Huang[114, 220], J. W. Lynn[114, 220], R. W. Erwin[114] and I. Troyanchuk[5]

Structures of $HgMo_{0.25}Ba_2CuO_{4+x}$ High T_c Superconductor
Q. Z. Huang[114, 220], M. Marezio[74], F. Licci[74] and A. Santoro[114]

Structures of $Ba_{0.8}Sr_{0.2}CoO_y$ Compounds
Q. Z. Huang[114, 220] and R. J. Cava[150]

Structures of $YM_2Cu_{2.85}Re_{0.15}O_{7+x}$ (M = Ba and Sr) High T_c Superconductors
Q. Z. Huang[114, 220], M. Marezio[74], F. Licci[74] and A. Santoro[114]

Structure Change of $BaRuO_3$ Under High Pressure
Q. Z. Huang[114, 220], S. F. Trevino[114, 12], A. Santoro[114] and R. J. Cava[150]

Structure and Magnetic Ordering of $M[N(CN)_2]_2$ (M = Co, Ni, Mn)
J. L. Manson[245], C. R. Kmety-Stevenson[138], Q. Z. Huang[114, 220], J. W. Lynn[114], G. Bendele[168], S. Pagola[168], P. W. Stephens[168], L. M. Kiable-Sands[23], A. L. Rheingold[23], A. J. Epstein[138] and J. S. Miller[245]

Studies of Charge, Spin and Orbital Ordering in the System $Bi_{1-x}Ca_xMnO_3$
P. Woodward[138], J. Goldberger[138] and P. Santosh[138]

Studies of Magnetic Critical Scattering in Strained and Lattice-Matched (Y/Lu)|Ho|(Y/Lu) Films
P. M. Gehring[114], C. F. Majrkzak[114], L. D. Gibbs[23], A. Vigliante[23], A. C. Lake[143], J. Goff[143] and R. A. Cowley[143]

Studies of Spin Waves in the Ladder Compound $La_5Ca_9Cu_24O_{41}$
M. Matsuda[78], G. Shirane[23], S.-H. Lee[114, 220] and P. M. Gehring[114]

Study of Low-Energy Excitations in a Weakly-Coupled Quantum Spin Chain System
A. Zheludev[23], K. Uchinokura[71], C. Broholm[82, 114] and S.-H. Lee[114, 220]

Study of the Relax or Based Ferroelectric PZN-PT
P. M. Gehring[114], G. Shirane[23], R. E. Park[146] and T. R. Shnut[146]

Superconductivity in $La_{2-x}Sr_xCuO_4$
S. Wakimoto[182], S. Ueki[182], K. Hirota[182], K. Yamada[182], Y. Endoh[182], R. J. Birgeneau[94], Y. S. Lee[94], M. A. Kastner[94], G. Shirane[23], S.-H. Lee[114, 220] and P. M. Gehring[114]

Superconductivity, Magnetic Fluctuations and Magnetic Order in $TbSr_2Cu_{2.69}Mo_{0.31}O_7$
W.-H. Li[104], W. Y. Chuang, S. Y. Wu[104], K. C. Lee[104], J. W. Lynn[114], H. L. Tsay[108] and H. D. Yang[108]

Surface Spin Ordering in $LaFeO_3$ Thin Films
J. A. Borchers[114], J. Stohr[63] and M. Toney[63]

TbNiBC Diffraction and Critical Scattering
F. Bourdaut[114], Q. Z. Huang[114, 220] and J. W. Lynn[114]

Temperature Dependence of the Exchange Coupling in Fe/Cr Superlattices
A. Schreyer[220], C. F. Majrkzak[114] and T. Schmitte[157]

Temperature-Dependent Crystallography and Zero-Field Magnetic Order of $Mn[N(CN)_2]_2(pyrazine-d_4)$
J. L. Manson[245], J. W. Lynn[114] and J. S. Miller[245]

Temperature Evolution of the Spin Excitation Spectrum in a Reentrant Spin Glass $Fe_{0.7}Al_{0.3}$
W. Bao[91], S. Shapiro[23] and S.-H. Lee[220,114]

Three-Dimensional Spin Structure of $Sr_2CuO_2Cl_2$: Field Dependent Neutron Scattering Study

T. Yildirim[114], S. Skanthakumar[8] and J. W. Lynn[114]

Ultra-High Energy Resolution Studies of the Second Length Scale in Single Crystal Terbium

J. E. Lorenzo[76], B. Farago[76], B. F. Frick[76], P. M. Gehring[114], C. F. Majkrzak[114] and G. Shirane[23]

Vortex Lattice in $ErNi_2BC$

P. Gamme[193], S. Lopez[193], D. C. Dender[114], S. Choi[114, 220], J. W. Lynn[114] and P. Cawield[80]

Vortex Lattice Structure in High-Tc Bi-2212

B. Keimer[150, 95], T. Fong[150] and J. W. Lynn[114]

BIOMOLECULAR SCIENCE

Conformational Changes of Chaperonin Complexes Involved in Protein Refolding

E. Eisenstein[29], J. Zondlo[29] and S. T. Krueger[114]

Determination of the Bending of DNA Bound to Cyclic AMP Receptor Protein in Solution

F. Schwarz[29] and S. T. Krueger[114]

Determination of the Location of the Lipid Anchor in Outer Surface Protein A of Borrelia Burgdorfei by SANS

D. Schneider[23], C. Lawson[23] and V. Graziano[23]

Gelation of Methylcellulose

C.-I. Huang[223] and T. Lodge[223]

Interaction of the Peptide Penetration with Phospholipid Double Bilayers

G. Fragneto[76], E. Bellet-Amalric[76], F. Graner[76] and L. Perino

Interfacial Morphologies of Phospholipid Membrane Systems

B. Gaulin[98], P. Mason[33] and R. Epand[98]

Internal Organization of Peptide-Nucleic Acid Complexes Derived from SANS

F. Schwarz[29] and S. T. Krueger[114]

Interpretation of Specular and Off-Specular Reflectivity Data from Patterned Thiahexaethyleneoxide Alkane Surfaces

N. F. Berk[114], C. F. Majkrzak[114], A. Munter[114], J. Woodward[116], C.W. Meuse[116], A. L. Plant[116] and S. T. Krueger[114]

In-Situ Measurements of Melittin Insertion into Hybrid Bilayer Membranes

S. T. Krueger[114], C. F. Majkrzak[114], J. A. Dura[114], A. L. Plant[116] and C. Meuse[116]

Lysozyme Adsorption at the Air/Water Interface

J. Erickson[82] and K. J. Stebe[82]

Magnetic Field Alignment of Mixed Lipid Discotic Micelles

J. Katsaras[33], R. Prosser[85], S. T. Krueger[114], C. J. Glinka[114] and M. Nieh[146]

Membrane Active Peptides: Phase Transitions and Supramolecular Assemblies of Peptides in Membranes

H. W. Huang[153], W. Heller[153], T. Harroun[153] and L. Yang[153]

Motion in Alpha-Lactalbumin and Alpha-Lactalbumin Molten Glouble Studied by Quasielastic Neutron Scattering

B. Zimei[124], D. A. Neumann[114] and C. C. Han[124]

Neutron Diffraction Studies of Peptides in Fluid Lipid Bilayers

S. White[200] and K. Hristova[200]

Neutron Reflectivity Studies of Protein Adsorption/Desorption on the Surfaces of Self-Assembled Monolayers

M. D. Foster[196], S. Petrash[196] and C. F. Majkrzak[114]

Ordering in Protein/Polelectrolyte Multilayers

J. Rusling[207] and Y. Lvov[111]

Protein Adsorption at Solid/Liquid Interfaces

J. R. Lu[235], T. J. Su[235] and B. Green[235]

Quasielastic Neutron Scattering Study of the Dynamics of Water in Saccharide Solutions

A. Tsai[29], M. Feeney[150], P. G. Debenedetti[150] and D. A. Neumann[114]

RNase-A Dynamics by Time of Flight Neutron Scattering: A Case Study in Protein Dynamics and its Implications for Drug Design, Formulation and Delivery

A. Tsai[29], T. J. Udovic[114], J. R. D. Copley[114], D. A. Neumann[114], J. J. Rush[114], M. Tarek[114, 231], D. Tobias[200] and G. Gilliland[116]

SANS Studies of Calmodulin/Target Enzyme Interactions

J. Krueger[91], J. Trewhella[91], N. Bishop[91] and A. Wang[116]

SANS Study of Catechol Dioxygenases from Pseudomonas Putida SH1

S.-L Huang[104], W.-H. Li[104] and J. W. Lynn[114]

SANS Study of Cyclic-AMP-Dependent Protein Kinase

J. Zhao[91], J. Trewhella[91], D. Walsh[199] and R. Bruschia[199]

SANS Study of the DNA/Flap Endonuclease Complex

J. Trewhella[91], C. Kim[91] and S. Gallagher[91]

SANS Study of Protein Folding Mechanisms

R. M. Briber[220], R. Perez-Salaz[220] and S. T. Krueger[114]

SANS Study of the Ferredoxin TOL Component of Toluence Dioxygenase from Pseudomonas Putida F1

S.-L. Huang[104], D. T. Gibson[218], W.-H. Li[104] and J. W. Lynn[114]

Self Assembly of Peptide Amphiphiles

H. Bianco[223], T. Gore[223], Y. Dori[223] and M. Tirrell[223]

Structure of G-Actin in Solution

R. Ivkov[114], P. Shantharaj[220], J. Forbes[220] and S. Greer[220]

Structure of Hybrid Bilayer Membranes by Direct Inversion of Neutron Reflectivity Data

C. F. Majkrzak[114], N. F. Berk[114], C. W. Meuse[116], V. Silin[116], A. L. Plant[116] and S. T. Krueger[114]

Structure of Intact Influenza Hemagglutinin Protein Containing the Viral Membrane Spanning Region

R. Blumenthal[107], D. Remeta[159], S. Durell[107] and S. T. Krueger[114]

Structure of Microtubule-Based Cellular Motors Investigated by SANS

R. A. Mendelson[203], D. B. Stone[203] and R. P. Hjelm[91]

Vectorially-Oriented Protein Monolayers: Neutron Reflectivity Studies

J. K. Blasie[231], L. Kneller[231], E. Nordgren[231], J. Strzalka[231] and A. Edwards[231]

CHEMICAL PHYSICS OF MATERIALS

A Quasi-Elastic and Inelastic Neutron Scattering Study of Hydrogen in Zeolite

P. Sokol[146] and R. M. Dimeo[114]

Bond Lengths and Ground State Structure of the Fulleride Polymer K_1C_{60}

G. M. Bendele[91], A. Huq[168] and P. W. Stephens[168]

Deposition Interdiffusion at Room Temperature and the Kinetics of Interlayer Diffusion in Barium Stearate Langmuir-Blodgett Films at the Temperature Just below the Melting Point

L. A. Feigin[77] and I. I. Samoilenko[77]

Dynamics of Arsenic-Selenium Glasses

B. Effey[139], R. L Cappelletti[139] and W. A. Kamitakahara[114]

Dynamics of Hydrogen in Laves Phase Hydrides

A. V. Skripov[99], J. C. Cook[114, 220], T. J. Udovic[114] and D. A. Neumann[114]

The Dynamics of Hydrogen in Single-Walled Nanotubes

W. M. Brown[114, 220], T. Yildirim[114] and D. A. Neumann[114]

Dynamics of Hydrogen Trapped by Defects in Pd

R. Kirchheim[234], T. J. Udovic[114] and J. J. Rush[114]

Dynamics of Layered Silicates: Intercalated Water

N. Wada[183] and W. A. Kamitakahara[114]

Dynamics of Li-Doped Carbon Electrode Materials

P. Papanek[114, 231], J. E. Fischer[223, 231] and W. A. Kamitakahara[114]

The Dynamics of Potassium Crytand Complexes

N. C. Maliszewskyj[114], D. A. Neumann[114], D. J. Gilbert[101] and J. L. Dye[101]

Dynamics of Selenium-Arsenic-Bromine Glasses

R. L. Cappelletti[114] and B. E. Schwickert[196]

The Effects of Confinement on Tunneling in Methyl Iodide

R. M. Dimeo[114]

Evolution of the Structure of the K_2NiF_4 Phases of $La_{2-x}Sr_xNiO_{4+\epsilon}$ with Oxidation State: Octahedral Distortion and Phase Separation ($0.2 < x < 1.0$)

J. E. Millburn[143], M. A. Green[143], M. J. Rosseinsky[143] and D. A. Neumann[114]

First-Principles Calculations and Neutron Scattering

T. Yildirim[114] and O. Gulseren[231]

First-Principles Calculations of Structural, Vibrational and Electronic Properties of Solid Cubane

T. Yildirim[114], C. Kilic[20] and S. Ciraci[20]

First-Principles Investigation of Structure and Dynamics of Negative Thermal Expansion Materials

T. Yildirim[114]

Fulleride Superconductors

T. Yildirim[114]

High Resolution Powder Diffraction of $CeRh_2Si_2$

G. M. Bendele[91], W. Bao[91], R. A. Robinson[91] and J. L. Sarrao[91]

Hydrogen Dynamics in K_3MnH_5

G. Auffermann[195], T. J. Udovic[114], J. J. Rush[114] and T. Yildirim[114]

Hydrogen Dynamics in $ZrBeH_{1.5}$

T. J. Udovic[114] and B. Hauback[72]

Incoherent Scattering from Lipid Bilayers and Bilayers with Channel Proteins Imbedded

S. H. Chen[94], C. Liao[94] and T. Weiss[153]

Inelastic Neutron Scattering Study of the Dynamics of Crown Ethers in Potassium Electrides

N. C. Maliszewskyj[114], D. A. Neumann[114], M. Wagner[57] and J. L. Dye[101]

Inelastic Neutron Scattering Study of the Dynamics of Guanidinium-Based Clathrate Materials

A. Pivovar[223], M. Ward[223], D. A. Neumann[114], T. Yildirim[114] and J. J. Rush[114]

Inelastic Neutron Scattering Study of the Hydration of Tricalcium Silicate

S. A. FitzGerald[137], J. J. Thomas[133], J. C. McLaughlin[133], D. A. Neumann[114] and R. A. Livingston[51]

Inelastic Neutron Scattering Study of Rare Earth Trihydrides and Trideuterides

T. J. Udovic[114], J. J. Rush[114] and Q. Z. Huang[114, 220]

Inelastic Neutron Scattering Study of Al Charged with Hydrogen

T. J. Udovic[114], J. J. Rush[114], C. Buckley[216] and H. K. Birnbaum[216]

Inelastic Scattering in Ce- and U-Based Non-Fermi Liquid Systems

W. Beyermann[201], T. Kelly[201], R. Robinson[91] and B. Maple[202]

In Situ Neutron Reflectometry Study of Self-Assembled Poly(Dimethyl Siloxane) Film

M.-W. Tsao[209], J. Rabolt[209], A. Kalambur[209], L. Sung[114, 220] and C. F. Majkrzak[114]

Isotopic Ordering in La(D_xH_{1-x})$_3$

T. J. Udovic[114], Q. Z. Huang[114, 220] and J. J. Rush[114]

Location of H and/or D Dissolved in Crystalline Pd$_3$P$_{0.8}$

T. J. Udovic[114], Q. Z. Huang[114, 220] and Y. Andersson[243]

The Microscopic Glass Transition in Viscous Metallic Liquids

A. Meyer[114, 220], R. Busch[25], J. Neuhaus[175] and H. Schober[76]

Neutron and X-ray Reflectometry Studies of Rough Interfaces in a Langmuir Blodgett Film

H. Kepa[141], L. J. Kleinwalks[181], N. F. Berk[114], C. F. Majkrzak[114], T. S. Berzina, V. I. Troitsky[177], R. Antolini[242] and L. A. Feigin[77]

Neutron Investigation of Molecular Reorientations in Solid Cubane

T. Yildirim[114], P. M. Gehring[114], D. A. Neumann[114], P. E. Eaton[206] and T. E. Emrick[206]

Neutron Scattering Studies of Hydration Reaction of Tricalcium Silicate and Portland Cement

S. A. FitzGerald[137], J. J. Thomas[133], D. A. Neumann[114] R. A. Livingston[51] and J. McLanghlin[133]

Neutron Scattering Studies of the Dynamics of Hydrofluorocarbons Encaged in NaX and NaY Zeolites

C. Karmonik[239], N. C. Maliszewskyj[114], T. J. Udovic[114], J. J. Rush[114], M. K. Crawford[45], D. R. Corbin[3] and R. R. Cavanagh[128]

Neutron Scattering Studies on the Vibrational Excitations and the Structure of Ordered Niobium Hydrides

B. Hauer[70], E. Jansen[70], W. Kockelmann[70], W. Schafer[70], D. Richter[70], R. Hempelmann[193], T. J. Udovic[114] and J. J. Rush[114]

Neutron Scattering Study of the Structure of Na$_2$C$_{60}$ as a Function of Pressure and Temperature

T. Yildirim[114], D. A. Neumann[114], S. F. Trevino[114, 12] and J. E. Fischer[231]

Neutron Scattering Study of the Dynamics of Hydrogen and Deuterium Solved in Crystalline Pd$_9$Si$_2$

C. Karmonik[239], T. J. Udovic[114], Q. Z. Huang[114, 220], J. J. Rush[114], Y. Andersson[246] and T. B. Flanagan[246]

Neutron Scattering Study of the Role of Diffusion in the Hydration Reaction of Tricalcium Silicate

S. A. FitzGerald[137], J. J. Thomas[133], D. A. Neumann[114] and R. A. Livingston[51] and J. McLanglin

Neutron Scattering Study of the Vibrational Modes of Cubane

T. Yildirim[114], P. M. Gehring[114], D. A. Neumann[114], P. E. Eaton[206] and T. E. Emrick[206]

Neutron Spectroscopy of Single-Walled Nanotubes

P. Papanek[114], J. E. Fischer[223, 231] and A. Clay[231]

Neutron Vibrational Spectroscopy of Pd$_3$P$_{0.8}$H(D)$_x$

T. J. Udovic[114,], Q. Z. Huang[114, 220] and Y Andersson[246]

Neutron Vibrational Spectroscopy of Sr$_2$IrH$_5$

T. J. Udovic[114] and R. O. Moyer[185]

Layer Shearing Modes in Li-Graphite Compounds

W. A. Kamitakahara[114] C. Bindra[231] and J. E. Fischer[223, 231]

Low Energy Dynamics of Alkali Silicate Glasses

J. Toulouse[90] and D. A. Neumann[114]

Orientational Dynamics of P$_4$ Molecules in White Phosphorus

W. A. Kamitakahara[114], T. Yildirim[114], D. A. Neumann[114] and F. Gompf[84]

Preferential Isotopic Site Occupation in Rare-Earth Hydrides

T. J. Udovic[114], Q. Z. Huang[114, 220] and J. J. Rush[114]

Phonon Density of States in Sc$_2$(WO$_4$)$_3$

C. Broholm[82], C. Urich[82] and G. Gasparovic[82]

Pressure Dependence of Phonon Density of States in Zr$_2$W$_2$O$_8$

C. Broholm[82], C. Ulrich[82] and A. P. Ramirez[93]

Proton Dynamics in Hydrated Nafions

T. J. Udovic[114], S. F. Trevino[114, 12] and M. K. Crawford[45]

Proton Dynamics in Strontium Cerate and Zirconate Ceramics

C. Karmonik[239], T. Yildirim[114], T. J. Udovic[114], J. J. Rush[114] and R. L. Paul[115]

Quasielastic Scattering Study of the Liquid-Glass Transition Intertramethyl-Heptane

J. Toulouse[34], H. Cummins[34] and S. Goiqing[34]

Relaxational Dynamics in GeO$_2$

A. Meyer[114, 220], J. Neuhaus[175] and H. Schober[76]

Rotational Dynamics of C$_{60}$ in (ND$_3$)K$_3$C$_{60}$

S. Margadonna[236], K. Prassides[236], D. A. Neumann[114], H. Shimoda[2] and Y. Iwasa[2]

Search for Bragg Peaks in Se-As-Br Glasses

R. Cappelletti[114] and B. Schwickert[198]

Search for Sublattice Ordering in PrD$_{2+x}$

T. J. Udovic[114] and Q. Z. Huang[114, 220]

Slow Motion in Bulk-Glass Forming Zr$_{46.8}$Ti$_{8.2}$Cu$_{7.5}$Ni$_{10}$Be$_{27.5}$

A. Meyer[114, 220], J. Wuttke[175], W. Petry[175] and H. Schober[76]

Structural Investigation of the High Temperature Protonic Conductors

C. Karmonik[239], Q. Z. Huang[114, 220], T. J. Udovic[114] and J. J. Rush[114]

Structural Ordering in LaD$_{3-x}$

T. J. Udovic[114], Q. Z. Huang[114, 220] and J. J. Rush[114]

Structure and Dynamics of Amorphous Carbon

P. Papanek[114, 231], W. A. Kamitakahara[114] and J. E. Fischer[223, 231]

Structure and Dynamics of Hydrogen in C$_{60}$

S. A. FitzGerald[137], T. Yildirim[114], L. J. Santodonato[114], D. A. Neumann[114], J. R. D. Copley[114], J. J. Rush[114] and F. Trouw[8]

Structure and Dynamics of Hydrogen in Na$_x$C$_{60}$

S. A. FitzGerald[137], T. Yildirim[114], L. J. Santodonato[114] and D. A. Neumann[114]

Structure and Dynamics of an Ultrahard Carbon

W. A. Kamitakahara[114], S. F. Trevino[114, 12] and S. G. Buga[75]

Structure of the Ruddlesdon-Popper, (Ln,Ca)$_{n+1}$Mn$_n$O$_{3n+1}$ Series (Ln = Lanthanide)

M. Green[156] and J. Waldron[156]

Vibrational Densitites of States for Cubic and Hexagonal Boron Nitride

W. A. Kamitakahara[114], D. A. Neumann[114], G. Doll[56], B Sweeting[56] and A. W. Moore[1]

The Vibrational Isocoordinate Rule in Se-As-Ge Glasses

B. Effey[139], R. L. Cappelletti[114] and W. A. Kamitakahara[114]

INSTRUMENTATION

Assembly and Testing of the Filter Analyzer Spectrometer

A. W. Clarkson[114], D. J. Pierce[114] J. Reardon[114], S. Slifer[114] and G. M. Baltic[114]

Characterization of Fe/Si Reference Layers for Reflectivity Data Inversion

C. F. Majkrzak[114]

"DARTS": A New Neutron Diffractometer for Residual Stress Measurement, Texture Determination and Single Crystal Diffraction

P. C. Brand[114], H. J. Prask[114] and T. Gnäupel-Herold[220]

Data Acquisition and Analysis Software for the Backscattering Spectrometer

N. C. Maliszewskyj[114] and R. M. Dimeo[114]

Data Analysis Software for the Fermi Chopper Spectrometer

T. Yildirim[114] and C. M. Brown[220]

Design of a Cable and Hose Management System for the NSE Spectrometer

D. Fulford[114]

Design of the Disk Chopper Spectrometer

C. W. Brocker[114, 220]

Design of the Filter Analyzer Spectrometer

D. J. Pierce[114], R. Christman[114] and J. T. Kenney[114]

Design and Performance Testing of the DCS Data Acquisition System Electronics

J. Ziegler[114], J. Raebiger[70], P. Klosowski[114] N. C. Maliszewskyj[114] and H. Layer[114]

Design and Testing of Vertically Polarized Heusler Alloy Monochrometer/Analyzer

J. W. Lynn[114], J. A. Borchers[114] and K. T. Forstner[114]

Design of the Perfect Crystal SANS Diffractometer

J. J. Moyer[114], J. T. Kenney[114] and J. G. Barker[114]

Development and Design of the Next-Generation Triple-Axis Spectrometer
C. W. Wrenn[114, 220], M. Murbach[114, 220], P. C. Brand[114] and J. W. Lynn[114]

Development and Installation of a Leak-Tight, Top-Loading, Horizontal Field Superconducting Magnet
D. C. Dender[114, 220] and R. W. Erwin[114]

Development and Installation of a Radial Collimator and Horizontally Focussed Pb Analyzer for BT-2
J. G. LaRock[114] and A. W. Carkson[114]

Development and Testing of Fe/Si Supermirror Plates for the NSE Analyzer
N. Rosov[114], S. Rathgeber[114, 220], C. F. Majkrzak[114] and J. Wood[142]

Development of a Radially-Focussed Polarizing Supermirror Analyzer Array
M. Murbach[114, 220], P. C. Brand[114] and N. Rosov[114]

Development of a Robust Static Thermal Switch for Fixed Sample Environment Temperatures from 15-650K
L. Santodonato[114]

Development of the HFBS Doppler Drive
R. M. Dimeo[114], A. Meyer[114, 220], R. Christman[114] and P. C. Brand[114]

Development of Synthetic Mica Monochromators
K. T. Forstner[114] and L. Passell[23]

Development of a Vacuum Rated Preamplifier/Amplifier/-Discriminator for $_3$He Neutron Detectors
J. Ziegler[114]

Dy/SPP Neutron Detector
Y.-T. Cheng[113, 114] and J. K. Stalick[114] and B. H. Toby[114]

The Disk Chopper Time-of-Flight Spectrometer(DCS)
J. R. D. Copley[114], J. C. Cook[114, 220] and F. B. Altorfer[114, 145]

Evaluation of New Neutron Area-Detectors
Y. T. Cheng[115, 113]

Evaluation of a Beryllium Single Crystal as a Monochromator for"DARTS"
P. C. Brand[114] and T. Gnäupel-Herold[220]

The Filter Analyzer Spectrometer
D. A. Neumann[114], P. Papanek[231], J. E. Fischer[231], J. J. Rush[114], M. L. Klein[231] and A. C. Cheetham[204]

The High Flux Backscattering Spectrometer (HFBS)
R. M. Dimeo[114], D. A. Neumann[114], C. Karmonik[239], A. Meyer[114, 220] and P. M. Gehring[114]

Hydrogen Cold Source Development
R. E. Williams[114], P. A. Kopetka[114] and J. M. Rowe[114]

In-Situ Real-Time Neutron Beam Imaging
K. T. Fortner[114] and N. C. Maliszewskyj[114]

Installation and Testing of the New Thermal Beam Tube Shutter Design Using a Remote Actuated Cast System
J. J. Moyer[114], C. W. Wrenn[114, 220], P. C. Brand[114], A. W. Clarkson[114], G. M. Baltic[114], D. L. Clem[114], M. J. Rinehart[114] and S. Slifer[114]

Installation of a New Heusler Alloy Polarizing Analyzer for BT-2
K. T. Forstner[114], J. A. Borchers[114] and J. W. Lynn[114]

Installation of Dedicated Crystal Alignment Spectrometer at BT-7 Beamline for Construction of FANS Double Focusing Copper Monochromator
K. T. Forstner[114] and A. W. Clarkson[114]

Installation of the Sample Chamber, Flight Chamber and Detector Assembly for the DCS
C. W. Brocker[114, 220], M. J. Rinehart[114], G. M. Baltic[114] and S. Slifer[114]

Laue Focussing and Its Applications
V. K. Kvardakov[87], V. A. Somenkov[87], S. S. Shilstein[87], J. W. Lynn[114], D. F. R. Mildner[115] and H. H. Chen-Meyer[115]

MBE Chamber for In-Situ Neutron Scattering: Instrument Development
J. A. Dura[114]
Mica and Ge Reflectivity
K. T. Forstner[114] and C. F Majkrzak[114]

Monte Carlo Methods for Nuclear Applications
R. E. Williams[114]

Monte Carlo Simulation of the NIST Cold Neutron Beamlines
J. C. Cook[114, 220]

Neutron Scattering Properties and Materials Properties Testing of the Null Scattering Titanium Alloy to be used for High Pressure Cells
S. F. Trevino[114, 12], K. T. Forstner[114] and R. Fields[123]

The NIST Neutron Spin Echo Spectrometer (NSE)
N. Rosov[114], S. Rathgeber[114, 220] and M. Monkenbusch[70]

Osmic and Mica Supermirror Tests
K. T. Forstner[114] and C. F. Majkrzak[114]

Performance Tests of the Phase Space Transform Chopper on NG-2
P. M. Gehring[114], D. A. Neumann[114] and C. Karmonik[239, 114]

SANS Polarization Analysis with Nuclear-Spin-Polarized $_3$He
T. R. Gentile[120], G. L. Jones[120], A. K. Thompson[120], J. G. Barker[114], C. J. Glinka[114], B. Hammouda[114] and J. W. Lynn[114]

Search for Effects on Neutron Transmission Due to Multiple Reflection by Glass Capillary Walls
R. E. Beneson[22, 24], H. H. Chen-Mayer[22] and J. W. Lynn[114]

Spin Echo Supermirror Development
N. Rosov[114] and C. F. Majkrzak[114]

Supermirror Reflectivity Measurements
C. F. Majkrzak[114]

TANQENS-A New Utility for the Analysis of Quasiolate Neutron Scattering Data
T. Yildirim[114]

Tests of Compound Refractive Optics for SANS
S.-M. Choi[114, 220], J. G. Barker[114], C. J. Glinka[114], P. L. Gammel[93] and Y. T. Cheng[113]

NEUTRON PHYSICS

Accurate Determination of Neutron Capture Flux
M. S. Dewey[120], M. Arif[120], D. M. Gilliam[120], G. L. Greene[91], W. M. Snow[67], J. Pauwels[73] and R. Scott[96]

Benchmark Measurements and Calculations of Neutron Transport
D. M. Gilliam[120], M. S. Dewey[120], J. S. Nico[120], C. M. Eisenhauer[120], J. Grundl[120] and H. Gerstenberg[10]

Certified Neutron Fluence Standards from the Cavity Fission Source
J. M. Adams[120] and J. Grundl[120]

Defined-Geometry Alpha Counting
D. M. Gilliam[120] and J. S. Nico[120]

Determination of the Neutron Lifetime
M. S. Dewey[120], J. S. Nico[120], D. M. Gilliam[120], W. M. Snow[67], G. L. Greene[91] and X. Fei[67]

Highly Accurate Neutron Wavelength Measurements
M. S. Dewey[120], K. J. Coakley[127], W. M. Snow[67] and M. Arif[120]

Intercomparison of NIST and PNL Calibration Facilities
A. Thompson[120], R. B. Schwartz[120], J. McDonald[16] and M. Murphy[16]

LASER Polarization of $_3$He for Neutron Spin Filters and Medical MRI
A. K. Thompson[120], T. R. Gentile[120], M. S. Dewey[120], G. L. Jones[120, 67], F. E. Wietfeldt[120, 59], W. M. Snow[67] and R. Rizi[231]

Neutron Calorimetry
W. M. Snow[67], Z. Chowdhuri[67], X. Fei[67] and M. S. Dewey[120]

Neutron Fluence Rate Measurements
D. M. Gilliam[120], J. S. Nico[120] and J. M. Adams[120]

Neutron Interferometry and Optics
M. Arif[120], D. L. Jacobson[120], R. Clothier[19], A. K. Thompson[120], S. A. Werner[224], A. Ioffe[224, 120], A. Zeilinger[217], K. Raum[226], B. Schillinger[226], C. Rausch[226] and W. Richards[96]

Neutron Radiography/Tomography
T. R. Gentile[120], M. Arif[120] and D. L. Jacobson[120]

Parity Non-Conserving Neutron Spin Rotation
B. Heckel[248], D. Markoff[248], E. Adelberger[248], S. Penn[248] and F. E. Wietfeldt[120, 59]

Quality Assurance Checks on Masses and Impurities in Neutron Dosimeters for NRC Reactor Pressure Vessel Embrittlement Surveillance
J. M. Adams[120], D.Gilliam[120] and J. Grundl[120]

Response of Albedo Dosimeters Versus Distance from a Neutron Source
R. B. Schwartz[120] and A. K. Thompson[120]

Response of Albedo Neutron Dosimeters as a Function of Angle
R. B. Schwartz[120]

Study of Time Reversal Invariance in Neutron Beta Decay
J. Wilkerson[253], E. Wasserman[198], J. S. Nico[120], R. G. H. Robertson[198], S. Freedman[198], A. Garcia[228], T. Chupp[24], K. Coulter[24], M. S. Dewey[120], G. L. Greene[91], A. K. Thompson[120], B. Fujikawa[198], G. L. Jones[120, 67], J. M. Adams[120], F. E. Wietfeldt[120, 59], L. Lising[198], S. Hwang[24] and T. Steiger[248]

Trapping of Ultra Cold Neutrons
J. M. Doyle[59], S. K. Lamoreaux, R. Golub[58], G. L. Greene[91], M. S. Dewey[120], P. R. Huffman[59], C. R. Brome[59], C. E. H. Mattoni[59], J. S. Butterworth[59] and D. N. McKinsey[59]

Utilization of the Materials Dosimetry Reference Facility-Tests of New IRMM $_{237}$Np and $_{238}$U Fast Neutron Dosimeters
J. M. Adams[120], J. Grundl[120], C. M. Eisenhauer[120], D. M. Gilliam[120] and P. Simpson[24]

MATERIALS ANALYSIS

A Bender-Focuser for Prompt Gamma Activation Analysis
E. A. Mackey[115], H. H. Chen-Mayer[115], R. M. Lindstrom[115], D. F. R. Mildner[115], R. L. Paul[115], Q.-F. Xiao[247] and V. A. Sharov[256]

Analytical Applications of Cold Neutrons
H. H. Chen-Mayer[115], R. Demiralp[115], R. R. Greenberg[115], G. P. Lamaze[115], J. K. Langland[115], R. M. Lindstrom[115], E. A. Mackey[115], D. F. R. Mildner[115], R. L. Paul[115] and V. A. Sharov[256]

Application of Radioisotope-Induced X-Ray Emission to the Identification of Lead and Other Elements in Ceramic Glazes and Housewares
D. L. Anderson[53] and W. C. Cunningham[53]

Archeological Applications of NAA
R. Bishop[165] and M. J. Blackman[115]

Bromation in Breadmaking
W. C. Cunningham[53] and C. R. Warner[53]

Bio-Analytical and Specimen Bank Research
K. A. Fitzpatrick[115], R. R. Greenberg[115], G. V. Iyengar[126], J. K. Langland[115], E. A. Mackey[115], B. J. Porter[115] and R. Zeisler[115]

Certification of Standard Reference Materials by Neutron Activation Analysis
D. A. Becker[115], R. Demiralp[115], R. R. Greenberg[115], R. M. Lindstrom[115], E. A. Mackey[115] and R. Zeisler[115]

Characterization of Sources and Fluxes of Particulate Pollutants Depositing to Great Waters
P. F. Caffrey[220], A. E. Suarez[220] and J. M. Ondov[220]

Characterization of Submicrometer Aerosol Particles
J. M. Ondov[220], S. F. Heller-Zeisler[220] and R. Zeisler[115]

Determination of Hydrogen by PGAA
R. R. Greenberg[115], R. M. Lindstrom[115], E. A. Mackey[115] and R. L. Paul[115]

Determination of Phosphorus via RNAA with Beta Counting
R. L. Paul[115]

Development of Radiochemical Separation for NAA
D. A. Becker[115], R. R. Greenberg[115] and E. A. Mackey[115]

Evaluation of Accuracy and Precision in INAA of Botanical Materials
D. A. Becker[115]

Evaluation of Errors and Interferences in NAA
D. A. Becker[115], M. J. Blackman[165], R. R. Greenberg[115], R. M. Lindstrom[115] and R. Zeisler[115]

Focusing Methods for Radiography and Topography
H. H. Chen-Mayer[115], D. F. R. Mildner[115], K. M. Podurets[87] V. A. Sharov[256] and S. S. Shilstein[87]

High Sensitivity Gamma-Ray Spectrometry
R. M. Lindstrom[115]

Homogeneity and Composition of Small Solid Samples
R. Zeisler[115]

Hydrogen Detection in Industrial Materials by Incoherent Neutron Scattering
H. H. Chen-Mayer[115], V. V. Kvardakov[87] D. F. R. Mildner[115], V. A. Somenkov[87] and D. Kozlenko[83]

Improvements to INAA Methodology
D. A. Becker[115], R. Demiralp[115], R. R. Greenberg[115], R. M. Lindstrom[115], E. A. Mackey[115] and R. Zeisler[115]

Improvements to PGAA Methodology
D. L. Anderson[53], R. M. Lindstrom[115], E. A. Mackey[115] and R. L. Paul[115]

Lithium Migration in Electrochromic Thin Films
G. P. Lamaze[115], H. H. Chen-Mayer[115], M. Badding[160], A. Gerouk[186] and R. Goldner[186]

Multielement Analysis of Foods and Related Materials by NAA
D. L. Anderson[53] and W. C. Cunningham[53]

Neutron Absorption Measurements Using Converging Beams
H. H. Chen-Mayer[115], E. A. Mackey[115], D. F. R. Mildner[115] and R. L. Paul[115]

Neutron Autoradiography of Paintings
Y.-T. Cheng[113, 115] and J. Olin[140]

Neutron Beam Spatial Distributions Using Imaging Plate Technology
H. J. Bahre[54], H. H. Chen-Mayer[115], Y.-T. Cheng[113, 115], D. F. R. Mildner[115] and V. A. Sharov[256]

Neutron Depth Profiling of AlN Thin Films
H. H. Chen-Mayer[115], G. P. Lamaze[115] and S. McGuire[38]

Neutron Depth Profiling of c-BN
H. H. Chen-Mayer[115], G. P. Lamaze[115] and L. Pilione[16]

Nitrogen Profiling of Thin Titanium Nitride Films
G. P. Lamaze[115], H. H. Chen-Mayer[115], N. Cox[79] and E. B. Steel[128]

Neutron Focusing for Analytical Chemistry
H. Chen-Mayer[115], G. P. Lamaze[115], J. K. Langland[115], R. M. Lindstrom[115], E. A. Mackey[115], D. F. R. Mildner[115], V. A. Sharov[256] and J. R. Swider[128]

Neutron Distribution Measurements by Neutron Induced Autoradiography
Z. En[247], J. S. Brenizer[247] and D. A. Becker[115]

Neutron Dosimetry for Instrument Development
R. M. Lindstrom[115]

Neutron Scattering Effects on PGAA
R. R. Greenberg[115], R. M. Lindstrom[115], E. A. Mackey[115], R. L. Paul[115] and M. Blaauw[174]

Neutron Transmission through Tapered Capillaries
H. H. Chen-Mayer[115], D. F. R. Mildner[115] and V. A. Sharov[256]

New Developments in Monitor Activation Analysis
G. P. Lamaze[115], R. M. Lindstrom[115], E. A. Mackey[115] and R. L. Paul[115]

New Developments in NDP
H. H. Chen-Mayer[115], G. P. Lamaze[115] and J. K. Langland[115]

Quality Assurance Improvements for NAA
D. A. Becker[115], R. Demiralp[115], R. R. Greenberg[115], R. M. Lindstrom[115], E. A. Mackey[115] and R. Zeisler[115]

Quality Assurance Programs
D. L. Anderson[53] and W. C. Cunningham[53]

Reactor Characterization for NAA
D. A. Becker[115]

Radionuclides in Foods
D. L. Anderson[53] and W. C. Cunningham[53]

Revalidation of Food SRMs
D. L. Anderson[53] and W. C. Cunningham[53]

Size Distribution and Deposition of Toxic Elements to Lake Michigan, by Size and by Source.
P. F. Caffrey[220] and J. M. Ondov[220]

Studies in Elemental Speciation
D. A. Becker[115], E. A. Mackey[115] and R. Zeisler[115]

Test of a Novel High Sensitivity Neutron Detector
B. Feller[134], H. H. Chen-Mayer[115] and G. Lamaze[115]

Trace Elemental Characterization of Silicon Semiconductor Materials
D. A. Becker[115] and R. M. Lindstrom[115]

54 Fuji Medical Systems USA, Incorporated
55 General Electric Corporate Research
56 General Motors Research and Development Center
57 George Washington University
58 Hahn-Meitner Institute, Germany
59 Harvard University
60 Hongik University, South Korea
61 Howard University
62 IAP Research, Incorporated
63 IBM, Almaden
64 Idaho National Engineering and Environment Laboratory
65 Imaging and Sensing Technology
66 Imperial College, United Kingdom
67 Indiana University
68 Institute of Physics, Peoples Republic of China
69 Institut Für Physikalische Chemie, Germany
70 Institut für Festkorperforschung, Germany
71 Institute for Chemical Research, Japan
72 Institute for Energiteknikk, Norway
73 Institute for Reference Materials and Measurements, Belgium
74 Institute for Special Materials, CNR, Italy
75 Institute for Superhard and Novel Carbon Materials, Russia
76 Institut Laue-Langevin, France
77 Institute of Crystallography, Russia
78 Institute of Physical and Chemical Research, Japan
79 Intel Corporation
80 Iowa State University
81 John Deere Corporation
82 Johns Hopkins University
83 Joint Institute for Nuclear Research, Russia
84 Karlsruhe Nuclear Research Center, Germany
85 Kent State University
86 Kiel University, Germany
87 Kurchatov Institute, Russia
88 Kyunghee University
89 Kyoto University, Japan
90 Lehigh University
91 Los Alamos National Laboratory
92 Los Alamos Neutron Science Center
93 Lucent Technologies, Bell Laboratories
94 Massachusetts Institute of Technology
95 Max-Planck Institut, Germany
96 McClellan Nuclear Radiation Center
97 McGill University, Canada
98 McMaster University, Canada
99 Metal Physics Institute, Russia
100 Michigan Molecular Institute
101 Michigan State University
102 Moscow Steel and Alloys Institute, Russia
103 National Aeronautics and Space Administration, Johnson Space Center
104 National Central University, Taiwan
105 National Cheng Kung University, Taiwan

106 National Institute for Research in Inorganic Materials, Japan
107 National Institute of Health
108 National Sun Yat-Sen University, Taiwan
109 National Taiwan University, Taiwan
110 National Tsing Hua University, Taiwan
111 Naval Research Laboratory
112 NEC Research Institute Incorporated
113 Neutek Incorporated
114 NIST Center for Neutron Research
115 NIST, Analytical Chemistry Division
116 NIST, Biotechnology Division
117 NIST, Building Materials Division
118 NIST, Ceramics Division
119 NIST, Electron and Optical Physics Division
120 NIST, Ionizing Radiation Division
121 NIST, Materials Evaluation
122 NIST, Materials Reliability Division
123 NIST, Metallurgy Division
124 NIST, Polymers Division
125 NIST, Semiconductor Electronics Division
126 NIST, Standard Reference Materials Program
127 NIST, Statistical Engineering Division
128 NIST, Surface and Microanalysis Science Division
129 NIST, Thermophysics Division
130 North Carolina State University
131 Northeastern University
132 Northern Illinois University
133 Northwestern University
134 Nova Scientific
135 Oak Ridge Institute for Science and Education
136 Oak Ridge National Laboratory
137 Oberlin College
138 Ohio State University
139 Ohio University
140 Olin Conservation Incorporated
141 Oregon State University
142 OSMIC, Incorporated
143 Oxford University, United Kingdom
144 Pacific Lutheran University
145 Paul Scherrer Institute, Switzerland
146 Pennsylvania State University
147 Philips Research Laboratories, The Netherlands
148 Polytechnic University
149 PPG Industries
150 Princeton University
151 Queen's University, Canada
152 Raychem Corporation
153 Rice University
154 Rothe Development, Incorporated
155 Royal Institute of Technology, Sweden
156 Royal Institution, United Kingdom
157 Ruhr University, Germany
158 Russian Academy of Sciences, Russia
159 Rutgers University
160 SAGE Electrochromics
161 Sandia National Laboratory
162 Seoul National University

163 Sid Richardson Carbon Company
164 Siemens
165 Smithsonian Institute
166 Stanford Linear Accelerator
167 Stanford University
168 State University of New York, Stony Brook
169 Struck, Incorporated, Germany
170 Sydney University, Australia
171 Tata Institute of Fundamental Research, India
172 TEC
173 Technical University Darmstadt, Germany
174 Technical University Delft, The Netherlands
175 Technical University Munchen, Germany
176 Technical University of Linz, Austria
177 Technobiochip
178 Tel Aviv University, Israel
179 Texaco Research and Development Center
180 Texas Materials Institute
181 Thomas Jefferson High School
182 Tohoku University, Japan
183 Toyo University, Japan
184 Tokyo University, Japan
185 Trinity College
186 Tufts University
187 U. S. Department of Transportation
188 U. S. Drug Administration, ARS
189 Universidad de la Republica Argentina
190 Universitat Autònoma de Barcelona, Spain
191 Universität Duisberg, Germany
192 Universitet de Montpellier Ii, France
193 Universität des Saarlandes, Germany
194 University di Brescia, Italy
195 University of Aachen, Germany
196 University of Akron
197 University of Antwerp, Belgium
198 University of California at Berkeley
199 University of California at Davis
200 University of California at Irvine
201 University of California at Riverside
202 University of California at San Diego
203 University of California at San Francisco
204 University of California at Santa Barbara
205 University of Central Florida
206 University of Chicago
207 University of Connecticut
208 University of Cincinnati
209 University of Delaware
210 University of Florida
211 University of Geneva, Switzerland
212 University of Göettingen, The Netherlands
213 University of Grenoble, France
214 University of Guelph, Canada
215 University of Houston
216 University of Illinois
217 University of Innsbruck, Austria
218 University of Iowa
219 University of Manitoba

220 University of Maryland at College Park
221 University of Massachusetts
222 University of Michigan
223 University of Minnesota
224 University of Missouri at Columbia
225 University of Missouri-Rolla
226 University of Munich, Germany
227 University of Nebraska
228 University of Notre Dame
229 University of Oklahoma
230 University of Oslo, Norway
231 University of Pennsylvania
232 University of Rhode Island
233 University of South Australia, Australia
234 University of Stuttgart, Germany
235 University of Surrey, United Kingdom
236 University of Sussex, United Kingdom
237 University of Sydney, Australia
238 University of Tennessee
239 University of Texas
240 University of Tokyo, Japan
241 University of Toronto, Canada
242 University of Trento, Italy
243 University of Uppsala
244 University of Uruguay
245 University of Utah
246 University of Vermont
247 University of Virginia
248 University of Washington
249 University of Waterloo, Canada
250 Uppsala University, Sweden
251 W. R. Grace
252 Walter Reed Army Institute of Research
253 Washington University
254 West Virginia University
255 Worcester Polytechnic Institute
256 X-Ray Optical Systems

Abdurashitov, J. N., Gavrin, V. N., Girin, S. V., Gorbachev, V. V., Ibragimova, T. V., Kalikhov, A.V., Khairnasov, N. G., Knodel, V. N., Kornoukhov, V. N., Mirmov, I. N., Shikhin, A. A., Verentenkin, E. P., Vermul, V. M., Yants, V. E., Zatsepin, G. T., Khomyakov, Y. S., Zvonarev, A. V., Bowles, T. J., Nico, J. S., Teasdale, W. A., Wark, D. L., Cherry, M. L., Karaulov, V. N., Levitin, V. L., Maev, P. I., Nazarenko, P. I., Shkol'nik, V. S., Skorikov, N.V., Cleveland, B. T., Daily, T., Davis, R., Lande, K., Lee, C. K., Wildenhain, P. S., Elliott, S. R., Wilkerson, J. F., "Measurement of the Response of a Gallium Metal Solar Neutrino Experiment to Neutrinos from a ^{51}Cr Neutrino Source", Phys. Rev. C **59**, 2246 (1999).

Abdurashitov, J. N., Gavrin, V. N., Girin, S. V., Gorbachev, V. V., Ibragimova, T. V., Kalikhov, A.V., Khairnasov, N. G., Knodel, V. N., Mirmov, I. N., Shikhin, A. A., Verentenkin, E. P., Vermul, V. M., Yants, V. E., Zatsepin, G. T., Bowles, T. J., Teasdale, W. A., Wark, D. L., Cherry, M. L., Nico, J. S., Cleveland, B. T., Davis, R., Lande, K., Wildenhain, P. S., Elliott, S. R., Wilkerson, J. F., "Measurement of the Solar Neutrino Capture Rate with Gallium Metal", Phys. Rev. C **60**, 55801 (1999).

Abdurashitov, J. N., Gavrin, V. N., Girin, S. V., Gorbachev, V. V., Ibragimova, T. V., Kalikhov, A.V., Khairnasov, N. G., Knodel, V. N., Mirmov, I. N., Shikhin, A. A., Verentenkin, E. P., Vermul, V. M., Yants, V. E., Zatsepin, G. T., Bowles, T. J., Teasdale, W. A., Wark, D. L., Cherry, M. L., Nico, J. S., Cleveland, B. T., Davis, R., Lande, K., Wildenhain, P. S., Elliott, S. R., Wilkerson, J. F., "Measurement of the Solar Neutrino Capture Rate by SAGE and Implications for Neutrino Oscillations in Vacuum", Phys. Rev. Lett., in press.

Adams, J. M., "Results from the NIST Round Robin Test of Fissionable Dosimeters in a Reactor Leakage Spectrum", in *Reactor Dosimetry*, edited by J. G. Williams, D. W. Vehan, F. H. Ruddy, and D. M. Gilliam, in press.

Aeppli, G., Bishop, D. J., Broholm, C., Bucher, E., Cheong, S. W., Dai, P., Fisk, Z., Haysedn, S. M., Kleiman, R., Mason, T. E., Mook, H. A., Perring, T. G., Schoeder, A., "Neutron Scattering and the Search for Mechanisms of Superconductivity", Physica C **318**, 9 (1999).

Agnew, S. R., Elliott, B. R., Youngdahl, C. J., Hemker, K. J., Weertman, J. R., "Structure and Mechanical Properties of Nanocrystalline", in *Metals with Opportunities for Modeling 19th Risø International Symposium on Materials Science* (Risø National Laboratory, Roskilde, Denmark), in press.

Amis, E. J., Bauer, B. J., Groehn, F. I., Prosa, T. J., Liu, D. W., Barnes, K. A., Jackson, C. L., Viers, B. D., Karim, A, Douglas, J. D., "Preparation and Characterization of Polymer/Dendrimer Blends Progress Report for 1999", NISTIR 6353.

Amos, T. G., Yokochi, A., Sleight, A. W., "Phase Transition and Negative Thermal Expansion in Tetragonal NbOPO$_4$", J. Solid State Chem. **141**, 303 (1998).

Anderson, C. R., Andersen, K. H., Bossy, J., Stirling, W. G., Dimeo, R. M., Sokol, P. E., Cook, J. C., Brown, D. W., " High Resolution Neutron Scattering Study of the Roton in Confined Superfluid ^{4}He", Phys. Rev. B **59**, 13588 (1999).

Anderson, M. L., Morris, C. A., Stroud, R. M., Merzbacher, C. I., Rolison, D. R., "Colloidal Gold Aerogels: Preparation, Properties, and Characterization", Langmuir **15**, 674 (1999).

Armstrong, D. W., Schneiderheinze, J., Nair, U., Magid, L. J., Butler, P. D., "Self-Association of Rifamycin B: Possible Effects on Molecular Recognition", J. Phys. Chem. B **103**, 4338 (1999).

Balbach, J. J., Conradi, M. S., Hoffmann, M. M., Udovic, T. J., Adolphi, N. L., "NMR Evidence of Disorder and Motion in Yttrium Trideuteride", Phys. Rev. B **58**, 14823 (1998).

Balsara, N. P., "Multicomponent Polyolefin Blends with Ordered and Disordered Microstructures", Curr. Opin. Sld. St. Mtls. Sci. **3**, 589 (1998).

Balsara, N. P., Lefebvre, A. A., Lee, J. H., Lin, C. C., Hammouda, B., "The Search for a Model Polymer Blend", AIChE J. **44**, 2515 (1998).

Bandyopadhyay, S., Klein, M. L., Martyna, G. J., Tarek, M., "Molecular Dynamics Studies of the Hexagonal Mesophase of Sodium Dodecylsulfate in Aqueous Solution", Mol. Phys. **95**, 377 (1998).

Bandyopadhyay, S., Tarek, M., Klein, M. L., "Nature of Lipid-DNA Interactions: A Molecular Dynamics Study of DNA Intercalated into a Lipid Bilayer", J. Phys. Chem., in press.

Bandyopadhyay, S., Tarek, M., Lynch, M. L., Klein, M. L., "C$_{12}$EO$_2$/Water System: A Molecular Dynamics Study", Langmuir, in press.

Balizer, E., DeReggi, A. S., Neumann, D. A., Bateman, F., "Polarization and Structural Transitions of Irradiated Vinylidene Fluoride-Trifluorethylene Copolymer" in *1999 Conference on Electrical Insulation and Dielectric Phenomena*, Vol. 1, (IEEE Publ. No 99CH36319, 1999) p.104.

Bao, W., Broholm, C., Aeppli, G., Carter, S. A., Dai, P., Rosenbaum, T. F., Honig, J. M., Metcalf, P., Trevino, S. F., "Magnetic Correlations and Quantum Criticality in the Insulating Antiferromagnetic, Insulating Spin Liquid, Renormalized Fermi Liquid, and Metallic Antiferromagnetic Phases of the Mott System V$_2$O$_3$", Phys. Rev. B **58**, 12727 (1999).

Barilo, S. N., Bychkov, G. L., Kurnevich, L. A., Shiryaev, S. V., Lynn, J. W., Vasiliu-Doloc, L., "Seeded Growth from Flux and Neutron Study of La$_{1-x}$Ba$_x$MnO$_3$ (0.2 < x < 0.5) Single Crystals", J. Cryst. Growth, in press.

Barilo, S. N., Shiryaev, S. V., Gatalskaya, V. I., Lynn, J. W., Baran, M., Szymczak, H., Szymczak, R., Dew-Hughes, D., "Scaling of Magnetization and Some Basic Parameters of Ba$_{1-x}$K$_x$BiO$_{3+y}$ Superconductors near T$_c$", Phys. Rev. B **58**, 12355 (1998).

Barilo, S. N., Shiryaev, S.V., Gatalskaya, V. I., Zhigunov, D. I., Pushkarev, A. V., Fedotova, V. V., Szymczak, H., Szymczak, R., Baran, M., Lynn, J. W., Rosov, N., Skanthakumar, S., "A New Method for Growing Ba$_{1-x}$K$_x$BiO$_3$ Single Crystals and Investigation of their Properties", J. Cryst. Growth **199**, 636 (1999).

Barilo, S. N., Shiryaev, S. V., Zhigunov, D. l., Pushkarev, A. V., Gatalskaya, V. I., Fedotova, V. V., Lynn, J. W., Skanthakumar, S., Rosov, N., Szymczak, H., Szymczak, R., Baran, M., Nabyalek, A., "Investigation of Electrochemical Growth Conditions for Ba$_{1-x}$K$_x$BiO$_3$ Single Crystal Superconductor and Its Magnetic Properties", *in International Conference on Crystal Growth*, (OBNIS, 1998), p.30.

Barker, J. G., Weertman, J. R., Pedersen, J. S., "Strain Rate Dependence of the Growth Rate of Grain Boundary Cavities during the High Cycle High Temperature Fatigue of Copper" in *Advanced Materials for the 21st Century: The 1999 Julia R. Weetman Symposium*, edited by Y. W Chung, D. C. Dunand, P. K. Liaw, G. B. Olson (The Minerals, Metals & Materials Society, Pennsylvania, 1999) p.71.

Barnes, K. A., Morrison, F. A., Nakatani, A. I., "The Effects of Steady Shear on the Order and Orientation of Diblock Copolymer Melt Using In-Situ Small-Angle Neutron Scattering", SPE ANTEC, in press.

Bateman, F. B., Boukharouba, N., Brient, C. E., Carlson, A. D., Grimes, S. M., Haight, R. C., Massey, T. N., Wasson, O. A., "New Measurements of the H (n, n) H Angular Distribution", in *Reactor Dosimetry*, edited by J. G. Williams, D. W. Vehan, F. H. Ruddy and D. M. Gilliam, in press.

Bauer, B. J., Prosa, T. J., Liu, D. W., Jackson, C. L., Tomalia, D. A., Amis, E. J., "Molecularly Dispersed Dendrimers in a Polymeric Matrix", ACS reprint **40**, 406 (1999).

Bauer, B. J., Ramzi, A., Liu, D. W., Scherrenberg, R. L., Froehling, P., Joosten, J., "Blends of Fatty Acid Modified Dendrimers with Polyolefins", J. Polym. Sci. Phys., in press.

Becker, D. A., "30 Years of Reactor Characterization on the NBSR", J. Radioanal. Nucl. Chem., in press.

Becker, D. A., "Accurate Determination of Trace Elements in Sediment CRMs by Instrumental Neutron Activation Analysis", Czech. J. Phys. **49**, 271 (1999).

Becker, D. A., Porter, B. J., Mackey, E. A., Schantz, M. M., Demiralp, R., "National Marine Mammal Tissue Bank and Quality Assurance Program: Protocols, Inventory, and Analytical Results", NISTIR 6279.

Bellows, R. J., Lin, M. Y., Arif, M., Thompson, A. K., Jacobson, D., "Neutron Imaging Technique for In-Situ Measurement of Water Transport Gradients within Nafion in Polymer Electrolyte Fuel Cells", J. Electrochem. Soc. **146**, 1099 (1999).

Benenson, R. E., Chen-Mayer, H. H., Lynn, J. W., "Search for Effects on Neutron Transmission Due to Multiple Reflection by Glass Capillary Walls", in Proceedings of SPIE Annual Meeting, in press.

Blackman, M. J., Badaljan, R. S., Kikodze, Z. K., Kohl, P. L., "Chemical Characterization of Caucasian Obsidian: Geological Sources", in *Synthese Sur l'Obsidienne au Proche-Orient: Du Volcan a l'Outil*, (BAR Publication, London), in press.

Blackman, M. J., Redford, S., "Northern Syrian Luster and Fritware: Petrographic and Chemical Implications for Productions and Distribution", Antiquity, in press.

Bode, P., de Nadai Fernandes, E. A., Greenberg, R., "INAA as a Primary Method in Metrology for Chemical Measurements", Proceedings Metrolsul. '99, in press.

Bode, P., de Nadai Fernandes, E. A., Greenberg, R. R., "Metrology for Chemical Measurements and the Position of INAA", J. Radioanal. Nucl. Chem., in press.

Bödeker, K., Schreyer, A., Zabel, H., "Spin Density Waves and Reorientation Effects in Thin Epitaxial Cr Films Covered with Ferromagnetic and Paramgnetic Layers", Phys. Rev. B **59**, 9408 (1999).

Borchers, J. A., Dura, J. A., Majkrzak, C. F., Hsu, S. Y., Lolee, R., Pratt, W. P., Bass, J., "Polarized Neutron Reflectivity Characterization of Weakly Coupled Co/Cu Multilayers", Physica B, in press.

Borchers, J. A., Dura, J. A., Unguris, J., Tulchinsky, D., Kelley, M. H., Majkrzak, C. F., Hsu, S. Y., Loloee, R., Pratt Jr., W. P., Bass, J., "Observation of Antiparallel Magnetic Order in Weakly Coupled Co/Cu Multilayers", Phys. Rev. Lett. **82**, 2796 (1999).

Borchers, J. A., Ijiri, Y., Lind, D. M., Ivanov, P. G., Erwin, R. W., Lee, S. -H., Majkrzak, C. F., "Polarized Neutron Diffraction Studies of Exchange-Coupled Fe_3O_4/NiO Superlattices", J. Appl. Phys. **85**, 5883 (1999).

Borchers, J. A., Majkrzak, C. F., "Magnetic Epitaxial Layers", in *Encyclopedia of Electronics and Electrical Engineering*, edited by John G. Webster (Wiley and Sons, 1999) p.699.

Bossy, J., Anderson, K. H., Cook, J.C., Randle, O. R., "High Resolution Neutron Measurements of Roton Lineshape Under Pressure", Physica B, in press.

Briber, R. M., Fodor, J. S., Miller, R. D., Carter, K. R., Russell, T. P., Hedrick, J. L., "Characterization of Thin Polymeric Nanofoam Films by Transmission Electron Microscopy and Small Angle Neutron Scattering", Materials Research Society Symposium, in press.

Brown, C. M., Taga, S., Gogia, B., Kordatos, K., Margadonna, S., Prassides, K., Iwasa, Y., Tanigaki, K., Fitch, A. N., Pattison, P., "Structural and Electronic Properties of the Noncubic Superconducting Fullerides A′ C-4 (60) (A′ = Ba, Sr)", Phys. Rev. Lett. **83**, 2258 (1999).

Brown, D. W., Sokol, P. E., FitzGerald, S. A., "Rotational Dynamics of n-H_2 in Porous Vycor Glass", Phys. Rev. B **59**, 13258 (1999).

Brunner-Popela, J., Mittelbach, R., Strey, R., Schubert, K.V., Kaler, E. W., Glatter, O., "Small-Angle Scattering of Interacting Particles. III. D_{20}-$C_{12}E_5$ Mixtures and Microemulsions with N-Octane", J. Chem. Phys. **110**, 10623 (1999).

Buckley, C.E., "Investigation of the Aluminium Hydrogen System using Small Angle X-Ray (SAXS) and Small Angle Neutron scattering (SANS)", in *Proceedings of the 1998 Joint Conference: WA Society for Electron Microscopy and Australian X-Ray Analytical Association Inc.*, edited by B.J. Griffin, A. van Riessen (Australia, 1998), p. 18.

Buckley, C.E., Birnbaum, H.K., "SANS Study of the Aluminum Hydrogen System", Physica B **241**, 344 (1998).

Butler, B. D., Muzny, C. D., Hanley, H. J. M., "Scaling of Small-Angle Neutron Scattering Intensities from Gelling Colloidal Silica", Int. J. Thermophys. **20**, 35 (1999).

Butler, P. D., "Near Surface Small Angle Scattering as a Means of Probing the Effects of Fluid Flow on Surfactant Aggregates Near a Solid Surface", in *Supramolecular Structure in Confined Geometries*, edited by Manne, S., Warr, G. G., ACS Symp. Series 736, (Amer. Chem. Soc, Washington, DC, 1999) p.73.

Butler, P. D., "Shear Induces Structures and Transformations in Complex Fluids", Curr. Opin. Colloid Interf. **4**, 214 (1999).

Cava, R. J., Ramirez, A. P., Huang, Q., Krajewski, J. J., "Compounds with the $YbFe_2O_4$ Structure Type: Frustrated Magnetism and Spin-Glass Behavior", J. Solid State Chem. **140**, 337 (1998).

Chen, W. C., Heuser, B. J., King, J. S., "SANS Investigation of Deuteride (hydride) Precipitation and Decompostion Morphology in Single Crystal Pd", J. Appl. Crystallogr., in press.

Chen-Mayer, H. H., Lamaze, G. P., "Depth Distribution of Boron Determined by Slow Neutron Induced Lithium Emission", Nucl. Instrum. Meth. B **135**, 407 (1998).

Chen-Mayer, H. H., Mackey, E. A., Paul, R. L., Mildner, D. F. R., "Quantitative Prompt Gamma Analysis Using a Focused Cold Neutron Beam", J. Radioanal. Nucl. Chem., in press.

Chen-Mayer, H. H., Mildner, D. F. R., Lamaze, G. P., Paul, R. L., Lindstrom, R. M., "Neutron Focusing using Capillary Optics and Its Applications to Elemental Analysis", in *Applications of Accelerators in Research and Industry*, edited by J.L. Duggan, I. L. Morgan, AIP Conference Proceedings 475 (The American Institute of Physics, Woodbury, New York, 1999), p. 718.

Choi, S., Briber, R. M., Bauer, B. J., Topp, A., Gauthier, M., Tichagwa., L., "Small Angle Neutron Scattering of Solutions of Arborescent Graft Polystryrenes", Macromol. **32**, 7879 (1999).

Choi, S., Liu, X., Briber, R. M., "Small Angle Scattering of Polymer Blends of Polyvinylmethylether at Dilute Concentration in deuterated Polystyrene", J. Polym. Sci. **36**, 1 (1998).

Choi, S. -M., Barker, J. G., Glinka, C. J., Cheng, Y. T., Gammel, P. L., "Focusing Cold Neutrons with Multiple Biconcave Lenses for Small-Angle Neutron Scattering", J. Appl. Crystallogr., in press.

Clutter, L. K., edited by, "NIST Center for Neutron Research-Annual Report-October 1997 through September 1998", NISTIR 6251.

Copley, J. R. D., "Neutron Powder Diffraction", in *Proceedings of Workshop on Cold Neutron in Contemporary Materials Research* (Institute of Nuclear Energy Research, Taiwan, 1999), p.74.

Copley, J. R. D., "Neutron Time-of-Flight Spectroscopy", in *Proceedings of Workshop on Cold Neutrons in Contemporary Materials Research* (Institute of Nuclear Energy Research, Taiwan, 1999), p. 240.

Copley, J. R. D., Hayes, C., Lartigue, C., "Performance Comparisons for the ILL Neutron Spin Echo Spectrometer IN15 in its Standard and Focusing Mirror Configurations", in *Proceedings of Conference on EUV, X-Ray and Neutron Optics and Sources*, edited by C. MacDonald (SPIE, Bellingham, Washington, 1999), in press.

Cosgrove, T., King, S. M., Griffiths, P. C., "SANS Methods in Polymer Adsorption Studies", in *Colloid-Polymer Interactions: From Fundamentals to Practice,* edited by R.Farinato and P. Dubin (Wiley), in press.

Cosgrove, T., Mears, S. J., Obey, T., Thompsen, L., Wesley, R. D., "Polymer, Particles, Surfactant Interactions", Colloid Surface **149**, 329 (1999).

Crawford, M. K., Dobbs, K. D., Smalley, R. J., Corbin, D. R., Maliszewskyj, N. C., Udovic, T. J., Cavanagh, R. R., Rush, J. J., Grey, C. P., "A Raman Spectroscopy Study of the Separation of Hydrofluorocarbons Using Zeolites", J. Phys. Chem. B **103,** 431 (1999).

Dadmun, M. D., Clingman, S., Ober, C. K., Nakatani, A. I., "The Flow Induced Structure in a Thermotropic Liquid Crystalline Polymer as Studied by SANS", J. Polym. Sci. Polym. Phys. **36**, 3017 (1998).

Daniel, C., Jao, T. –C., Bauer, B. J., Amis, E. J., "Study of Ethylene-Propylene Copolymer Thermoreversible Gels", Macromol., in press.

Deegan, R. D., Leheny, R. L., Menon, N., Nagel, S. R., Vnerus, D. C., "Dynamic Shear Modulus of Tricresyl Phosphate and Squalane", J. Phys. Chem. **103**, 4066 (1999).

Denecke, B., Eykens, R., Pauwels, J., Robouch, P., Gilliam, D. M., Hodge, P., Hutchison, J. M. R., Nico, J. S., "Characterization of Actinide Targets by Low Solid-Angle Alpha Particle Counting", Nucl. Instrum. Meth. A, in press.

Dewey, M. S., Kessler, E. G., "Precision Measurements of Fundamental Constants using GAMS4. J. Res. Natl. Inst. Stan., in press.

Dimeo, R. M., Sokol, P. E., Anderson, C. R., Stirling, W. G., Andersen, K. H., Adams, M. A., "Confinement Effects on Superfluid Helium", J. Low Temp. Phys. **113**, 369 (1998).

Dimeo, R. M., "Fourier Transform Solution to the Semi-Infinite Resistance Ladder", Am. J. Phys., in press.

Dimeo, R. M., Sokol, P. E., Anderson, C. R., Stirling, W. G., Andersen, K. H., Adams, M.A, "Localized Collective Excitations in Superfluid Helium in Vycor", Phys. Rev. Lett. **81**, 5860 (1998).

Downing, R. G., Ivengar, G. V., "Methodological Issues in the Analytical Determination of Boron", Environ. Health Perspect., in press.

Downing, R. G., Strong, P. L., "A Round-Robin Determination of Boron in Botanical and Biological Samples", Biological Trace Element Research **66**, 23 (1998).

Duan, N., Kameswari, U., Sleight, A. W., "Further Contraction of ZrW_2O_8", J. Chem. Soc. **121**, 10432 (1999).

Dulloo, A. R., Ruddy, F. H., Seidel, J. G., Adams, J. M., Nico, J. S., Gilliam, D. M., "The Neutron Response of Miniature Silicon Carbide Semiconductor Detectors", Nucl. Instrum. Meth. A **422**, 47 (1999).

Dura, J. A., Richter, C. A., Majrkzak, C. F., Nguyen, N. V., "Neutron Reflectivity, X-Ray Reflectivity, and Spectroscipic Ellipsometry Characterization of Thin SiO_2 on Si", Appl. Phys. Lett. **73**, 2131 (1998).

Effey, B., Cappelletti, R. L., "Neutron Inelastic Scattering Study of Se-As-Ge Glasses: A Test of the Vibrational Isocoordinate Rule", Phys. Rev. B **59**, 4119 (1999).

Einarsrud, M. A., "Light Gels by Conventiobal Drying", J. Non-Cryst. Solids **225**, 1 (1998).

En, Z., Brenizer, J. S., Hostica, B., Becker, D. A., "Use of Nuclear Track Technique to Study Boron and Nitrogen Distribution in Alloys", J. Radioanal. Nucl. Chem., in press.

En, Z., Brenizer, J.S., Hostica, B., Gao, J., Becker, D. A., "Nitrogen Distribution Measurements by Neutron Induced Autoradiography", J. Radioanal. Nucl. Chem. **234**, 59 (1998).

Fischer, P., Ioffe, A., Jacobson, D. L., Arif, M., Mezei, F., "4π-Periodicity of the Spinor Wave Function Under Space Rotation", Nucl. Instrum. Meth. A., in press.

FitzGerald, S. A., Neumann, D. A., Rush, J. J., Kirkpatrick, R. J., Cong, X., Livingston, R. A., "Inelastic Neutron Scattering Study of the Hydration of Tricalcium Silicate", J. Mater. Res. **14**, 1160 (1999).

FitzGerald, S. A., Yildirim, T., Santodonato, L. J., Neumann, D. A., Copley, J. R. D., Rush, J. J., Trouw, F., "Quantum Dynamics of Interstitial H_2 in Solid C_{60}", Phys. Rev. B **60**, 6439 (1999).

Flanagan, T. B., Noh, H., Clewley, J. D., Barker, J. G., "Evidence for H-Enhanced Metal Atom Diffusion in Pd-Ni Alloys from SANS and H_2 Solubilities", Scripta Mat., in press.

Fodor, J. S., Briber, R. M., Russell, T. P., Carter, K. R., Hedrick, J. L., Miller, R. D., "Non-Uniform Composition Profiles in Thin Film Polymeric Nanofoams", Polymer **40**, 2547 (1999).

Fong, H. F., Keimer, B., Lynn, J. W., Hayashi, A., Cava, R. J., "Spin Structure of the Dopable Quasi-One Dimensional Copper Oxide $Ca_2Y_2Cu_5O_{10}$", Phys. Rev. B **59**, 6873 (1999).

Foster, M. D., Greenberg, C. C., Teale, D. M., Cloutet, E., Turner, C. M., Quirk, R. P., "Quantifying Surface Segregation in Blends of Linear and Star Branched Molecules", Am. Chem. S. **39**, 1203 (1998).

Foster, M. D., Greenberg, C. C., Teale, D. M., Turner, C. M., Corona-Galvan, S., Cloutet, E., Butler, P. D., Hammouda, B., Quirk, R. P., "Effective X and Surface Segregation in Blends of Star and Linear Polystyrene", in *Proceedings of the Mainz Conference* (1999), Macromol. Symposia, in press.

Forster, P. M., Sleight, A.W., "Negative Thermal Expansion in $Y_2W_3O_{12}$", Int. J. Inorg. Chem. **1**, 123 (1999).

Gardner, J.S., Gaulin, B. D., Lee, S.H., Broholm, C., Raju, N. P., Greedan, J.E., "Glassy Statics and Dynamics in the Chemically-Ordered Pyrochlore Antiferromagnet, $Y_2Mo_2O_7$", Phys. Rev Lett. **83**, 211 (1999).

Gentile, T. R., Jones, G. L., Thompson, A. K., Barker, J., Glinka, C. J., Hammouda, B., Lynn, J. W., "SANS Polarization Analysis with Nuclear-Spin-Polarized ^{3}He", J. Appl. Crystallogr., in press.

Gentile, T. R., Jones, G. L., Thompson, A. K., Rizi, R. R., Dimitrov, I. E., Roberts, D., Gefter, W., Schnall, M. D., Leigh, J. S., "A Compact Compressor for Application of Metastability-Exchange Optical Pumping of ^{3}He to Human Lung Imaging", Magn. Reson. Med., in press.

Gibaud, A., Sella, C., Maaza, M., Sung, L., Dura, J., Satija, S. K., "Neutron and X-Ray Reflectivity Analysis of Ceramic-Metal Materials", Thin Solid Films **340**, 153 (1999).

Gibbons, M. R., Richards, W. J., Shields, K., Paul, R. L., Lindstrom, R. M., "Correction of Scattering and Beam Hardening in Thermal Neutron Tomography for Quantitative Detection of Hydrogen", IEEE Trans. Nucl. Sci., in press.

Gnäupel-Herold, T., Brand, P. C., Prask, H. J., "Accessing the Elastic Properties of Cubic Materials with Diffraction Methods", Advances in X-ray Analysis, in press.

Gnäupel-Herold, T., Brand, P. C., Prask, H. J., "The Calculation of Single Crystal Elastic Constants for Cubic Crystal Symmetry from Powder Diffraction Data", J. Appl. Crystallogr. **31**, 929 (1998).

Gnäupel-Herold, T., Brand, P. C., Prask, H. J., "Neutron Diffraction Investigation of Residual Stresses in Transverse/Oblique Rail Slices Subjected to Different Grinding Strategies", NISTIR 6305.

Gnäupel-Herold, T., Brand, P. C., Prask, H. J., "Residual Stress Analysis for Engineering Applications by Means of Neutron Diffraction", Trans. Amer. Nucl. Soc. **80**, 101 (1999).

Goldmints, I., Yu, G., Booth, C., Smith, K. A., Hatton, T. A., "Structure of (Deuterated PEO)-(PPO)-(Deuterated PEO) Block Copolymer Micelles as Determined by Small Angle Neutron Scattering", Langmuir **15**, 1651 (1999).

Green, M. A., Neumann, D. A., "Synthesis, Structure and Electronic Properties of $LaCa_2Mn_2O_7$", Chem. Mater., in press.

Green, M. A., Prassides, K., Stalick, J. K., Day, P., "The Crystal Structure of $SrSnO_3$", Inorg. Chem., in press.

Greenberg, C. C., Foster, M. D., Turner, C. M., Corona-Galvan, S., Cloutet, E., Butler, P. D., Hammouda, B., Quirk, R. P., "Effective Interaction Parameter Between Topologically Distinct Polymers", Polymer **40**, 4713 (1999).

Greenberg, R. R., Lindstrom, R. M., Simons, D. S., "Instrumental Neutron Activation Analysis for Certification of Ion-Implanted Arsenic in Silicon", J. Radioanal. Nucl. Chem., in press.

Griffith, P. C., Cosgrove, T., Shar, J., King, S. M., Yu, G. E., Booth, C., Malmsten, M., "Role of Copolymer Architecture on Adsorption at the Solid/Liquid Interface", Langmuir 14, 1779 (1998).

Guerrero, H. M., Cappelletti, R. L., Neumann, D. A., Yildirim, T., "Structure and Lattice Dynamics of K_1C_{60} in the Orthorhombic Phase: A Neutron Scattering Study", Chem. Phys. Lett. 297, 265 (1998).

Gygax, F. N., Solt, G., Amato, A., Anderson, I. S., Pinkpank, M., Schenk, A., Udovic, T. J., "The Light 'Hydrogen' Isotope μ^+ in Sc and α-ScH_x Solid Solutions", Phys. Rev. B, in press.

Hamilton, W. A., Butler, P. D., Magid, L. J., Han, Z., Slawecki, T. M., "Fast Relaxation of a Hexagonal Poiseuille Shear-Induced Near-Surface Phase in a Threadlike Micellar Solution", Phys. Rev. E. 60, R1146 (1999).

Hammar, P. R., Stone, M. B., Reich, D. H., Broholm, C., Gibson, P. J., Turnbull, M. M., Landee, C. P., Oshikawa, M., "Characterization of a Quasi-One-Dimensional Spin-1/2 Magnet which is Gapless and Paramagnetic for $g\mu_B H \leq J$ and $k_B T << J$", Phys. Rev. B 59, 1008 (1999).

Hanley, H. J. M., Muzny, C. D., Butler, B. D., Straty, G. C., Bartlett, J., Drabarek, E., "Shear-Induced Restructuring of Concentrated Colloidal Silica Gels", J. Phys. Condens. Matt. 11, 1369 (1999).

Harris, V. G., Fatemi, D. J., Hathaway, K. B., Huang, Q., Mohan, A., Long, G. J., "Atomic Structure and Magnetism of Ordered and Disordered $Al_{0.5}Fe_{0.5-x}Mn_x$ Alloys", J. Appl. Phys. 85, 5181 (1999).

Harris, V. G., Huang, Q., Shah, V.R., Markandeyulu, G., Rao, K. V. S. R., Huang, M. Q., Sirisha, K., McHenry, M. E., "Neutron Diffraction and Extended X-Ray Absorption Fine Structure Studies of $Pr_3(Fe_{1-x}Co)_{27.5}Ti_{1.5}$ Permanent Magnet Compounds", IEEE Trans. Magn.. 35, 3286 (1999).

Harroun, T. A., Heller, W. T., Weiss, T. M., Yang, L., Huang, H. W., "Experimental Evidence of Hydrophobic Matching and Membrane-Mediated Interactions in Lipid Bilayers Containing Gramicidin", Biophys. J. 76, 937 (1999).

Harroun, T. A., Heller, W. T., Weiss, T. M., Yang, L., Huang, H. W., "Theoretical Analysis of Hydrophobic Matching and membrane-Mediated Interactions in Lipid Bilayers Containing Gramicidin', Biophys. J. 76, 3176 (1999).

Hawari, A. I., Adams, J. M., "A Method for the Minimization of the HPGe Detector Efficiency Bias in the Measurement of the Spectral Index", in Reactor Dosimetry, edited by J. G. Williams, D. W. Vehan, F. H. Ruddy and D. M. Gilliam, in press.

Hedrick, J. L., Carter, K. R., Labadie, J. W., Miller, R. D., Volksen, W., Hawker, C. J., Yoon, D. Y., Russell, T. P., McGrath, J. E., Briber, R. M., "Nanoporous Polyimides", Progr. Polyimide Chem. II 141, 1 (1999).

Heller, W. T., Waring, A. J., Lehrer, R. I., Huang, H. W., "Multiple States of Beta-Sheet Peptide Protegrin in Lipid Bilayers", Biochem. 37, 17331 (1998).

Heller-Zeisler, S., Ondov, J., Zeisler, R., "Collection and Characterization of a Bulk $PM_{2.5}$ Air Particulate Matter Material for Use in Reference Materials", J. Bio. Trace Ele. Res. 71, 195 (1999).

Henrickson, R. C., Blackman, M. J., "Hellenistic Production of Terra Cotta Roof Tiles Among the Ceramic Industries at Gordian", Oxford J. Archaeology 18, in press.

Heuser, B. J., King, J. S., Chen, W. C., "SANS Measurements of Deuteride (Hydride) Formation in Single Crystal PD", J. Alloys Compnds. 292, 134 (1999).

Ho, D. L., Briber, R. M., Jones, R. L., Kumar, S. K., Russell, T. P., "Small Angle Neutron Scattering Studies on Thin Films of Isotopic Polystyrene Blends", Macromol. 31, 9247 (1998).

Hobbie, E. K., Kim, S., Yu, J., Han, C. C., "Pattern Formation and Scaling in Critical Polymer Mixtures Under Simple Shear Flow", II Nuovo Cimento 20, 2303 (1998).

Huang, C. –I., Chapman, B. R., Lodge, T. P., Balsara, N. P., "Quantifying the 'Neutrality' of Good Solvents for Block Copolymers: Poly (styrene-b-isoprene) in Toluene, Benzene, and THF", Macromol. 31, 9384 (1998).

Huang, H. W., "Pores in Lipid Bilayers", in Materials Research using Cold Neutrons, edited by P. Thiyagarajan, F. Trouw, B. Marzec (World Scientific, Singapore, 1999), p. 70.

Huffman, P. R., Brome, C. R., Butterworth, J. S., Coakley, K. J., Dewey, M. S., Dzhosyuk, S.N., Golub, R., Greene, G. L., Habicht, K., Lamoreaux, S. K., Mattoni, C. E. H., McKinsey, D. N., Wietfeldt, F. E., Doyle, J. M., "Magnetic Trapping of Neutrons", Nature, in press.

Huffman, P. R., Brome, C. R., Butterworth, J. S., Coakley, K. J., Dewey, M. S., Dzhosyuk, S. N., Gilliam, D. M., Golub, R., Greene, G. L., Habicht, K., Jones, G. L., Lamoreaux, K. S., Mattoni, C. E., McKinsey, D. N., Wietfeldt, F. E., Doyle, J. M., "Progress Towards Magnetic Trapping of Ultracold Neutrons", Nucl. Instrum. Meth. A, in press.

Huibers, P. D. T., Bromberg, L. E., Robinson, B. H., Hatton, T. A., "Reversible Gelation in Semidilute Aqueous Solutions of Associative Polymers: A Small Angle Neutron Scattering Study", Macromol. 32, 4889 (1999).

Hunt, W. J., Zukoski, C. F., "The Equilibrium Properties and Microstructure of Mixture of Colloidal Particles with Long Range, Soft Repulsions", JCIS 210, 332 (1999).

Idemoto, Y., Izumi, F., Huang, Q., Santoro, A., Matsuzawa, M., Koura, N., "Effects of Sr Substitution on the T_c and Crystal Structure of $T_{12}(Ba_{1-x}Sr_x)_2Ca_2Cu_3O_y$", in Chemistry and Technology of High-Temperature Superconductors (HTSC) and Related Advanced Materials, edited by G. van Tendeloo (Kluwer, Dordrecht, 1999), p. 129.

Ikeda, T., Miyazawa, K., Izumi, F., Huang, Q., Santoro, A., "Structural Study of the Aluminophosphate $AlPO_{4-5}$ by Neutron Powder Diffraction", J. Phys. Chem. Solids 60, 1531 (1999).

Ilavsky, J., Long, G. G., Allen, A. J., Herman, H., Berndt, C. C., "Use of Small Angle Neutron Scattering for the Characterization of Anisotropic Structures Produced by Thermal Spraying", Ceramics-Silikaty 42, 81 (1998).

Ilavsky, J., Stalick, J. K., "Phase Composition and Its Changes during Annealing of Plasma-Sprayed YSZ", Surface and Coating Technology, in press.

Ioffe, A., Arif, M., Jacobson, D. L., Mezei, F., "Precision Neutron Interferometric Search for Evidence of Nuclear Quantum Entanglement in Liquid H_2O-D_2O Mixtures", Phys. Rev. Lett. 82, 2322 (1999).

Ivkov, R., Gehring, P. M., Maliszewskyj, N. C., Krishnamoorti, R., "Structure and Dynamics of Polymers in Confined Geometries: Neutron Studies of Intercalated Clay-Polymer Nanocomposites", in Proceedings of Society Plastics Engineers—ANTEC '99, in press.

Izumi, F., Ikeda, T., "A Rietveld-Analysis Program RIETAN-98 and Its Applications to Zeolites", Proceeding of the Sixth European Conference on Powder Diffraction, Materials Science Forum, in press.

Jacobson, D. L., Arif, M., Bergmann, L., Ioffe, A., "Development of the Neutron Phase Contrast Imaging Technique and its Application in Materials Science Research." in Proceedings, SPIE Conference, Denver, July 17-23, 1999, in press.

Jeon, H. S., Lee, J. H., Balsara, N. P., Newstein, M. C., "An Experimental Study of the Thermodynamics of Multi component Polyolefin Blends with Ordered and Disordered Phases", Macromol. 31, 3340 (1998).

Jeon, H. S., Lee, J. H., Balsara, N. P., "Predicting the Thermodynamics of Multi-Component Polymer Blends from Measurements on 'Two-Component Systems'", Macromol. 31, 3328 (1998).

Johnson, G. M., Reisner, B. A., Tripaathi, A., Corbin, D. R., Toby, B. H., Parise, J. B., "Flexibility and Cation Distribution upon Lithium Exchange of AlSi- and AlGe-RHO Framework Materials", Chem. Mat. 11, 2780 (1999).

Jones, G. L., Adams, J. M., Anaya, J. M., Bowles, T. J., Chupp, T. E., Coulter, K. P., Dewey, M. S., Freedman, S. J., Fujikawa, B. K., Garcia, A., Greene, G. L., Hwang, S. -R., Lising, L. J., Nico, J. S., Robertson, R. G. H., Steiger, T. D., Teasdale, W. A., Thompson, A. K., Wietfeldt, F. E., and Wilkerson, J. F., "Time Reversal in Polarized Neutron Decay - The EMIT Experiment", Nucl. Instrum. Meth. A, in press.

Jones, G. L., Gentile, T. R., Thompson, A. K., Chowdhuri, Z., Dewey, M. S., Snow, W. M., Wietfeldt, F. E., "Test of ^{3}He-based Neutron Polarizers at NIST", Nucl. Instrum. Meth. A, in press.

Jones, R. L., Kumar, S. K., Ho, D. L., Briber, R. M., Russell, T. P., "Chain Conformation in Ultrathin Polymer Films", Nature **400**, 146 (1999).

Jolly, M., Bender, J., Carlson, J. D., "Properties and Applications of Commercial Magnetorheological Fluids", Proc. SPIE **3327**, 262 (1998).

Kaduk, J. A., Wong-Ng, W., Greenwood, W., Dillingham, J., Toby, B. H., "Crystal Structures and Reference Powder Patterns of BaR_2ZnO_5 (R = La, Nd, Sm, Eu, Gd, Dy, Ho, Y, ER and Tm)", J. Res. Natl. Inst. Stan. **140**, 147 (1999).

Kamitakahara, W. A., Wada, N., "Dynamics of Intercalated Water Molecules in Synthetic Layered Silicates", Mol. Cryst. Liq. Cryst., in press.

Karen, P., Kjekshus, A., Huang, Q., Karen, V. L., "The Crystal Structure of Magnesium Dicarbide", J. Alloys Compnds. **282**, 72 (1999).

Karim, A., "Interactions of Polymers with Fillers and Nanocomposites, NIST June 18-19, 1998", NISTIR 6312.

Kasper, N. V., Troyanchuk, I. O., Khalyavin, D. D., Hamad, N., Haupt, L., Frobel, P., Barner, K., Gmelin, E., Huang, Q., Lynn, J. W., "Effect of Oxygen Content and Oxygen Vacancy Ordering on Properties of $TbBaCo_{2-x}O_{6-\delta}$ (x ≤ 0.5) Perovskites", Phys. Status Solidi B **215**, 697 (1999).

Kent, M. S., Majewski, J., Smith, G. S., Lee, L. T., Satija, S. K., "Tethered Chains in Poor Solvent Conditions: An Experimental Study Involving Angmuir Diblock Copolymer Monolayers", J. Chem. Phys. **110**, 3553 (1999).

Kent, M. S., McNamara, W. F., Baca, P. M., Wright, W., Domeier, L. A., Wong, A. P. Y., Wu, W. L., "Water Adsorption in Interfacial Silane Layers by Neutron Reflection: II. Epoxy + Silane on Silicon Wafers", J. Adhesion **69**, 139 (1999).

Kerch, H. M., Long, G. G., Krueger, S., Allen, A. J., Gerhardt, R., Cosandey, F., "Characterization of Porosity over Many Length Scales: Application of Colloidal Gels", J. Mater. Res. **14**, 1444 (1999).

Kernick III, W. A., Wagner, N. J., "The Role of LCP Pheology on the Evolving Microstructure of Immiscible Blrnds Containning LCPs", J. Rheol. **43**, 521 (1999).

Kesler, O., Matejicek, J., Sampath, S., Suresh, S., T., Brand, P. C., Prask, H. J., "Measurement of Residual Stress in Plasma-Sprayed Metallic, Ceramic and Composite Coatings", J. Mater. Sci. Eng. **257**, 215 (1998).

Kessler, E. G., Dewey, M. S., Deslattes, R. D., Henins, A., Borner, H. G., Jentschel, M., Doll, C., Lehmann, H., "The Deuteron Binding Energy and the Neutron Mass", Phys. Rev. Lett. **255**, 221 (1999).

Kholifah, P., Erwin, R. W., Lynn, J. W., Huang, Q., Batlogg, B., Cava, R. J., "The Magnetic and Electronic Characterization of Quasi-One-Dimensional La_3RuO_7", Phys. Rev. B **60**, 9573 (1999).

Kilic, C., Yildirim, T., Mehrez, H., Ciraci, S., "A First-Principles Study of the Structure and Dynamics of C_8H_8, Si_8H_8 and Ge_8H_8 Molecules", J. Phys. Chem., in press.

Kim, Y. J., Aharony, A., Birgeneau, R. J., Chou, F. C., Entin-Wohlman, O., Erwin, R. W., Greven, M., Harris, A. B., Kastner, M. A., Korenblit, I., Ya, Lee, Y. S., Shirane, G., "Ordering due to Quantum Fluctuations in $Sr_2Cu_3O_4Cl_2$", Phys. Rev. Lett. **83**, 852 (1999).

Kimura, H., Hirota, K., Matsushita, H., Yamada, K., Endoh, Y., Lee, S. -H., Majkrzak, C. F., Erwin, R. W., Shirane, G., Greven, M., Lee, Y. S., Kastner, M. A., Birgeneau, R. J., "Neutron Scattering Study of Static Antiferromagnetic Correlations in $La_{2-x}Sr_xCu_{1-y}Zn_yO_4$", Phys. Rev. B **59**, 6517 (1999).

Kitade, S., Ochiai, N., Takahashi, Y., Noda, I., Matsushita, Y., Karim, A., Nakatani, A. I., Kim, H., Han, C. C., "Lamellar Orientation of Diblock Copolymer Solutions Under Steady Shear Flow", Macromol. **31**, 8083 (1998).

Kline, S. R., "Polymerization of Rod-Like Micelles", Langmuir **15**, 2726 (1999).

Kline, S. R., "Structural Evolution During Micelle Polymerization", J. Appl. Crystallogr., in press.

Kmety, C. R., Manson, J. L., Huang, Q., Lynn, J. W., Erwin, R. W., "Collinear Ferromagnetism and Spin Orientation in the Molecule-Based Magnets $M[N(CN)_2]_2$ (M = Co,Ni)", Phys. Rev. B **60**, 60 (1999).

Kmety, C. R., Manson, J. L., Huang, Q., Lynn, J. W., Erwin, R. W., Miller, J. S., Epstein, A. J., "Magnetic Phase Transitions in $M^{II}[N(CN)_2]_2$", J. Mol. Liq. Cryst., in press.

Kossuth, M. B., Morse, D. C., Bates, F. S., "Viscoelastic Behavior of Cubic Phases in Block Copolymer Melts", J. Rheology **43**, 167 (1999).

Koubi, L., Tarek, M., Klein, M. L., Scharf, D., "Distribution of Volatile General Anesthetics in a Model Membrane from Molecular Dynamics Simulation", Biophy. J., in press.

Krishnamoorti, R., Silva, A. S., Modi, M. A., Hammouda, B., "Small Angle Neutron Scattering Study of a Cylinder to Sphere Order-Order Transition in Block Copolymers", Macromol., in press.

Krone, C. A., Robisch, P. A., Tilbury, K. L., Stein, J. E., Mackey, E. A., Becker, P. R., O'Hara, T. M., Philo, L. M., "Elements in Liver Tissues of Bowhead Whales (*Balaena mysticetus*)", Marine Mammal Sci. **15**, 123 (1999).

Lamaze, G. P., Chen-Mayer, H. H., "Nitrogen Analysis in Thin Films Using Cold Neutron Depth Profiling", in *Proc. 9th Intl. Conf. on Modern Materials and Technologies*, edited by P. Vincenzini, (TECHNA, Faenza, Italy), in press.

Lamaze, G. P., Chen-Mayer, H. H., Badding, M., Laby. L., "In Situ Measurements of Lithium Movement in Thin Film Electrochromic Coatings Using Cold Neutron Depth Profiling", J. Surf. Interface Anal. **27**, 644 (1999).

Lamaze, G. P., Chen-Mayer, H. H., Langland, J. K., "Recent Developments in Neutron Depth Profiling at NIST", in *Proc. 1998 Intl. Conf. Characterization and Metrology for Ultra Large Scale Integration Technology*, edited by D. G. Deiler, A. C. Diebold, W. M. Bulis, T. J., Shaffner, R. McDonald, E. J. Walter, (American Institute of Physics, 1998) p.883.

Lee, S.-H., Broholm, C., Aeppli, G., Cheong, S.-W., "Short-Range Spin Correlations in a Geometrically Frustrated Magnet, $SrCr_{9p}Ga_{12-9p}O_{19}$", in *Proceedings of the International Workshop on Cold Neutron Utilization* (Korean Atomic Energy Institute, Taejon, South Korea), in press.

Lee, S.-H., Broholm, C., Cheong, S.-W., Kim, T. H., Ratcliff II, W., "Local Spin Resonance and Spin-Peirls Like Phase Transition in the Geometrically Frustrated Antiferromagnet $ZnCr_2O_4$", Phys. Rev. Lett., in press.

Lee, S.-H., Majkrzak, C. F., "A New Technique for Polarized Neutron Diffraction", Physica B **268**, 341 (1999).

Lee, S.-H., Majkrzak, C. F., "Polarized Neutron Diffraction with an Area-Sensitive Detector", J. Neutron Res. **7**, 131 (1999).

Lee, S.-H., Majkrzak, C. F., Sinha, S. K., Stassis, C., Kawano, H., Lander, G. H., Brown, P. J., Fong, H. F., Cheong, S. W., Matsushita, H., Yamada, K., Endoh, Y., "Search for Orbital Moments in Underdoped Cuprate Metals—A Sisyphian Task", Phys. Rev. B **60**, 10405 (1999).

Lee, Y. S., Birgeneau, R. J., Kastner, M. A., Endoh, Y., Wakimoto, S., Yamada, K., Erwin, R. W., Lee, S. H., Shirane, G., "Neutron Scattering Study of Spin Density Wave Order in the Superconducting State of Excess-Oxygen-Doped La_2CuO_{4+y}", Phys. Rev. B **60**, 3643 (1999).

Lefebvre, A. A., Balsara, N. P., Hammouda, B., Jeon, H. S., La, R. J., Lee, J. H., "Initial Stages of Nucleation During Liquid-Liquid Phase Separation in Polymer Blends", J. Chem. Phys. **111**, 6082 (1999).

Lefebvre, A. A., Lee, J. H., Balsara, N. P., Hammouda, B., Krishnamoorti, R., "Relationship between Internal Energy and Volume Change on Mixing in Pressurized Polymer Blends", Macromol. **32**, 5460 (1999).

Lefebvre, K. K., Lee, J. H., Balsara, N. P., Hammouda, B., Krishnamoorti, R., Kumar, S., "Relationship Between Internal Energy and Volume Change of Mixing in Pressurized Polymer Blends", Macromol. **32**, 5460 (1999).

Leheny, R.L., Christianson, R. J., Birgeneau, R. J., Erwin, R. W., "Spin Correlations in an Isotropic Spin – 5/2 Two-Dimensional Antiferromagnetic", Phys. Rev. Lett. **82**, 418 (1999).

Leheny, R. L., Nagel, S. R., "Dielectric Susecptibility Studies of the High-Frequency Shape of the Primary Relaxation in Supercooled Liquids", J. Non-Cryst. Solids **235**, 278 (1998).

Li, W.-H., Wu, S. Y., Lee, K. C., Lynn, J. W., "Magnetic Ordering of Mn in Ca-doped $NdMnO_3$", Physica B, in press.

Li, W.-H., Wu, S. Y., Lee, K. C., Lynn, J. W., Liu, R. S., Wu, J. B., Huang, C. Y., "Magnetic Order and Spin Reorientation in $Nd_{0.45}Ca_{0.55}MnO_3$", J. Appl. Phys. **85**, 5588 (1999).

Li, W.-H, Wu, S. Y., Lin, Y. C., Lee, K. C, Lynn, J. W., Weng, S. S., Hong, I. P., Lin, J. –Y., Yang, H. D., "Magnetic Ordering in Double-Chain $PrBa_2Cu_4O_8$", Phys. Rev. B **60**, 4212 (1999).

Li, Z. G., Harlow, R. L., Foris, C. M., Li, H., Ma, P., Vickery, R. D., Maurin, M. B., Toby, B. H., "Polymorph Determination for the GPIIb/IIIa Antagonist, Roxifiban, Using a Combination of Electron Diffraction and Synchrotron X-ray Powder Diffraction Techniques", J. Pharmctl. Sci. **88**, 297 (1999).

Liang, J. K., Huang, Q., Santoro, A., Liu, Q. L., Chen, X. L., "A Neutron Powder Diffraction Study of the System $La_2(Co_{1-x}Fe_x)_{16}Ti$ for x = 0.0, 0.2, and 0.4", J. Appl. Phys. **86**, 1226 (1999).

Liang, J. K., Huang, Q., Santoro, A., Wang, J. L., Yang, F. M., "Magnetic Structure and Site Occupancies in $YFe_{11-x}Co_xTi$ (x = 1, 3, 7, 9)", J. Appl. Phys. **86**, 2155 (1999).

Licci, F., Marezio, M., Huang, Q., Santoro, A., Bougerol-Chaillout, C., Masini, R., "Synthesis, Structure and Superconductivity of $Hg_{0.75}Mo_{0.25}Ba_2CuO_{4+\delta}$", Physica C, in press.

Lin, E. K., Kolb, R., Satija, S. K., Wu, L. U., "Reduced Polymer Mobility Near the Polymer/Solid Interface as Measured by Neutron Reflectivity", Macromol. **32**, 3753 (1999).

Lin, E. K., Kolb, R., Wu, W. L., Satija, S. K., "Enhanced Polymer Segment Exchange Kinetics due to an Applied Shear Field", Macromol. **32**, 4741 (1999).

Lin, E. K., Pochan, D. J., Kolb, R., Wu, W. L., Satija, S. K., "Neutron Reflectivity for Interfacial Materials Characterization", in *Characterization and Metrology for ULSI Technology*, edited by D. G. Seiler, A. C., Diebold, W. M. Bullis, T. J. Shaffner, R. McDonlad, E. J. Watters, AIP Conference Series 449 (American Institute of Physics, Woodbury, NY, 1998), p.879.

Liu, Y., Chen, S.-H., Huang, J. S., "Small-Angle Neutron Scattering Analysis of the Structure and Interaction of Tri-Block Copolymer Micelles in Aqueous Solution", Macromol. **31**, 2236 (1998).

Long, G. G., Krueger, S., Allen, A. J., "Multiple Small-Angle Neutron Scattering", J. Neutron Res. **7**, 195 (1999).

Lynn, J. W., "Magnetic Neutron Scattering", in *Methods in Materials Research*, edited by Kaufman (John Wiley & Sons), in press.

Lynn, J. W., "Spin Dynamics of Magnetoresistive Oxides", in *The Physics of Manganites*, edited by Kaplan and Mahanti (Plenum Publishing, 1999), p. 149.

Lynn, J. W., "Spin Dynamics of the Magnetoresistive Oxides", Int. J. Mod. Phys. **12**, 3355 (1998).

Lynn, J. W., Rosov, N., Barilo, S. N., Kurnevitch, L., Zhokhov, A., "Pr Magnetic Order and Spin Dynamics in the Cuprates", Chin. J. Phys., in press.

Lynn, J. W., Skanthakumar, S., "Neutron Scattering Studies of Rare Earth Magnetic Ordering", *Handbook on the Physics and Chemistry of Rare Earths*, edited by K. A. Gschneider, Jr., L. Eyring, M. B. Maple (Elsevier Science), in press.

Mackey, E. A., Demiralp, R., Fitzpatrick, K. A., Porter, B. J., Wise, S. A., Greenberg, R. R., "Quality Assurance in Analysis of Cryogenically Stored Specimens from the NIST National Biomonitoring Specimen Bank", Sci. Total Environ. **226**, 165 (1999).

Magid, L. J., "The Surfactant-Polyelectrolyte Analogy", J. Phys. Chem. B. **102**, 4064 (1998).

Magid, L. J., Han, Z., Li, Z., Butler, P.D., "Tuning Microstructure of Cationic Micelles on Multiple Length Scales: The Role of Electrostatics and Specific Ion Binding", Langmuir, in press.

Majkrzak, C. F., "Neutron Applications in Materials Science and Engineering", J. Neut. Res., in press.

Majkrzak, C. F., "Neutron Reflectometry Studies of Thin Films and Multilayered Materials", Acta Physica Polonica A **96**, 81 (1999).

Majkrzak, C. F., Berk., N. F., "Exact Determination of the Phase in Neutron Reflectometry by Variation of the Surrounding Media", Phys. Rev. B **58**, R15416 (1998).

Majkrzak, C. F., Berk, N. F., "Experimental Demonstration of Phase Determination in Neutron Reflectometry by Variation of the Surrounding Media", Physica B, in press.

Majkrzak, C. F., Berk, N. F., "Inverting Neutron Reflectivity from Layered Film Structures Using Polarized Beams", Physica B **268**, 168 (1999).

Mang, J. T., Hjelm, R. P., "Small Angle Neutron Scattering Studies of Vesicle Stability", Intl. J. Thermophys **19**, 461 (1998).

Margadonna, S., Brown, C. M., Lappas, A., Prassides, K., Tanigaki, K., Knudsen, K. D., le Bihan, T., Mezouar, M., "Pressure and Temperature Evolution of the Structure of the Superconducting Na_2CsC_{60} Fulleride", J. Solid State Chem. **145**, 471 (1999).

Margadonna, S., Prassides, K., Neumann, D. A., Shimoda, H., Iwasa, Y., "Rotational Dynamics of C_{60} in $(ND_3)K_3C_{60}$", Phys. Rev. B **59**, 943 (1999).

Matejicek, J., Sampath, S., Brand, P. C., Prask, H. J., "Quenching, Thermal, and Residual Stress in Plasma Sprayed Deposits: NiCrAlY and YSZ Coatings", Acta Mater. **47**, 67 (1999).

Maurer, R. H., Roth, D. R., Fainchtein, R., Goldsten, J. O., Kinnison, J. D., Thompson, A. K., "Portable Real Time Neutron Spectrometry", *in Proceedings of the Space Technology and Applications International Forum (STAIF-99)*, Conference on International Space Station Utilization, in press.

McKinsey, D. N., Brome, C. R., Butterworth, J. S., Dzhosyuk, S. N., Golub, R., Habicht, K., Huffman, P. R., Lamoreaux, S. K., Mattoni, C. E. H., Doyle, J. M., "Radiative Decay of the Metastable Molecule $He_2(a^3\Sigma_u^+)$ Molecule in Liquid Helium", Phys. Rev. A **59**, 200 (1999).

Merfeld, G. D., Karim, A., Majumdar, B., Satija, S. K., Paul, D. R., "Interfacial Thickness between Immiscible Bilayers of Poly(phenylene oxide) and Styrenic Copolymers", J. Poly. Sci. Part B, in press.

Merzbacher, C. I., Barker, J. G., Long, J. W., Rolison, D. R., "The Morphology of Nanoscale Deposits of Ruthenium Oxide in Silica Aerogels", Nanostructured Mater., in press.

Meyer, A., Busch, R., Schober, H., "Time-Temperature Superposition of Structural Relaxation in a Viscous Metallic Liquid", Phys. Rev. Lett., in press.

Meyer, A., Wuttke, J., Petry, W., "Two-Step Relaxation in a Viscous Metallic Liquid", J. Non-Cryst. Solids, in press.

Migler, K. B., Han, C. C., "Pressure Effects on Diblock Copolymers: Optical Birefringence and Neutron Scattering", Macromol., in press.

Mildner, D. F. R., "Self Shielding for Thick Slabs in a Converging Neutron Beam", Nucl. Instrum. Meth. A **432**, 399 (1999).

Mildner, D. F. R., Chen-Mayer, H. H., "Neutron Absorption Measurements Using Converging Beams—Increased Reaction Rate", Nucl. Instrum. Meth. A **422**, 21 (1999).

Mildner, D. F. R., Lamaze, G. P., "Neutron Transmission of Simple Crystal Sapphire", J. Appl. Crystallogr. **31**, 835 (1998).

Modi, M. A., Krishnamoorti, R., Tse, M. F., Wang, H. C., "Viscoelastic Characterization of an Order-Order Transition in a Mixture of Di- and Triblock Copolymers", Macromol. **32**, 4088 (1999).

Morkved, T. L., Chapmen, B. R., Bates, F. S., Lodge, T. P., Stepanek, P., Almdal, K., "Dynamics of Ternary Polymer Blends: Disordered, Ordered, and Bicontinuous Microemulsion Phases", Faraday Discuss. 112, in press.

Nakatani, A. I., "Phase Separation Kinetics During Shear in Compatibilized Polymer Blends", in *Scattering from Polymers*, edited by B. S. Hsiao, P. Cebe, D. J. Lohse (ACS Symp. Series, Washington, DC), in press.

Newstein, M. C., Wang, H., Balsara, N. P., Lefebvre, A. A., Shnidman, Y., Watanabe, H., Osaki, K., Shikita, T., Niwa, H., Morishima, Y., "Microstructural Changes in a Colloidal Liquid in the Shear Thining and Shear Thickening Regimes", J. Chem. Phys., in press.

Nico, J. S., Abdurashitov, J. N., Gavrin, V. N., Girin, S. V., Gorbachev, V. V., Ibragimova, T. V., Kalikhov, A. V., Khairnasov, N. G., Knodel, V. N., Mirmov, I. N., Shikhin, A. A., Verentenkin, E. P., Vermul, V. M., Yants, V. E., Zatsepin, G. T., Bowles, T. J., Teasdale, W. A., Wark, D. L., Cherry, M. L., Cleveland, B. T., Davis, R., Lande, K., Wildenhain, P. S., Elliott, S. R., Wilkerson, J. F., "Solar Neutrino Results from SAGE", in *Proceedings of the 10th International Baksan School: Particles and Cosmology*, in press.

Nikolaev, A. V., Michel, K. H., Copley, J. R. D., "Orientational Disorder and Order in C_{60}-Fullerite and in MC_{60}-Alkali Metal Fullerides", in *Correlations, Coherence, and Order*, edited by D. V. Shopova, D. I. Uzunov (Plenum Press, London-New York, 1999), p. 183.

Nisato, G., Ivkov, R., Amis, E. J., "Structure of Charged Dendrimer Solutions as Seen by SANS", Macromol. **32**, 5895 (1999).

Norman, B. R., Igengar, G. V., "Further Applications of Pre-irradiation Combustion and Neutron Activation Analysis Technique for the Determination of Iodine in Food and Environmental Reference Materials: Merits and Demerits", Fresen. J. Anal. Chem., in press.

Oakey, J., Marr, D. W. M., Schwartz, K. B., Wartenberg, M., "The Influence of Polyethlene and Carbon Black Morphology on Void Formation in Conductive Composite Materials – a SANS Study", Macromol. **32**, 5399 (1999).

Ondov, D. J., Ondov, J. M., "Data Management and Acquisition System for INAA", Trans. Amer. Nucl. Soc. **78**, in press.

Osborn, R., Rosenkranz, S., Argyriou, D. N., Vasiliu-Doloc, L., Lynn, J. W., Sinha, S. K., Mitchell, J. F., Gray, K. E., Bader, S. D., "Neutron Scattering Investigation of Magnetic Bilayer Correlations in $La_{1.25}Sr_{1.8}Mn_2O_7$: Evidence of Canting above T_C", Phys. Rev. Lett. **81**, 3964 (1998).

Overholser, R., Wuttig, M., Neumann, D. A., "Chemical Ordering in Ni-Mn-Ga Heusler Alloys", Scripta Mat. **40**, 1095 (1999).

Pan, Y.-M., Page, R. A., Long, G. G., Krueger, S., "The Role of Zirconia Addition in Pore Development and Grain Growth in Alumina Compacts", J. Mater. Res., in press.

Papanek, P., Fischer, J. E., Sauvajol, J. L., Dianoux, A. J., McNeillis, P. M., Mathis, C., Francois, B., "Low-Frequency Phonons in Pristine and Doped Phases of Polyacetylene: An Inelastic Neutron Scattering Study", J. Chem. Phys., in press.

Pardo, H., Ortiz, W. A., Araujo-Moreira, F. M., Suescun, L., Toby, B. H., Negreira, C. A., Prassides, K., Mombru, A. W., "A New Structure in the $REBaCuFeO_{5+\delta}$ Series: $LaBaCuFeO_{5+\delta}$. Structure and Magnetic Properties in the $La_{1-x}Pr_xBaCuFe_{5+\delta}$ System", Physica C **313**, 105 (1999).

Paul, R. L., "Determination of Nitrogen in Some Reference Materials by Cold Neutron Prompt Gamma-ray Activation Analysis", J. Radioanal. Nucl. Chem., in press.

Paul, R. L., "Determination of Phosphorus in Steels by Radiochemical Neutron Activation Analysis", J. Radioanal. Nucl. Chem., in press.

Paul, R. L., "Measurement of Phosphorus in Metals by Radiochemical Neutron Activation Analysis", J. Radioanal. Nucl. Chem., in press.

Pochan, D. J., Lin, E. K., Wu, W. L., Satija, S. K., Cheng, S. Z. D., "Thermal Expansion and Glass Transition Behavior of Thin Polymer Films with and without a Free Surface via Neutron Reflectometry", in *Dynamics in Small Confining Systems IV*, edited by J. M. Drake, G. S. Grest, J. Klafter, R. Kopelman, MRS Symp. Series 543, (Materials Research Society, Warrendale, PA, 1999), in press.

Podurets, K. M., Mildner, D. F. R., Sharov, V. A., "Application of Capillary Optics to Neutron Radiography", Rev. Sci. Instrum. **69**, 3541 (1998).

Pommé, S., Simonits, A., Lindstrom, R. M., DeCorte, F., Robouch, P., "Determination of Burnup Effects Prior to Reactor Neutron Field Characterization", J. Radioanal. Nucl. Chem., in press.

Prask, H. J., Choi, C. S., "Nondestructive Determination of Subsurface Residual Stresses by Means of Neutron Diffraction", in *Multiazial Fatiqul of an Induction Hardened Shaft*, edited by T. Cordes, K. Leasly (Society Auto Engineering, 1999) p.45.

Prask, H. J., Gnäupel-Herold, T., Clark, A. V., Hehman, C. S., Nguyen, T. N., "Neutron and Ultrasonic Determination of Residual Stress in an Aluminum Ring-Plug", in *Proceedings of the 26th Annual Review of Progress in Quantative NDE* (Montreal, July 1999), in press.

Prince, E., "Neutron Scattering Instrumentation: A Tutorial Review", App. Spectrosc. Rev. **34**, 159 (1999).

Qi, S., Chakraborty, A. K., Wang, H., Lefebvre, A. A., Balsara, N. P., Shaknovich, E. I., Xenidou, M., Hadjichristidis, N., "Microphase Ordering in Melts of Randomly Grafted Copolymers", Phy. Rev. Lett., in press.

Ramzi, A., Bauer, B. J., Scherrenberg, R., Froehling, P., Joosten, J., Amis, E. J., "Fatty Acid Modified Dendrimers in Bulk and Solution: Single Chain Neutron Scattering from Dendrimer Core and Fatty Acid Shell", Macromol. **32**, 4983 (1999).

Richter, C. A., Nguyen, N. V., Dura, J. A., Majkrzak, C. F., "Characterization of Thin SiO_2 on Si by Spectroscopic Ellipsometry, Neutron Reflectivity, an X-Ray Reflectivity", in *Characterization and Metrology for ULSI Technology*, edited by D. G. Seiler (AIP, New York, 1998), p. 185.

Rijssenbeek, J. T., Huang, Q., Erwin, R. W., Zandbergen, H. W., Cava, R. J., "The Crystal Structure of $Ba_3CuRu_2O_9$ and Comparison to $Ba_3MRu_2O_9$ (M = In, Co, Ni, and Fe)", J. Sol. State Chem. **146**, 65 (1999).

Rijssenbeek, J. T., Matl, P., Batlogg, B., Huang, Q., Ong, N. P., Cava, R. J., "Crystal Structure and Physical Properties of a Series of Ternary Barium Metal Ruthenates: $Ba_3MRu_2O_9$, M = Fe, Co, Ni, and In", Phys. Rev. B, in press.

Rosenkranz, S., Osborn, R., Mitchell, J. F., Vasiliu-Doloc, L., Lynn, J. W., Sinha, S. K., "Low-energy Spin Wave Excitations in the Bilayer Manganite $La_{1.2}Sr_{1.8}Mn_2O_7$", J. Appl. Phys., in press.

Rosenkranz, S., Osborn, R., Mitchell, J. F., Vasiliu-Doloc, L., Lynn, J. W., Sinha, S. K., "Spin Correlations of the Magnetoresistive Bilayer Manganite $La_{1.2}Sr_{1.8}Mn_2O_7$", Int. J. Mod. Phys. B, in press.

Rosov, N., Rathgeber, S., Monkenbusch, M., "Neutron Spin Echo Spectroscopy at the NIST Center for Neutron Research", ACS Proceedings of the PSME Symposium Scattering and Polymers **216**, 4865 (1998).

Rush, J. J., Udovic, T. J., Berk, N. F., Richter, D., Magerl, A., "Excited-State Vibrational tunnel Splitting of Hydrogen Trapped by Nitrogen in Niobium", Europhys. Lett., in press.

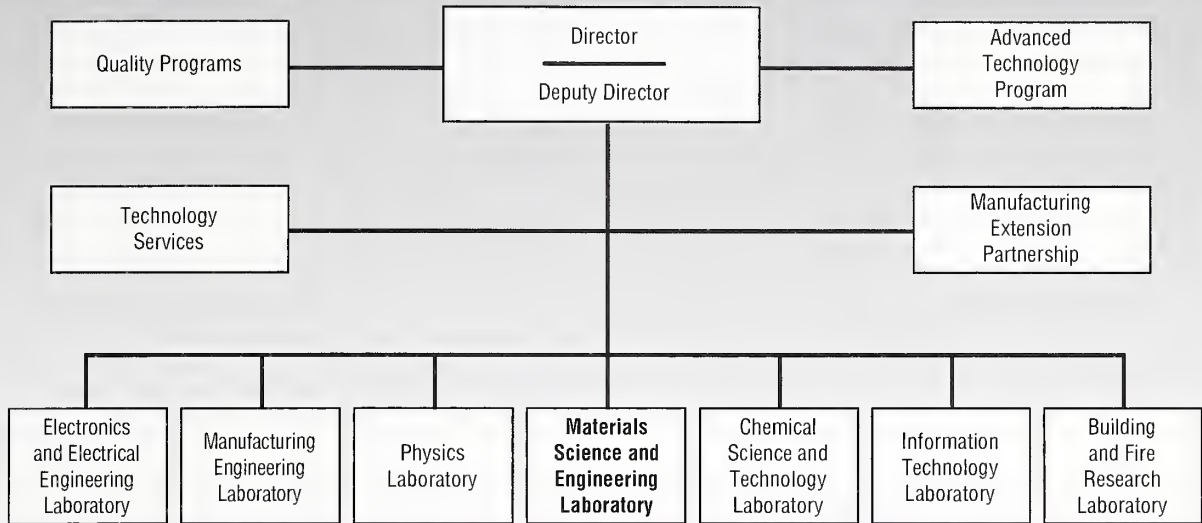Russell, T. P., "Neutron Reflectivity on Thin Film Symmetric Diblock Polymers", Am. Cryst. Assoc. Trans., in press.

Ruzette, A.-V. G., Banerjee, P., Mayes, A. M., Pollard, M., Russell, T. P., Jerome, R., Slawecki, T., Hjelm, R., Thiyagarajan, P., "Phase Behavior of Diblock Copolymers Between Styrene and N-Alkyl Methacrylates" Macromol. **31**, 8509 (1998).

Ryan, L. D., Kaler, E. W., "Microstructure Properties of Alkyl Polyglucoside Microemulsions", Langmuir **15**, 92 (1999).

Salamat, G., de Uries, R., Kaler, E. W., Satija, S. K., Sung, L. P., "Undulations in Salt-Free Charged Lamellar Phases Detected by Small Angle Neutron Scattering and Neutron Reflectivity", Langmuir, in press.

Salamat, G., Kaler, E. W., "Colloidal Dispersions in Lyotropic Lamellar Phases", Langmuir **15**, 5414 (1999).

Sanders, P. G., Eastman, J. A., Weertman, J. R., "Pore Distributions in Nanocrystalline Metals from Small-Angle Neutron Scattering", Acta Materialia **46**, 4195 (1998).

Santoro, A., Natali Sora, I., Huang, Q., "Bond-Valence Analysis of the Structure of $(Ba_{0.875}Sr_{0.125})RuO_3$", J. Solid State Chem. **143**, 69 (1999).

Sayer, E. V., Yener, A. K., Joel, E. C., Blackman, M. J., Özbal, "Stable Lead Isotope Studies of Black Sea Anatolian Ore Sources and Related Bronze Age and Phrygian Artifacts from Nearby Archaeological Sites. Appendix: New Central Taurus Ore Data", Archaeometry, in press.

Schmidt-Winkel, P., Glinka, C. J., Stucky, G. D., "Microemulsion Templates for Mesoporous Silica", Langmuir, in press.

Schober, H., Cook, J. C., Mezei, F., "Upgrade of the IN5 Cold Neutron Time-of-Flight Spectrometer", J. Neutron Res., in press.

Schober, H., Losert, C., Mezei, F., Cook, J. C., "Chopper Cascades: An Analytical Treatment of the Contamination Problem", J. Neutron Res., in press.

Schreyer, A., Majkrzak, C. F., Berk, N. F., Grüll, H., Han., C. C., "Using Polarized Neutrons to Determine the Phase Reflection from Thin Film Structures", J. Phys. Chem. Sol. **60**, 1045 (1999).

Schulz, J. C., Warr, G. G., Hamilton, W. A., Butler, P. D., "Neutron Reflectometry of Adsorbed Surfactant Aggregates", J. Phys. Chem. B, in press.

Seehra, M. S., Babu, V. S., Lynn, J. W., "Magnetism of Ferrihydrite Nanoparticles Studied by Neutron Scattering and Magnetometry", Phys. Rev. B, in press.

Shen, L. F., Laibinis, P. E., Hatton, T. A., "Aqueous Magnetic Fluids Stabilized by Surfactant Bilayers", J. Magn. Magn. Mater. **194**, 37 (1999).

Shi, Y., Wang, S., Krueger, S., Schwarz, F. P., "Effect of Mutations at the Monomer-Monomer Interface of CAMP Receptor Protein on Specific DNA Binding", J. Bio. Chem. **274**, 6946 (1999).

Skanthakumar, S., Lynn, J. W., "Rare Earth Magnetic Order in RNi_2B_2C and RNiBC", Physica B **261**, 576 (1999).

Skripov, A. V., Cook, J. C., Karmonik, C., Kozhanov, V. N., "Hydrogen Motion in C15-Type $ZrMo_2H_x$: Quasielastic Neutron Scattering and Nuclear Magnetic Resonance Studies", Phys. Rev. B **60**, 7238 (1999).

Slawecki, T. M., Glinka, C. J., Hammouda, B., "Shear Induced Micellar Crystal Structures in an Aqueous Triblock Copolymer Solution", Phys. Rev. E **58**, 4084 (1998).

Smith, M. D., Stalick, J. K., zur Loye, H. C., "Sr3PbNiO6-Trigonal Prismatic Lead in an Unprecedented Inverse K_4CdC_{16}-Type Pseudo One-Dimensional Oxide", Chem. Mater. **11**, 2984 (1999).

Snow, W. M., Bazhenov, A., Biessinger, C. S., Bowman, J. D., Chupp, T. E., Coulter, K. P., Freedman, S. J., Fujikawa, B. K., Gentile, T. R., Greene, G. L., Hansen, G., Hogan, G. E., Ishimoto, S., Jones, G. L., Knudson, J. N., Kolomenski, E., Lamoreaux, S. K., Leuschner, M. B., Masaike, A., Masuda, Y., Matsuda, Y., Morgan, G. L., Morimoto, K., Morris, C. L., Nann, H., Penttila, S. I., Pirozhkov, A., Pomeroy, V. R., Rich, D. R., Serebrov, A., Sharapov, E. I., Smith, D. A., Smith, T. B., Welsh, R. C., Wietfeldt, F. E., Wilburn, W. S., Yuan, V. W., and Zerger, J., "Measurement of the Parity Violating Asymmetry $A\gamma$ in $n + p \rightarrow d + \gamma$", Nucl. Instrum. Meth. A, in press.

Snow, W. M., Chowdhuri, Z., Dewey, M. S., Fei, X., Gilliam, D. M., Greene, G. L., Nico, J. S., Wietfeldt, F. E., "Measurement of the Neutron Lifetime by Counting Trapped Protons", Nucl. Instrum. Meth. A, in press.

Sokolov, M. A., Spooner, S. E., Odette, G. R., Wirth, B. D., Lucas, G. E., "SANS Study of High-Copper RPV Welds in Irradiated and Annealed Conditions", in *Effects of Radiation on Materials: 18th International Symposium*, ASTM STP I325, edited by R. K. Nanstad, M. L. Hamilton, F. A. Garner, and A. S. Kumar (ASTM, West Conshohocken, PA, 1999), in press.

Stanka, M. B., Adams, J. M., Eisenhauer, C. M., "Proton Recoil Measurements of the ^{252}Cf Fission Neutron Leakage Spectrum from an Iron Sphere", Nucl. Sci. Eng., in press.

Stone, D. B., Hjelm, R. P., Mendelson, R. A., "Solution Structures of Dimeric Kinesin and NCD Motors", Biochem. **38**, 4938 (1999).

Stull, J. T., Lin, P. J., Krueger, J. K., Trewhella, J., Zhi, G., "Myosin Light Chains: Functional Domains and Structural Motifs", Acta Physiol. Scand. **164**, 471 (1999).

Sung, L., Karim, A., Douglas, J. F., Han, C. C., "Modification of Thin Film Phase Separation by a Surfactant", Macromol., in press.

Tarek, M., Tobias, D. J., "Environmental Dependence of the Dynamics of Protein Hydration Water", J. Am. Chem. Soc. **121**, 9740 (1999).

Tarek, M., Tu, K., Klein, M. L., Tobias, D. J., "Molecular Dynamics Simulations of Supported Phospholipid/Alkanethiol Bilayers on a Gold (111) Surface", Biophys. J. **77**, 964 (1999).

Their, K. F., Goze, C., Mehring, M., Rachdi, F., Yildirim, T., Fischer, J. E., "Metallic Properties of the Ternary Fullerides ABa_2C_{60} (A = K, RB, Cs)", Phys. Rev. B **59**, 10536 (1999).

Thiyagarajan, P., Crawford, R. K., Mildner, D. F. R., "Neutron Transmission of Single Crystal MgO Filter", J. Appl. Crystallogr. **31**, 841 (1998).

Thomas, J. J., Jennings, H. M., Allen, A. J., "The Surface Area of Hardened Cement Paste as Measured by Various Techniques", Con. Sci. Eng., in press.

Toby, B. H., "Diffraction Analysis and Crystallographic Structure Determination", in *Handbook of Ceramic Engineering*, edited by M. N. Rahaman, in press.

Toby, B. H., Khosrovani, N., Dartt, C. B., Davis, M. E., Parise, J. B., "Structure-Directing Agents and Stacking Faults in the CON System: A Combined Crystallographic and Computer Simulation Study", Microporous and Mesoporous Mater., in press.

Toby, B. H., Purnell, S., Hu, R., Peters, A., Olson, D. H., "An Attempt to Locate Protons in the ZSM-5 Structure by Combined Synchrotron and Neutron Diffraction", in *Proceedings of the 12th International Zeolite Conference*, edited by M. M. J. Tracy, B. K. Marus, M. E. Bisher and J. B. Higgins (Material Research Society, Warrendale, PA, 1999), p. 2413.

Topp, A., Bauer, B. J., Klimash, J. W., Spindler, R., Tomalia, D. A., Amis, E. J., "Probing the Location of the Terminal Groups of Dendrimers in Dilute Solution", Macromol. **32**, 7226 (1999).

Topp, A., Bauer, B. J., Prosa, T. J., Scherrenberg, R., Amis, E. J., "Size Change of Dendrimers in Concentrated Solution", Macromol., in press.

Topp, A., Bauer, B. J., Tomalia, D. A., Amis, E. J., "Effect of Solvent Quality on the Molecular Dimensions of PAMAM Dendrimers", Macromol. **32**, 7232 (1999).
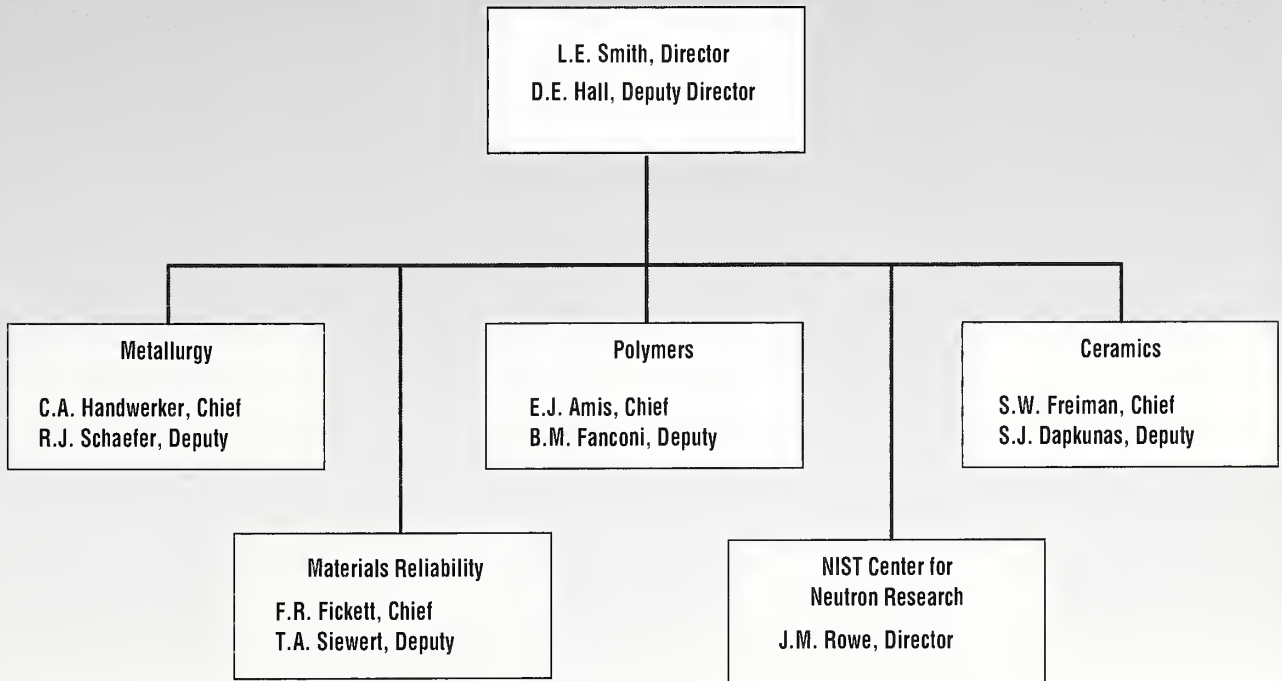
Trevino, S. F., Ivkov, R., Matyas, G., Lebeda, F. J., "Small-Angle Neutron Scattering of Bilayer Vesicles Made with Synthetic Phospholipids", in *Polymeric Materials-Drugs, Delivery and Devices* (Materials Research Society. Nov. 30-Dec. 4, 1998), in press.

Troyanchuk, I. O., Kasper, N. V., Khalyavin, D. D., Tonoyan, A. A., "Structure, Phase Transitions, and Magnetotransport Properties of $TbBaCo_{2-x}Fe_xO_{6-x}(x \leq 0.5)$ Perovskites", Phy. Rev B., in press.

Tsui, O. K. C., Rockford, L., Huang, E., Russell, T. P., "Manipulating Copolymers with Confinement and Interfacial Interactions", in *Supramolecular Structures in Confined Geometries* (Manne/Warr, 1999), in press.

Tu, K. C., Tarek, M., Klein, M. L., Scharf, D., "Effects of Anesthetics on the Structure of a Phospholipid Bilayer: Molecular Dynamics Investigation of Halothane in the Hydrated Liquid Crystal Phase of Dipalmitoylphosphatidylcholine", Biophy. J. **75**, 2123 (1998).

Udovic, T. J., Huang, Q., Karmonik, C., Rush, J. J., "Structural Ordering and Dynamics of LaH_{3-x}", J. Alloys Compounds, in press.

Udovic, T. J., Huang, Q., Lynn, J. W., Erwin, R. W., Rush, J. J., "Neutron Scattering Study of the Nuclear and Magnetic Structure of DyD_3 and Associated Vibrational and Magnetic Excitations", Phys. Rev. B **59**, 11852 (1999).

Udovic, T. J., Yildirim, T., Karmonik, C., Huang, Q., "The Applications of Neutron Seattering Methods to the Study of High-Temperature Protonic Conductors", in *Solid State Ionics V,* edited by G.A. Nazri, C. Julien, A. Rougier, MRS Symp. Series 548 (MRS, Pittsburgh, 1999), in press.

Unguris, J., Tulchinsky, D., Kelley, M. H., Borchers, J. A., Dura, J. A., Majkrzak, C. F., Hsu, S. Y., Loloee, R., Pratt, W. P., Bass, J., "Magnetic Depth Profiling Co/Cu Multilayers to Investigate Magnetoresistance", J. Appl. Phys., in press.

van der Zaag, P. J., Feiner, L. F., Wolf, R. M., Borchers, J. A., Ijiri, Y., Erwin, R. W., "The Blocking and Neel Temperature in Exchange Biased Fe_3O_4/CoO Multilayers", Physiea B, in press.

Vanderah, T. A., Wong-Ng, W., Toby, B. H., Browning, V. M., Shull, R. D., Geyer, R. G., Roth, R. S., "Characterization of Ternary Compounds in the $BaO:Fe_2O_3:TiO_2$ System: $Ba_6Fe_{45}Ti_{17}O_{106}$ and $BaFe_{11}Ti_3O_{23}$", J. Solid State Chem. **143**, 182 (1999).

Vasiliu-Doloc, L., Lynn, J. W., Moudden, A. H., de Leon-Guevara, A. M., Revcolevschi, A., "Structure and Spin Dynamics of $La_{0.85}Sr_{0.15}Mn_2O_7$", Phys. Rev. B **58**, 14913 (1998).

Vasiliu-Doloc, L., Rosenkranz, S., Osborn, R., Sinha, S. K., Lynn, J. W., Mesot, J., Seeck, O., Lee, W. K., Mitchell, J. F., "Charge Melting and Polaron Collapse in Colossal Magnetoresistive Oxides", Phys. Rev. Lett., in press.

Vaynberg, K. A., Wagner, N. J., Sharma, R., Martic, P., "Structure and Extent of Adsorbed Gelatin on Acrylic Latex and Polystyrene Colloidal Particles", J. Coll. Int. Sci. **205**, 131 (1998).

Velev, O. D., Kaler, E. W., Lenhoff, A. M., "Protein Interactions in Solution Charaeterized by Light and Neutron Scattering: Comparison of Lysozyme and Chymotrypsinogen", Biophys. J. **75**, 2682 (1998).

Viisanen, Y., Wagner, P., Strey, R., "Measurement of the Molecular Content of Binary Nuclei – IV – Use of the Nucleation Rate Surfaces for the N-Nonane-N-Alchol Series", J. Chem. Phys. **108**, 4257 (1998).

Wakimoto, S., Shirane, G., Endoh, Y., Hirota, K., Ueki, S., Yamada, K., Birgeneau, R. J., Kastner, M. A., Lee, Y. S., Gehring, P. M., Lee, S.-H., "Observation of Incommensurate Magnetic Correlations at the Lower Critical Concentration for Superconductivity in $La_{2-x}Sr_xCuO_4$ (x = 0.05)", Phys. Rev. B **60**, 769 (1999).

Wakimoto, S., Yamada, K., Ueki, S., Shirane, G., Lee, Y. S., Lee, S.-H., Kastner, M. A., Hirota, K., Gehring, P. M., Endoh, Y., Birgeneau, R. J., "Neutron Scattering Study of Elastic Magnetic Signals in Superconducting $La_{1.94}Sr_{0.06}CuO_4$", J. Phys. Chem. Solids, in press.

Wallace, W. E., Jacobson, D. L., Arif, M., Ioffe, A., "Application of Neutron Interferometry to the Measurement of Thin Film Density", Appl. Phys. Lett. **74**, 469 (1999).

Wang, H., Newstein, M. C., Krishnan, A., Balsara, N. P., Garetz, B. A., Hammouda, B., Krishnamoorti, R., "Ordering Kinetics and Alignment of Block Copolymer Lamellae Under Shear Flow", Macromol. **32**, 3695 (1999).

Watanabe, H., Yao, M. L., Osaki, K., Shikata, T., Niwa, H., Morishima, Y., Balsara, N. P., Wang, H., "Nonlinear Rheology and Flow Induced Structure in a Concentrated Spherical Silica Suspension", Rheol. Acta **37**, 1 (1998).

Watkins, J. J., Brown, G. D., Rao, V. S. R., Pollard, M. A., Russell, T. P., "Phase Separation in Polymer Blends and Diblock Copolymers Induced by Compressible Solvents", Macromol., in press.

Welp, K. A., Co, C., Wool, R. P., "Improved Reflectivity Fitting Using SERF: Spreadsheet Environment Reflectivity Fitting", J. Neut. Res., in press.

Welp, K. A., Wool, R. P., Agrawal, G., Satija, S. K., Pispas, S., Mays, J., "Direct Observation of Polymer Dynamics: Mobility Comparison Between Central and End Section Monomers", Macromol., in press.

Wietfeldt, F. E., Schima, F. J., Coursey, B. M., Hoppes, D. D., "Long-Term Measurement of the Half-Life of ^{44}Ti", Phys. Rev. C **59**, 528 (1999).

Wilemski, G., "Small Angle Neutron Scattering from Aerosols: Crossed Beam Kinematics and Guinier Analysis", Phys. Rev. E, in press.

Wirth, B. D., Odette, G. R., Pavinich, W. A., Lucas, G. E., Spooner, S. E., "Small Angle Neutron Scattering Study of Linde 80 RPV Welds", in *Effects of Radiation on Materials: 18th International Symposium*, ASTM STP 1325, edited by R. K. Nanstad, M. L. Hamilton, F. A. Garner and A. S. Kumar (ASTM, West Conshohocken, PA, 1999), in press.

Wu, S. Y., Hwang, S. R., Li, W. H., Lee, K. C., Lynn, J. W., Liu, R. S., "Jahn-Teller Distortion, Charge Ordering, and Magnetic Transitions", Chin. J. Phys., in press.

Wu, S. Y., Kuo, C. M., Wang, H. Y., Li, W. H., Lee, K. C., Lynn, J. W., Liu, R. S., "Magnetic Structure and Spin Reorientation of the Mn Ions in $NdMnO_3$", J. App. Phys., in press.

Wu, W. L., Wallace, W. E., Lin, E. K., Lynn, G. W., Glinka, C. J., Ryan, E. T., Ho, H. M., "Properties of Nanoporous Silica Thin Films Determined by High Resolution X-Ray Reflectivity and Small-Angle Neutron Scattering", J. Appl. Phys., in press.

Wyslouzil, B. E., Wilemski, G., Cheung, J. L., Strey, R., Barker, J. G., "Doppler Shift Anistropy in Small Angle Neutron Scattering", Phys. Rev. E **60**, 4330 (1999).

Yamaura, K., Cava, R. J., Erwin, R.W., Huang, Q. Z., Lynn, J. W., "Anomalous Crystal Structure Distortion at the Antiferromagnetic Transition in the Layered Cobalt Oxide $Sr_2Y_{0.8}Ca_{0.2}Co_2O_6$", Phys. Rev. B. **60**, 9623 (1999).

Yamaura, K., Huang, Q., Cava, R. J., "Synthesis, Crystal Structure, Electrical and Magnetic Properties of the New Layered Cobalt Oxides: $(Sr, Ca, Ln)_3Co_2O_{6\pm\delta}$ (Ln = Sm, Eu, Gd, Tb, Dy, Ho, and Y)", J. Sol. State Chem **146**, 277 (1999).

Yang, L., Harroun, T. A., Heller, W. T., Weiss, T. M., Huang, H., W., "Supermoleeular Structures of Peptide Assemblies in Membranes by Neutron Off-Plane Scattering: Method of Analysis", Biophys. J., in press.

Yang, L., Slawecki, T. M., Alexandridis, P., "Shear Induced Orientation and Structural Transitions in Micellar Cubic Crystals Formed by Solvated Block Copolymers: A SANS Investigation", Macromol., in press.

Yildirim, T., "Ordering Due to Disorder in Frustrated Quantum Magnetic Systems", Turkish J. Phys. **23**, 47 (1999).

Yildirim, T., Gehring, P. M., Neumann, D. A., Eaton, P. E., Emrick, T., "Neutron Scattering Investigation of Molecular Reorientations in Solid Cubane", Phys. Rev. B **60**, 314 (1999).

Yildirim, T., Kilic, C., Ciraci, S., Gehring, P. M., Neumann, D. A., Eaton, P. E., Emrick, T., "Vibrations of the Cubane Molecule: Inelastic Neutron Scattering Study and Theory", Chem. Phys. Lett. **309**, 234 (1999).

Yildirim, T., Neumann, D. A., Trevino, S. F., Fischer, J. E., "Neutron Scattering Study of Na_2C_{60} in Pressure-Temperature Plane", Phys. Rev. B **60**, 10707 (1999).

Yildirim, T., Zhou, O., Fischer, J. E., "Intercalation Compounds of Fullerenes I: Synthesis, Characterization, and Solid State Properties", in *Physics and Chemistry of Materials with Low-Dimensional Structures*, edited by W. Andreoni, in press.

Yildirim, T., Zhou, O., Fischer, J. E., "Intercalation Compounds of Fullerenes II: Structure and Superconductivity of Alkali Metal Fullerides", in *Physics and Chemistry of Materials with Low-Dimensional Structures*, edited by W. Andreoni, in press.

Yildirim, T., Zhou, O., Fischer, J. E., "Intercalation Compounds of Fullerenes III: Other Fullerides and Intercalated Nanotubes", in *Physics and Chemistry of Materials with Low-Dimensional Structures*, edited by W. Andreoni, in press.

Yim, H., Kent, M., McNamara, W. F., Ivkov, R., Satija, S., Majewski, J., "Structure within Thin Epoxy Films Revealed by Solvent Swelling: A Neutron Reflectivity Study", Macromol., in press.

Zeisler, R., "Investigations by INAA for the Development of Natural Matrix Standard Reference Materials (SRMs) Suitable for Small Sample Analysis", J. Radioanal. Nucl. Chem., in press.

Zeisler, R., "Maintaining Accuracy in Gamma-Ray Spectrometry at High Count Rates", J. Radioanal. Nucl. Chem., in press.

Zeisler, R., Greenberg, R. R., "Determination of Sub-Nanomole Elemental Levels by NAA and Their Possible Impact on Human Health Related Issues", J. Bio. Trace Ele. Res. **71**, 283 (1999).

Zhao, J., Wang, J., Chen, D. J., Peterson, S. R., Trewhella, J., "The Solution Structure of the DNA Double-Strand Break Repair Protein Ku and its Complex with DNA: A Small-Angle Neutron Scattering Study", Biochem. **38**, 21512 (1999).

Zhao, J., Hoye, E., Boylen, S., Walsh, D. A., Trewhella, J., "Quaternary Structures of a Catalytic Subunit-Regulatory Subunit Dimeric Complex and the Holoenzyme of the CAMP-Dependent Protein Kinase by Neutron Contrast Variation", J. Bio. Chem. **273**, 30448 (1998).

Zheludev, A., Maslov, S., Shirane, G., Tsukada, I., Masuda, T., Uchinokura, K., Zaliznyak, I., Erwin, R. W, Regnalt, L.P., "Experimental Evidence for Kaplan-Shekhtman-Entin-Wohlman-Aharony Interactions in Ba_2CuGeO_7", Phys Rev. Lett. **81**, 5410 (1998).

Zheludev, A., Maslov, S., Shirane, G., Tsukada, I., Masuda, T., Uchinokura, K., Zaliznyak, I., Erwin, R. W., Regnault, L. P., "Magnetic Anisotropy and Low-Energy Spin Waves in the Dzyaloshinskii-Moriya Spiral Magnet $Ba_2CuGe_2O_7$", Phys. Rev. B, in press.

Zheludev, A., Maslov, S., Zaliznyak, I., Regnault, L. P., Masuda, T., Uchinokura, K., Erwin, R.W., Shirane, G., "Experimental Evidence for Shekhtman-Entin-Wohlman-Aharony Interactions in $Ba_2CuGe_2O_7$", Phys. Rev. B, in press.

Zhou, C., Hobbie, E. K., Bauer, B. J., Han, C. C., "Equilibrium Structure of Hydrogen-Bonded Polymer Blends", J. Polym. Sci. Polm. Phys., in press.

National Institute of Standards and Technology

| Quality Programs |
| Director |
| Deputy Director |
| Advanced Technology Program |

| Technology Services |
| Manufacturing Extension Partnership |

| Electronics and Electrical Engineering Laboratory | Manufacturing Engineering Laboratory | Physics Laboratory | **Materials Science and Engineering Laboratory** | Chemical Science and Technology Laboratory | Information Technology Laboratory | Building and Fire Research Laboratory |

Materials Science and Engineering Laboratory

L.E. Smith, Director
D.E. Hall, Deputy Director

Metallurgy

C.A. Handwerker, Chief
R.J. Schaefer, Deputy

Polymers

E.J. Amis, Chief
B.M. Fanconi, Deputy

Ceramics

S.W. Freiman, Chief
S.J. Dapkunas, Deputy

Materials Reliability

F.R. Fickett, Chief
T.A. Siewert, Deputy

NIST Center for Neutron Research

J.M. Rowe, Director

CENTER OFFICE (856)

Rowe, J. M., Director
Weiss, S. H., Deputy Director
Hill, J. M., Secretary
Sullivan, D. A., Admin. Off.
Neal, S. L., Admin. Asst.
Clutter, L. K., User. Coord.
Barker, J. G.
Cappelletti, R. L.
Kamitakahara, W. A.
Prask, H. J.

REACTOR OPERATIONS & ENGINEERING

Raby, T. M., Chief
Torrence, J. F., Deputy
Poole, L. M., Secretary

Operations

Beasley, R.D.
Bickford, N. A.
Bobik, P. A.
Cassells, M. G.
Clark, F. C.
Dilks, H. W.
Flynn, D. J.
Guarin, E. L.
Lindstrom, L. T.
McDonald, M. J.
Mueller, W. W.
Myers, T. J.
Pierce, S. C.
Ring, J. H.
Slaughter, S. G.
Sprow, R. P.
Stiber, R. F.
Thompson, R. G
Toth, A. L.
Wilkison, D. P.
Wright, K. D.

Engineering

Suthar, M. A., Chief
Beatty, J. A.
Boyd, J. M.
Brady, D. E.
Hall, K. D.
Liposky, P. J.
Reilly, G. D.
Shuman, L.A.

Guest Researchers

Anderson, D. A.
Dahan, S.
Cunningham, W. C.
Yee, K.

NEUTRON CONDENSED MATTER SCIENCE GROUP

Rush, J. J., Leader
Runkles, C. L., Secretary
Bowen, M. L., Automat. Asst.
Berk, N. F.
Yildirim, T.

Chemical Physics of Materials

Copley, J. R. D.
Dimeo, R. M.
Forstner, K. T.
McLaughlin, J. C.
Neumann, D. A., Team Leader
Tsai, A. M.
Udovic, T. J.

Crystallography

Reisner, B. A.
Santoro, A.
Stalick, J. K.
Toby B. H., Team Leader

Magnetism and Superconductivity

Borchers, J. A.
Erwin, R. W.
Gehring, P. M.
Lynn, J. W., Team Leader
Santodonato, L.

Macromolecular and Microstructure

Butler, P. D.
Glinka, C. J., Team Leader
Hammouda, B.
Hernandez, Y.
Kline, S. R.
Munter, A. E.
Rosov, N.

Surfaces and Interfaces

Dura, J. A.
Krueger, S. T.
Ivkov, R.
Majkrzak, C. F., Team Leader
Satija, S. K.

Guest Researchers

Adams, C.
Broholm, C.
Brown, C. M.
Bu, Z.
Choi, S.-M.
Cook, J.
Dender, D.
Gnäupel-Herold, T.
Gulseren, O.
Ho, D.
Huang, Q. Z.
Lee, S.-H.
Lin, M. Y.
Meyer, A.
Nieh, M.
Papanek, P.
Pagoda, C.
Park, S.
Prince, E.
Raebiger, J.
Rathgeber, S.
Sitepu. H.
Tarek, M.
Trevino, S. F.
Ulrich, C.
Vasiliu-Doloc, L.

RESEARCH FACILITY OPERATIONS

Gallagher, P. D. Leader
Ruhl, K. J., Clerk Typist
Baltic, G. M.
Bostian, C. D.
Brand, P. C.
Clarkson, A. W.
Clem, D. L.
Clow, W. R.
Dickerson, W. E.
English, M. C.
Fravel, D. H.
Fulford, D.
Greene, G. C.
Heald, A. E.
Klosowski, P.

Knill, W. C.
Kopetka, P. H.
Kulp, D. L.
LaRock, J. G.
Maliszewskyj, N. C.
Pierce, D. J.
Reardon, J. P.
Rinehart, M. J.
Schröder, I. G.
Slifer, S.
Thai, T. T.
Tobin, P. J.
Williams, R. E.
Ziegler, J. B.

Guest Engineers

Brocker, C. W.
Christman, R.
Kenney, J. T.
Moyer, J. J.
Murbach, M.
Wrenn, C. W.

OTHER NIST GROUPS

NEUTRON INTERACTIONS & DOSIMETRY GROUP (846)

Gilliam, D. M., Leader
Chin, C. R., Secretary
Adams, J. M.
Arif, M.
Clarkson, N.
Dewey, M. S.
Gentile, T. R.
Huffman, P. R.
Jacobson, D. L.
Nico, J. S.
Thompson, A. K.

Guest Researchers

Brome, C. R.
Butterworth, J.S.
Chowdhuri, Z. S.
Doyle, J. M.
Dzhosyuk, S. N.
Eisenhauer, C. M.
Hansen, G. L.
Ioffe, A.
Jones, G. L.
Mattoni, C. E. H.
McKinsey, D.
Rich, D. R.
Schwartz, R. B.
Snow, W. M.
Weitfeldt, F. E.

NUCLEAR METHODS GROUP (839)

Greenberg, R. R., Leader
Wilson, J. M., Secretary
Becker, D. A.
Chen-Mayer, H. H.
Demiralp, R.
Lamaze, G. P.
Langland, J. K.
Lindstrom, R. M.
Mackey, E. A.
Mildner, D. F. R.
Paul, R. L.
Porter, B. J.
Zeisler, R. L.

Guest Researchers

Berger, A.
Bishop, R. L.
Blackman, M. J.

HEALTH PHYSICS (354)

Slaback, L. A., Leader
Thomas, C. L., Secretary
Brown, D. R.
Campbell, C. D.
Cassells, L. H.
Clark, J. S.
Deardorff, G. E.
Fink, L. E.
Mengers, T. F.
Shubiak, J. J.

RESEARCH AND ENGINEERING STAFF

J. G. Barker
  SANS instrumentation and research
  Microstructure of materials

N. F. Berk
  Condensed matter theory
  Scattering theory for microstructure analysis
  Computer software for graphics and data analysis

N. A. Bickford
  Reactor operations
  Reactor irradiations
  Reactor utilization

J. A. Borchers
  Magnetism
  Thin-film analysis
  Artificially modulated materials

D. E. Brady
  Electrical/electronic engineering
  Nuclear reactor instrumentation
  NDE diffraction methods

P. C. Brand
  Engineering physics
  Materials engineering
  Neutron residual stress measurements

J. M. Boyd
  Electrical/electronic engineering
  Nuclear reactor instrumentation

P. D. Butler
  Microstructure of complex fluids
  SANS instrumentation

R. L. Cappelletti
  Dynamics of disordered solids
  Condensed matter physics
  Science information management

J. R. D. Copley
  Time-of-flight spectrometer development
  Neutron instrumentation
  Conceptual design
  Condensed matter physics

W. E. Dickerson
  Neutron scattering instrumentation
  Microcomputer interfacing
  Nuclear and engineering physics

R. M. Dimeo
  Condensed matter physics
  Cold neutron instrumentation
  Molecules in porous media
J. A. Dura
  Combined molecular beam
  epitaxy and neutron reflectivity
  Instrumentation
  Surface, interfacial, and epitaxial
  physics
M. C. English
  Electrical engineering
  Instrument development
  Facility operations
R. W. Erwin
  Magnetic materials
  Phase transformations
  Cryogenics
K. T. Forstner
  Instrumentation
  Monochromator development
D. B. Fulford
  Mechanical engineering
P. D. Gallagher
  Neutron instrumentation
  Interfacial phenomena in polymer
  systems and complex fluids
  Phase transitions and critical
  phenomena
P. M. Gehring
  Back-scattering and triple-axis
  instrumentation
  Transitions in magnetic and
  ferroelectric materials
  Dynamics of high T_c materials
C. J. Glinka
  Microstructure characterization by
  SANS
  CHRNS project director
  Cold neutron instrument
  development
G. C. Greene
  System and user software for cold
  neutron instrumentation
  Spectrometer and data acquisition
  systems interfaces
B. Hammouda
  SANS from polymers, liquid
  crystals, and colloids
  Dynamics of polymers in solution
  Scattering from sheared fluids
Y. Hernandez
  Chemical technology
  Sample preparation and
  characterization
A. E. Heald
  Design engineering
  Neutron instrumentation
  Shielding

W. A. Kamitakahara
  Dynamics of disordered solids
  Condensed matter physics
  NCNR user program
S. R. Kline
  Microstructure of colloids and
  microemulsions
  Novel surfactant systems
  SANS instrumentation
R. Ivkov
  Dynamics of filled polymers and
  polymer composites
  Neutron reflectometry
  Structure of polymer and protein
  solutions, polymer brushes thin
  films
P. Klosowski
  Scientific data visualization
  Numerical computer modeling
  Data acquisition software and
  hardware
P. A. Kopetka
  Mechanical engineering
  Cold source design
  Electro-mechanical systems
S. T. Krueger
  Structure of biological materials
  SANS and neutron reflectometry
  methods
  Computer software development
J. G. LaRock
  Mechanical engineering
  Neutron instrumentation design
P. J. Liposky
  Design engineering
  Nuclear systems and components
J. W. Lynn
  Condensed matter physics
  Magnetic and superconducting
  materials
  Neutron scattering methods
C. F. Majkrzak
  Condensed matter physics
  Polarized neutron scattering and
  instrumentation development
  Neutron reflectivity measurements
N. C. Maliszewskyj
  Computer software development
  Time-of-flight instrumentation
  Condensed matter physics
J. C. McLaughlin
  Materials chemistry
  Neutron scattering
  Nanoscale properties of cements
A. E. Munter
  Neutron SANS and reflectometry
  Computer software development
T. J. Myers
  Reactor operations
  Safety analysis

D. A. Neumann
  Molecular and layered materials
  Condensed matter physics
  Neutron and X-ray scattering
  instrumentation
D. J. Pierce
  Mechanical engineering
  Neutron instrumentation design
H. J. Prask
  Residual stress measurement
  methodology
  Neutron NDE applications and
  instrumentation
T. M. Raby
  Reactor operations and standards
  Nuclear engineering
  Nuclear systems and components
G. D. Reilly
  Design engineering
  Nuclear systems and
  components
B. A. Reisner
  Solid state chemistry
  Crystallographic methods
  Neutron scattering
N. Rosov
  Spin echo techniques
  Phase transformations
  Magnetic materials
J. M. Rowe
  Orientationally disordered solids
  Cold source development
  Cold neutron research and
  instrumentation
J. J. Rush
  Catalysts and molecular materials
  Hydrogen in metals
  Inelastic scattering methods
L. Santodonato
  Condensed matter physics
  Cryogenics
A. Santoro
  Crystal structure of oxide
  ceramics
  Theory of crystal lattices
  Powder diffraction methods
S. K. Satija
  Low-dimensional molecular
  systems
  Fractal aspects of microporous
  media
  Neutron reflectometry
I. G. Schröder
  Cold neutron instrumentation
  development
  Nuclear and engineering physics
  Optical devices for neutron
  transport

J. K. Stalick
  Neutron and X-ray diffraction
  Inorganic chemistry
  Crystal database development
M. A. Suthar
  Design engineering
  Nuclear systems and components
B. H. Toby
  Neutron and synchrotron X-ray
  diffraction
  Zeolite crystallography
  Structure determination methods
J. F. Torrence
  Reactor supervision
  Reactor maintenance
  Nuclear engineering
A. M. Tsai
  Biochemical engineering
  Dynamics of biological systems
  Inelastic neutron scattering
T. J. Udovic
  Neutron time-of-flight
  instrumentation
  Properties of catalysts and
  adsorbates
  Hydrogen in metals
S. H. Weiss
  Reactor operations and standards
  Reactor licensing and regulations
  Electrical Engineering
R. E. Williams
  Cold neutron source development
  Nuclear engineering
  Reactor physics simulations
T. Yildrim
  Condensed matter theory
  Neutron scattering methods
  Solid state synthesis
J. B. Ziegler
  Electrical engineering
  Electronic design
  Instrument development

NIST CENTER FOR NEUTRON RESEARCH

For additional information on the facility, contact:

J. Michael Rowe
(301) 975-6210
mike.rowe@nist.gov

John J. Rush
(301) 975-6231
john.rush@nist.gov

To obtain guidelines for preparing proposals to conduct research at the facility, contact:

William Kamitakahara
(301) 975-6878
william.kamitakahara@nist.gov

Location of all contacts:

NIST Center for Neutron Research
Building 235, Room E151, Mail Stop 8562
National Institute of Standards and
Technology
Gaithersburg, MD 20899-8562

Details are also available on the
NCNR Web site:
www.ncnr.nist.gov.